(2)

The Study of Surface Condition Control of Lithium Metal Anode for Rechargeable Lithium Batteries

1999

Soshi Shiraishi

Contents

General Introduction

Background

Attraction and problem of rechargeable lithium battery with lithium metal

Recently, people have demanded higher energy density batteries for larger power sources and portable electrical devices. Especially, rechargeable lithium batteries have been widely used as power sources for small devices and are also expected as large power sources for load leveling systems or electric vehicles because of their high energy density (Figure 1)[1-4]. Rechargeable lithium batteries are composed of a lithium metal anode or a

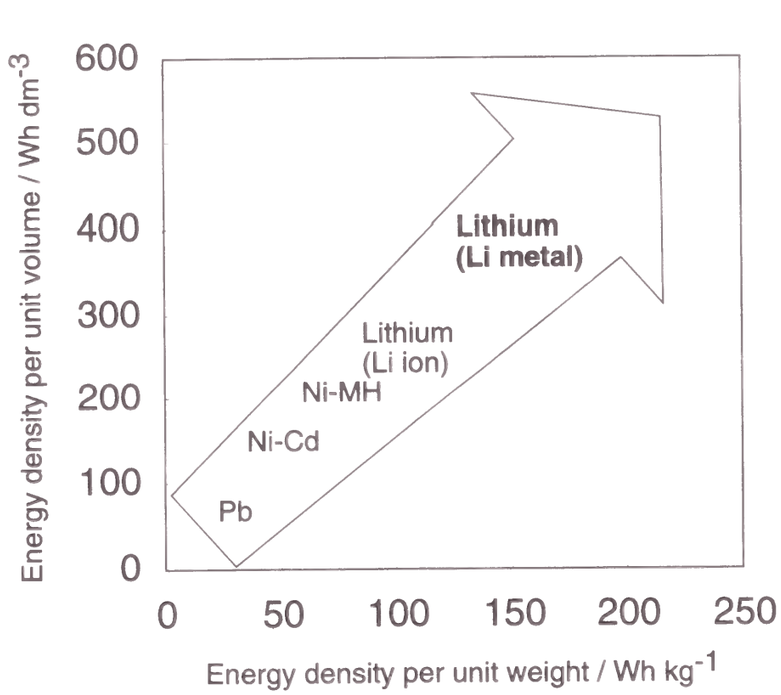

Figure 1 Energy density of various rechargeable batteries.
Pd: lead storage battery, Ni-Cd; nickel cadminum battery, Ni-MH; nickel hydrogen battery, Lithium (Li-ion); rechargeable lithium battery (Li-ion type), Lithium (Lithium metal); rechargeable lithium battery with lithium metal anode

lithium ion source anode, a lithium ion conducting electrolyte (nonaqueous electrolyte containing lithium salts), and a lithium ion accepting cathode material (for example, transition metal dicalcogenides and oxides). A schematic illustration for this system is shown in Figure 2 [4]. The charge and discharge reactions for the cathodes are the intercalation (doping) and deintercalation (undoping) of lithium ions into/from the cathode matrix, respectively. On the other hand, the charge and discharge reactions of lithium metal correspond to the electrochemical deposition and dissolution of lithium, as shown by the following reaction.

$$Li^+ + e^- \underset{\text{discharge : dissolution}}{\overset{\text{charge : deposition}}{\rightleftarrows}} Li \qquad E^0 = -3.05 \text{ V vs. SHE}$$

The energy density of the anode or cathode material for a battery depends on the electrode

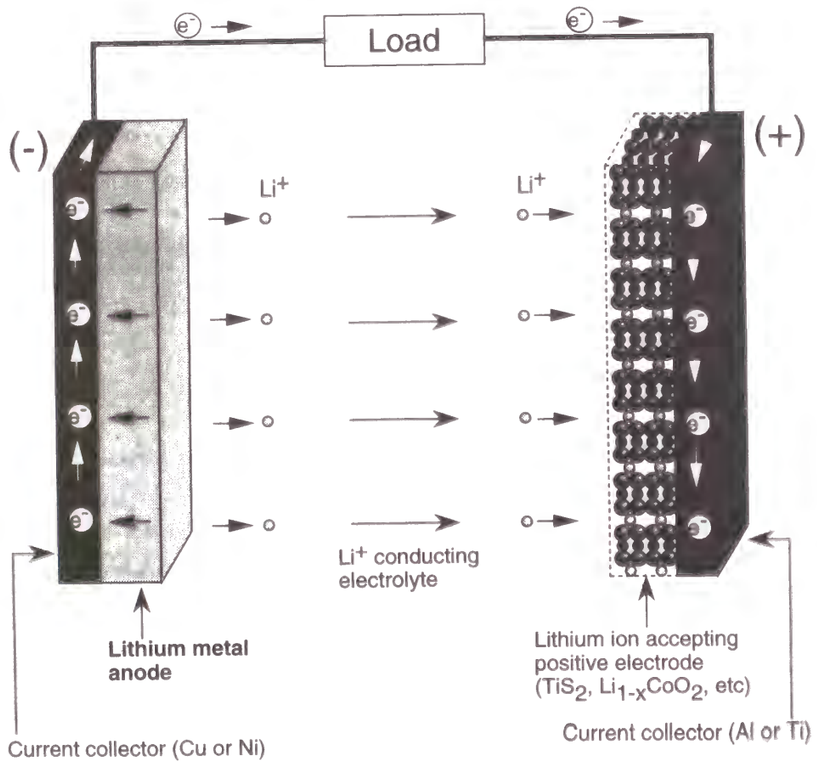

Figure 2 Schematic illustration for the discharge process of rechargeable lithium metal battery.

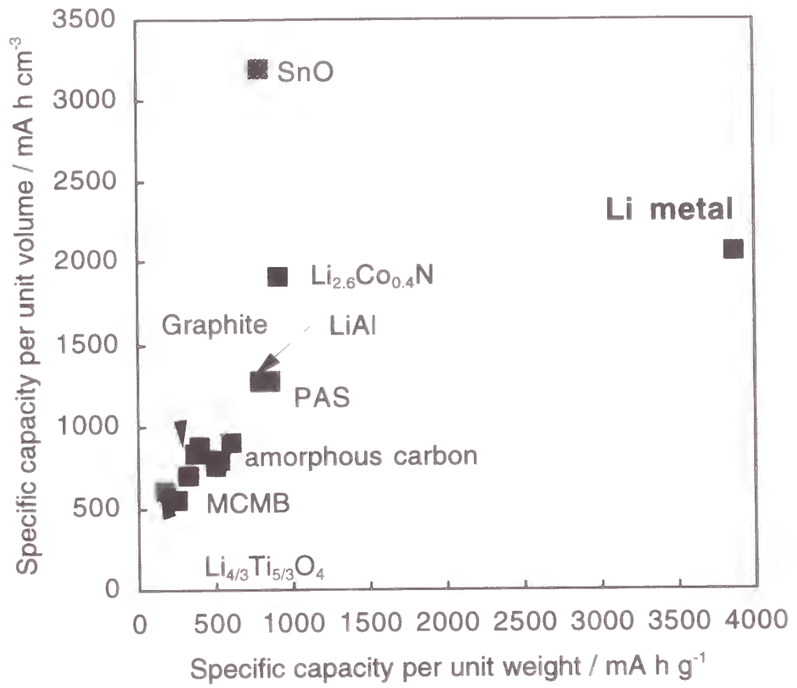

Figure 3 Energy density of various anode materials for rechargeable lithium battery.

potential and the molar mass. Lithium metal has the most negative electrode potential and very small molar mass. Therefore, lithium metal theoretically has the highest energy density (coulombic energy density per unit weight: 3860 mAh g^{-1}) among all anode materials for rechargeable lithium batteries, as shown in Figure 3 [5,6]. However, the charge-discharge cycle efficiency and safety of lithium metal anode are too low to be used for practical batteries. These are caused by both the high reactivity of lithium with nonaqueous electrolytes and the morphology of lithium electrodeposited during charging [7-10]. To overcome these problems, various alternative anodes have been developed and utilized as lithium ion sources [3,4]. In the "Lithium Ion Battery", carbon materials (for example, graphite and amorphous carbon) are used as the anode. The charge-discharge reaction of the carbon anode is the intercalation (doping) and deintercalation (undoping) of lithium ions into/ from the carbon matrix. So, this "Lithium ion battery" has been commercialized most

successfully among various candidates for practical rechargeable lithium batteries. However, this battery is still not practical for large power sources. On the other hand, rechargeable lithium batteries with lithium metal possess a high energy density that is two or three times higher than that of "Lithium Ion Batteries". Therefore, lithium metal anodes have to be studied in order to realize higher energy densities for future applications.

The reversibility of electrochemical deposition and dissolution of lithium metal

Lithium metal explosively reacts with water, therefore, aqueous electrolytes are not suitable for rechargeable lithium batteries with a lithium metal anode. In most cases, various nonaqueous electrolytes that are used for the batteries consist of aprotic organic solvents and lithium salts. Representative solvent, salt, and electrolyte conductivities are summarized in Table 1 and Table 2. When lithium metal is electrodeposited in these electrolytes, the morphology is usually in a dendritic shape. Figure 4 is a scanning electron micrograph for typical dendritic lithium. This dendritic lithium easily causes electrical or mechanical separation from a current collector, as shown in Figure 5. Lithium metal, which was separated from a current collector, is called "dead lithium". This dead lithium leads to a rapid decrease in reversibility of the lithium anode [9,10]. Selim et al. performed a chemical quantitative analysis of the amount of lithium metal electrodeposited and that

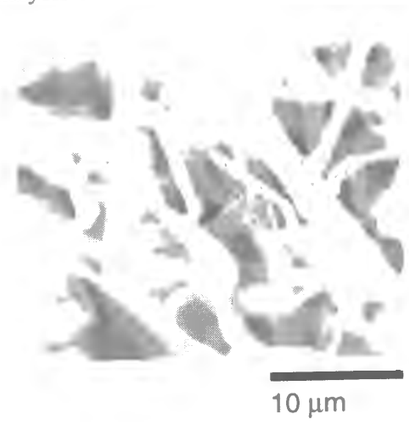

Figure 4 Scanning electron micrograph of typical dendritic lithium

Table 1 Physical parameters (25 C) of various solvents for nonaqueous electrolytes used in rechargeable lithium batteries [12]

Solvents	ε_r	η_0 [cP]	DN	mp [°C]	bp [°C]
Etylene carbonate (EC) [a]	90 (40°C)	1.9	16.4	37	238
Propylene carbonate (PC) [b]	65	2.5	15	-49	242
γ-Butyrolactone (γ-BL) [c]	42	1.7	18	-44	204
1,2-Dimethoxyethane (DME) [d]	7.2	0.46	20	-58	84
Tetrahydrofuran (THF) [e]	7.4	0.46	20	-109	66
2-Methyltetrahydrofuran (2MeTHF) [f]	6.2	0.47	18	-137	80
1,3-Dioxolane (DOL) [g]	7.1	0.59	-	-95	78
Metyl formate (MF) [h]	8.5	0.33	-	-99	32
Dimetyl carbonate (DMC) [i]	3.1	0.59	-	3	90
Ethyl methyl carbonate (EMC) [j]	2.9	0.65	-	-55	108
Diethyl carbonate (DEC) [k]	2.8	0.75	15.1	-43	127

ε_r: dielectric constant, η_0: viscosity, DN: donor number, mp: meting point, bp: boiling point

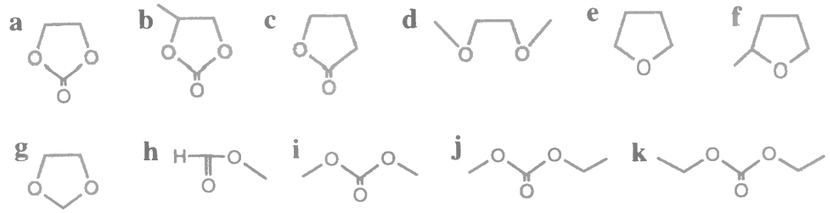

Table 2 Conductivity (25°C) of various nonaqueous electrolytes (1.0 mol dm^{-3}) [13-15]

	Conductivity [mS cm^{-1}]			
Salts	PC	γ-BL	THF	PC/EMC(1:1)
$LiClO_4$	5.6	10.9	3.3	5.7
$LiBF_4$	3.4	7.5	-	3.3
$LiAsF_6$	5.7	11.5	13.3	9.2
$LiCF_3SO_3$	1.7	4.3	-	1.7
$LiPF_6$	5.8	10.9	-	5.7
$Li(CF_3SO_2)_2N$	5.1	9.4	-	1.3

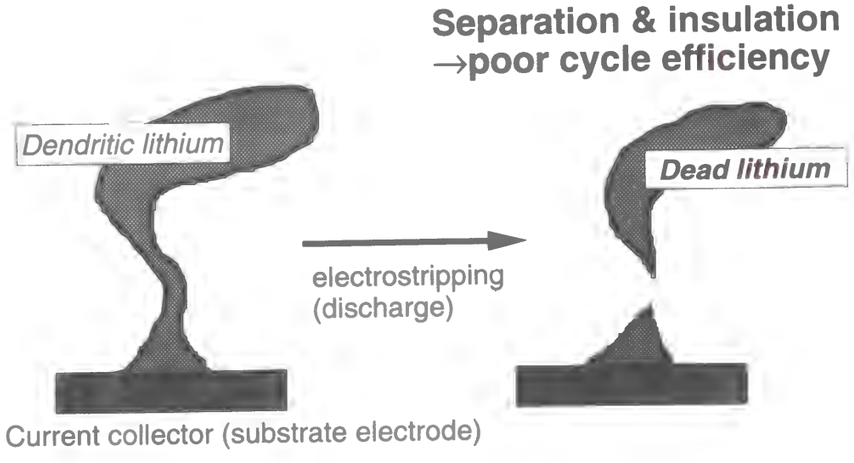

Figure 5 Formation of dead lithium by electrostripping (discharge process).

of the lithium metal electrodissolved [11]. Their results revealed the following points.

(1) lithium metal is electrodeposited with almost 100% coulombic efficiency.

(2) Only a part of the lithium metal electrodeposited can be electrochemically dissolved.

These facts indicate that the low reversibility for the deposition and dissolution cycle of lithium metal is related to the undesirable morphology of lithium deposits rather than consumption of lithium metal by chemical reaction with the electrolyte components. Therefore, morphology control of lithium metal is necessary to acquire a higher reversible deposition and dissolution of the lithium metal.

Surface film on lithium metal

The electrochemical behavior of the lithium metal anode has been investigated since the 1970's. During the initial period, the electrochemical parameters, such as the exchange current density of the lithium metal electrode [16,17], the efficiency of deposition/dissolution of the lithium metal [18,19], the diffusion coefficiency of the electrolyte [20], and so on, have been studied by many researchers. In 1979, E. Peled proposed a model for the lithium/electrolyte interface. This model is called the "Solid Electrolyte Interface (SEI)"

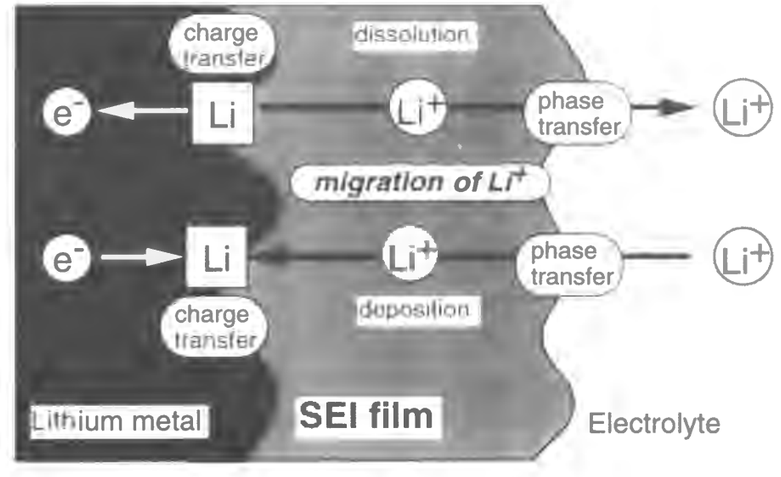

Figure 6 Schematic illustration of solid electrolyte interface (SEI) model [21].

model [21], and its schematic illustration is shown in Figure 6. In this model, lithium metal is covered with a surface film consisting of various lithium compounds which were formed by the chemical reactions with electrolyte or active gases in the atmosphere (O_2, H_2O, CO_2) during the preparation or storage of the lithium metal. The characteristic points in this model are

(1) the surface film works as a passive film to suppress further chemical reactions of the lithium metal with components of the nonaqueous electrolyte,

(2) the surface film is lithium ion conductive (approximately, the conductivity is in the range between $10^{-7} \sim 10^{-10}$ S cm^{-1}),

(3) the electrochemical deposition or dissolution of lithium takes place with the migration of Li^+ ions through the surface film, and

(4) the migration of Li^+ ions in the surface film is the rate determining step of the electrochemical deposition or dissolution of lithium.

These discussions suggest that the electrochemical behavior of lithium metal and the morphology of the electrodeposited lithium strongly depend on the state of the surface film. Therefore, surface chemistry on the lithium metal anode is very important to improve the performance of the lithium metal anode.

In fact, numerous studies have been conducted to obtain information about the chemical compositions and structure of the surface film. These studies were carried out using many kinds of spectroscopic, electrochemical, and microscopic analyses, for example, *in situ* and *ex situ* Fourier Transform Infrared Spectroscopy (FTIR) [27,28], *in situ* X-ray Diffraction (XRD) [29,40], Electron Probe Microanalysis (EPMA) [31,43], *in-situ* Raman Spectroscopy [41], X-ray Photoelectron Spectroscopy (XPS) [35,40], Auger electron spectroscopy (AES) [41,42], electrochemical impedance spectroscopy (EIS) [44,48], electrochemical quartz crystal microbalance (ECQCM) [48,53], the electrochemical scanning vibrating electrode technique (SVET) [54], and scanning probe microscopy (SPM) [55,56]. However, the condition of the surface film has not clarified yet in spite of these efforts by many researchers. Table 3 shows a summary of the results of the surface analysis of lithium metal in various electrolytes. In this table, different chemical compositions were reported even when the same electrolytes were used. This inconsistency complicates the understanding of the surface film condition. The following two points have been considered as reasons for this inconsistency.

(1) difference in the analytical techniques

(2) difference in the initial surface condition of the lithium metal

Especially, the latter had been neglected for a long time. The latter point seems to be the main reason for such confusion in the study of the lithium surface. The following points are the different initial conditions of the lithium metal used for analysis.

(1) as-received lithium metal (lithium metal without pre-treatment before analysis) [18,37]

(2) lithium metal with pre-treatment for exposure of fresh surface (lithium metal whose surface is cut by a stainless knife [24,44,61,62] or etched by anodic dissolution [22,64])

(3) electrodeposited lithium [53]

(4) lithium prepared by vapor-deposition [36,41,42]

(5) amalgamated lithium [30]

Based on these different conditions, it follows that the reports by each researcher can not

Table 3 Summary of the reports for chemical compositions of surface film on lithium metal in various nonaqueous electrolytes.

Electrolyte or solvent	Surface film	References
LiClO$_4$/PC	Li_2CO_3	[64]
	Li_2CO_3, LiCl, partially chlorinated hydrocarbon	[40]
	Li_2CO_3, LiCl, LiOCO$_2$R ($CH_3CHCH_2OCO_2Li$, $CH_2CHCHOCO_2Li$, $LiOCH_2(CH_2)CHOCO_2Li$)	22]
	Li_2O, LiOH, Li_2CO_3, LiCl (minor)	[37]
LiAsF$_6$/PC	Li_2CO_3, LiF, LiOCO$_2$R	[22]
	Li_2CO_3, LiOH, Li_2O, LiF	[37]
DEC	$CH_3CH_2OCO_2Li$, CH_3CH_2OLi	[22]
(LiClO$_4$/DEC)	Li_2CO_3, LiOH, Li_2O, LiOCO$_2$R, LiCl (minor)	[26]
(LiPF$_6$/DEC)	Li_2CO_3, LiOH, Li_2O, LiF	[26]
LiAsF$_6$/THF	BuOLi, LiF, -As-O-As-	[65]
	$LiOCH_2CH_2CH_2CH_3$	[66]
	LiOR, LiF, Li_xAsF_y	[23]
	Li_2CO_3, LiOH, Li_2O, LiF (minor)	[63]
	-O(CH$_2$)$_4$-THF, F, As-O-As-F$_2$	[34]
LiAsF$_6$/2MeTHF	$CH_3(CH_2)_4OLi$, $CH_3CH(OLi)CH_2CH_2CH_3$	[67]
LiAsF$_6$/DME	CH_3OLi, LiF	[65]
LiClO$_4$/γ-BL	$CH_3CH_2CH_2CO_2Li$, cyclic β-keto ester anion	[68]
	LiOCO$_2$R, Li_2CO_3, LiOH, Li_2O, LiCl (minor)	[63]
LiClO$_4$/DOL	CH_3OLi, CH_3CH_2OLi, $LiOCH_2CH_2(OCH_2CH_2)_nOX$ (X=OLi, H, OR)	[69]
LiClO$_4$/MF	CH_3OLi, LiOOCH	[70]

be easily compared to each other. Consequently, much attention must be paid to the initial state of the lithium metal in order to better clarify the conditions of the surface film on the lithium metal.

The determining factors for the morphology of electrodeposited lithium

The spectroscopic or electrochemical analyses of the stability of lithium metal and the chemical composition of the surface films were the main topics in the study of lithium metal anodes until the 1990's. However, during the past 10 years, the relationship between the morphology of the lithium deposits and the surface film has been actively studied [40,63,71,72]. The surface film is formed by the chemical reaction with the electrolyte, so it is easily expected that the morphology of the lithium is dependent on the type of electrolytes used in electrodeposition. However, different morphologies are often observed even if the same electrolyte is used [72]. Therefore, another factor needs to be considered for the electrodeposition of lithium. Such a factor could be the type of substrate electrode (current collector) used for the electrodeposition. Two types of substrate electrodes are as follows.

(1) lithium metal,

(2) inactive metals which do not alloy with lithium metal, such as nickel, copper, etc.,

For case (1), lithium metal is electrodeposited on the lithium metal substrate by the migration of lithium ions through the surface film on the substrate (Figure 7). Here, the important point is that a surface film (SEI film) on the lithium metal substrate is already present before the electrodeposition of the lithium metal. Especially, such an initial surface film, which was already formed prior to the immersion in the electrolyte, is called the "native surface film". On the other hand, in the case of (2), first, SEI films are formed on the electrode by reductive decomposition of the electrolyte [73]. After the formation of the SEI film on the substrate, the lithium metal is electrodeposited on the substrate electrode through the SEI film (Figure 8). According to the above mechanism, the significant difference

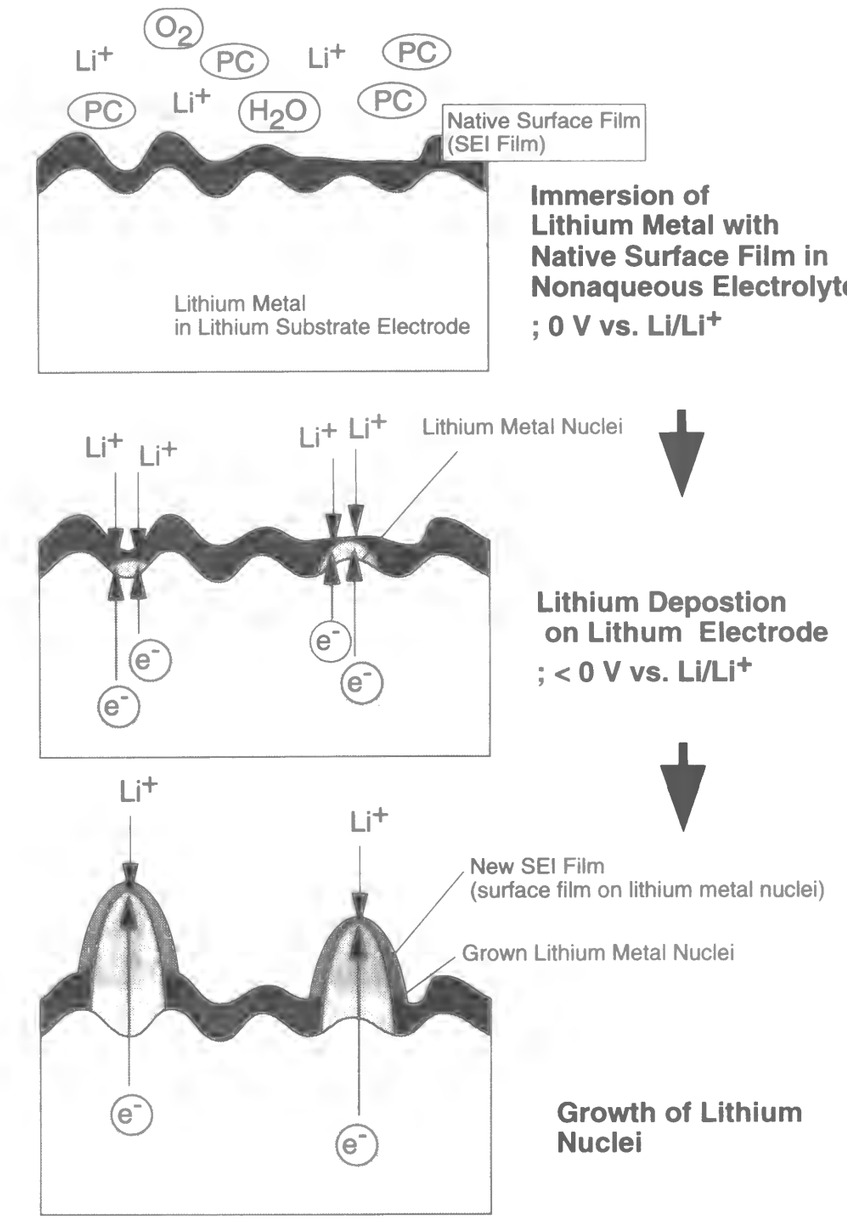

Figure 7 Schematic illustration of the initial stage of electrodepostion of lithium metal on lithium metal substrate electrode.

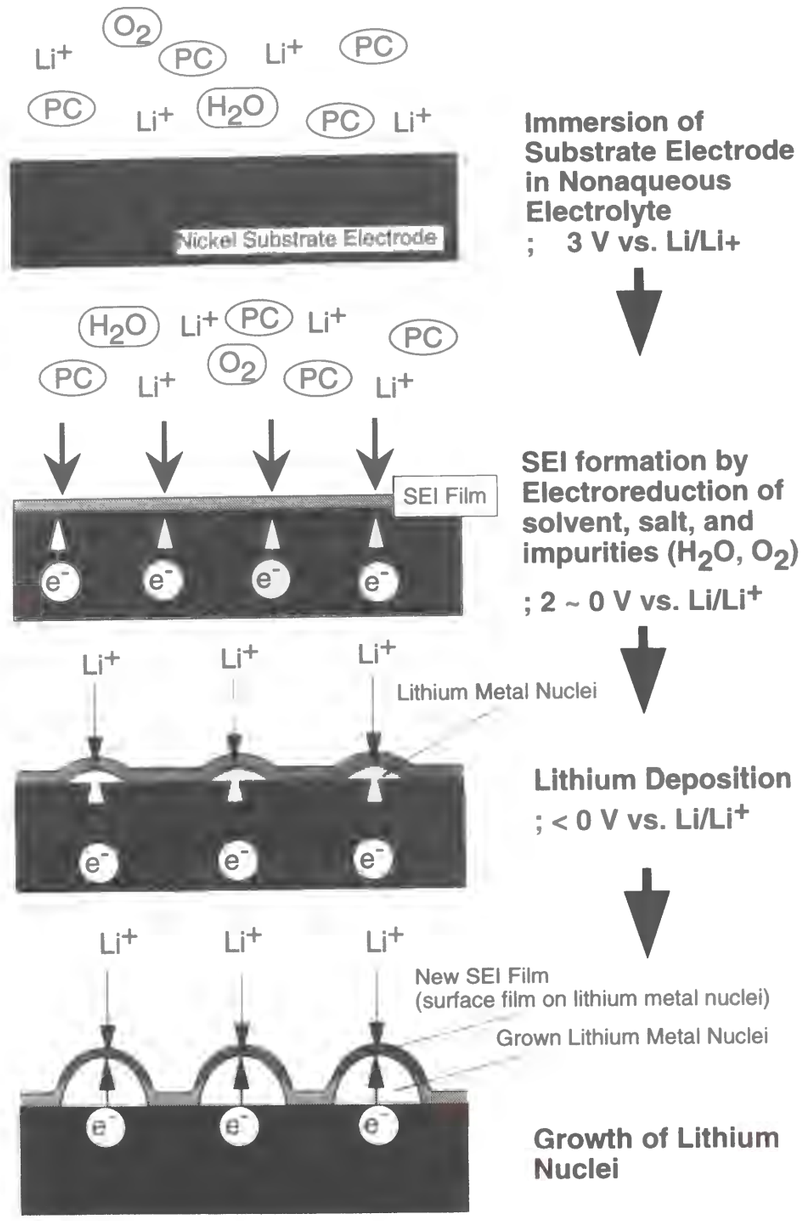

Figure 8 Schematic illustration of the initial stage of electrodepostion of lithium metal on inactive metal (nickel, copper, etc) substrate electrode.

between the type (1) and type (2) states is the initial condition of the substrate electrode for the electrodeposition. The condition of the native film should strongly affect the morphology of the electrodeposited lithium. This means that the substrate type is also a significant "key point" for determining the morphology of the electrodeposited lithium. However, this factor has not been considered by most researchers, which causes more complication when studying the electrochemical behavior of lithium metal.

Model for the formation of dendritic lithium metal

Although the relationship between the morphology of the electrodeposited lithium and the surface film is not yet clarified, recently, a common rough model is supported to explain the reason for the formation of the dendritic lithium metal [47,48,59,74,75]. This model is the combination of the SEI model and the conventional model for the formation of dendrite metal such as zinc. In the latter, the concentration of the current at the tip of electrodeposited metal generates dendrite formation [76,77]. So, applying this mechanism to lithium metal deposition, it can be proposed that the dendrite formation of lithium is caused by concentration of the current due to a non-uniformity (such as thinner part, higher lithium ion conductive part, crack, or pin-hole in the film) of the surface film (Figure 9).

On the other hand, the internal stress of lithium metal under the surface film is also proposed as another model. This model is derived from the formation of a whisker of tin by internal stress [78]. However, more details are not available because there is only one report of this model.

The morphology control of electrodeposited lithium metal

According to the combination model, the surface modification of lithium metal is an effective way to obtain a uniform surface film for the suppresses the dendrite formation of lithium. Some researchers have suggested that some additives such as CO_2 [79-81], 2-Me

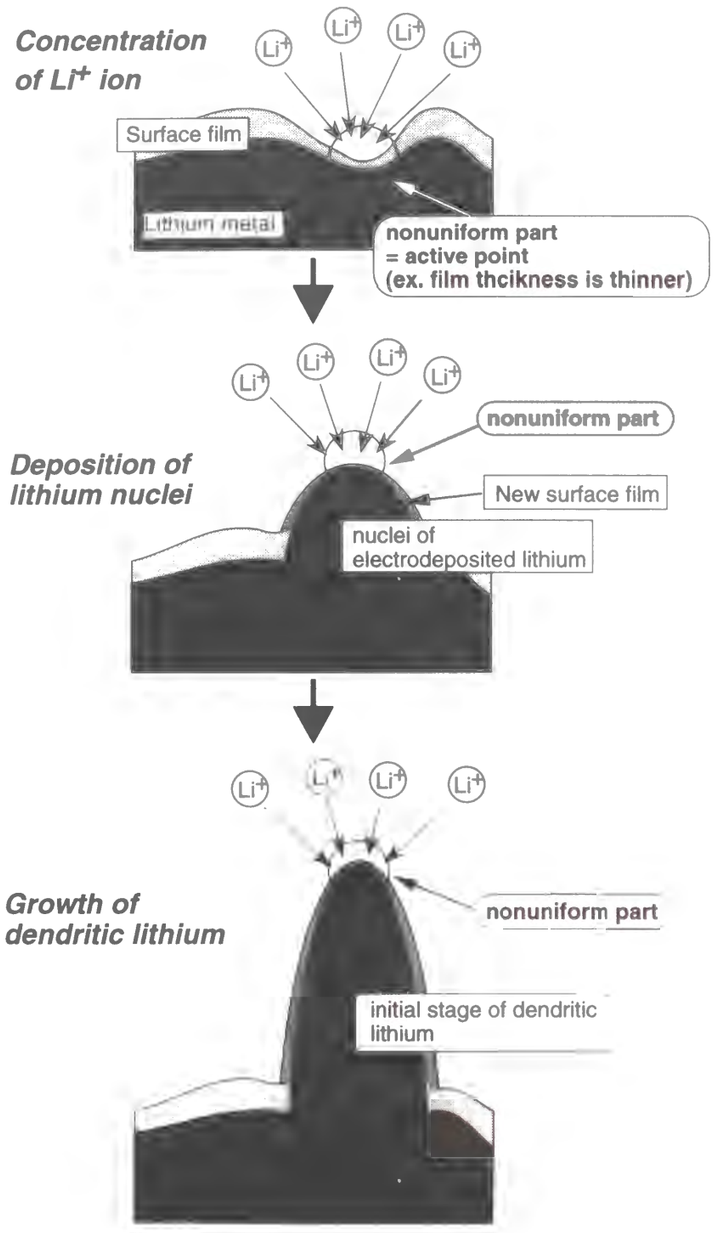

Figure 9 Possible Schematic illustration of dendritic lithium fomataion caused by ionic current concentration of Li^+ ion due to nonuniformity of surfcae film.

furan [54,82,83], AlI_3 [54], benzene [83], pyridine [84], and surfactants [48,85,86] may be effective in improving the reversibility of the deposition and dissolution of lithium metal. Unfortunately, even using these additives, the morphology of the electrodeposited lithium is not substantially improved (dendrite lithium is still deposited), so that the reversibility of the lithium anode is still not adequate for practical use. Thus, even now, many researchers and companies are searching for more adequate additives to optimize the surface film. However, such unperfected morphology control seems to fundamentally originate from the lack of understanding the relationship between the surface film and the electrochemical behavior of lithium metal. Consequently, more effective additives must be developed based on a more systematic investigation of the lithium/electrolyte interface.

Outline of this study

In this work, the analysis of the lithium/electrolyte interface plays an important role in order to improve the reversibility of the electrodeposition/dissolution of lithium. First, the surface film on lithium metal in nonaqueous electrolytes was characterized using various spectroscopic methods. The changes in the lithium surface in electrolyte were discussed from the view point of the reaction of the initial surface film (native film) with the electrolyte (Chapters 1 and 2). Second, possible additives for the suppression of the dendritic lithium was found based on the relationship between the condition of the surface film and the electrodeposited lithium. The electrochemical behavior of lithium metal in the presence of the additive (hydrogen fluoride: HF) was investigated using various spectroscopic and electrochemical analyses (Chapters 3~8). Finally, the most effective additive (HF complex) was proposed based on the HF results, and the possibility to realize a practical rechargeable lithium battery with a lithium metal anode was demonstrated using the charge-discharge cycle test (Chapter 9).

In Chapter 1, the surface of the lithium metal foil with the native film (as-received lithium) after immersion in propylene carbonate (PC) solutions containing various salts

($LiClO_4$, $LiCF_3SO_3$, $LiBF_4$, and $LiPF_6$) were analyzed by XPS, *in-situ* FTIR, and the electrochemical impedance method. The native film consisted of Li_2CO_3, LiOH, and Li_2O. During the immersion of lithium in the electrolytes, the native film reacted with impurity acid in the electrolyte to form a lithium halide (LiF or LiCl) on the lithium surface. The halide formation depended on the kind of salt. Especially, the chemical compositions of the surface film formed on the lithium metal after the immersion in PC containing 1.0 mol dm^{-3} $LiPF_6$ ($LiPF_6$/PC) was very different from those in the other electrolytes. Moreover, the surface film in $LiPF_6$/PC was thinner than those after immersion in the other electrolytes. These drastic changes in the native film are explained by an acid-base reaction of the native film with HF as an impurity (a hydrolysis product of PF_6^- ions) in the electrolyte. The morphology of the lithium electrodeposited on the lithium foil was influenced by the surface condition of the lithium foil. When the lithium foil was immersed in $LiPF_6$/PC for 72 h, the formation of the dendritic lithium was suppressed. These results indicate that a new surface film formed by the acid-base reaction with HF is important for the suppression of the dendritic lithium formation on the lithium foil.

In Chapter 2, a surface modification of the as-received lithium foil was performed by the acid-base reaction of the native film with various acids (HF, H_3PO_4, HI, HCl) dissolved in PC. The dendritic lithium was observed when using in $LiClO_4$/PC as the electrolyte, even though the lithium foil modified with any acids was used as the substrate electrode. On the other hand, spherical lithium particles were obtained by the electrodeposition in $LiPF_6$/PC when the lithium foil modified with HF was used. From the XPS results, the lithium foil modified by H_3PO_4, HI, or HCl was covered with a thick film which consists of Li_3PO_4, Li_2CO_3, LiOH, or Li_2O. The lithium foil modified with HF was covered with a thin bilayer structure film consisting of LiF and Li_2O. These results clearly show that the suppression of the dendritic lithium on the lithium foil can be accomplished by the surface modification of the native film with HF and the proper choice of electrolytes.

In Chapter 3, the chemical compositions of the surface films and the morphology of the deposits on a Ni substrate electrode in $LiClO_4$/PC, $LiAsF_6$/PC, $LiBF_4$/PC, or $LiPF_6$/PC were analyzed by XPS and scanning electron microscopy (SEM). The Ni substrate is used to eliminate the influences of the initial surface film such as the native film. The relationship between the surface film of lithium formed during the electrodeposition and the lithium morphology was deduced in this study. The dendrite formation was suppressed when using $LiPF_6$/PC as the electrolyte, which includes a small amount of HF as impurity. In this case, a very thin and tight surface film was formed on the surface of the lithium deposits. A similar surface film and morphology of the lithium deposits could be obtained by the addition of a small amount of hydrofluoric acid (46 wt.% HF aqueous solution), as a source of HF, into $LiClO_4$/PC. It was found that a small amount of HF in the electrolyte is also necessary for the suppression of lithium dendrites.

In Chapter 4, XPS and SEM methods were used for the analysis of the surface layers of lithium deposited at various current densities in $LiClO_4$/PC and using various amounts of HF, in order to investigate the effect of HF in electrolytes on the surface reaction of lithium during electrochemical deposition. The surface condition of lithium and the morphology of the lithium deposits are influenced by both the concentration of HF and the electrodeposition current. The first parameter for the electrodeposition of lithium is related to the chemical reaction rate of the lithium surface with HF and the second to the electrodeposition rate of lithium. These results suggest that surface modification is highly effective in suppressing lithium dendrite formation when the chemical reaction rate with HF is greater than the electrochemical deposition rate of lithium.

In the chapter 5, the condition of the surface film on lithium electrodeposited in various carbonate electrolytes containing HF was investigated in order to clarify the interfacial reaction and the electrodeposition process of lithium in carbonate electrolytes

in the presence of a small amount of HF. The surface composition and morphology of electrodeposited-lithium were strongly affected by the presence of HF in the carbonate electrolytes rather than the solvents or salts. Various basic lithium compounds in the surface film were converted into LiF through acid-base reactions with HF. These results suggested that the surface film on lithium and the morphology of lithium seem to be more sensitive to the minor component, HF, in the carbonate electrolytes. Moreover, the XPS analysis revealed that lithium electrodeposited in carbonate electrolytes containing HF was covered with a highly stable and ultrathin (20-50 Å) film consisting of a LiF/Li_2O bilayer. Based on these results, it can be concluded that such a stable thin surface film promotes the highly smooth deposition of lithium.

In Chapter 6, the dissolution-deposition cycle behavior of lithium metal electrodeposited in nonaqueous electrolyte containing HF was investigated. In the first deposition process, lithium particles were deposited with a smooth hemispherical shape on a Ni substrate electrode. After the first dissolution process, a residual film was observed on the entire surface of the Ni substrate. This residual film is partially derived from the surface film on the lithium particles. The residual film accumulated on the electrode during cycling. On the other hand, it was found that the coulombic efficiency of lithium during cycling was much improved by the addition of HF. However, the formation of dendritic lithium was observed after the 45th cycle, suggesting that the accumulated thick residual film on the lithium surface disturbs the supply of HF to the lithium surface during the deposition process. The formation of this residual film is a serious problem for suppression of the dendritic lithium for long cycles in an electrolyte containing HF.

In Chapter 7, the surface film on lithium metal was analyzed using tapping mode atomic force microscopy (TMAFM) and surface potential microscopy (SPoM). The difference between the surface film on lithium deposited in nonaqueous electrolytes with and without HF was detected in order to discuss the relationship between the uniformity

of the surface film and the morphology of the lithium. The TMAFM/SPoM images indicate a much higher uniformity of the surface films on the lithium particles deposited in electrolyte containing HF. This result directly proved that the HF in an electrolyte has the effect of forming a highly uniform surface film on the electrodeposited lithium.

In Chapter 8, the electrochemical dissolution of lithium in an electrolyte containing HF was analyzed using an Electrochemical Quartz Crystal Microbalance (ECQCM) and *in-situ* Fluid Tapping Mode Atomic Force Microscopy (F-TMAFM). The mass change obtained by ECQCM showed that the electrodeposited lithium was electrochemically dissolved and accompanied by a secondary chemical reaction of lithium with electrolyte and trapping of the electrolyte on the lithium surface. On the other hand, the local dissolution of electrodeposited lithium is clearly observed in the F-TMAFM images. These results show that the chemical reaction of lithium with the electrolyte caused by the breakdown of the surface film at dissolution process is a serious problem for the reversibility of deposition/dissolution of lithium in an electrolyte containing HF.

In Chapter 9, a new additive $(C_2H_5)_4NF(HF)_4$ (TEAFHF) to nonaqueous electrolytes was investigated in order to modify the surface condition of lithium metal and clarify the role of H_2O in the electrolyte containing HF. The coulombic efficiency of lithium metal anodes during the discharge and charge cycles was examined using $LiCF_3SO_3$/PC containing various concentrations of HF, H_2O, and TEAFHF. The additions of TEAFHF were effective for suppressing the dendrite formation of lithium, leading to the high performance of the lithium anode. The appropriate and proper amount of H_2O in PC containing HF or TEAFHF promoted the long cycle life of the lithium anode, but the coulombic efficiency was only about 80%. On the other hand, in the case of a $LiClO_4$/DME based electrolyte, large lithium particles were deposited with the surface film consisting of the bilayered LiF/Li_2O. These lithium particles also exhibited the highest performance with a coulombic efficiency of 92.5%. The is due to excluding H_2O in the

electrolyte and the high stability of the solvent with lithium metal. As a result of the charge-discharge cycle test using a quasi practical battery cell, it was found that the coulombic efficiency of lithium metal anode is significantly improved to almost 100%. This result strongly indicates the possibility to realize a practical rechargeable lithium battery using lithium metal anode.

Chapter 1
Surface Condition of Lithium Metal after Immersion in Various Propylene Carbonate Electrolytes

1-1 Introduction

Electrodeposition of lithium metal is a very important in the charging process of rechargeable lithium metal batteries. Usually, the morphology of lithium deposited in nonaqueous electrolytes has been found to be in dendritic shape. The dendritic lithium are related to a battery failure phenomenon occurring during discharge and charge cycles[1]. This morphological phenomenon of lithium has been discussed, based on surface condition of lithium metal in nonaqueous electrolytes. In the "solid electrolyte interface (SEI) model", the physical and chemical conditions of surface film on lithium metal strongly affect the electrochemical behavior of lithium metal anodes[2-4]. Therefore, many studies have been extensively performed to analyze surface films on lithium metal in nonaqueous electrolytes using various spectroscopic methods[2,5-9].

On the other hand, lithium metal foils are usually used as the anode of the rechargeable lithium battery. Especially, as-received lithium foil is important as a practical lithium anode. It is originally covered with an surface film formed by chemical reactions of lithium metal with active gases (O_2, H_2O, CO_2, etc.) in the atmosphere during preparation or storage of lithium foils[4,7]. Such surface films are called "native film", consisting of various basic lithium compounds (Li_2CO_3, LiOH, and Li_2O). The native film can not be ignored in the sense of electrodeposition of lithium on the as-received lithium foil. However, the condition of the native film in the electrolyte was not still well-known. In this chapter, surface reaction of as-received lithium foil in propylene carbonate (PC) electrolytes was investigated with various methods. Moreover, the morphology of lithium electrodeposited in the PC electrolytes were observed with scanning electron microscopy.

1-1 Experimental

1-1-1 Immersion of as-received lithium foil in various electrolytes and electrodeposition of lithium

As-received lithium foils were used as samples for this study. The as-received lithium foil was obtained from Kyokuto metal company (Japan). This lithium foil (1cm × 2cm) was immersed in various nonaqueous electrolytes. Propylene carbonate containing 1.0 mol dm^{-3} $LiClO_4$ ($LiClO_4$/PC), $LiCF_3SO_3$ ($LiCF_3SO_3$/PC), and $LiPF_6$ ($LiPF_6$/PC) were used for the electrolytes (Mitsubishi Chemical Co., Japan). The water contents of the electrolytes were estimated to be less than 20 ppm by analysis with a Karl Fischer Moisture Titrator (MKC-210, Kyoto Denshi Kogyo Co., Japan). After the immersion, lithium metal was electrodeposited on the lithium foils in the identical electrolyte. The electrodeposition was carried out under galvanostatic condition using the standard three electrode-electrochemical cell (Figure 1-1). The counter electrode was lithium foil (8 cm^2) and the reference electrode was Li/Li^+. The current density was set at 0.2 mA cm^{-2}, and the amount of electric charge was 1.0 C cm^{-2}. All procedures were conducted in an argon dry box at room temperature (dew point < -90 °C).

1-1-2 X-ray photoelectron spectroscopic (XPS) analysis

The surface analysis of the lithium foils was carried out with XPS (ESCA 850s, Shimadzu, Japan) analysis under ultra-high vacuum condition (less than 5×10^{-7} Pa). The Mg Kα line (8kV, 30 mA) was used as an X-ray source. The minimum resolution of this equipment is 0.7 eV. The Ag 3d5/2 peak of a clean silver standard substrate was observed at 368.2 eV in our XPS equipment, and only a hydrocarbon gas was detected as a contaminant in the XPS equipment. Any peaks showing an adsorption of O_2, H_2O, or CO_2 were not observed for 1 hour. Since a hydrocarbon gas is less active, it does not prevent the XPS analysis on lithium. Before the XPS analysis of lithium sample, the sample was washed with pure dry PC (Mitsubishi Chemical Co., Japan) to remove electrolyte salts and dried under vacuum at 1×10^{-3} Pa for 1 h. The sample was then transferred from the

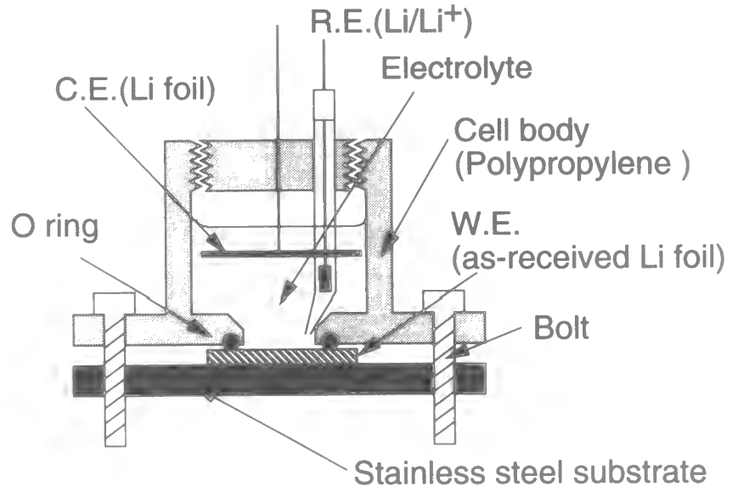

Figure 1-1 Schematic illustration of the standard three electrode-electrochemical cell for electrodeposition of lithium metal and impedance measurement.

argon dry box to a sub-chamber, which was filled with argon gas, connected to the XPS introduction chamber. A glass bottle with a ground stopper was used as a transfer vessel to avoid undesirable reaction with air during the transfer process. The schematic illustration of the sub-chamber of the XPS equipment is shown in Figure 1-2. The binding energy of the C1s peak at 285.0 eV was used as an internal standard to calibrate the binding energy scale. The binding energy for all lithium compounds were shown in Table A-1 (Appendix 1). The XPS depth analysis was also performed to obtain the information for three-dimensional structure of the condition of the surface film. The depth profiles can be obtained from the relative peak intensities in the XPS spectra for each element before and after the argon ion etching, and approximately indicates the relative molar ratio of each element in the surface film. They were calculated from the following equation [87].

$$I = I_0 / \sigma \qquad (1\text{-}1)$$

I, I_0, and σ mean the relative integrated intensity of XPS peak, the observed integrated intensity, and the cross section for ionization (relative sensitivity), respectively. The etching process was performed using an argon (ultra-high pure argon ; Kyoto Teisan Co., Japan) ion beam (accelerating voltage ; 2 keV, ion beam current ; 7~8 μA). Since the surface of

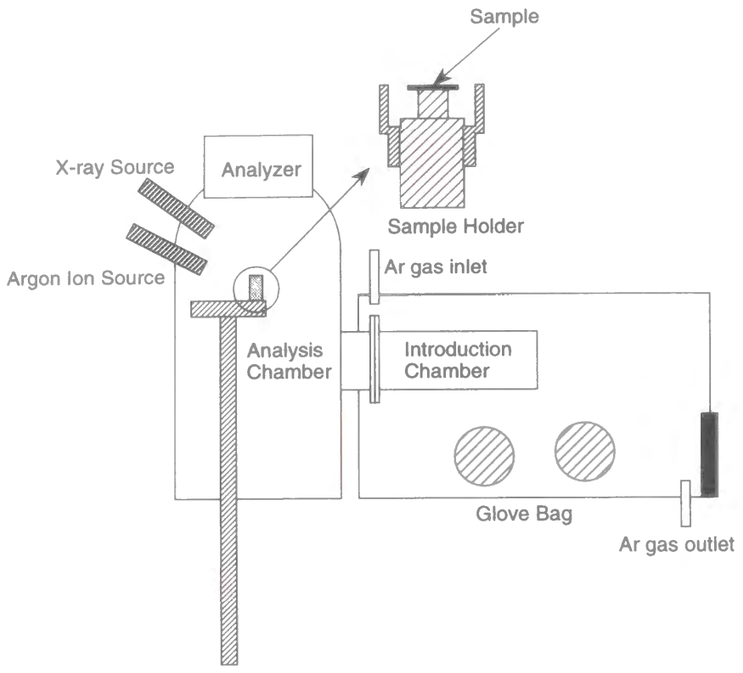

Figure 1-2 Schematic illustrations for the XPS analysis equipment and the sample holder.

samples are not ideally uniform and smooth, it was too difficult to measure the practical etching rate of various compounds from the experimental method. On the other hand, it has been reported in the literature [87] that the etching rate can be estimated by a calculation involving the atomic weight, material density, ion beam current density, and sputtering coefficient, ideally. In this study, the etching rate was estimated to be 5 Å min^{-1} by such a calculation according to reference [87]. Though the etching rate would be slightly changed by surface morphology and matrix effect, the etching rate obtained by the above calculation is good enough to estimate the thickness of the surface film on the lithium metal as a first rough approximation.

1-1-3 in-situ fourier transform infrared absorption spectroscopic (FTIR) analysis

An *in-situ* FTIR measurement was employed to observe the surface condition of the lithium foil during immersion in various PC electrolytes. The cell configuration for

in-situ FTIR measurement is shown in Figure 1-3. The external reflectance method was used in this study. A high reflectivity was necessary to obtain high-quality reflectance spectra, so that lithium foils were pressed to an IR window using a spring coil. The IR window was NaCl, the wavenumber resolution was 8 cm^{-1}, and the accumulation time was 150. In the cell, a thin layer (several μm) of the electrolyte was formed between the window and the lithium foil during the *in situ* FTIR measurement. The FTIR measurements were performed at 10 min intervals. In order to eliminate influences of strong absorption peaks of the solvent, substractively normalized interfacial FTIR spectroscopy (SNIFTIR) was adopted here [88]. The SNIFTIR (ΔR/R) spectrum at T_{i+1} was calculated according to the following equation (1-2).

$$\frac{\Delta R}{R} = \frac{R_{i+1} - R_i}{R_i} \qquad (1\text{-}2)$$

These procedures were repeated with potential increments (T_{i+1}-T_i) of 10 min until the immersion time reached 240 min.

1-1-4 Scanning electron microscopic (SEM) observation

The morphology of the electrodeposited lithium on the lithium foil was observed with a scanning electron microscope (SEM ; JEM-25D, JEOL, Japan). After the electrodeposition, the lithium foils were washed with the pure PC to remove electrolyte salts. The sample was transferred to the SEM in the same way as that used for the XPS analysis.

1-1-5 Electrochemical impedance spectroscopic (EIS) analysis

The resistance of the surface film on the lithium metal foils during immersion in the electrolytes was analyzed by an impedance measurement system (1250A Solartron, UK). The impedance measurement was performed at open circuit potential using the same electrochemical cell as that used for the electrodeposition. The amplitude of the applied alternating potential was ±5 mV, and its frequency was swept from 50 kHz to 0.01

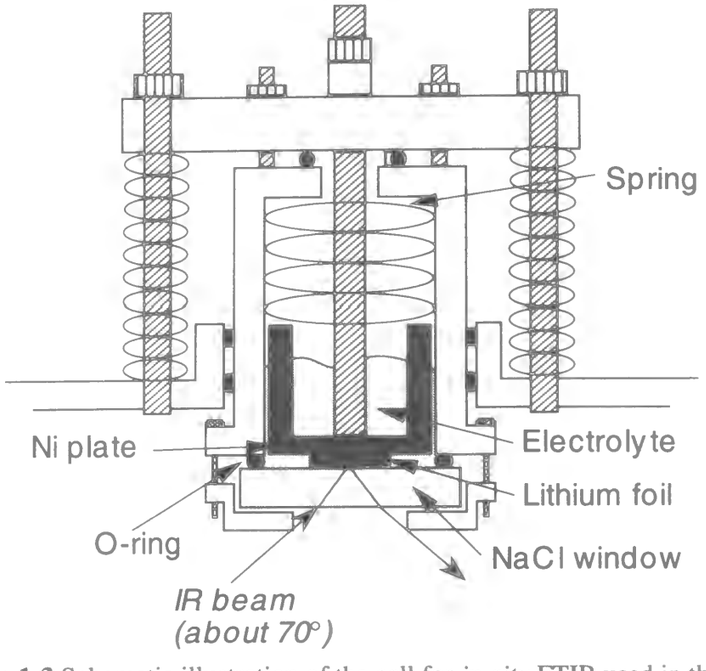

Figure 1-3 Schematic illustration of the cell for *in-situ* FTIR used in this study, IR window ; NaCl plate

Hz. The measurement was performed at 30±0.1°C under an argon atmosphere.

1-3 Results and Discussion

1-3-1 Changes in resistance of surface film on the lithium foil during immersion in electrolytes

The electrochemical behavior of the lithium electrode has been studied by many researchers using the electrochemical methods. It has been suggested that the impedance of the lithium foil electrode is related to the resistance and capacitance of the surface film formed on the lithium metal immersed in the electrolyte [43-48]. The interface of the lithium metal foil can be expressed as the equivalent parallel circuit consisting of the film resistance component and the film capacitance component. In the case of such equivalent circuit, a semicircle is observed in the Cole-Cole plots as shown at Figure 1-4. Figure 1-5 shows the Cole-Cole plots of the lithium electrode in various PC electrolytes. The diameter of

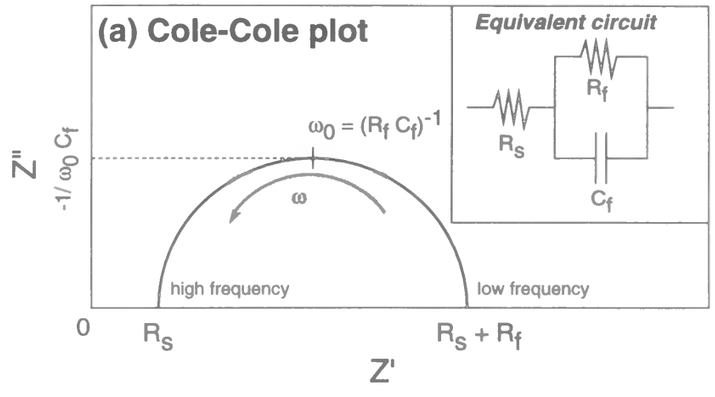

Figure 1-4 The typical Cole-Cole plots for lithium surface and its equivalent circuit, Rs: resistance of electrolyte (R_f : resistance of the surface film, C_f : capacitance of the surface film, ω_0 : characteristic angular frequency).

the semicircle in the Cole-Cole plots corresponds to the resistance of the surface film formed on the lithium metal. Figure 1-6 shows the resistance change of the lithium electrode during the immersion in PC containing various salts. The resistance change depended on the kind of salt. The resistance of the lithium electrode immersed in $LiClO_4$/PC slightly increased during the immersion for 100 h. The resistance of the lithium electrode immersed in $LiCF_3SO_3$/PC was almost constant for 96 h. The resistance of the lithium electrode immersed in $LiPF_6$/PC was high even just after the immersion in the electrolyte and then gradually increased. The resistance change of the lithium electrode in the PC electrolytes indicates that the condition of the surface film changes in the course of the immersion of the lithium foil in the electrolyte and the surface reaction of lithium is influenced by the kind of salt.

Next, in order to discuss the resistance change of the surface film from the view point of the reaction between the lithium surface and the electrolyte, first of all, the native film on the as-received lithium foil before the immersion in the electrolyte was analyzed with XPS.

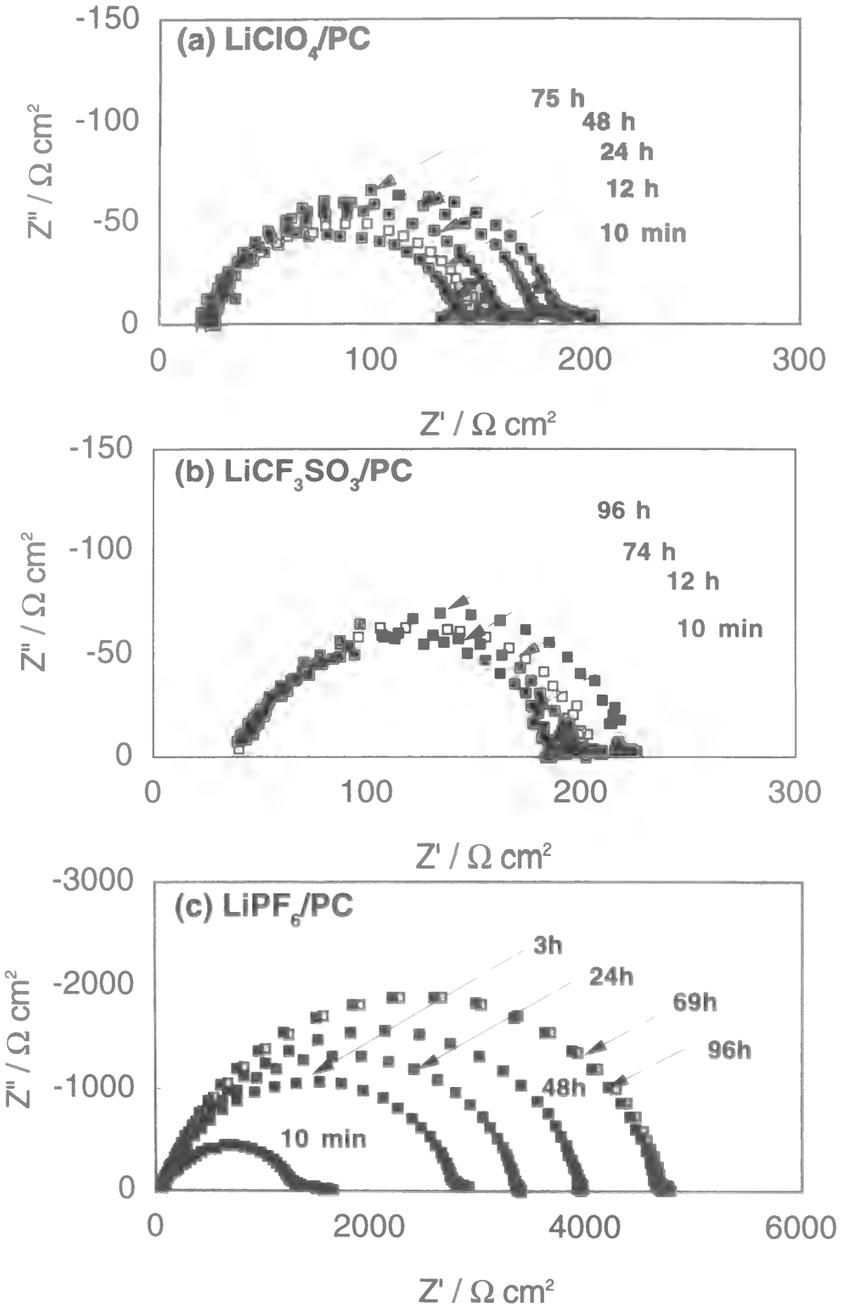

Figure 1-5 The Cole-Cole plots of the lithium electrode in PC containing 1.0 M (a) $LiClO_4$, (b) $LiCF_3SO_3$, and (c) $LiPF_6$ Time in figures indicates the immersion time.

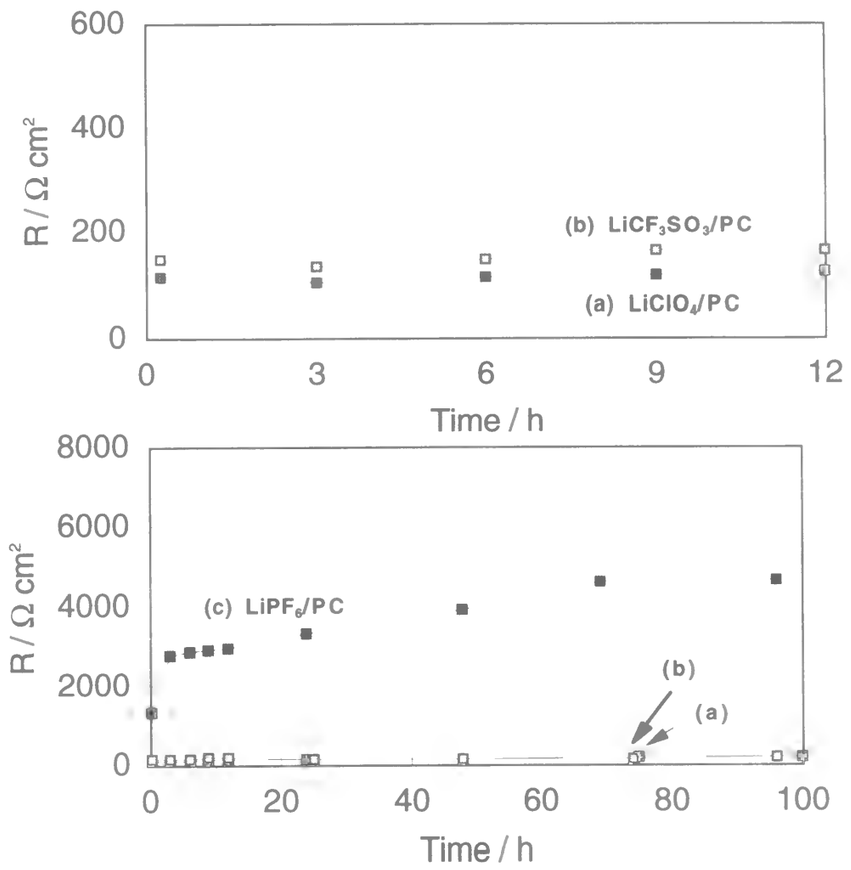

Figure 1-6 The resistance change of the surface film on the lithium electrode, obtained from the Cole- Cole plots in PC containing 1.0 M (a) $LiClO_4$, (b)$LiCF_3SO_3$, and (c) $LiPF_6$.

1-3-2 XPS analysis for as-received lithium foil

Figures 1-7 (a), (b), (c), and (d) show the XPS spectra of Li 1s, C 1s, O 1s, and their depth profile for the as-received lithium foil. These spectra were obtained after argon ion etching for various duration. A peak at 55.0 eV in the Li 1s spectra before the argon ion etching was attributed to Li_2CO_3, and another strong peak at 53.7 eV after the argon ion etching for 5 min was attributed to Li_2O. The peak intensity changes of Li_2O and Li_2CO_3 in the Li1s spectra show the presence of Li_2O under a Li_2CO_3 layer. The peak corresponding to lithium metal was clearly observed after the argon ion etching for 45

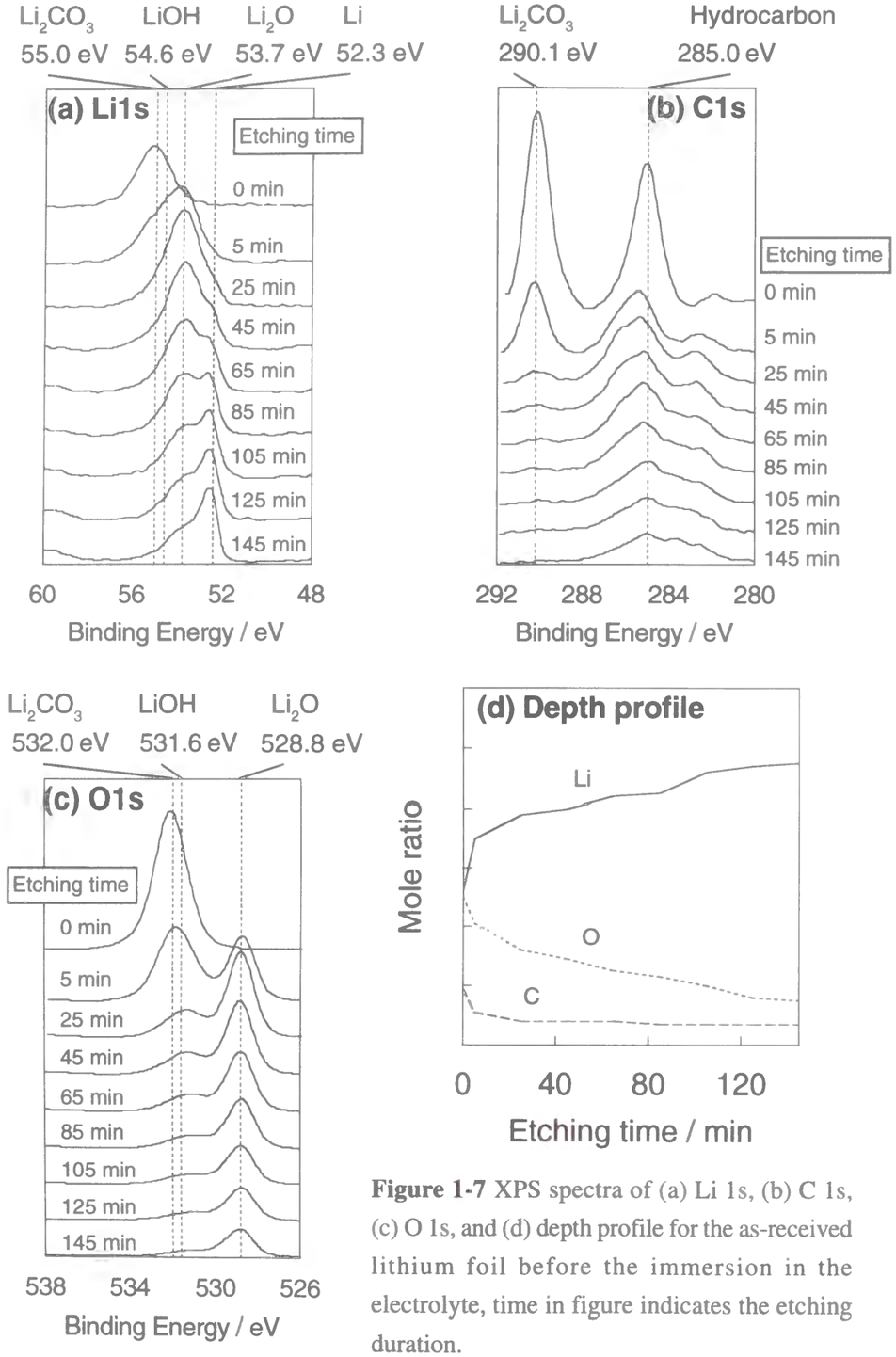

Figure 1-7 XPS spectra of (a) Li 1s, (b) C 1s, (c) O 1s, and (d) depth profile for the as-received lithium foil before the immersion in the electrolyte, time in figure indicates the etching duration.

min, and the pattern of Li 1s spectra was not changed by the following argon ion etching for 145 min. The peak of Li_2O was still observed after the argon ion etching for 145 min. This may be due to reactions of lithium metal with residual H_2O or O_2 in the XPS analysis chamber, or variation in the argon ion beam radiation of lithium metal due to the surface roughness (distribution of the argon ion beam etching). However, in preliminary experiment, it was already found that the oxidation of lithium metal did not significantly occur in our XPS equipment for 1 hour. Therefore, the observation of the Li_2O peak after the argon ion etching for 145 min is mainly due to the surface roughness of this lithium foil. A peak of 290.1 eV in the C1s spectra, attributed to Li_2CO_3, however, was diminished by the argon ion etching for 25 min. Therefore, it can be seen that Li_2CO_3 is present only at the outer part of the surface film on this lithium metal foil. A peak at 285.0 eV was attributed to hydrocarbon adsorbed on the lithium metal surface. Two peaks in the O 1s spectra before the argon ion etching were observed at 532.0 eV and 528.8 eV, corresponding to Li_2CO_3 and Li_2O, respectively. After the Ar ion etching for 25 min, the peak at 531.6 eV attributed to LiOH was observed. The peak of Li_2O was strongly observed after the argon ion etching for 5 min and its intensity gradually decreased during the argon ion etching after 25 min duration. From these XPS spectra, it is concluded that the native film on the lithium foil consists of the outer layer involving Li_2CO_3/LiOH and the inner layer including Li_2O (and the small amount of LiOH). From the peak corresponding to lithium metal in the Li1s spectra, the surface film seems to be almost removed by the argon ion etching for

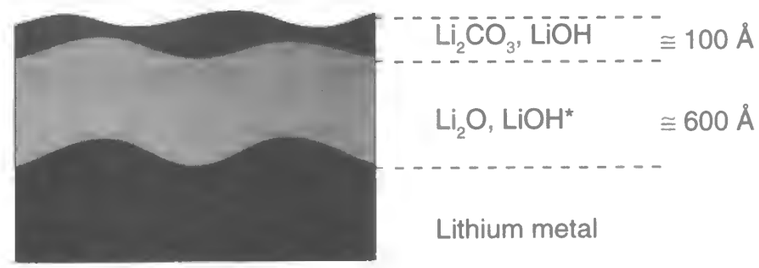

Figure 1-8 Schematic illustration of the native film formed on the as-received lithium.
*: minor species

145 min, indicating that the thickness of the surface film can be roughly estimated to be 700 Å (the thickness of the outer Li_2CO_3/LiOH layer is about 100 Å). From the XPS depth profiles, it is also confirmed that the amount of compounds involving oxygen such as Li_2CO_3 is larger at the outer layer in the surface film. The schematic illustration of the condition of the native film was shown in Figure 1-8.

1-3-3 XPS analysis of the lithium foil after immersion in various electrolytes

When the lithium foil is immersed in the PC electrolyte, the lithium surface may reacts with solvent, salt, and some impurities in electrolyte. Such reactions can be examined by the surface analysis for lithium immersed in electrolyte. Figure 1-9 shows the Li1s spectra for the lithium foil after the immersion in electrolyte for 72 h. For $LiClO_4$/PC and $LiCF_3SO_3$/PC, the peaks corresponding to LiOH and Li_2CO_3 were observed in the outer part of the surface film formed on the lithium metal. Moreover, the presence of Li_2O in the inner part of the film was deduced from these XPS spectra. These spectra were very similar to those for the native film formed on the lithium foil before the immersion in the electrolyte (Figure 1-7(a)). In these two electrolytes, the native film still remained after the immersion in the electrolyte for 72 h. The fact, that the change in the resistance of the lithium electrode in $LiClO_4$/PC and $LiCF_3SO_3$/PC were not so large, may be related to such a high stability of the native lithium in these electrolytes.

Figure 1-10 shows the C1s spectra for the lithium foil after the immersion of lithium in various PC electrolytes for 72 h. The peak corresponding to hydrocarbon was observed at 285.0 eV before the argon ion etching in all XPS spectra of C 1s. After the argon ion etching, this peak disappeared. Probably this peak is due to the adsorption of hydrocarbon existing in the XPS analysis chamber as an impurity. The strongly intensive peak attributed to Li_2CO_3 was observed at 290.1 eV in the C1s spectra for the lithium foil immersed in $LiClO_4$/PC or $LiCF_3SO_3$/PC. This peak also disappeared after the argon ion etching.

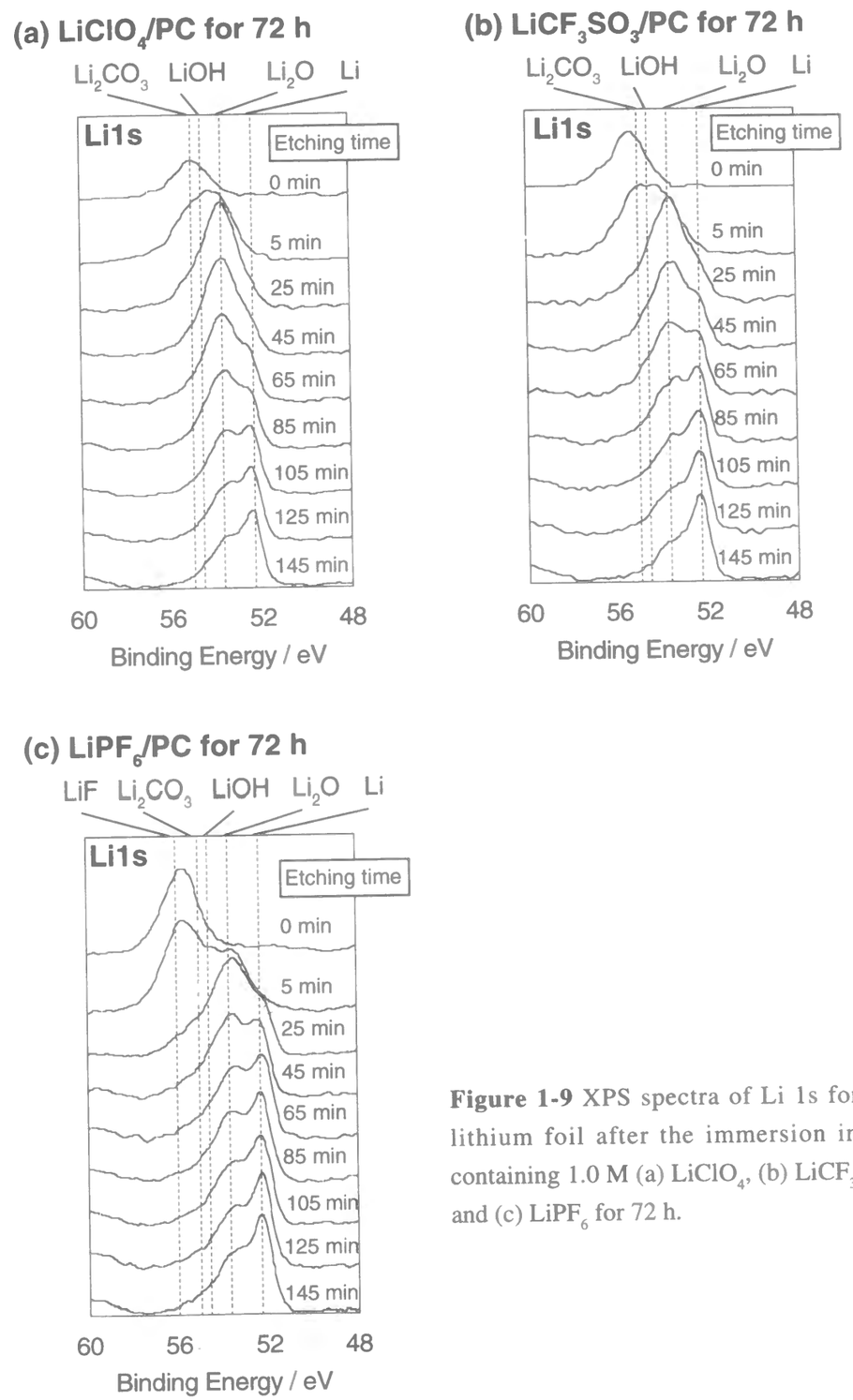

Figure 1-9 XPS spectra of Li 1s for the lithium foil after the immersion in PC containing 1.0 M (a) $LiClO_4$, (b) $LiCF_3SO_3$, and (c) $LiPF_6$ for 72 h.

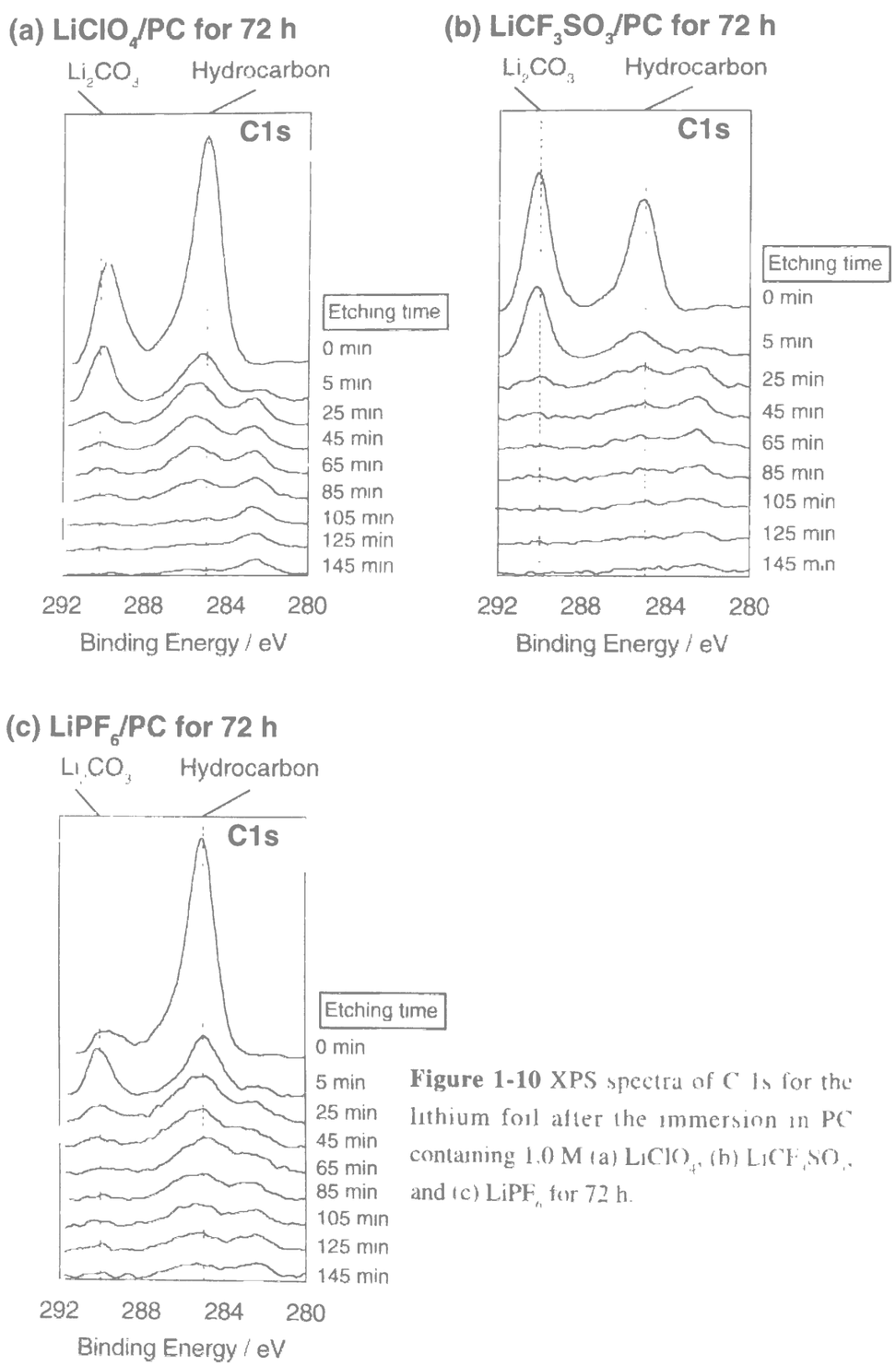

Figure 1-10 XPS spectra of C 1s for the lithium foil after the immersion in PC containing 1.0 M (a) $LiClO_4$, (b) $LiCF_3SO_3$, and (c) $LiPF_6$ for 72 h.

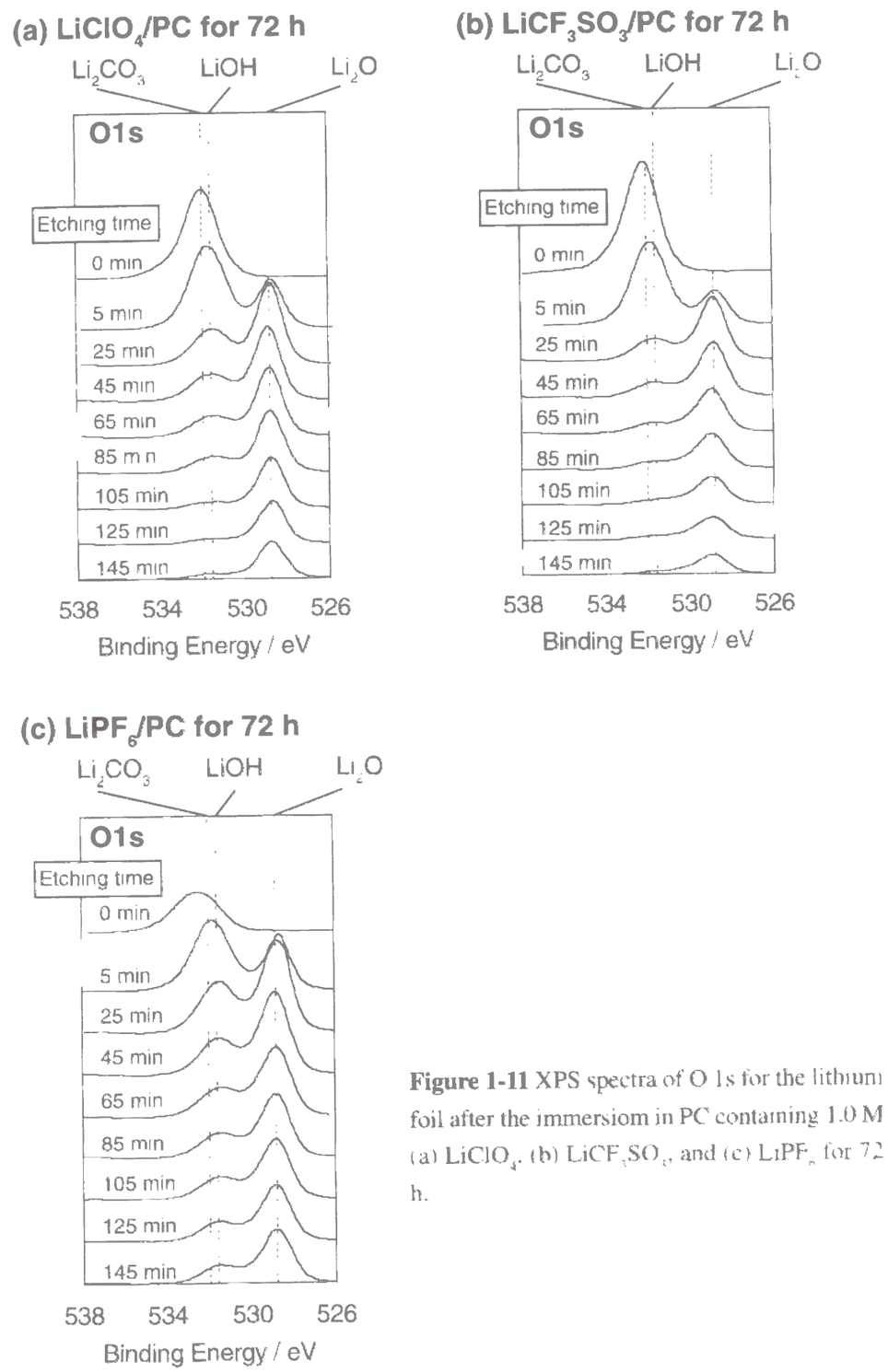

Figure 1-11 XPS spectra of O 1s for the lithium foil after the immersion in PC containing 1.0 M (a) $LiClO_4$, (b) $LiCF_3SO_3$, and (c) $LiPF_6$ for 72 h.

Figure 1-11 shows the O1s spectra for the lithium foil after the immersion of lithium in various electrolytes for 72 h. In the case of $LiClO_4$/PC or $LiCF_3SO_3$/PC, the peak attributed to LiOH or Li_2CO_3 were observed in the outer region of the surface film and that to Li_2O was observed in the inner part of the surface film. These O 1s spectra also shows that the native film was stable in $LiClO_4$/PC or $LiCF_3SO_3$/PC.

Figure 1-12 shows the C12p and F1s spectra for the lithium foil immersed in various electrolytes for 72 h. A peak at 199 eV in the Cl 2p spectra was assigned to LiCl. Peaks attributed to residual salt and LiF were observed in the F1s spectra. These results indicate that the small amount of LiCl or LiF was formed only in the upper region of the surface film after the immersion in $LiClO_4$/PC or $LiCF_3SO_3$/PC, respectively.

The XPS spectra for the lithium foil immersed in $LiPF_6$/PC were different from those for the native film. The formation of the large amount of LiF in the surface film was confirmed by the Li1s spectra for $LiPF_6$/PC, as shown in Fig. 1-9 (c). Moreover, from the C1s (Fig.1-10(c)) and O1s spectra (Fig.1-11(c)), it can be seen that LiOH and Li_2CO_3 decreased during the immersion of lithium in $LiPF_6$/PC. However, the LiF intensity in the Li1s spectra decreased after the argon etching for 5 min. From these results, it can be expected that the LiF layer was formed at only the outer part of the surface film. This phenomena can be confirmed by the F 1s spectra (Fig.1-12(c)). Moreover, in the Li 1s spectra for the lithium foil immersed in $LiPF_6$/PC, the shoulder peak corresponding to Li metal was observed after argon etching for 25 min. On the other hand, in the Li1s spectra for the native film (Fig.1-7(a)), the peak of Li metal was observed after the argon etching for 45 min. From the comparison of these Li1s spectra, it can be seen that the film formed on the lithium surface immersed in $LiPF_6$/PC is thinner than that for the native film.

Figure 1-13 shows the S2p and P2p spectra for the lithium foil after the immersion of lithium in various electrolytes. A weak peak assigned to $LiCF_3SO_3$ was observed in the S2p spectra. A peak attributed to $LiPF_6$ were observed in the P2p spectra, but the intensity was very weak. No peaks attributed to decomposition products of salts were observed in all spectra. From these results, it can be seen that the decomposition products of salts were

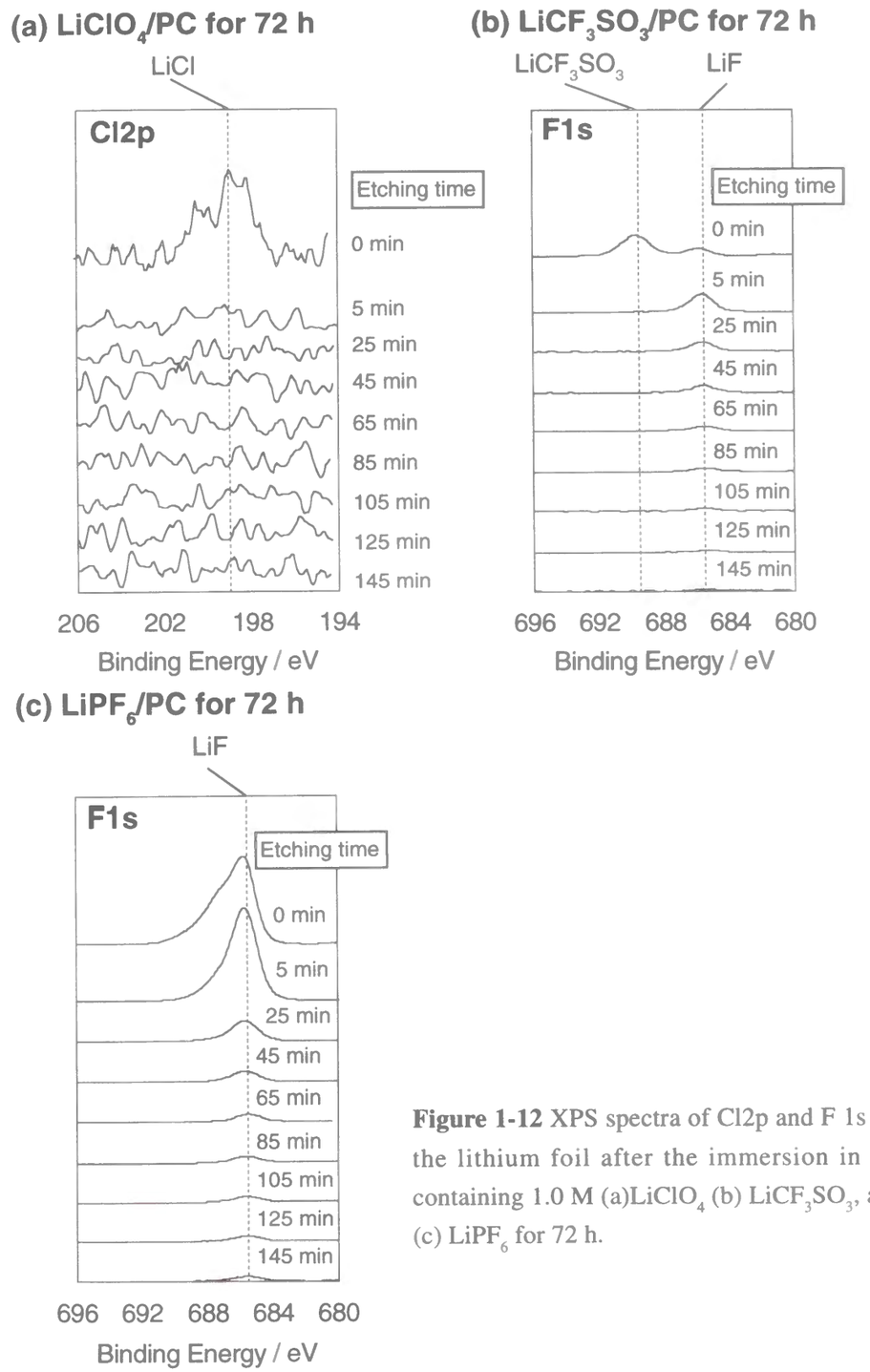

Figure 1-12 XPS spectra of Cl2p and F 1s for the lithium foil after the immersion in PC containing 1.0 M (a)$LiClO_4$ (b) $LiCF_3SO_3$, and (c) $LiPF_6$ for 72 h.

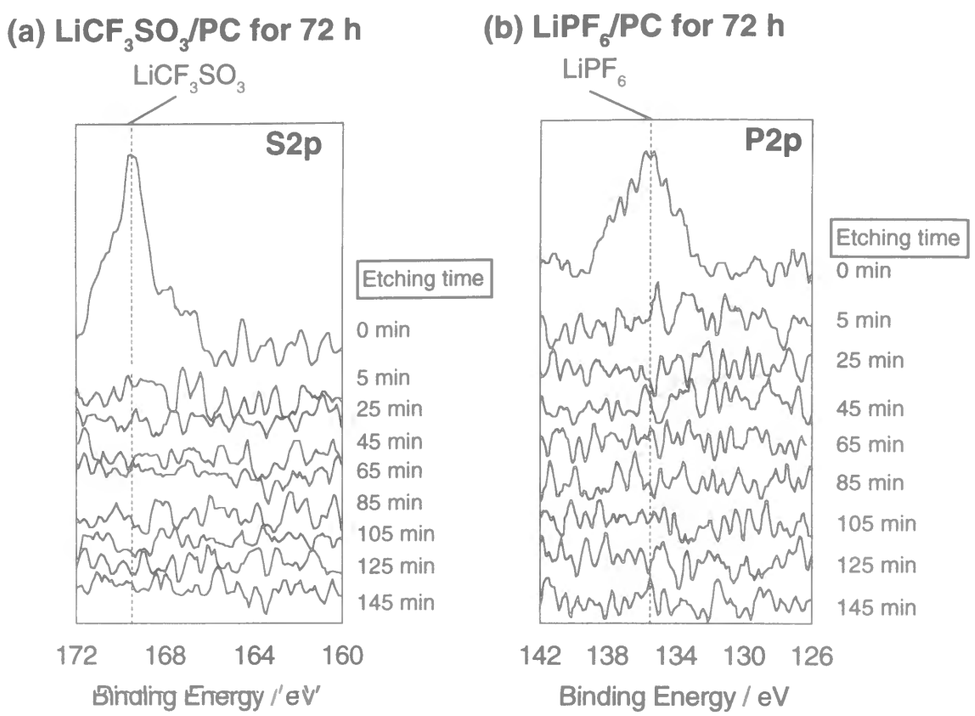

Figure 1-13 XPS spectra of S2p and P2p for the lithium foil after the immersion in PC containing 1.0 M (a) $LiCF_3SO_3$, and (b) $LiPF_6$ for 72h.

not present in the surface film immersed in $LiCF_3SO_3$/PC and $LiPF_6$/PC. This means that the formation of LiF in the film immersed in the PC electrolyte may not be due to the direct reaction between lithium and salt.

Figure 1-14 shows the depth profile of each element including in the surface film on the lithium foil immersed in various electrolytes. In the cases of $LiClO_4$/PC and $LiCF_3SO_3$/PC, the depth profiles were also very similar to that for the native film despite of the small Cl and F contents at the outer part of the surface film. Therefore, these depth profiles also show that the native film was stable in $LiClO_4$/PC and $LiCF_3SO_3$/PC electrolytes. In the case of $LiPF_6$/PC, the large amount of elemental F was observed at the outer part of the surface film. Moreover, the O and C content were smaller than F content at the outer part of the surface film. This indicates that Li_2CO_3, LiOH, and Li_2O in the

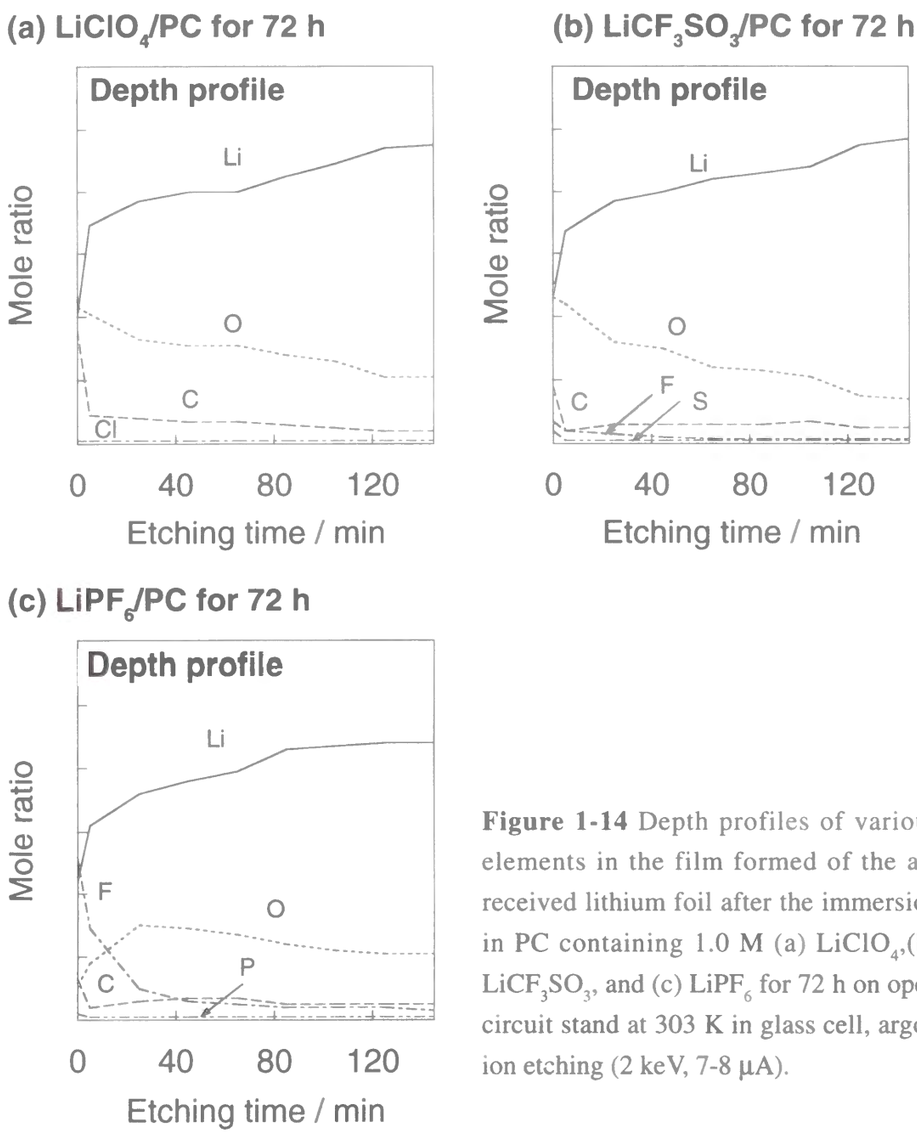

Figure 1-14 Depth profiles of various elements in the film formed of the as-received lithium foil after the immersion in PC containing 1.0 M (a) $LiClO_4$,(b) $LiCF_3SO_3$, and (c) $LiPF_6$ for 72 h on open circuit stand at 303 K in glass cell, argon ion etching (2 keV, 7-8 μA).

native film change to LiF by the immersion in $LiPF_6$/PC.

From the XPS analysis in this study, it can be said that one of the reactions of the lithium surface immersed in the PC electrolytes is the formation of lithium halide from LiOH, Li_2CO_3, or Li_2O which are the original components consisting the native film of lithium. Especially, in the case of $LiPF_6$/PC, the formation of lithium halide is seemed to be a main reaction at the lithium surface in the electrolytes. As the results of the impedance analysis for the lithium electrode in $LiPF_6$/PC, the resistance of the surface film became very large after the immersion in the electrolyte for 72 h. Because the ionic conductivity of LiF is higher than that of LiOH, Li_2CO_3, or Li_2O, the increasing resistance of the lithium electrode is related to the formation of the large amount of LiF in the surface film.

The possible reaction scheme for the formation of LiF in $LiPF_6$/PC may be written as follows.

(i) Decomposition of salt (shown in equation (1-3)) with residual H_2O in electrolyte and formation of HF as an impurity [90]:

$$LiMF_n + H_2O \rightarrow LiF + 2HF + MOF_{n-3} \quad (1\text{-}3)$$

It is known that hydrolysis of $LiPF_6$ leads to the formation of a relatively high concentration of HF (several tens ppm = several mmol dm^{-3}). Such hydrolysis may occur at the storage of the salt or at the dissolution of salt in the solvents containing residual moisture.

(ii) Reaction of lithium compounds consisting of the native film with HF:

$$LiOH + HF \rightarrow LiF \text{ (porous, weak)} + H_2O \quad (1\text{-}4)$$

$$Li_2O + 2HF \rightarrow 2LiF \text{ (porous, weak)} + H_2O \quad (1\text{-}5)$$

$$Li_2CO_3 + 2HF \rightarrow 2LiF \text{ (dense, tight)} + H_2CO_3 \quad (1\text{-}6)$$

These acid-base reactions indicate that a part of a native surface film, at least, is changed to a new surface film consisting of LiF. The reaction induced by acid-base reactions with HF causes volume changes in the surface films. The volume of lithium compounds per 1 mole of atomic lithium is shown in Table A-2 (Appendix 1). The volume of Li_2CO_3 (17.6 cm^3) or LiOH (16.4 cm^3) is much larger that of LiF (9.84 cm^3), and that of Li_2O (7.42 cm^3) is slightly smaller than that of LiF. Therefore, the volume of the surface film, involving a

Li_2CO_3/LiOH layer, decreases through the acid-base reactions with HF and the volume of the Li_2O layer does not change significantly. This means that a porous LiF surface film is formed from the Li_2CO_3/LiOH layer and a dense and rigid LiF surface film is produced from the Li_2O layer. These volume changes can explain the reason why the thickness of the surface film in $LiPF_6$/PC was less than that of the native film. The decrease in the surface film, namely, the etching of the surface film is due to a removal of the porous and weak LiF layer produced from the Li_2O layer. The etching reaction should be terminated by the formation of the LiF layer, produced from the Li_2O layer, because of the high rigidity and stability of the LiF layer. According to the results in the impedance analysis (Fig.1-6), the resistance of the surface film in $LiPF_6$/PC did not almost change after the immersion for 69 h. This result supports the termination of the acid-base reaction for the native film.

The possible schematic illustration of the surface film formed on the lithium foil immersed in various electrolytes were shown in Figure 1-15.

1-3-4 in-situ FTIR analysis for as-received lithium foil during immersion in electrolytes

According to the results of FTIR analysis by D. Aurbach's group, it has been reported that lithium alkyl carbonate is formed by the chemical reaction of propylene carbonate with lithium metal [22,24]. Therefore, it can be expected that such organic compounds is present in the surface film of lithium if the direct reaction of lithium metal with PC proceed by the immersion of the lithium foil in the PC electrolytes. Figure 1-16 and Figure 1-17 were the SNIFTIR spectra for the as-received lithium foil during the immersion in various electrolytes. In the SNIFTIR spectra, upward peaks correspond to disappearance of some compounds and downward peaks indicates an increase or a formation of some chemical species. In all spectra, downward or upward peak was observed at 2340 cm^{-1}. This peak is assigned to CO_2 in the dry air flowing in the FTIR measurement system. The broad downward peaks around 3500 cm^{-1} and 1400 ~ 1700 cm^{-1} were also observed at initial period of the immersion. These peaks can indicate that moisture in the FTIR

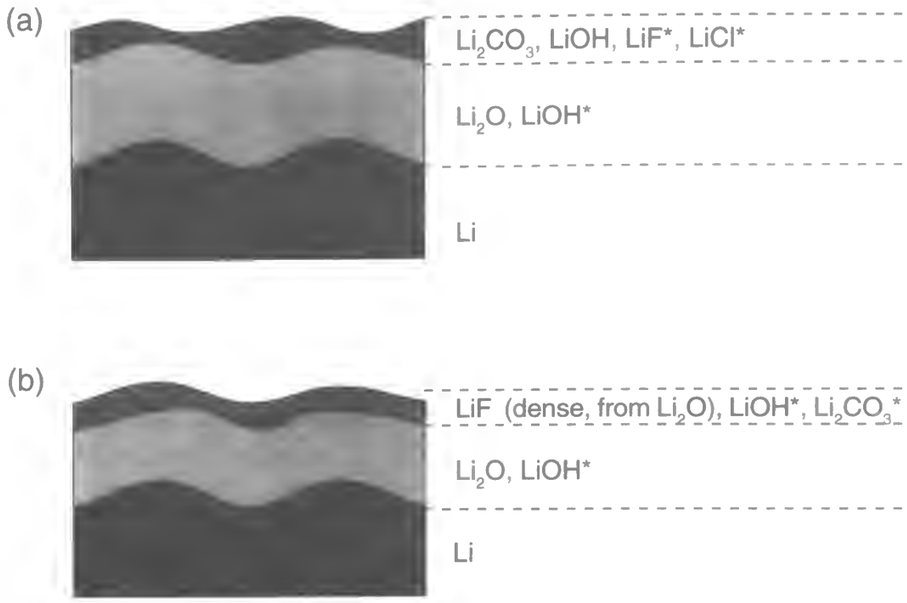

Figure 1-15 Schematic illustrations for the lithium surface immersed in PC containing 1.0 M (a) $LiClO_4$ or $LiCF_3SO_3$, and (b) $LiPF_6$. *: minor species

system was reduced during the measurement. Therefore, these peaks are not related to the surface reaction of the lithium foil. Any other peaks attributed to organic compounds or decomposition products of the salts were not observed in the spectra for all electrolytes. These results strongly show that lithium metal in the as-received lithium foil do not directly react the PC electrolytes through the contact (immersion) with the electrolyte. This is not in agreement with the results by D. Aurbach group [22,24,39]. The difference in the surface condition of lithium metal is derived from the difference in the initial condition of the lithium metal before experiment. D. Aurbach's group used the lithium metal treated with surface polishing in their reports, but the as-received lithium covered with the native film was employed in my study. The results obtained by FTIR analysis in the present study revealed that the native film on the as-received lithium foil effectively passive the surface of lithium metal from the PC electrolytes.

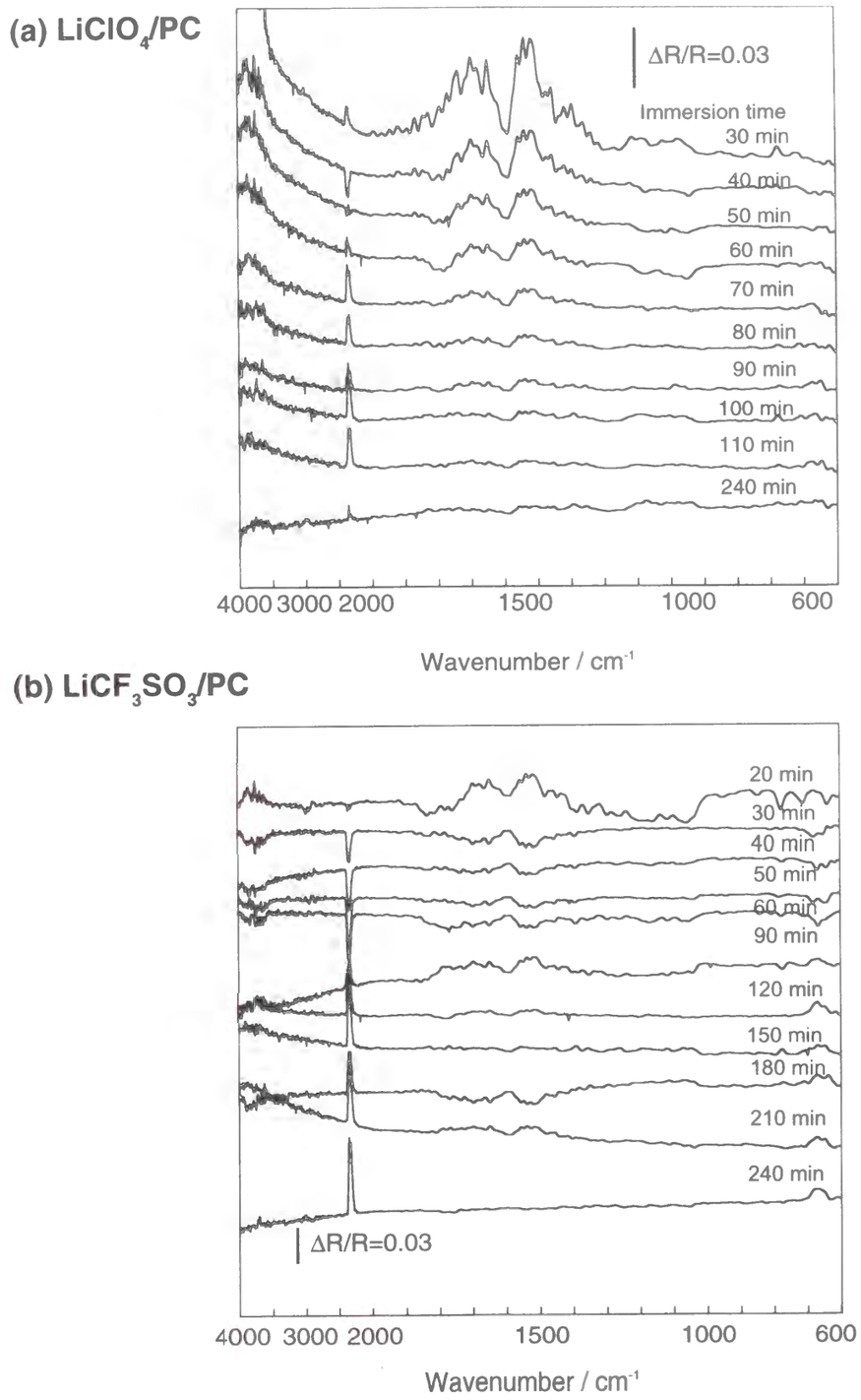

Figure 1-16 SNIFTIR spectra for the as-received lithium foil during the immersion in PC containing 1.0 M (a) $LiClO_4$ and (b) $LiCF_3SO_3$.

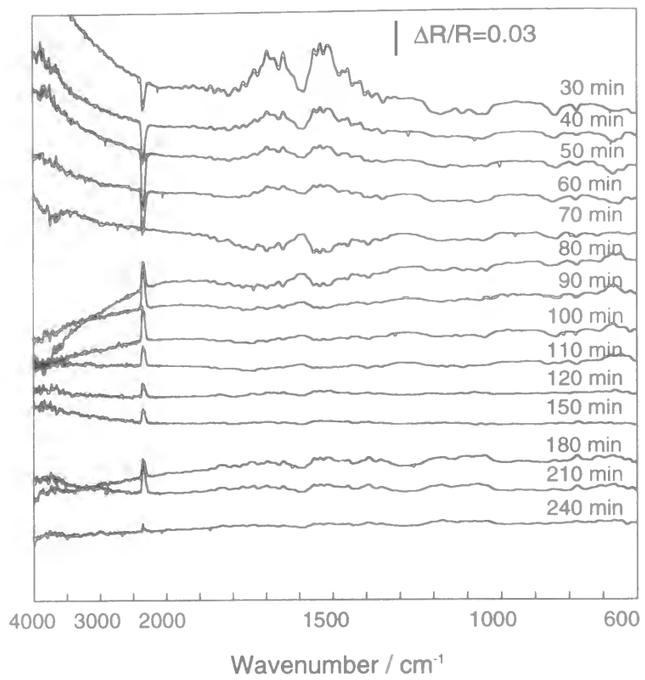

Figure 1-17 SNIFTIR spectra for the as-received lithium foil during the immersion in PC containing 1.0 M $LiPF_6$.

1-3-5 Electrodeposition of lithium on the lithium surface

Figure 1-18 shows the scanning electron micrographs of lithium deposited (0.2 mA cm^{-2}, 1.0 C cm^{-2}) on the lithium surface immersed in PC containing various salts for 72 h. The morphology of lithium deposited on the lithium surface depended on the kind of the salts. Figure 1-18 (a) and (b) show the scanning electron micrographs of lithium deposited in $LiClO_4$/PC and $LiCF_3SO_3$/PC. The dendrite formation of lithium was observed in the scanning electron micrographs of lithium deposited in $LiClO_4$/PC or $LiCF_3SO_3$/PC. The native film remained in the lithium surface immersed in these electrolytes. The chemical composition of the film formed on the lithium surface immersed in $LiCF_3SO_3$/PC is very similar to that immersed in $LiClO_4$/PC. These results show that the dendrite formation of lithium may be caused by the electrodeposition of lithium through the native film. Figure 1-18 (c) shows the electron micrograph of lithium deposited in $LiPF_6$/PC. The morphology

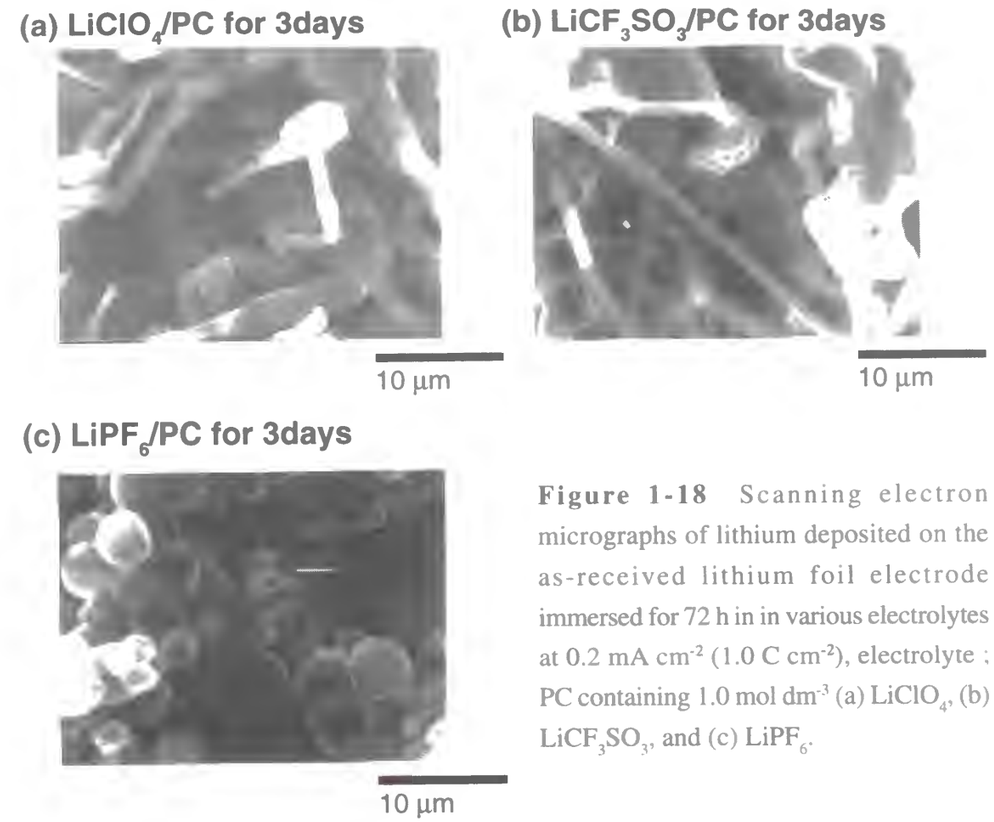

Figure 1-18 Scanning electron micrographs of lithium deposited on the as-received lithium foil electrode immersed for 72 h in in various electrolytes at 0.2 mA cm^{-2} (1.0 C cm^{-2}), electrolyte ; PC containing 1.0 mol dm^{-3} (a) $LiClO_4$, (b) $LiCF_3SO_3$, and (c) $LiPF_6$.

was different from dendrite. The semi-spherical lithium was deposited on the lithium surface. The surface of the lithium foil after the immersion in $LiPF_6$/PC for 72 h was covered with the thin and tight film which consists of LiF and Li_2O.

1-3-6 The dependence of morphology of lithium deposits on the immersion duration

In the previous section, it was found that the formation of dendritic lithium is suppressed when lithium was electrodeposited on the lithium foil after the immersion in $LiPF_6$/PC for 72 h. This may be due to the formation of the thin and tight film which consists of LiF and Li_2O through the acid-base reaction. Figure 1-19 shows the scanning electron micrographs of lithium deposited on the lithium surface immersed in $LiPF_6$/PC for 10 min. The dendritic lithium was observed on the lithium foil. This result indicates that the deposition of the dendritic lithium can not be suppressed when the chemical

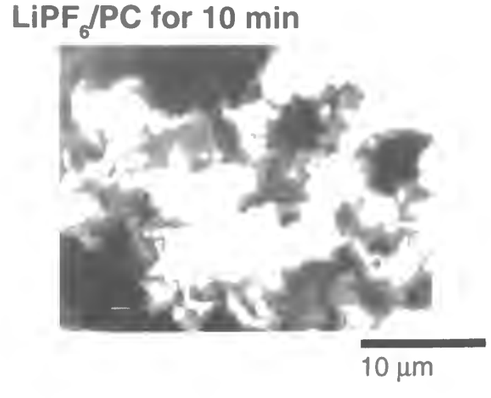

Figure 1-19 Scanning electron micrographs of lithium deposited on the as-received lithium foil electrode immersed for 10 min in in various electrolytes at 0.2 mA cm^{-2} (1.0 C cm^{-2}), electrolyte ; PC containing 1.0 M $LiPF_6$.

composition of the native film is not sufficiently changed with the immersion in $LiPF_6$/PC. Figure 1-20 shows the Li1s, C1s, O1s, and F1s spectra and the depth profile for the lithium foil after the immersion of lithium in $LiPF_6$/PC for 10 min. In the Li1s and F1s spectra, the peaks attributed to LiF were observed clearly. The depth profile exhibits that the LiF layer was formed at the upper region of the surface film by the immersion in the electrolyte. The conversion of Li_2CO_3 and LiOH, and Li_2O in the native film already proceeded by the immersion in $LiPF_6$/PC for 10 min. However, the amount of LiF in the surface film was less and the thickness of the surface film was not so different in the comparison with that of the native film. Therefore, it can be said that the surface film is not so well modified with HF in the electrolyte as to suppress the dendritic lithium when the immersion time in $LiPF_6$/PC electrolyte is short.

1-4 Conclusion

The results obtained in this chapter were summarized in the schematic illustration as shown in Figure 1-21. The as-received lithium surface covered with the native film, which consists of Li_2CO_3, Li_2O, and LiOH, reacts with a small amount of acid in the electrolyte to form lithium halide in the lithium surface during the immersion in the PC electrolytes. The formation of lithium halide strongly depended on the kind of salt. The native film in PC containing 1.0 mol dm^{-3} $LiClO_4$ or $LiCF_3SO_3$ was more stable than that in PC containing 1.0 mol dm^{-3} $LiPF_6$. This result may be due to the difference in the

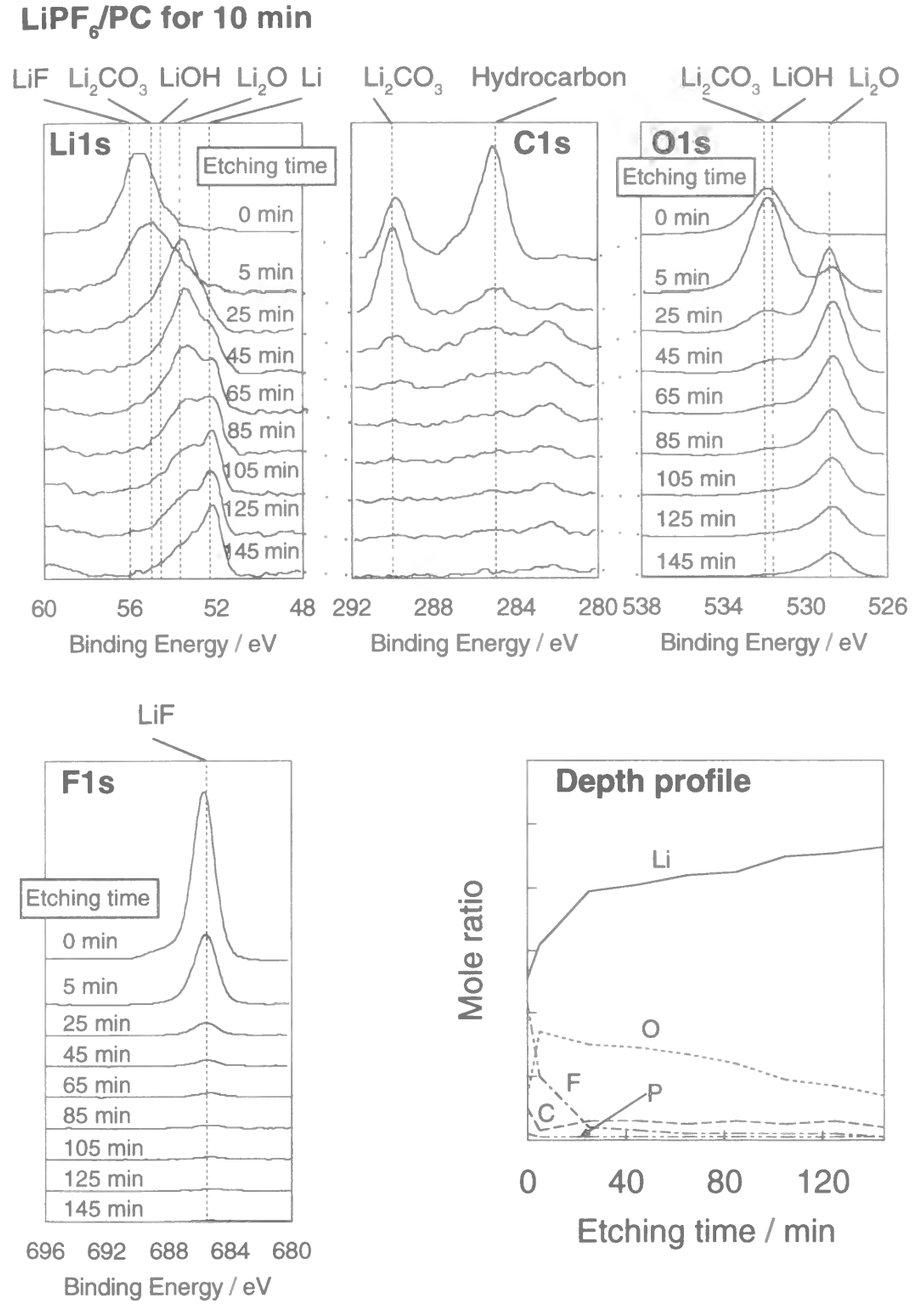

Figure 1-20 XPS spectra of Li1s, C1s, O1s, and F1s and depth profile for the lithium foil after the immersion in PC containing 1.0 M $LiPF_6$ for 10 min.

stability of salts against hydrolysis. Moreover, the film formed on the lithium surface immersed in the PC containing 1.0 mol dm^{-3} $LiPF_6$ was more tight and thinner than those immersed in any other electrolytes. The morphology of lithium deposited on such a peculiar surface of lithium was not dendrite.

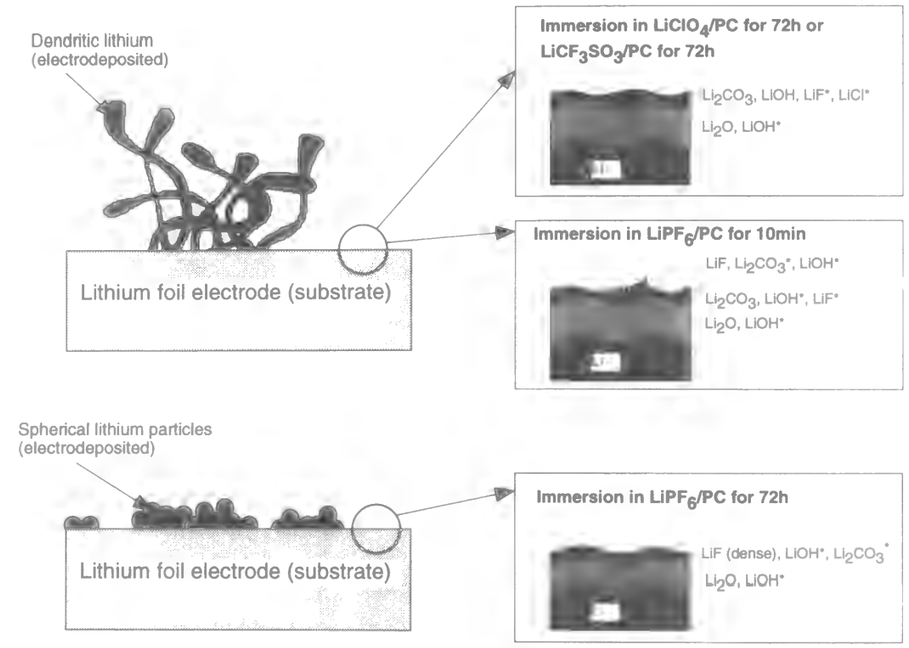

Figure 1-21 Schematic illustration of the relationship between the surface condition of the lithium foil electrode and the morphology of lithium electrodeposited on the lithium electrode. *; minor species

Chapter 2
Effect of Surface Modification Using Various Acids on Electrodeposition of Lithium

2-1 Introduction

In the previous chapter, it has been already found that the surface condition of a lithium foil changes with the immersion time in propylene carbonate containing $LiPF_6$, leading to the morphological change in the lithium particles electrodeposited on it. This result indicates that the morphology of lithium deposits is related to the surface condition of the lithium foil. The surface condition change of the lithium foil is caused by the acid-base reaction of the native film with HF which was present in electrolytes as impurities. It means that morphology control of lithium can be accomplished through the surface modification with a proper acid in nonaqueous solvent or electrolyte. Therefore, in this chapter, the surface modification of lithium was conducted by the acid-base reaction of the native film with various acids (HF, H_3PO_4, HCl, or HI) added in pure PC. The electrodeposition of lithium was performed in PC containing 1.0 mol dm^{-3} $LiClO_4$ or $LiPF_6$ using the modified lithium. The effects of this surface modification and the effect of electrolyte on the morphology of electrodeposited lithium were discussed.

2-2 Experimental

2-2-1 Surface Modification and Electrodeposition

As-received lithium foils (Kyokuto Co.) were used. The surface conditions of these lithium foils were analyzed by XPS in advance. The surface condition of the lithium foils used were same as described in the previous chapter. The as-received lithium foils were covered with the native film. Its outer part consisted of a mixture of Li_2CO_3 and LiOH, and the inner part consisted of Li_2O. The lithium foil was immersed in PC containing 0.2 mmol dm^{-3} HF, H_3PO_4, HI, or HCl for 3 days. PC was treated using molecular sieves (Wako pure Chemical Co.) for 2 days to remove water before use. After this dehydration,

the residual water in PC was less than 5 ppm, determined by Karl Fischer Moisture Titrator (MKC-210, Kyoto Denshi Kogyo Co.). PC containing acid was prepared from this pure PC and HF (46% by weight), H_3PO_4 (85% by weight), HCl (36% by weight), or HI (47% by weight) (Wako pure Chemical Co.). The water contents of PC solutions containing acids were estimated to be less than 20 ppm. After this treatment, these modified lithium foils were washed with pure PC (Mitsubishi Yuka Co.). The electrodeposition of lithium on the modified lithium foil (1 cm^2) was performed in PC containing 1.0 mol dm^{-3} $LiClO_4$ or $LiPF_6$ (Mitsubishi Yuka Co.) under galvanostatic conditions. The current density was 0.20 mA cm^{-2} and the duration was 80 min. The total quantity of electric charge was 0.96 C cm^{-2}. Lithium foil was used as counter (8 cm^2) and reference electrodes. These procedures were conducted on argon dry box (dew point < -90 °C) at room temperature.

2-2-2 XPS Analysis and SEM Observation

The characterization of the modified lithium surface was carried out using XPS (ESCA 850s, Shimadzu). The morphology of electrodeposited lithium was observed using Scanning Electron Microscopy (SEM ; JSM-25D, JEOL). The samples were washed with pure PC and dried under vacuum for one hour before being introduced to the XPS or SEM. The sample transfer and the analysis condition for the XPS or the SEM were conducted in the same way as described in the previous chapter.

2-3 Results and Discussion

2-3-1 The surface modification using HF or H_3PO_4 dissolved in propylene carbonate

Figure 2-1 presents the XPS spectra of P2p, O1s, C1s, and Li1s for the lithium surface after the immersion in PC containing 0.2 mmol dm^{-3} H_3PO_4 for 72 h. The upper spectrum was obtained before the argon ion etching, the middle and bottom spectra were obtained after the argon ion etching for 20 min and 40 min, respectively. These spectra correspond to the depth profile of each compound in the surface film. The peak observed at 133.6 eV in the XPS spectra of P2p is attributed to Li_3PO_4. The intensity of this peak

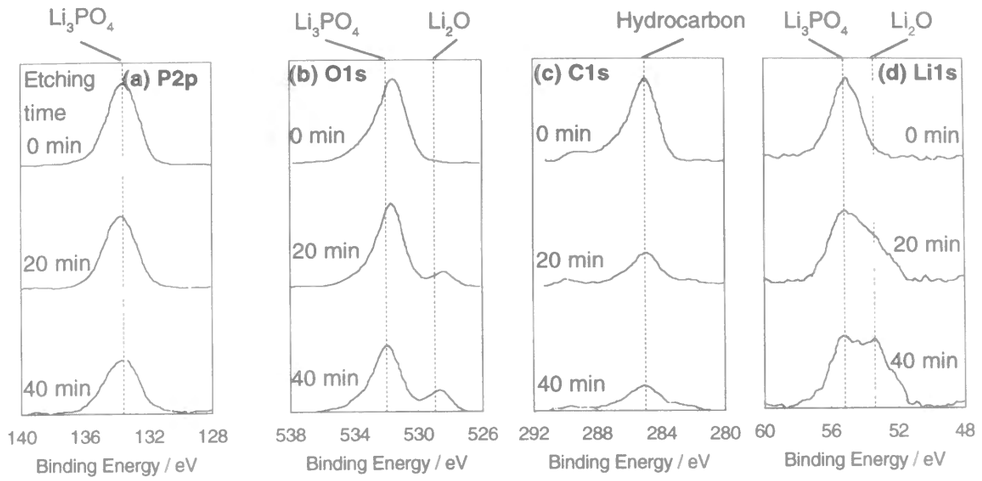

Figure 2-1 XPS spectra of (a) P2p, (b) O1s, (c) C1s, and (d) Li1s for the lithium foil after the immersion in the PC containing 0.2 mM H_3PO_4 for 72 h. Time indicate the duration of the argon ion etching.

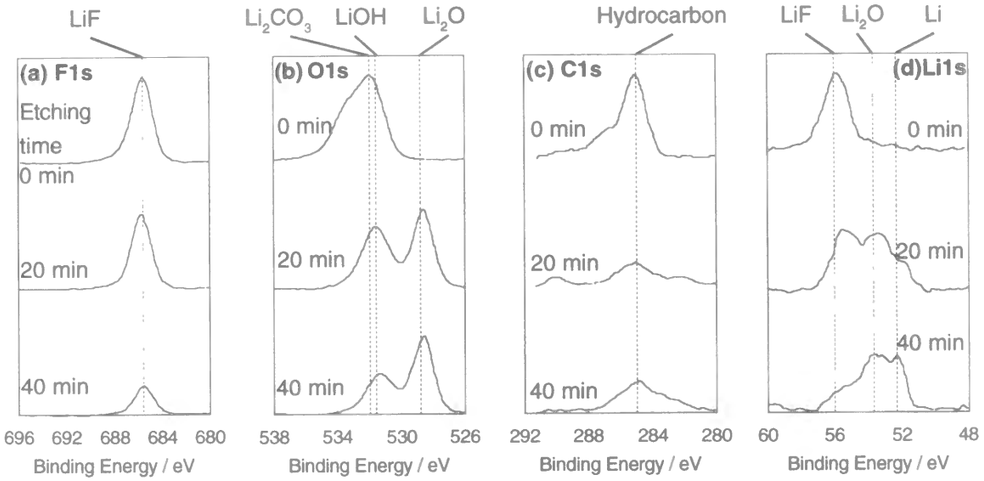

Figure 2-2 XPS spectra of (a) F1s, (b) O1s, (c) C1s, and (d) Li1s for the lithium foil after the immersion in the PC containing 0.2 mM HF for 72 h. Time indicate the duration of the argon ion etching.

was unchanged with argon ion etching. This means that a thick Li_3PO_4 layer is formed on the lithium surface. Peaks at 532.0 eV and 528.8 eV in the O1s spectra correspond to Li_3PO_4 and Li_2O, respectively. Peak corresponding to Li_2O was observed after the argon ion etching for 20 min. These spectra indicate that a layer of Li_2O is present under the

thick layer of Li_3PO_4. The peak at 285.0 eV in the C1s spectra is attributed to hydrocarbon, which is an impurity in the XPS measurement chamber. In the XPS spectra of Li1s, peak attributed to Li_3PO_4 was observed at 55.2 eV before and after the argon ion etching. Peak corresponding to Li_2O was observed at 53.7 eV after the argon ion etching for 20 min. These results were in good agreement with those obtained for the P2p and O1s spectra. Therefore, it can be concluded that the film formed on the lithium surface after the immersion in PC containing H_3PO_4 has a bilayer structure film consisting of the thick Li_3PO_4 and Li_2O.

Figure 2-2 shows the XPS spectra of F1s, O1s, C1s, and Li1s for the lithium surface after the immersion in PC containing 0.2 mol dm^{-3} HF for 3 days. The peak observed at 685.5 eV is attributed to LiF. This peak intensity remarkably decreased with the argon ion etching showing that LiF is formed at the outer part of the lithium surface film. In the XPS spectra of O1s the peak around 532 eV can be attributed to Li_2CO_3 or LiOH while the peak at 528.8 eV is attributed to Li_2O. These peak intensities were changed with the argon ion etching. This indicates that Li_2CO_3 or LiOH exists at the outer part of the surface film and Li_2O exists at the inner part of the film. The peak attributed to hydrocarbon was observed at 285.0 eV in the C1s spectra. The peak attributed to Li_2CO_3 (290.0 eV) could not be observed. This fact indicates that Li_2CO_3 is not present in the film. The peak attributed to LiF was observed at 56.0 eV in the XPS spectra of Li1s before the argon ion etching, while peaks corresponding to Li_2O and Li metal were also observed at 53.7 eV and 52.3 eV after the argon ion etching. The peak of Li metal was clearly observed after the argon ion etching for 20 min. The peak of Li metal was not observed in the XPS spectra for the as-received lithium used in this study even after the argon ion etching for 25 min. These results show that the surface film after the immersion in PC containing HF is thinner than the native film. From these results, it can be concluded that the lithium surface is modified by HF consists of a thin bilayer structure film consisting of LiF and Li_2O.

The formation of Li_3PO_4 and LiF may be explained by the chemical reaction of

lithium compounds (Li_2CO_3, LiOH, and Li_2O) consisting of the native film with acids (H_3PO_4, HF) in PC. These reactions can be described as follows.

$$Li_2CO_3 + 2/x\ H_xA \rightarrow 2\ Li_xA + H_2CO_3$$
$$LiOH + 1/x\ H_xA \rightarrow Li_xA + H_2O$$
$$Li_2O + 2/x\ H_xA \rightarrow 2Li_xA + H_2O$$
$$(H_xA\ ;\ H_3PO_4 \text{ or HF})$$

Moreover, the surface condition of lithium after the immersion in PC containing HF was very similar to that after the immersion in the PC containing 1.0 mol dm^{-3} $LiPF_6$ for 72 h, as discussed in the previous chapter. This fact proves that the surface state change of the as-received lithium in PC containing $LiPF_6$ is caused by the acid-base reaction of the native film with HF dissolved in the electrolyte as an impurity.

2-3-2 The surface modification using HCl or HI dissolved in PC

Figure 2-3 presents the XPS spectra of Cl2p, O1s, C1s, and Li1s for the lithium surface after the immersion in PC containing 0.2 mmol dm^{-3} HCl for 72 h. No peaks were observed in the XPS spectra of Cl2p neither before or after the argon ion etching. This indicates that compounds involving chlorine are not present in the lithium surface film. The peak at 532.0 eV in the XPS spectra of O1s before the argon ion etching corresponds to Li_2CO_3. Peaks attributed to LiOH and Li_2O were observed at 531.7 eV and 528.8 eV after the argon ion etching, respectively. The peak at 290.0 eV in the C1s spectra is attributed to Li_2CO_3. This peak was diminished with the argon ion etching. The peak corresponding to Li_2CO_3 was observed at 55.0 eV in the Li1s spectra before the argon ion etching. The peak attributed to Li_2O was observed at 53.7 eV after the argon ion etching. These XPS spectra show that the outer part of the surface film consists of Li_2CO_3 and LiOH, and that of the inner part consists of Li_2O.

Figure 2-4 shows the XPS spectra of I3d5/2, O1s, C1s, and Li1s for the lithium surface after the immersion in the PC containing 0.2 mmol dm^{-3} HI for 72 h. The peak attributed to LiI was observed at 629.8 eV in the I3d5/2 spectra. The intensity of this peak

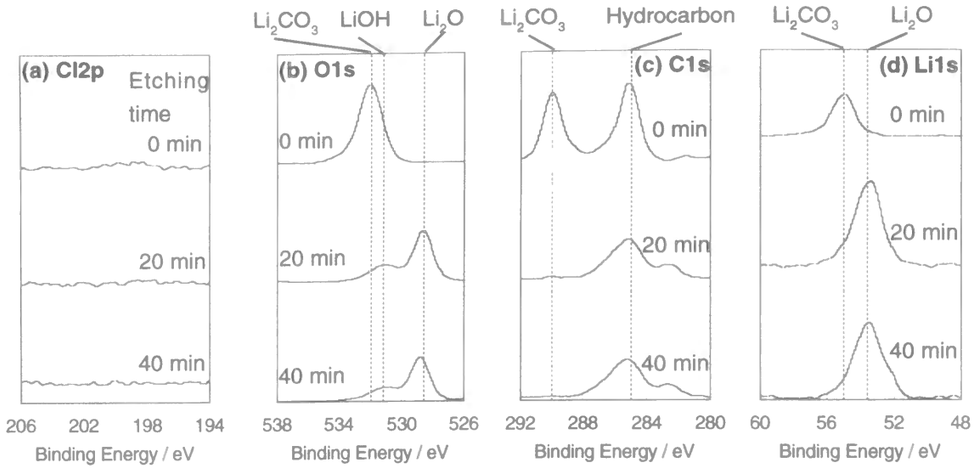

Figure 2-3 XPS spectra of (a) Cl2p, (b) O1s, (c) C1s, and (d) Li1s for the lithium foil after the immersion in the PC containing 0.2 mM HCl for 72 h. Time indicate the duration of the argon ion etching.

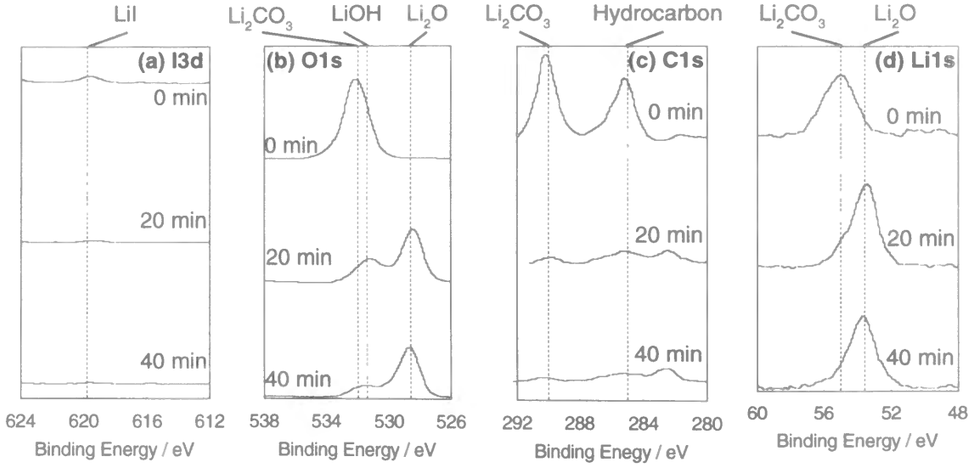

Figure 2-4 XPS spectra of (a) I3d5/2, (b) O1s, (c) C1s, and (d) Li1s for the lithium foil after the immersion in thePC containing 0.2 mM HI for 72 h. Time indicate the duration of the argon ion etching.

was much smaller than those of other elements. Probably, compounds containing iodine are at low concentration in the lithium surface film. The O1s, C1s, and Li1s spectra in Figure 2-4 were very similar to those in Figure 2-3. This result shows that the lithium surface after the immersion in PC containing HI is also covered with a bilayer structure

film consisting Li_2CO_3/LiOH and Li_2O.

From these XPS spectra, it can be said that the structure of the lithium surface after the immersion in PC containing HCl or HI resembles that of the native film. This result might be explained as follows. HCl and HI may not have high enough acidity in PC to react with Li_2CO_3, LiOH, and Li_2O, so that the native film remained on the lithium surface after the immersion in PC solutions containing these acids. Another possible explanation is the difference in solubility of lithium compounds in PC. Li_3PO_4 and LiF hardly dissolve in PC, while LiCl and LiI readily dissolve in PC. Therefore, the lithium surface after the immersion in the PC containing HCl or HI is still covered with insoluble Li_2CO_3, LiOH, and Li_2O. Probably, they are still remaining to react with acid, or produced by the chemical reaction of PC or residual water with lithium metal. The reactivity of acid can be guessed from proton affinity in a gas phase which corresponds to a basicity of ions in an aprotic nonaqueous solvent. F^- (1553 kJ mol^{-1}) has a larger proton affinity compared with those of Cl^- (1393 kJ mol^{-1}) or I^- (1314 kJ mol^{-1})[91]. From these values, it can be seen that HF is the weakest acid among three acids. HCl and HI should react with Li_2CO_3, LiOH, and Li_2O to form lithium halides on the lithium surface. Therefore the surface states of lithium after the immersion in PC containing HCl and HI may be due to the high solubility of LiCl and LiI. LiF is so insoluble in the PC that LiF remains on the surface film as a reaction product of HF and the native film. The LiF layer may be dense enough to suppress the further reaction of the native film.

2-3-3 XPS depth profile of the modified lithium surface

Figure 2-5 shows the depth profile for each element in the lithium surface film after the immersion in the PC containing (a) H_3PO_4, (b) HF, (c) HCl, or (d) HI. Figure 2-5 (a) shows that phosphorus uniformly distributes in the surface film after the immersion in PC containing H_3PO_4. The ratio among P, O, and Li in the film roughly corresponds to that for Li_3PO_4. Figure 2-5 (b) indicates that the amount of fluorine is concentrated on the outer part of the surface film after the immersion in PC containing HF for 72 h,

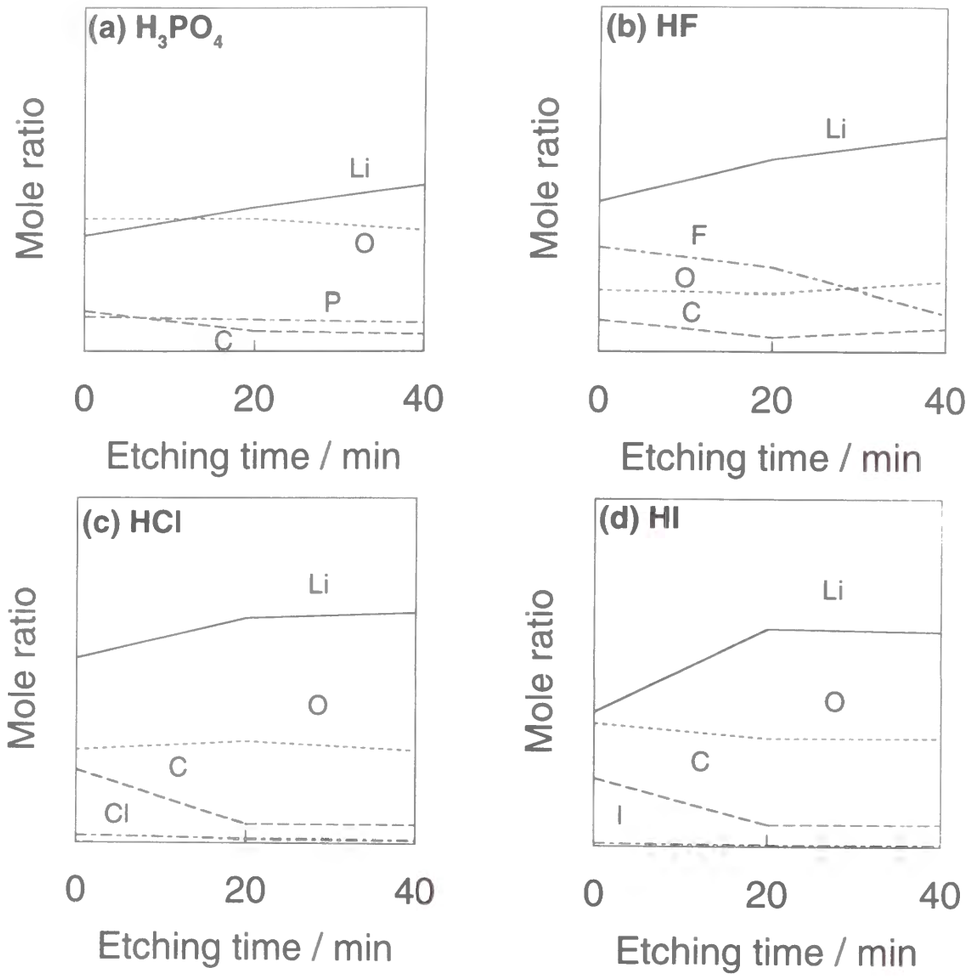

Figure 2-5 XPS depth profiles for each element in the surface film formed on the lithium foil after immersion in PC containing (a) 0.2 mM H_3PO_4, (b) 0.2 mM HF, (c) 0.2 mM HCl, and (d) 0.2 mM HI.

demonstrating that the main compound in the outer part of the film is LiF. On the other hand, it is clear that the amount of Cl element in the surface after the immersion in PC containing HCl for 72 h is much less than those of Li and O, as shown in Figure 2-5 (c). Additionally, the ratio of Li, O, and C in this profile resembled that in the native film. The depth profile in Figure 2-5 (d) was similar to that in Figure 2-5 (c), indicating that iodine is hardly present in the surface film after the immersion in PC containing HI for 72 h.

2-3-4 SEM observation of electrodeposited lithium

Figure 2-6 shows the scanning electron micrographs of lithium electrodeposited in PC containing 1.0 mol dm^{-3} $LiClO_4$ ($LiClO_4$/PC) on the lithium surface after immersion in PC containing H_3PO_4, HF, HCl or HI for 72 h. The typical dendritic form was observed for lithium electrodeposited on all lithium surfaces. A similar result was obtained for propylene carbonate containing 1.0 mol dm^{-3} $LiBF_4$ or $LiAsF_6$. Moreover the morphology of lithium deposited on the as-received lithium (without the surface modification) was dendritic (as shown in Figure 2-7) and independent of the kind of electrolyte. On the other hand lithium electrodeposited in PC containing 1.0 mol dm^{-3} $LiPF_6$ ($LiPF_6$/PC) after

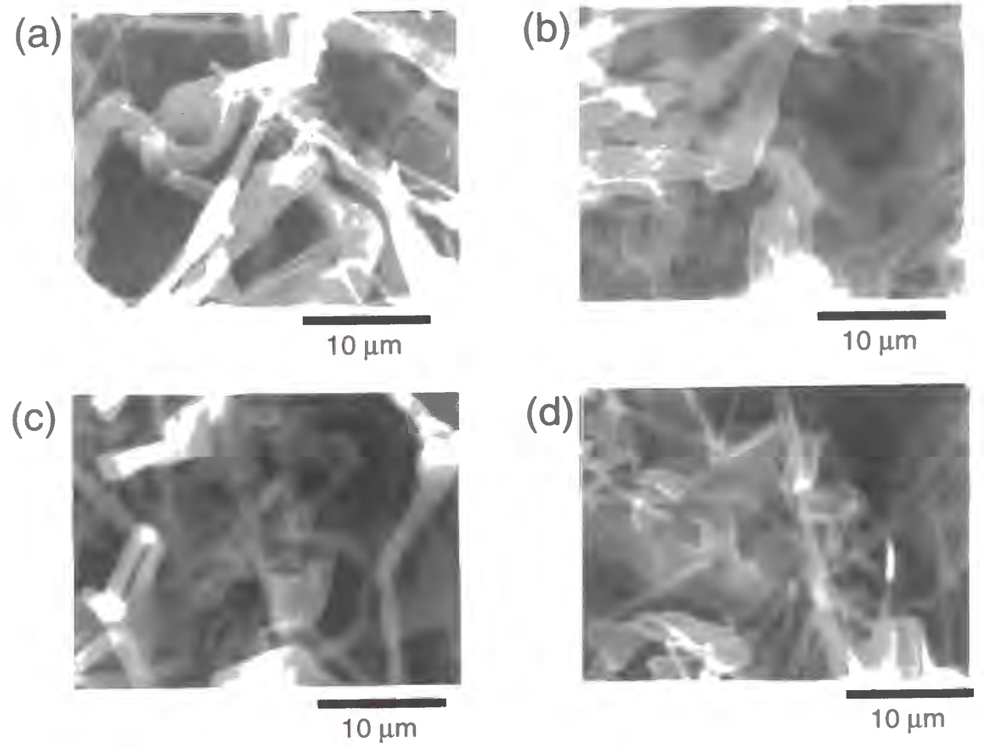

Figure 2-6 Scanning electron micrographs of lithium deposited on lithium foils after the immersion in the PC containing (a) 0.2 mM H_3PO_4, (b) 0.2 mM HF, (c) 0.2 mM HCl, or (d) 0.2 mM HI for 72 h (the electrodeposition current : 0.20 mA cm^{-2}, duration : 80 min, electrolyte : PC containing 1.0 M $LiClO_4$.).

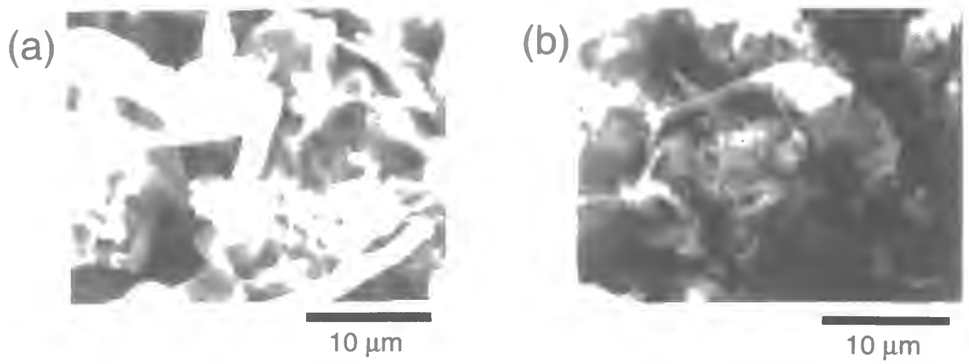

Figure 2-7 Scanning electron micrographs of lithium deposited in the PC containing (a) 1.0 M $LiClO_4$ or (b) 1.0 M $LiPF_6$ on the as-received lithium foils (the electrodeposition current : 0.20 mA cm^{-2}, duration : 80 min.).

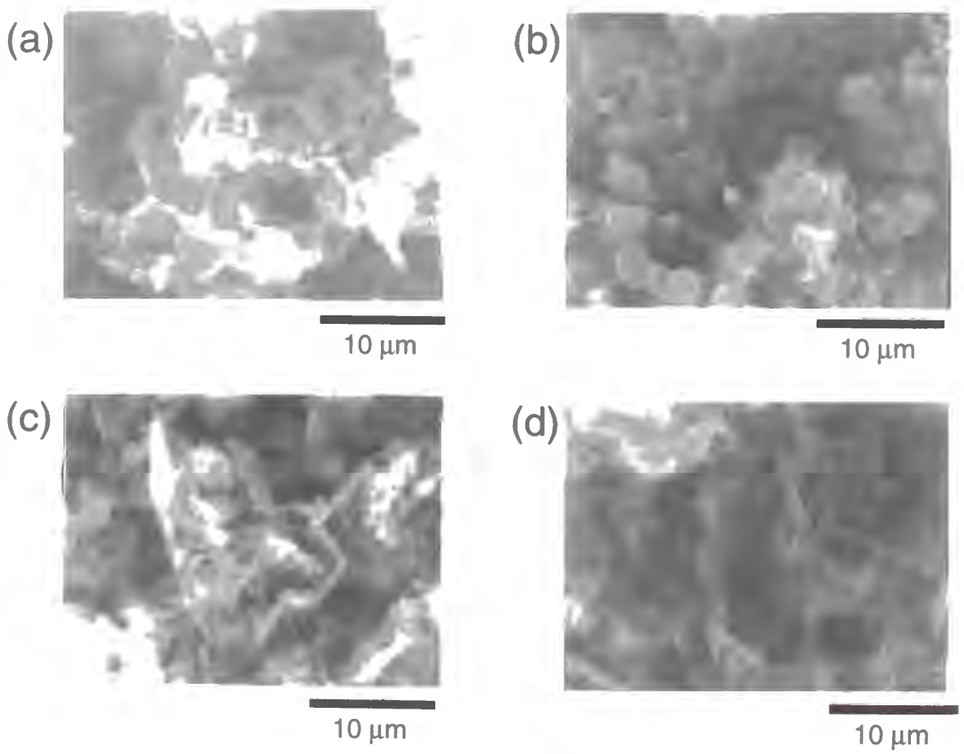

Figure 2-8 Scanning electron micrographs of lithium deposited on lithium foils after the immersion in the PC containing (a) 0.2 mM H_3PO_4, (b) 0.2 mM HF, (c) 0.2 mM HCl, or (d) 0.2 mM HI for 72 h (the electrodeposition current : 0.20 mA cm^{-2}, duration : 80 min, electrolyte : PC containing 1.0 M $LiPF_6$.).

immersion in PC containing HF for 72 h had a spherical morphology, as shown in Figure 2-8. However the morphology of lithium electrodeposited in $LiClO_4$/PC was not dependent on the surface modification. The dendrite was always observed. Thus, the surface treatment of lithium with HF is very effective for the suppression of the dendrite formation of lithium only when $LiPF_6$/PC is used as electrolyte for electrodeposition of lithium.

2-4 Conclusion

The surface condition of lithium was treated by the acid-base reaction of the native film of lithium with various acids dissolved in PC. HF produced the most favorable surface condition of lithium for the suppression of the dendritic form of lithium when using $LiPF_6$/PC was used as electrolyte. The surface film has a thin bilayer structure consisting of LiF and Li_2O. This indicates that the such surface film may enhance spherical lithium formation. However, when $LiClO_4$/PC was used, even though the lithium surface is modified by HF dissolved in PC, lithium dendrites were formed during electrodeposition. This results indicates that a appropriate electrolyte salt is necessary for the suppression of the dendritic lithium even when the surface modification with HF was performed. From this study, the following two points were clarified for the morphology control of lithium when the lithium foil with the native film was used as the substrate.

(1) as-received lithium foil needs to be modified by acid-base reaction of the native film with HF.

(2) Besides above surface modification of as-received lithium foil, a proper electrolyte salt must be selected.

Maybe, components in $LiPF_6$ /PC have a significant effect on the electrodeposition process of lithium. One possible component may be HF involved in the electrolyte. PF_6^- ion is hydrolysed to form HF in the electrolyte, as seen in the previous chapter. It can be easily predicted that a small amount of HF in the $LiPF_6$/PC also plays a significant role at lithium/ electrolyte interface during the electrodeposition. In order to confirm this, the relationship between the morphology and the surface condition of electrodeposited lithium has to be

examined under the condition which eliminates the influences of the native film.

Chapter 3
Morphology and Chemical Compositions of Surface Films of Lithium Deposited on a Ni Substrate in Nonaqueous Electrolytes

3-1 Introduction

In the previous chapter, it was seen that a small amount of HF in $LiPF_6$/PC operates on the lithium/electrolyte interface during the electrodeposition to suppress the formation of the dendritic lithium. Therefore, the surface condition of the electrodeposited lithium must be analyzed to understand the role of HF in sense of the influences on the morphology. However, when lithium foil electrodes is used as substrate electrode for the electrodeposition of lithium, the morphology of the electrodeposited lithium depends on the condition of both the surface film of the lithium foil and the surface film of the lithium electrodeposited. This case is thus not suitable for investigating the influence of the surface condition of lithium deposits on their morphology. On the other hand, in the case of electrodeposition of lithium on nonactive metal (e.g. nickel, copper) electrodes, SEI films are formed on the electrode by reductive decomposition of electrolyte before lithium bulk deposition [73,92]. Therefore, the electrodeposition of lithium on nonactive metal is not influenced by native film, and thus constitutes a suitable means for investigating for the relationship between the condition of SEI film formed on the electrodeposited lithium in nonaqueous electrolytes and the morphology of deposits. Therefore, in this chapter, an electrochemical deposition of lithium on Ni substrates was performed in propylene carbonate containing various salts.

3-2 Experimental

A Ni substrate was obtained from Nilaco Company, which was 7 mm × 10 mm. Before experiments, the Ni substrate was polished with fine alumina powders (0.05 μm) to obtain a mirror surface and then was washed with water and acetone. Lithium was electrodeposited on the Ni substrate under galvanostatic condition using the standard three electrode-electrochemical cell. The counter electrode was lithium foil (8 cm^2) and the

reference electrode was Li/Li^+. The current density was set at 1.0 mA cm^{-2}, and the amount of electric charge was 1.0 C cm^{-2}. Propylene carbonate containing 1.0 mol dm^{-3} $LiClO_4$ ($LiClO_4$/PC), $LiBF_4$ ($LiBF_4$/PC), $LiAsF_6$ ($LiAsF_6$/PC), and $LiPF_6$ ($LiPF_6$/PC) were used in this chapter (Mitsubishi Chemical Co., Japan). After the lithium deposition, the lithium deposited on the Ni substrate was washed with pure PC to remove electrolyte salts remaining on the electrode surface, and then it was dried under vacuum at ambient temperature for an hour to eliminate solvents. All procedures were conducted in an argon dry box at room temperature (dew point < -90 °C). The surface condition of the lithium electrodeposited on the Ni substrate was analyzed with XPS. The morphology of the lithium electrodeposited was observed with SEM. The sample transfer from the argon dry box to the XPS or the SEM equipment was conducted in the same way as described in the chapter 1. The analysis condition for the XPS or the SEM were same as that in the previous chapter.

3-3 Results and Discussion

Figure 3-1 shows the XPS spectra for lithium deposited on the Ni substrate in propylene carbonate containing 1.0 mol dm^{-3} $LiClO_4$ ($LiClO_4$/PC). Peaks at 55.0 eV in the XPS spectra of Li 1s correspond to Li_2CO_3. Peaks at 532.0 eV in the XPS spectra of O 1s correspond to Li_2CO_3. Peaks at 290.1 eV and at 289.0 eV in the XPS spectra of C 1s is assigned to Li_2CO_3 and lithium alkylcarbonate ($LiOCO_2R$), respectively. A peak at 285.0 eV in the XPS spectra of C 1s are assigned to a hydrocarbon. A hydrocarbon exists in the XPS analysis chamber, as a contaminant. The hydrocarbon adsorbed on samples in the XPS analysis chamber can be eliminated by the argon ion sputtering. However, after the etching for 1 min, the peak was still observed. Therefore, it can be seen that the hydrocarbon observed in the C 1s spectra is not only due to a hydrocarbon as a contaminant, but also is due to organic compounds involved in the surface film. The XPS spectra were changed by the following consecutive argon ion etching processes. A peak appearing at 528.8 eV in the XPS spectra of O 1s corresponds to Li_2O, showing the presence of Li_2O at the inner part of the surface film. In the XPS spectra of Li 1s, the shape and position of the peak

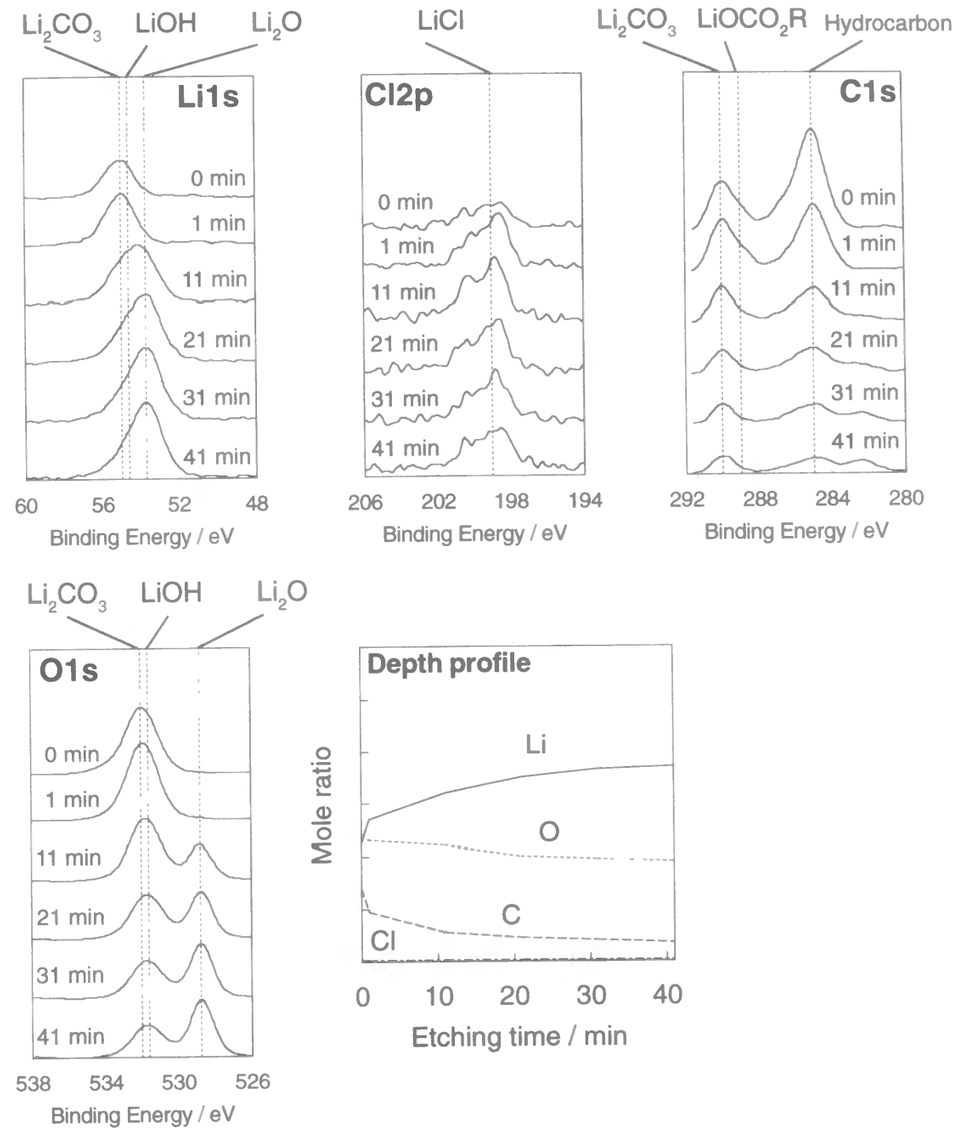

Figure 3-1 XPS spectra of Li 1s, Cl 2p, C 1s, and O 1s for lithium deposited on the Ni substrate in $LiClO_4$/PC at 1.0 mA cm^{-2} (1.0 C cm^{-2}), and depth profile of each element in the surface film. The time in each figure indicates the duration of the Ar ion etching.

were changed by the consecutive etching processes. Probably, the peak is a mixture of several peaks corresponding to LiOH, Li_2CO_3, and Li_2O even after the etching for 11 min, and then LiOH and Li_2CO_3 are decreased and Li_2O is increased by the argon ion etching. This chemical composition change was also confirmed from the XPS spectra of O 1s. Both Li 1s and O 1s spectra propose that the outer and inner parts of the surface film involve Li_2CO_3 and Li_2O as the main product of the surface film, respectively. In the XPS spectra of Cl 2p, a peak was observed at around 199 eV. This peak is assigned to LiCl. The formation of LiCl in the surface film can be explained by the chemical reaction of ClO_4^- ions and lithium or acid-base reactions between basic lithium compounds (LiOH, Li_2CO_3, and Li_2O) and HCl included in the electrolyte as an impurity. The depth profile for each element in the surface film can be calculated from the peak area and the cross-section for the ionization of each element. The amount of C element at the outer part of the surface film was larger than that at the inner part. Cl and O elements were observed in the entire region of the surface film and their quantities were uniform. The amount of Cl element was much smaller than those of C and O elements. The amount of O element at the inner part of the surface film was two times as large as that of C element. From these results, it can be seen that the lithium surface is covered with a layer consisting of Li_2CO_3, LiOH, Li_2O, and organic compounds. The surface film can be illustrated as shown in Figure 3-5 (a).

Figure 3-2 shows the XPS spectra for lithium deposited on the Ni substrate in propylene carbonate containing 1.0 mol dm^{-3} $LiAsF_6$ ($LiAsF_6$/PC). The spectra of Li 1s, C 1s, and O 1s were very similar to those for lithium deposited in $LiClO_4$/PC, so that it can be said that the chemical compositions of the surface film obtained in $LiAsF_6$/PC are very similar those of the surface film formed in $LiClO_4$/PC. The difference between two surface films was only the kind of lithium halides. In $LiAsF_6$/PC, the formation of LiF was confirmed from the XPS spectra of F 1s, while LiCl was formed in $LiClO_4$/PC. The formation of LiF can be understood by acid-base reactions between basic lithium compounds and HF or a reaction of lithium with AsF_6^- ions. When AsF_6^- ions are reduced with lithium,

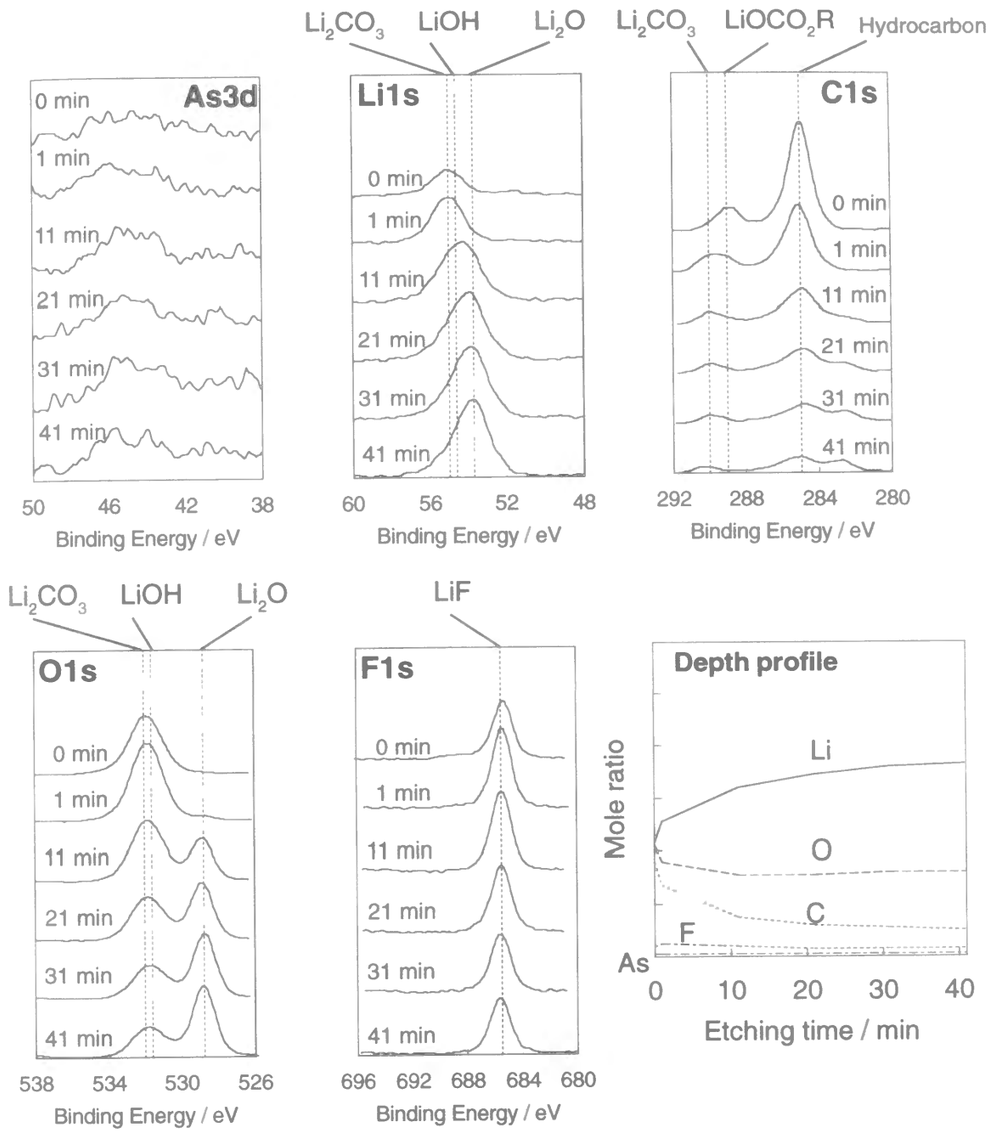

Figure 3-2 XPS spectra of As 3d, Li 1s, C 1s, O 1s, and F 1s for lithium deposited on the Ni substrate in $LiAsF_6$/PC at 1.0 mA cm^{-2} (1.0 C cm^{-2}), and depth profile of each element in the surface film. The time in each figure indicates the duration of the Ar ion etching.

As compounds in reduced state remains on lithium. However, As element was not observed in the XPS spectra. This means that LiF is mainly formed by the acid-base reaction. The depth profile for the surface film obtained in $LiAsF_6$/PC was very similar to that in Figure 3-1. The surface film can be illustrated as shown in Figure 3-5 (a).

Figure 3-3 shows the XPS spectra for lithium deposited on the Ni substrate in propylene carbonate containing 1.0 mol dm^{-3} $LiBF_4$ ($LiBF_4$/PC). There was no significant difference in the XPS spectra of Li 1s, C 1s, and O 1s, compared with those in Figure 3-2. The formation of LiF was confirmed from the XPS spectra of F 1s. The XPS spectra of B 1s show that reaction products from BF_4^- ions are not present in the surface film. Correspondingly, the depth profiles were also very similar to those in Figure 3-2. These results propose that the surface film formed in $LiBF_4$/PC is similar to that obtained in $LiAsF_6$/PC. Therefore, the schematic diagram for the surface film can be given by Figure 3-5 (a).

Figure 3-4 shows the XPS spectra of lithium deposited on the Ni substrate in propylene carbonate containing 1.0 mol dm^{-3} $LiPF_6$ ($LiPF_6$/PC). The XPS spectra of Li 1s was completely different from those observed for other PC electrolytes. Peaks were observed at 56.0 eV and 52.3 eV in the XPS spectra of Li 1s before and after the etching for 1 min. These peaks correspond to LiF and Li, respectively. While the peak intensity of LiF was decreased by the etching procedure, the peak intensity of Li was increased. The appearance of Li metal indicates that the surface film of lithium deposited in this electrolyte is much thinner than the surface films formed in other electrolytes. After the etching for 11 min, several overlapped broad peaks were observed in the binding energy region from 56 eV to 52 eV. After the etching for 21 min, a peak was observed at 53.7 eV. This peak is assigned to Li_2O. The XPS spectrum change of Li 1s suggests that LiF exists at the outer part of the surface as a main compound, and the inner part mainly consists of Li_2O. The presence of LiF was also confirmed from the XPS spectra of F 1s. A peak corresponding to LiF was observed at 685.5 eV and its intensity was decreased by the etching process. The formation of LiF is due to the chemical reaction of electrolyte salts with lithium metal

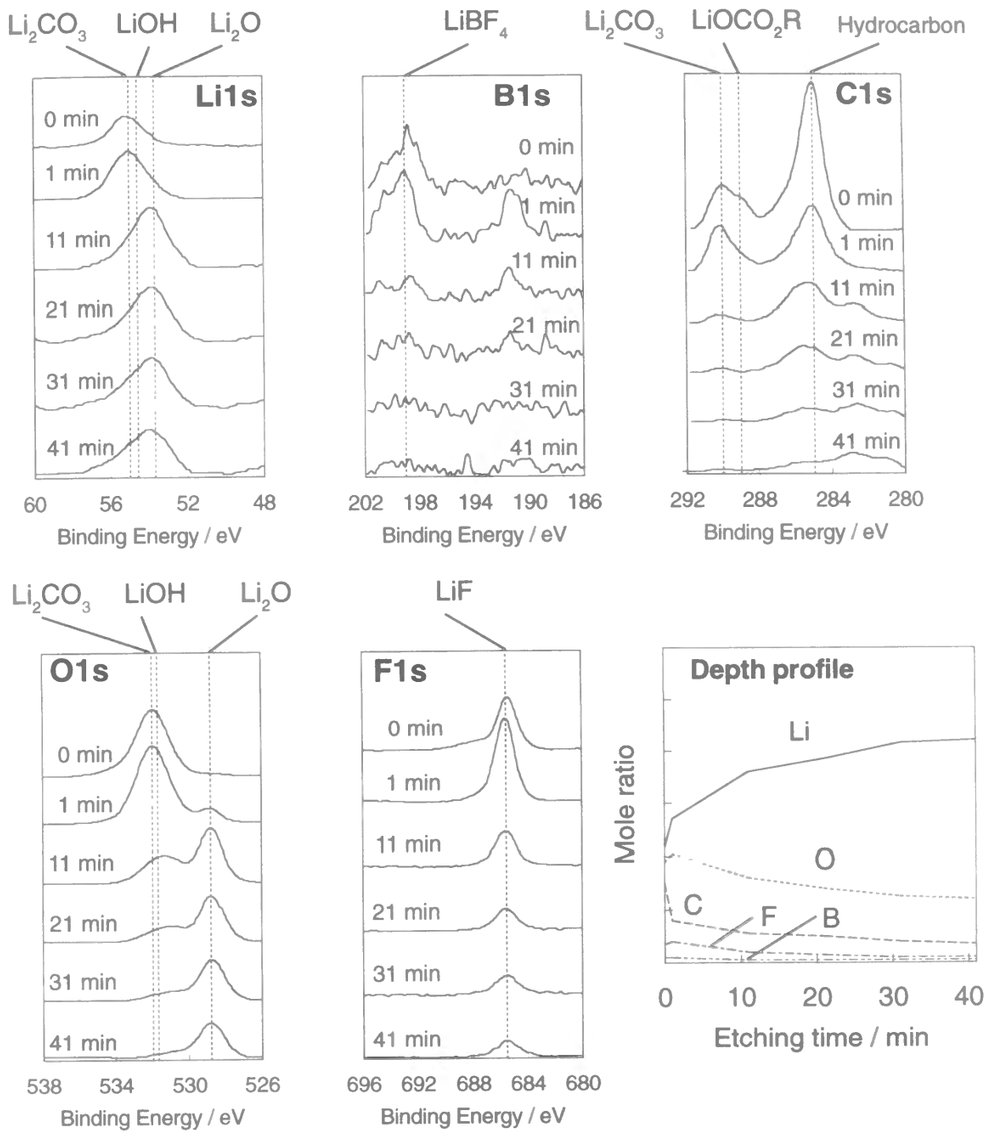

Figure 3-3 XPS spectra of Li 1s, B 1s, C 1s, O 1s, and F 1s for lithium deposited on the Ni substrate in $LiBF_4$/PC at 1.0 mA cm^{-2} (1.0 C cm^{-2}), and depth profile of each element in the surface film. The time in each figure indicates the duration of the Ar ion etching.

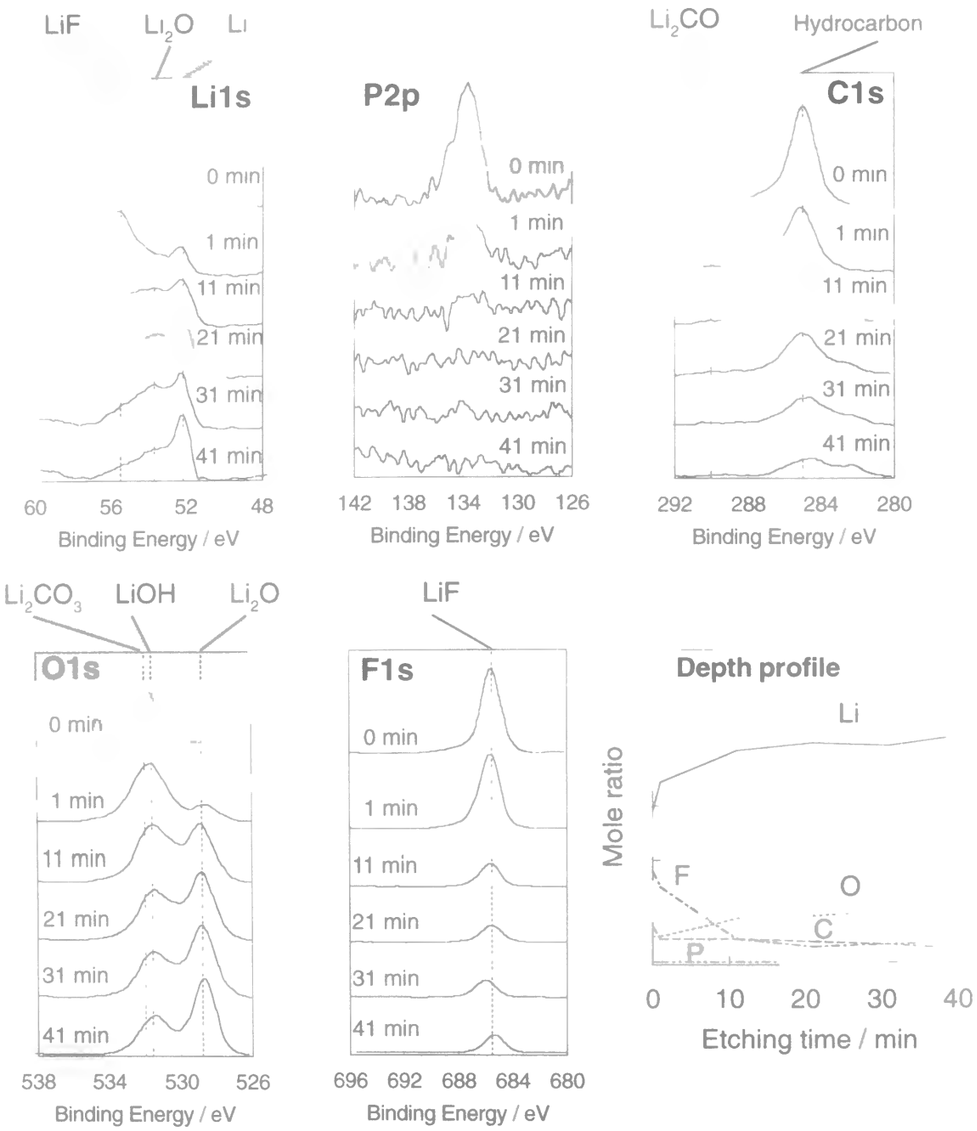

Figure 3-4 XPS spectra of Li 1s, P2p, C 1s, O 1s, and F 1s for lithium deposited on the Ni substrate in $LiPF_6$/PC at 1.0 mA cm^{-2} (1.0 C cm^{-2}), and depth profile of each element in the surface film. The time in each figure indicates the duration of the Ar ion etching.

and acid-base reactions between basic lithium compounds and HF in the electrolyte. There were no strong peaks in the XPS spectra of P 2p, so that LiF would be formed by the acid-base reaction. The presence of Li_2O was observed from the XPS spectra of O 1s and its intensity was increased by the etching process. The presence of a hydrocarbon was observed from this C 1s spectra. These XPS spectra for lithium deposited in $LiPF_6$/PC were very unique. The interesting feature of the surface film was also observed in the depth profile of each element in the surface film. The amount of F element was the largest at the outer part of the surface film, while the amount of O element (Li_2O) was the largest at the inner part. This indicates that the surface film comprises of LiF and Li_2O. Thus the surface film of lithium deposited in $LiPF_6$/PC can be illustrated as shown in Figure 3-5 (b), differing

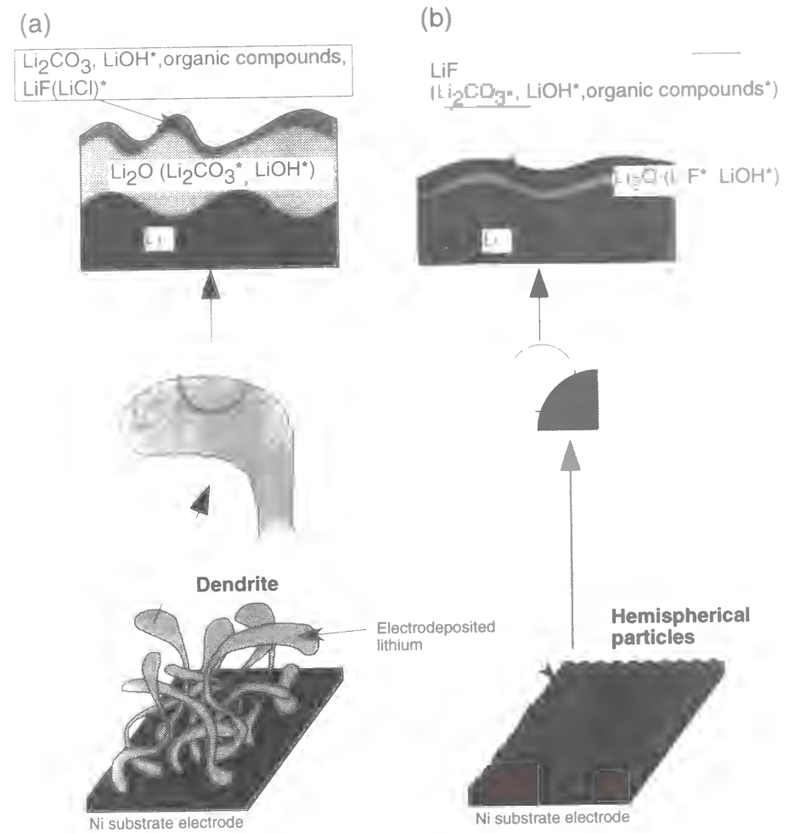

Figure 3-5 Schematic illustrations of the surface condition and the morphology of lithium deposited on the Ni substrate (a) in $LiAsF_6$, $LiBF_4$, and $LiClO_4$/PC and (b) in $LiPF_6$/PC. *: minor species

from other electrolytes.

The thickness of the surface film is important. However, it is very difficult to determine the etching rate for various compounds involved in the surface film. The etching rate was roughly estimated to be 5 Å min^{-1}. If it is correct, the thickness of the surface film formed in $LiPF_6$/PC can be calculated to be less than several tens Å. Since the peak corresponding to lithium metal was not observed even after the etching for 41 min in other three electrolytes, the thickness of the surface film would be more than 200 Å. From these estimation for the thickness of the surface film, it can be said that the very thin and uniform surface film, having a adequate tightness for the protection of the lithium metal surface, is formed on lithium deposited in $LiPF_6$/PC, otherwise solvents and salts react with lithium directly to form various compounds leading to destruction of a lithium metal.

The surface film of lithium deposited on the Ni substrate includes the following chemical compounds, hydrocarbon, LiOH, Li_2CO_3, Li_2O, and LiF (or LiCl). The surface film of lithium has been analyzed by FTIR method which is useful to detect organic species. The presence of various kinds of organic products (lithium alkylcarbonate; $LiOCO_2R$) in the surface film of lithium has been proposed from such FTIR measurement [22,24]. In this study, the surface film of lithium was analyzed by XPS which is suitable for the detection of inorganic compounds, not organic compounds, and this method should be an *ex-situ* measurement. Therefore, it is difficult to discuss on the chemical condition of organic products from the XPS spectra. However, a hydrocarbon was observed in the XPS spectra of C 1s for all surface films. At least, it can be said that propylene carbonate decomposes during the electrochemical deposition of lithium metal. Moreover the formation of Li_2CO_3 and $LiOCO_2R$ might be an indication for electrochemically reductive decomposition of PC. On the other hand, the formation of LiOH and Li_2O may be explained by electrochemically reductive decomposition of H_2O in the electrolyte, salt and solvent. The formation of LiF is due to the chemical reaction of LiOH, Li_2CO_3, and Li_2O with HF dissolved in the electrolyte as an impurity. Thus the surface film of lithium is strongly influenced by impurities (H_2O and acid) as well as solvents and salts.

When a migration of lithium ions through the surface film takes place during the electrodeposition of lithium, such a surface film should influence the electrochemical characteristics and the morphology of lithium. Since the surface film of lithium depends on the kind of electrolyte salts, the morphology of lithium is influenced by the kind of electrolyte salts. The morphology of lithium was observed with scanning electron microscope. Figure 3-6 shows the scanning electron micrographs of lithium deposited on the Ni substrate in PC containing various electrolyte salts. Two different types of morphology were observed in these scanning electron micrographs. One is a typical dendrite

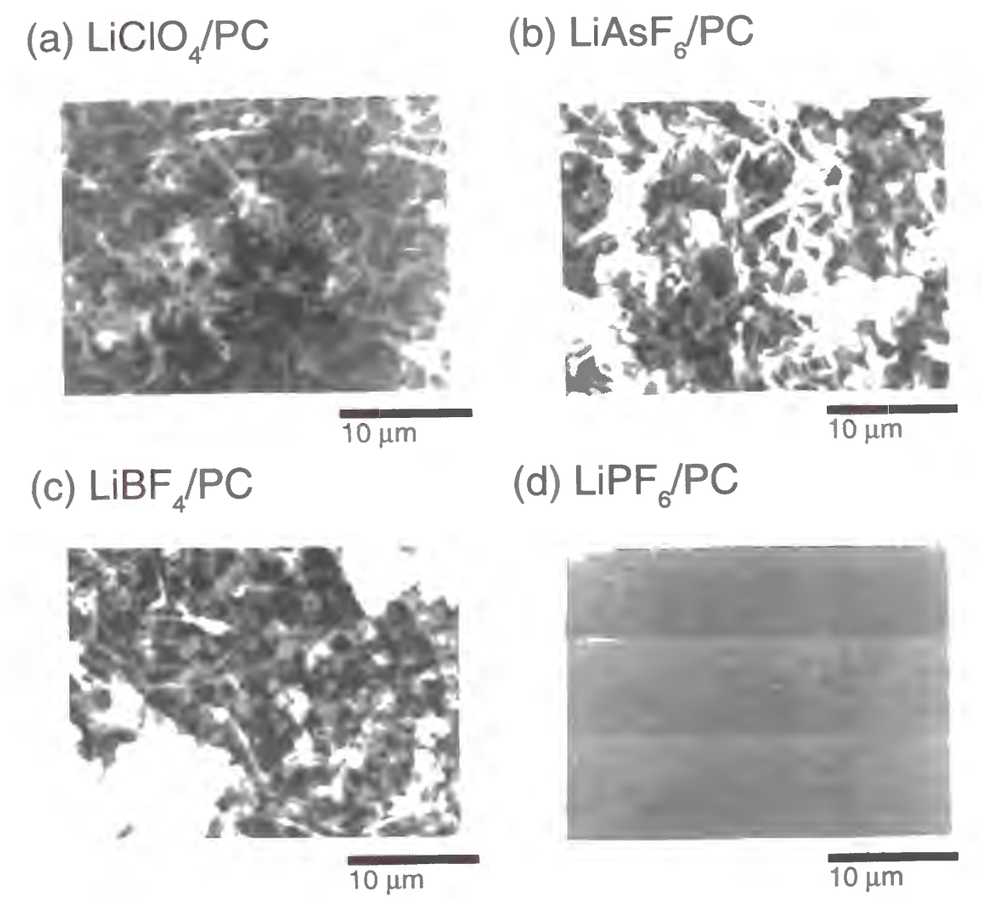

Figure 3-6 Scanning electron micrographs of lithium deposited on the Ni substrate in various propylene carbonate electrolytes at 1.0 mA cm^{-2} (1.0 C cm^{-2}), (a) $LiClO_4$, (b) $LiAsF_6$, (c) $LiBF_4$, and (d) $LiPF_6$.

form, and another is a hemispherical form. The hemispherical one was obtained in the case of the electrodeposition in $LiPF_6$/PC. These scanning electron micrographs well correspond to the surface film of lithium formed during the electrochemical deposition, so that the morphology of lithium deposits may be determined by its surface film. From these results, it can be seen that the formation of lithium dendrite is reduced by the suitable structure of the surface film formed on lithium which is obtained by the suitable selection of electrolyte. There are many differences between $LiPF_6$/PC electrolyte and other three electrolytes. If the morphology of lithium is controlled by the surface film of lithium formed during the electrochemical deposition, the flat electrochemical deposition (or a hemispherical lithium deposition) can be accomplished by the reproducible formation of the similar surface film as obtained in $LiPF_6$/PC. The most different feature of the surface film among four PC electrolytes is the distribution of LiF (or LiCl) in the surface film. If LiF is formed by acid-base reactions of basic lithium compounds and HF, the addition of HF into electrolytes will provide the similar surface film as observed for the surface film obtained in $LiPF_6$/PC. Therefore, the electrochemical deposition of lithium was performed in $LiClO_4$/PC containing a small amount of aqueous HF (46 weight %). HF concentration was 5.0 mmol dm^{-3}. Figure 3-7 shows the scanning electron micrograph of lithium deposited in this electrolyte. The morphology of lithium was a hemispherical type and the lithium

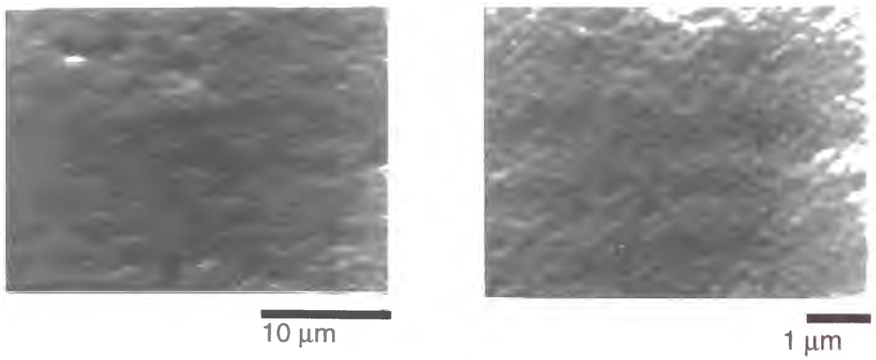

Figure 3-7 Scanning electron micrographs of lithium deposited on the Ni substrate in propylene carbonate containing 1.0 mol dm^{-3} $LiClO_4$ and 5×10^{-3} mol dm^{-3} HF at 1.0 mA cm^{-2} (1.0 C cm^{-2}).

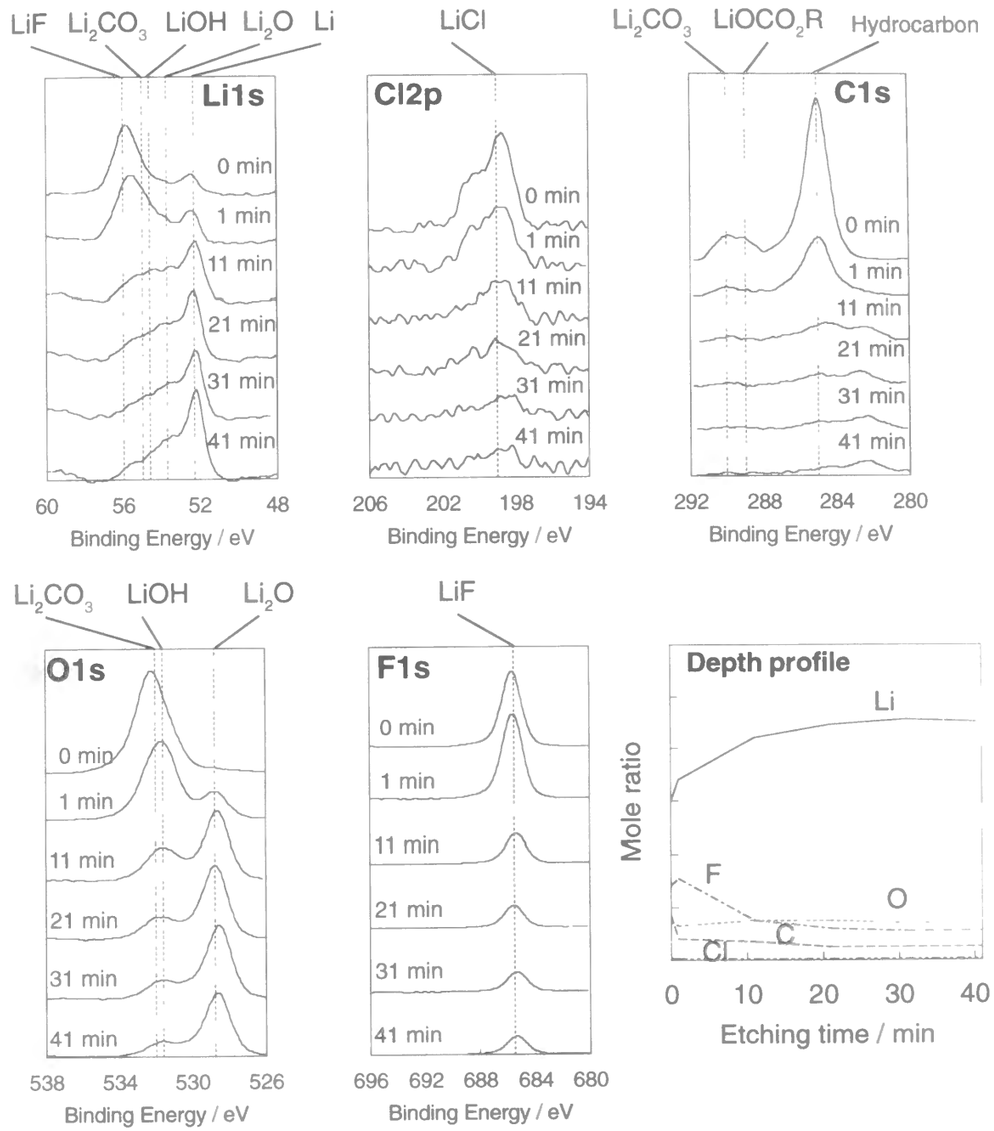

Figure 3-8 XPS spectra of Li 1s, Cl 2p, C 1s, O 1s, and F 1s for lithium deposited on the Ni substrate in propylene carbonate containing 1.0 M $LiClO_4$ and 5.0 mM HF at 1.0 mA cm^{-2} (1.0 C cm^{-2}). The time in each figure indicates the duration of the Ar ion etching.

surface was very smooth and flat, which was like a shining mirror surface. The surface film of this lithium was analyzed by XPS and the spectra were shown in Figure 3-8. All spectra were very similar to those observed in Figure 3-4 and were completely different from those in Figure 3-1. From this result, it can be concluded that the surface film of lithium is very sensitive to a small amount of acid which is an important key factor for the morphology control of lithium.

3-4 Conclusion

The chemical compositions of surface films of lithium deposited on a Ni substrate in propylene carbonate (PC) containing 1.0 mol dm^{-3} $LiClO_4$, $LiAsF_6$, $LiBF_4$, or $LiPF_6$ were analyzed by XPS and the morphology of lithium deposited in these electrolytes were observed with SEM. In the case of PC electrolytes, the relationship between the surface film of lithium formed during the electrochemical deposition and the morphology of lithium was deduced in this study. The dendrite formation was suppressed when using $LiPF_6$/PC which includes a small amount of HF as a decomposition product of PF_6^- ions. The similar surface film could be obtained by the addition of small amount of HF in $LiClO_4$/PC. Therefore, the suppression of lithium dendrites is mainly due to a small amount of HF which may provide the thin and tight surface film.

Chapter 4
Electrochemical Deposition of Highly Smooth Hemispherical Lithium Using Nonaqueous Electrolytes Containing HF

4-1 Introduction

In the previous chapter, it has been seen that lithium electrodeposited on nickel substrate electrodes in electrolytes containing HF has an extremely smooth hemispherical form. This can be attributed to the modification of the surface film formed on the lithium deposits. In this chapter, the competitive action between electrodeposition rate (electrodeposition current density) and chemical reaction rate of the lithium surface (concentration of HF) is used as a basis for a discussion of the effect of the surface film on lithium electrodeposition in order to throw light on the mechanism of dendritic lithium deposition.

4-2 Experimental

4-2-1 Electrodeposition

A nickel plate (Nilaco Corporation, Japan ; 6×20 mm) was used as a substrate electrode. Before the experiments, the nickel substrate was polished with fine alumina powders (0.05 μm) to obtain a mirror surface and then was dipped in an ultrasonic bath containing pure water and acetone to remove residual alumina powders. Lithium metal foil (Honjoh Metal Company, Japan) was used as the reference and for the counter electrodes (8 cm^2). Propylene carbonate (PC) containing 1.0 mol dm^{-3} $LiClO_4$ (Mitsubishi Chemical, Japan) was used as a base electrolyte, and an aqueous HF solution (46% weight, Wako Chemical, Japan) was added before the electrodeposition of lithium. Concentrations of HF and H_2O in the electrolytes used in this study are summarized in Table 4-1. Electrochemical deposition was performed under galvanostatic conditions at currents ranging from 10.0 mA cm^{-2} to 0.2 mA cm^{-2}. The electrical charge for all electrodepositions was set at 1.0 C cm^{-2}. After the electrodeposition of lithium, the electrode was washed

with pure PC (Mitsubishi Chemical, Japan) to remove electrolyte salts. All procedures were conducted in an argon dry box at room temperature (dew point < -90°).

Table 4-1 Concentrations of HF and H_2O in propylene carbonate 1.0 M $LiClO_4$ and various amount of HF.

C_{HF} / mmol dm^{-3}	C_{H_2O} / mmol dm^{-3}
0	0.5
0.50	1.2
2.5	3.8
5.0	7.0
10	14
20	27

4-2-2 XPS analysis and SEM observation

The surface condition of the lithium electrodeposited on the Ni substrate was analyzed with XPS. The morphology of the lithium electrodeposited was observed with SEM. The sample transfer from the argon dry box to the XPS or the SEM equipment was conducted in the same way as described in the chapter 1. The analysis condition for the XPS or the SEM were the same as that in the previous chapter.

4-2-3 Impedance analysis

The electrochemical behavior of the interface of lithium was analyzed by means of impedance measurement (1250A, Solartron, U.K.). The impedance measurement for lithium was performed at an open circuit voltage after the electrodeposition of lithium. The amplitude of the alternating current was 5 mV, and the frequency range 50 kHz - 0.01 Hz. The measurement was performed at 30 ± 0.1 °C under an argon atmosphere.

4-3 Results and discussion

Several chemical reactions taking place on lithium in electrolytes containing HF as a contaminant (e.g. PC containing $LiPF_6$) were proposed at the previous chapter ; these reactions are formulated as follows:

$$Li_2CO_3 + 2HF \rightarrow 2LiF + H_2CO_3 \quad (1)$$

$$LiOH + HF \rightarrow LiF + H_2O \quad (2)$$

$$Li_2O + 2HF \rightarrow 2LiF + H_2O \quad (3)$$

$$LiOR + HF \rightarrow LiF + ROH \quad (4)$$

$$LiOCO_2R + HF \rightarrow LiF + ROH + CO_2 \quad (5)$$

$$Li + HF \rightarrow LiF + 1/2H_2 \quad (6)$$

These basic compounds, such as $LiOCO_2R$, Li_2CO_3, LiOR, LiOH, and Li_2O, are produced by electrochemically reductive decomposition of the solvent, residual water, and oxygen in the electrolytes. Equations (1) - (5) represent acid-base reactions of some basic lithium compounds with HF. Equation (6) shows the direct reaction of lithium metal with HF. All equations show that LiF is a final product on the lithium surface in electrolytes containing HF as a contaminant. When a small amount of HF is added to propylene carbonate containing 1.0 mol dm^{-3} $LiClO_4$, lithium, deposited on a Ni substrate, has an ultra smooth surface covered with a thin LiF/Li_2O surface film which is formed by the effect of HF. This suggests that HF works effectively to suppress the dendrite formation of lithium. In fact, when the deposition is performed without the addition of HF, lithium electrodeposited on a Ni substrate has a dendritic form and the surface is covered with a thick film (mainly LiOH, Li_2CO_3 and Li_2O). If surface reactions of lithium occur during the electrochemical deposition of lithium, the morphology of lithium deposited on the substrate depends on both the electrochemical deposition kinetics and the rate of the surface reaction of lithium; the first parameter can be changed by changing current density and the second can be controlled by the concentration of HF. The morphology of lithium probably becomes dendritic when the surface reaction of lithium with HF is not fast enough to form the LiF/ Li_2O film which is effective for the suppression of lithium dendrites or when the electrochemical deposition rate is too fast to modify the surface film of lithium.

4-3-1 Influence of electrodeposition current density (deposition rate)

Figure 4-1 shows the scanning electron micrographs of lithium deposited from PC containing 1.0 mol dm^{-3} $LiClO_4$ and 5.0 mmol dm^{-3} HF (obtained from the appropriate

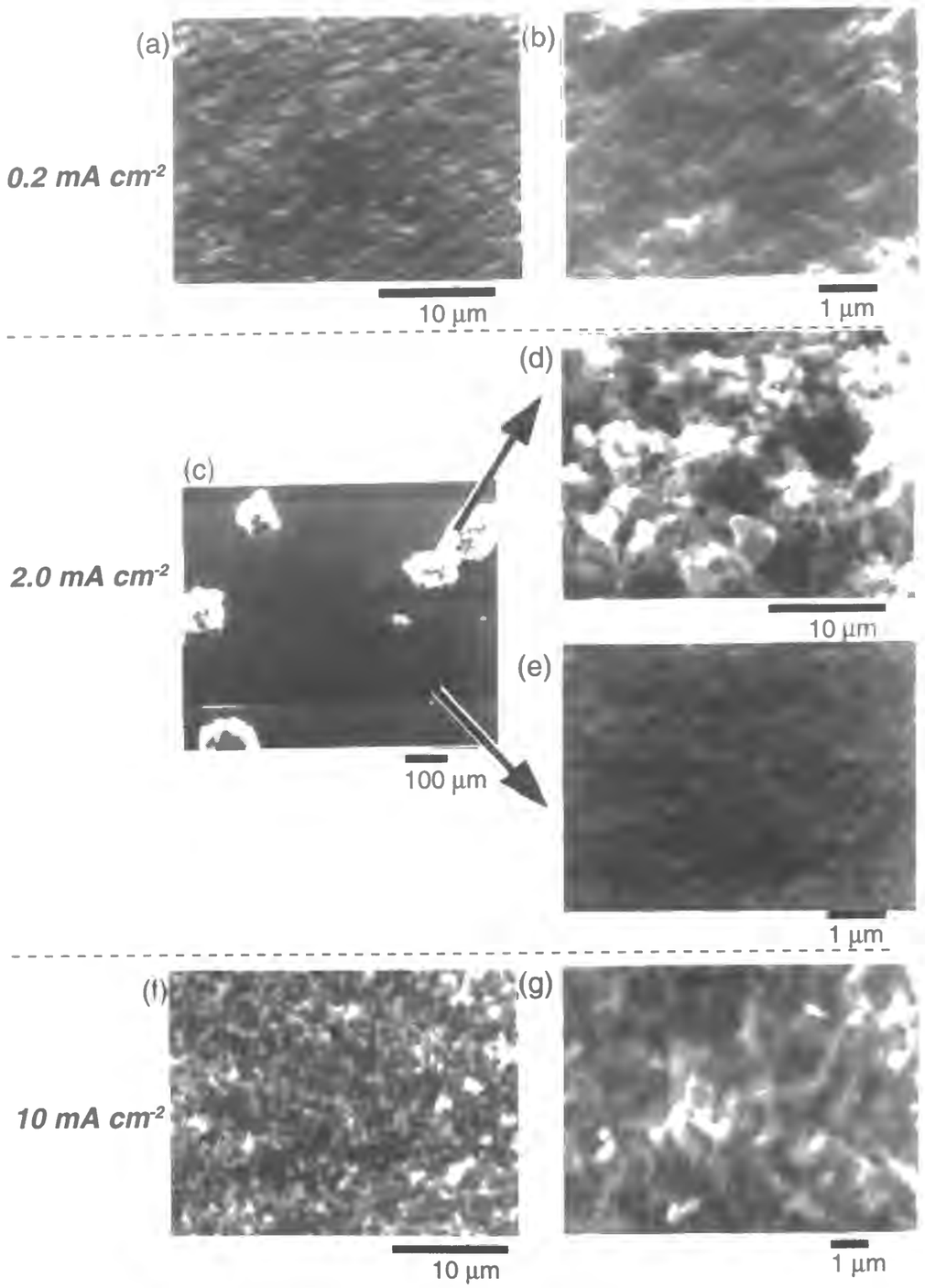

Figure 4-1 Scanning electron micrographs of lithium deposited on the Ni substrate from PC containing 1.0 M $LiClO_4$ and 5.0 mM HF at various electrodeposition currents [(a, b) 0.2 mA cm^{-2}; (c-e) 2.0 mA cm^{-2}; (f, g) 10.0 mA cm^{-2}].

volume of 46 wt.% aqueous solution) at various electrodeposition currents. The morphology of the lithium deposited on the Ni substrate at 0.2 mA cm^{-2} was a hemisphere with a diameter of about 0.3 µm as shown in Figures 4-1 (a) and (b). The lithium deposition under this condition resulted in an ultra smooth surface of lithium and a homogeneous deposition over the Ni substrate. Figures 4-1 (c-e) show the scanning electron micrographs of lithium deposited at 2.0 mA cm^{-2}. The electrode was mostly covered with very smooth deposits, but agglomerates of lithium were also observed at several points. The lithium particles in the smooth part have a hemispherical shape as shown in Figure 4-1 (e). On the other hand, the agglomerates consist of dendritic lithium deposits as shown in Figure 4-1 (d). At 10.0 mA cm^{-2}, all lithium deposited was dendritic as shown in Figures 4-1 (f) and (g). Thus, the proportion of the agglomerates consisting of lithium dendrites increased with an increase in the electrodeposition current, and finally the surface was entirely covered with dendritic lithium deposits. If the lithium surface were uniformly modified by HF, the hemispherical form would be obtained even at 10 mA cm^{-2} electrodeposition current. However, the formation of the dendritic lithium at a high electrodeposition current shows that the modification is not uniformly accomplished under that condition. These results led us to expect that the efficiency of the surface modification would depend on the electrodeposition current. Therefore, in this study the surface conditions of these lithium deposits were analyzed with XPS in order to discover the relationship between the form of the deposition and the surface conditions.

Figures 4-2 (a), (b), and (c) show the XPS spectra of Li 1s for lithium deposited at 0.2 mA cm^{-2}, 2.0 mA cm^{-2}, and 10.0 mA cm^{-2} from PC containing 1.0 mol dm^{-3} $LiClO_4$ and 5.0 mmol dm^{-3} HF, respectively. Several spectra are shown in each figure; these were obtained after argon ion etching for various durations, corresponding to the depth profile. Etching durations were from top to bottom 0 min, 1 min, 11 min, 21 min, 31 min, and 41 min. The etching rate is roughly estimated to be 5 Å min^{-1} from the sputtering coefficient and the ion beam current.

Two peaks and a shoulder peak were observed at 56.0 eV, 52.3 eV, and 53.7 eV in

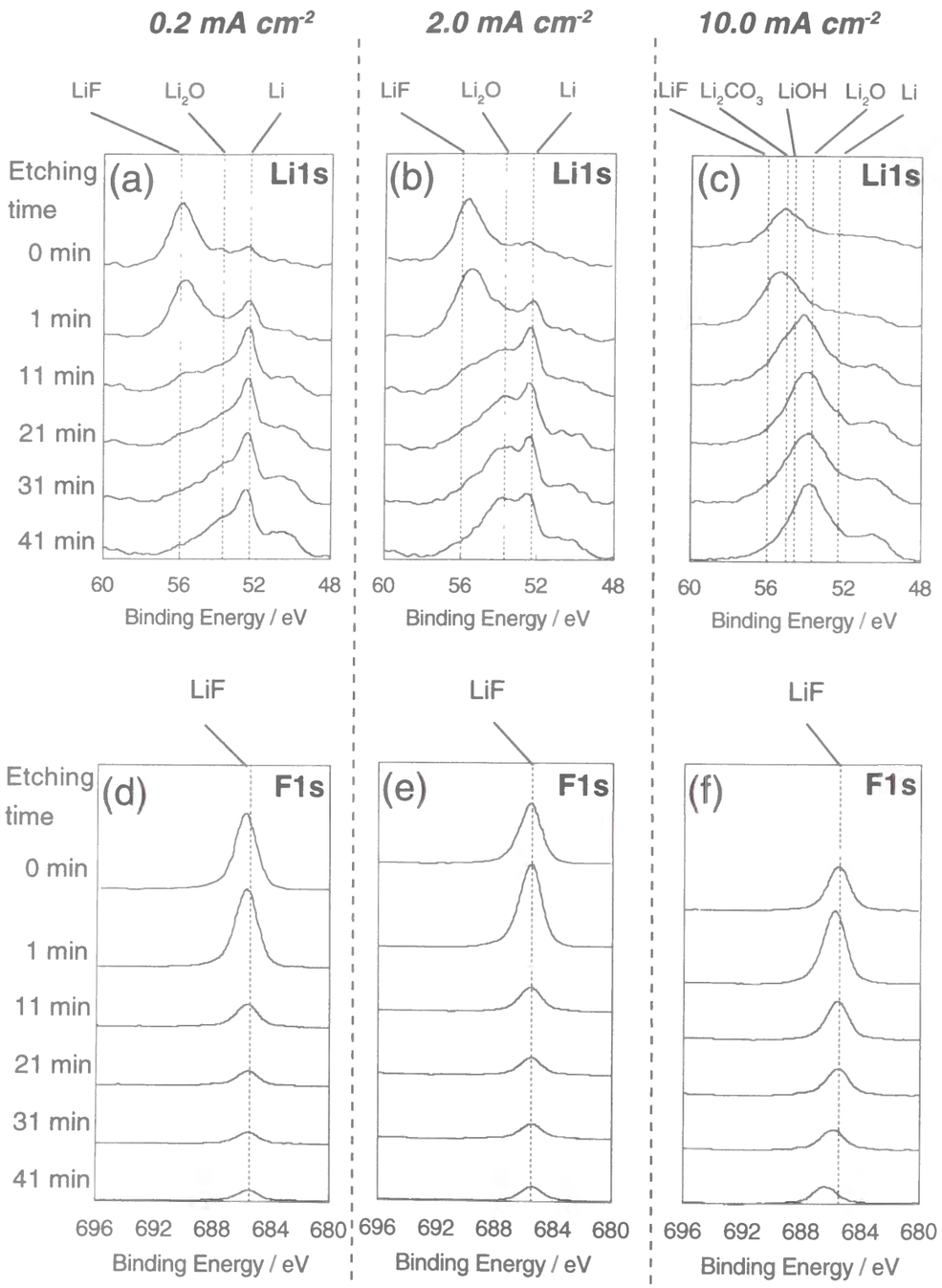

Figure 4-2 XPS spectra of Li1s and F1s for lithium deposited on the Ni substrate at (a, d) 0.2 mA cm^{-2}, (b, e) 2.0 mA cm^{-2}, and (c, f) 10.0 mA cm^{-2} from PC containing 1.0 M $LiClO_4$ and 5.0 mM HF; time indicates the duration of the argon ion etching.

the XPS spectra of Li 1s for lithium deposited at 0.2 mA cm^{-2} (Figure 4-2 (a)); these peaks can be attributed to LiF, Li, and Li_2O, respectively. The LiF peak was strong before the argon ion etching and then decreased with progression of the etching process. The peak from Li metal became gradually more intense with the argon ion etching, and finally became the main peak after argon ion etching for 41 min. This peak was accompanied by a shoulder peak corresponding to Li_2O at 53.7 eV. These results suggest that the surface of lithium is covered with a layer consisting of LiF (outer part) and Li_2O (inner part). Because the XPS spectrum remained unchanged after argon ion etching for 11 min, the thickness of this surface film is roughly estimated to be 50 Å. But, taking into account variations in the argon ion beam radiation to the sample and the oxidation of lithium metal by residual oxygen and moisture in the XPS analysis chamber, it might be expected to be less than 50 Å. The spectra in Figure 4-2 (b) were similar to those in Figure 4-2 (a), except for the intensity of Li_2O after the argon ion etching. This result shows that the smooth (hemispherical) part of lithium electrodeposited at 2.0 mA cm^{-2} (see SEM Figures 1 (c-e)) is covered with the same surface film observed for lithium deposited at 0.2 mA cm^{-2}. However, the Li_2O peak after the argon ion etching exhibits the effect of dendritic lithium formed as a minor morphology. The XPS spectra of Li 1s for lithium deposited at 10.0 mA cm^{-2} were very different from those for lithium deposited at 0.2 mA cm^{-2} (Figure 4-2 (c)). The peak observed at 55.0 eV and 54.6 eV can be attributed to Li_2CO_3 ($LiOCO_2R$) and LiOH, respectively. Since the binding energy of LiOH is almost the same as that of Li_2CO_3 or $LiOCO_2R$, the ratio of the three compounds was not be determined from the Li 1s spectra. However, since the Li_2O peak was the main peak after the argon ion etching for 11 min, it can be concluded that the surface film formed on lithium deposited at 10.0 mA cm^{-2} consists of an upper layer involving LiOH, Li_2CO_3, or $LiOCO_2R$ and a thick inner Li_2O layer (more than 200 Å).

Figures 4-2 (d), (e), and (f) show the XPS spectra of F1s for lithium electrodeposited from PC containing 1.0 mol dm^{-3} $LiClO_4$ and 5.0 mmol dm^{-3} HF at various electrodeposition current densities. Figure 4-3 shows the depth profiles for the mole ratios

of each element. The peaks observed at 685.5 eV in the F1s spectra can be attributed to LiF and were strong before the argon ion etching and after etching for 1 min. The intensity of this peak in Figure 4-2 (f) is weaker than that in Figure 4-2 (d) and (e), as shown in the depth profile of each element in Figure 4-3. Therefore, the amount of LiF in the surface film formed on lithium deposited at 10.0 mA cm^{-2} is smaller than that on lithium deposited at 0.2 mA cm^{-2} and 2.0 mA cm^{-2}. This result corresponds to the Li 1s XPS spectra, indicating that the surface films of lithium deposited at 0.2 mA cm^{-2} and 2.0 mA cm^{-2} mainly consist of LiF and the surface film of lithium deposited at 10.0 mA cm^{-2} consists of Li_2O.

A peak was observed at 285.0 eV in all the XPS spectra of C1s, as seen in Figures 4-4 (a), (b), and (c). This peak can be attributed to carbon in a hydrocarbon structure. This structure may be due to a residual gas in the XPS analysis chamber, or the reaction product

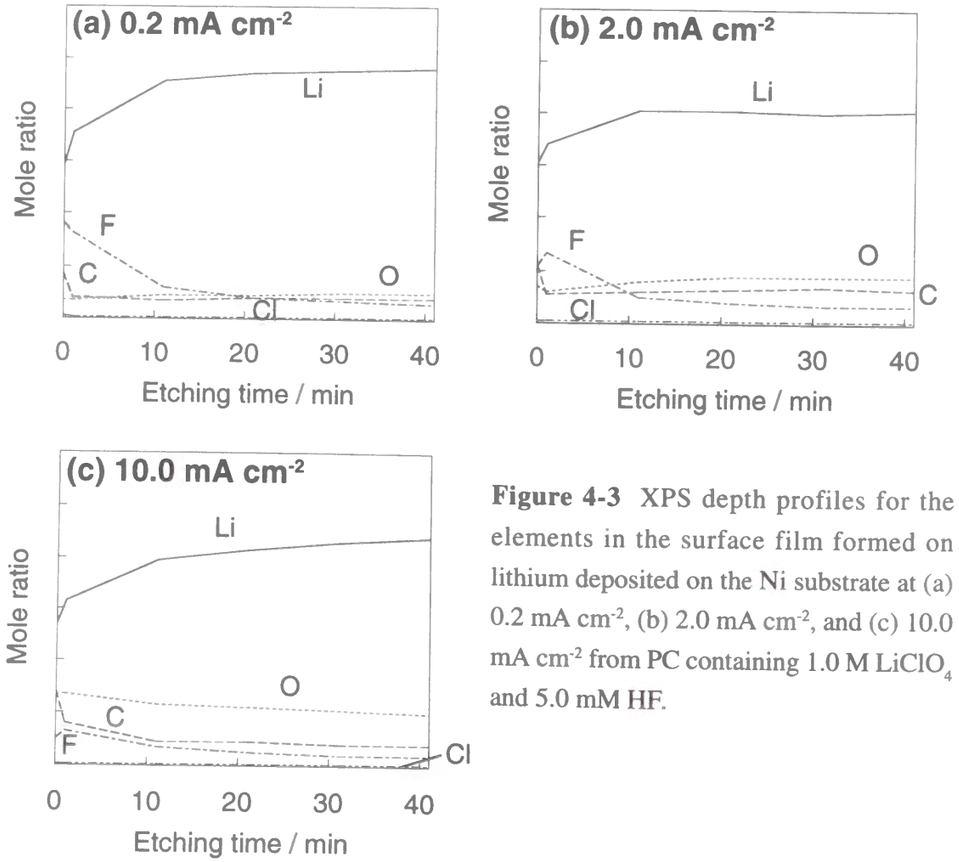

Figure 4-3 XPS depth profiles for the elements in the surface film formed on lithium deposited on the Ni substrate at (a) 0.2 mA cm^{-2}, (b) 2.0 mA cm^{-2}, and (c) 10.0 mA cm^{-2} from PC containing 1.0 M $LiClO_4$ and 5.0 mM HF.

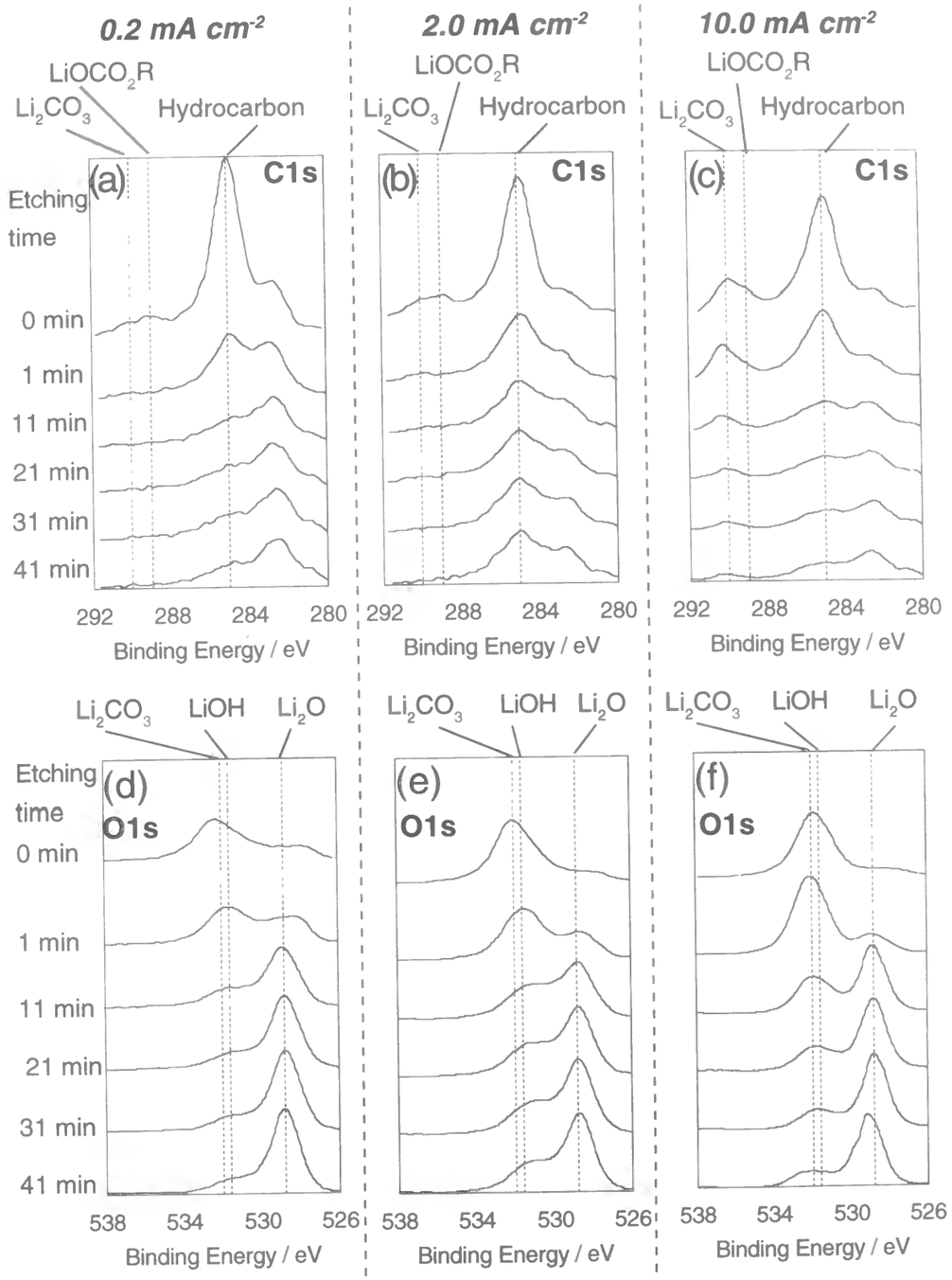

Figure 4-4 XPS spectra of C1s and O1s for lithium deposited on the Ni substrate at (a, d) 0.2 mA cm^{-2}, (b, e) 2.0 mA cm^{-2}, and (c, f) 10.0 mA cm^{-2} from PC containing 1.0 M $LiClO_4$ and 5.0 mM HF; time indicates the duration of the argon ion etching.

of solvent with lithium. If this peak was due to hydrocarbon gas adsorbed on the surface of lithium, the peak intensity of this hydrocarbon should have been significantly decreased by argon ion etching for a short time. In Figure 4-4 (a), the peak at 285.0 eV in fact markedly decreased after the argon ion etching, indicating that the peak at 285.0 eV was indeed due to the hydrocarbon gas adsorbed on the electrode surface. On the other hand, the peak at 285.0 eV in Figure 4-4 (b) and (c) did not markedly decrease, suggesting that the hydrocarbon in Figure 4-4 (b) and (c) should be attributed to the reduction product of PC. These conclusions are confirmed by the peaks observed at the binding energy region from 289 eV to 290 eV, which can be attributed $LiOCO_2R$ and Li_2CO_3, respectively. These compounds can be produced by the reductive decomposition of PC. In addition, the peak intensity change in the XPS spectra of C 1s in Figures 4-4 (b) and (c) accompanying the argon ion etching suggests the presence of Li_2CO_3 and $LiOCO_2R$ in the upper part of the surface film.

Peaks observed at 532.0 eV, 531.6 eV, and 528.8 eV in Figures 4-4 (d), (e), and (f) can be attributed to Li_2CO_3 ($LiOCO_2R$), LiOH, and Li_2O, respectively. In all figures, the peak corresponding to Li_2O was observed after the argon ion etching, showing that Li_2O was present in the inner part of the surface film. However, the depth profile in Figure 4-3 shows that the amount of Li_2O is larger in Figure 4-4 (f) than in Figures 4-4 (d) and (e). This suggests that a thick Li_2O layer is related to the formation of lithium dendrites when the electrodeposition is performed at 10.0 mA cm^{-2}. This result is in good agreement with the results of the discussion of the XPS spectra of Li1s.

From the XPS spectra of Cl 2p, some chloride compounds (mainly LiCl) were observed, but very few of these occurred in the surface film as shown in the depth profile in Figure 4-3. Therefore, the XPS spectra of Cl 2p strongly suggests that $LiClO_4$ does not react significantly with lithium metal.

The modification used in this study is explained by the chemical reaction of lithium with HF or several lithium compounds formed on the lithium surface with HF, as shown in equations (1)-(6). When the chemical reactions are too slow to modify the lithium surface,

lithium deposits in a dendritic form. On the other hand, when the chemical reactions proceed more quickly, than to the electrodeposition of lithium, lithium deposits in a hemispherical shape. The XPS spectra suggest that the modification of the surface film on lithium during the electrochemical deposition is not achieved at a high electrodeposition current. A comparison of the scanning electron micrographs with the XPS spectra shows that the surface film of the lithium is incomplete at several localized points. We consider that such a non-uniformity of the surface film causes a two-dimensional distribution of the film resistance. Therefore, the dendrite formation of lithium may be related to the current distribution resulting from the distribution of the film resistance.

4-3-2 Influence of concentration of HF (surface modification rate)

Figures 4-5 and 4-6 show the scanning electron micrographs for lithium deposited on the Ni substrate at 0.2 mA cm^{-2} from PC containing 1.0 mol dm^{-3} $LiClO_4$ and various concentrations of HF. All lithium deposits were a hemispherical when the PC electrolyte contained more than 5.0 mmol dm^{-3} HF (as shown in Figures 4-1 (a-b), 4-5 (a-b)). On the other hand, when the concentration of HF was lower than 0.50 mmol dm^{-3} HF, no hemispherical lithium can be seen in Figure 4-6. The dependence of the morphology of the deposited lithium on the HF concentration suggests that the chemical reaction rate with HF influences the modification of the surface film on lithium deposits. When the concentration of HF was 2.5 mmol dm^{-3} HF, both dendritic and hemispherical forms were observed. The dendritic deposits were observed at several localized points, as shown in Figures 4-5 (c-e), with conditions for the dendritic deposition similar to those in Figures 4-1 (c-e). This result suggests that the deposition of dendritic lithium is due to local variations in the surface film.

Figure 4-7 shows the XPS spectra of Li 1s for lithium deposited on the Ni substrate at 0.2 mA cm^{-2} from PC containing 1.0 mol dm^{-3} $LiClO_4$ and various concentrations of HF. Figure 4-7 (a) shows that the surface film on the hemispherical lithium deposited from the PC electrolyte containing 10 mmol dm^{-3} HF (see SEM Figures 4-5 (a, b)) has almost the

same structure as that deposited from the PC electrolyte containing 5.0 mmol dm^{-3} HF (see XPS Figure 4-2 (a)) and consists of both an outer LiF layer and an inner Li_2O layer. The thickness of this surface film is roughly estimated to be 50 Å because the XPS spectrum was unchanged after argon ion etching for 11 min. This result suggests that the concentration of HF from the PC electrolyte does not significantly affect the surface film at a concentration range of more than 5.0 mmol dm^{-3} when the electrodeposition current is 0.2 mA cm^{-2}. This

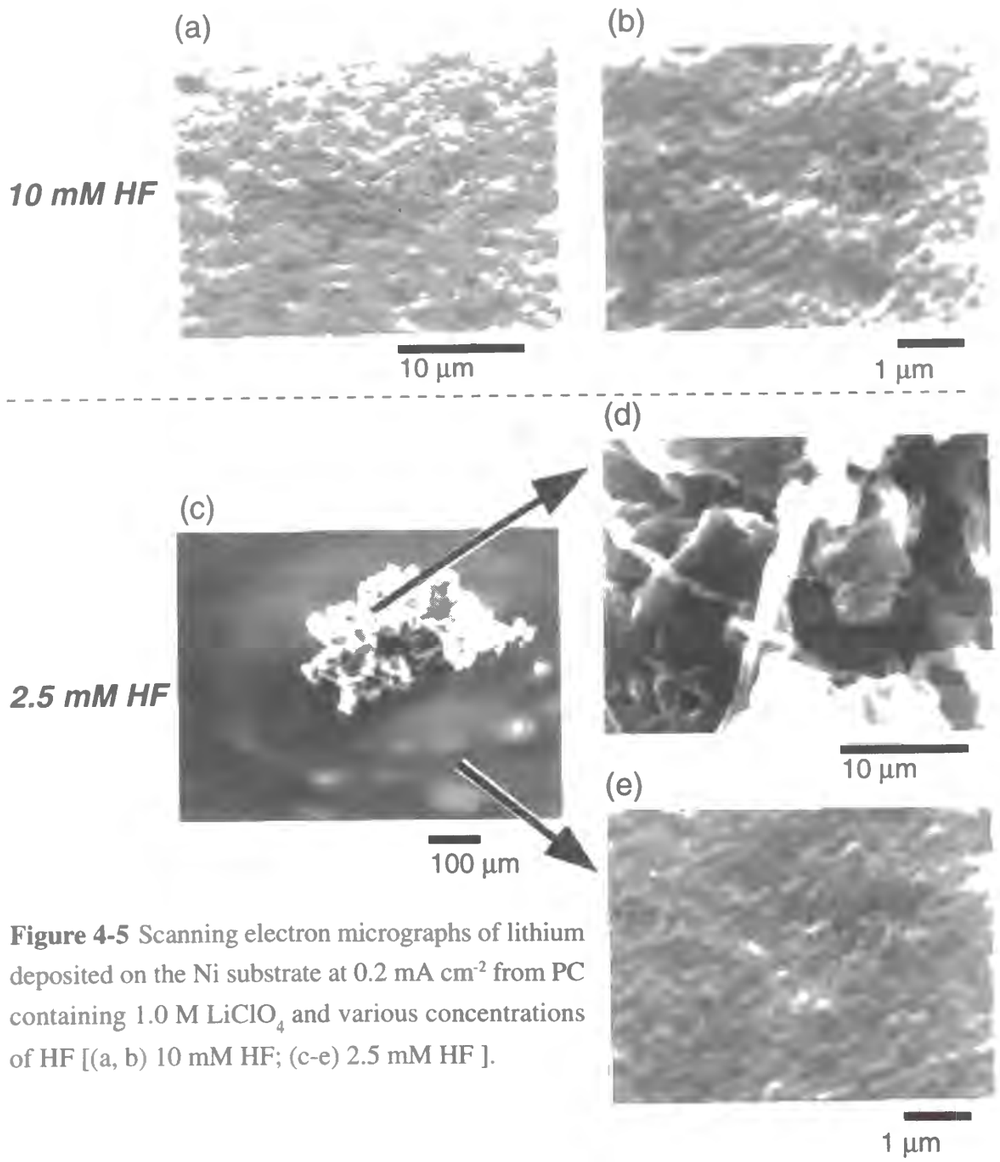

Figure 4-5 Scanning electron micrographs of lithium deposited on the Ni substrate at 0.2 mA cm^{-2} from PC containing 1.0 M $LiClO_4$ and various concentrations of HF [(a, b) 10 mM HF; (c-e) 2.5 mM HF].

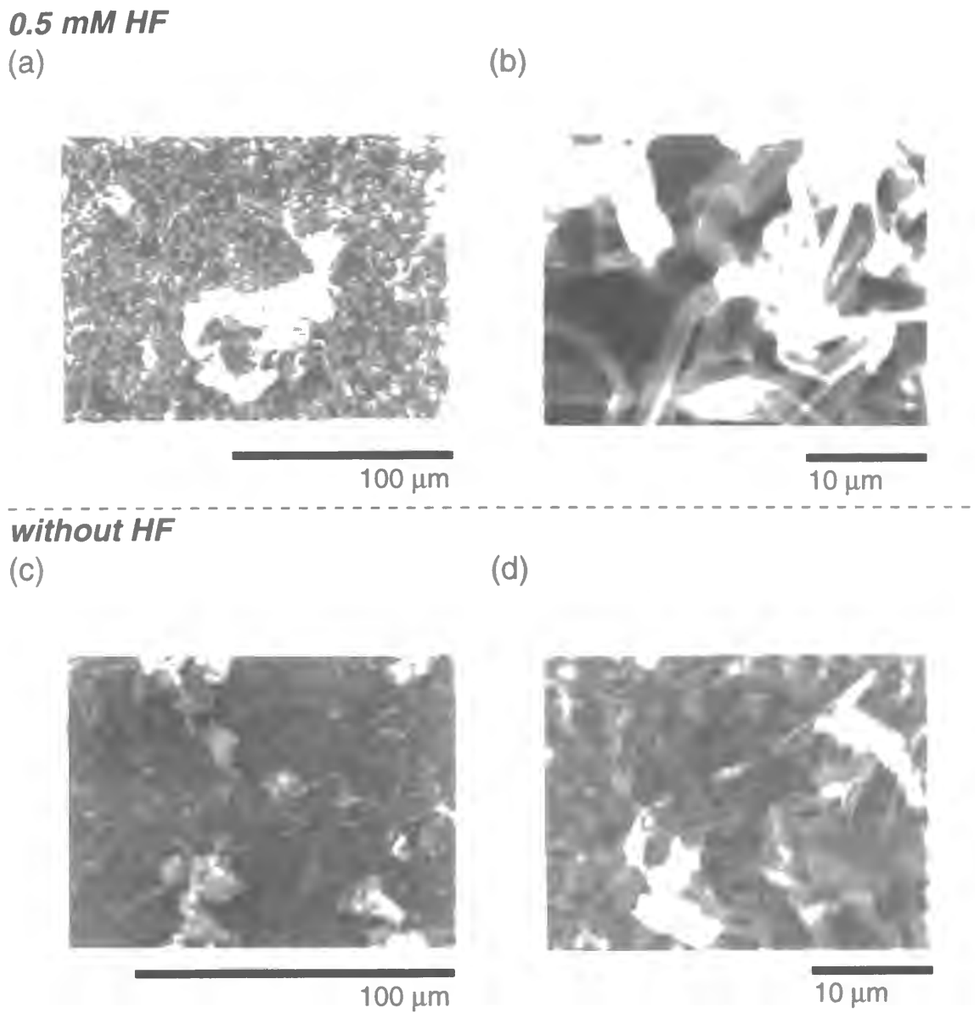

Figure 4-6 Scanning electron micrographs of lithium deposited on the Ni substrate at 0.2 mA cm^{-2} from PC containing 1.0 M $LiClO_4$ and various concentrations of HF [(a, b) 0.50 mM HF; (c, d) without HF].

may indicate that the chemical reaction rate for the modification from a PC electrolyte containing 5.0 mmol dm^{-3} HF is significantly faster than the electrodeposition rate of lithium. Figure 4-7 (b) shows the XPS spectra for the surface film on the hemispherical lithium deposited from a PC electrolyte containing 2.5 mmol dm^{-3} HF. These XPS spectra resemble those in Figure 4-7 (a), indicating that the surface film of the lithium deposited from this electrolyte is the same as that observed for the lithium deposited from a PC electrolyte

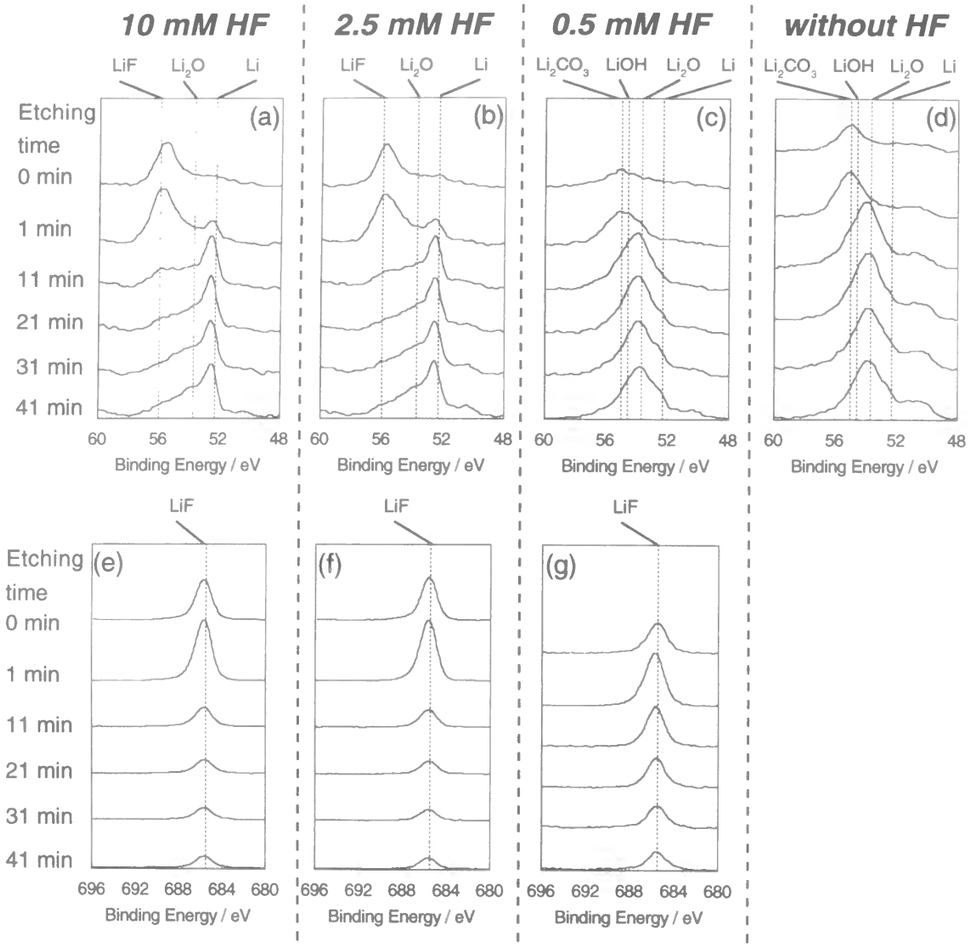

Figure 4-7 XPS spectra of Li1s and F1s for lithium deposited on the Ni substrate at 0.2 mA cm^{-2} from PC containing 1.0 M $LiClO_4$ and (a, e) 10 mM HF, (b, f) 2.5 mM HF, (c, g) 0.50 mM HF, or (d) without HF; time indicates the duration of the argon ion etching.

containing 5.0 mmol dm^{-3}. Although hemispherical lithium was observed for lithium deposited from PC containing 2.5 mmol dm^{-3} HF, there were also a few agglomerates of lithium dendrites on the electrode surface (see SEM Figures 4-5 (c-e)). Thus, the area where part for the agglomerate forms probably has a different character from the section providing the hemispherical lithium form. Figures 4-7 (c) and (d) show the XPS spectra of Li 1s for lithium deposited from a PC electrolyte containing 0.50 mmol dm^{-3} HF and

without HF. Both surface films included LiOH, Li_2CO_3, or $LiOCO_2R$ (at the outside) and Li_2O (at the inside), the same as observed for the dendritic lithium in Figure 4-6.

Figures 4-7 (e-g), and 4-8 show the XPS spectra of F 1s, C 1s, and O 1s for lithium electrodeposited at 0.2 mA cm^{-2} from PC containing 1.0 mol dm^{-3} $LiClO_4$ and various concentrations of HF. Figure 4-9 is the XPS depth profile, showing the mole

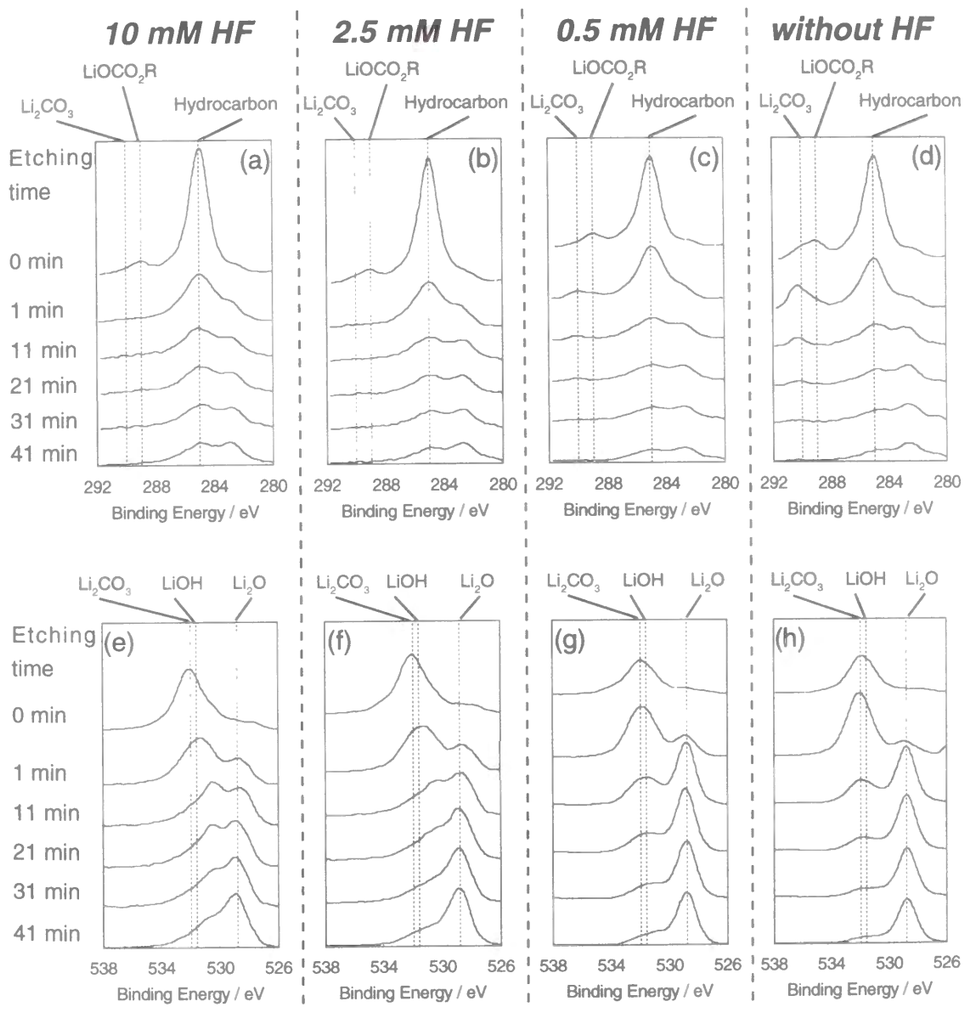

Figure 4-8 XPS spectra of C1s and O1s for lithium deposited on the Ni substrate at 0.2 mA cm^{-2} from PC containing 1.0 M $LiClO_4$ and (a, e) 10 mM HF, (b, f) 2.5 mM HF, (c, g) 0.50 mM HF, or (d, h) without HF; time indicates the duration of the argon ion etching.

ratios for each of the elements, after argon ion etching. The XPS spectra of F1s, C1s, and O1s did not show a clear difference in the structure of the surface film due to the concentration of HF in the PC electrolyte, indicating that the materials existing in the surface film are independent of the addition of HF into PC electrolyte. However, the depth profile shows a clear difference between the amount of LiF in the outer part and the amounts of oxide compounds (LiOH or Li_2O) in the inner part of the surface film. The amount of LiF increased and that of the oxide compounds decreased with increasing concentrations of HF in the PC electrolyte.

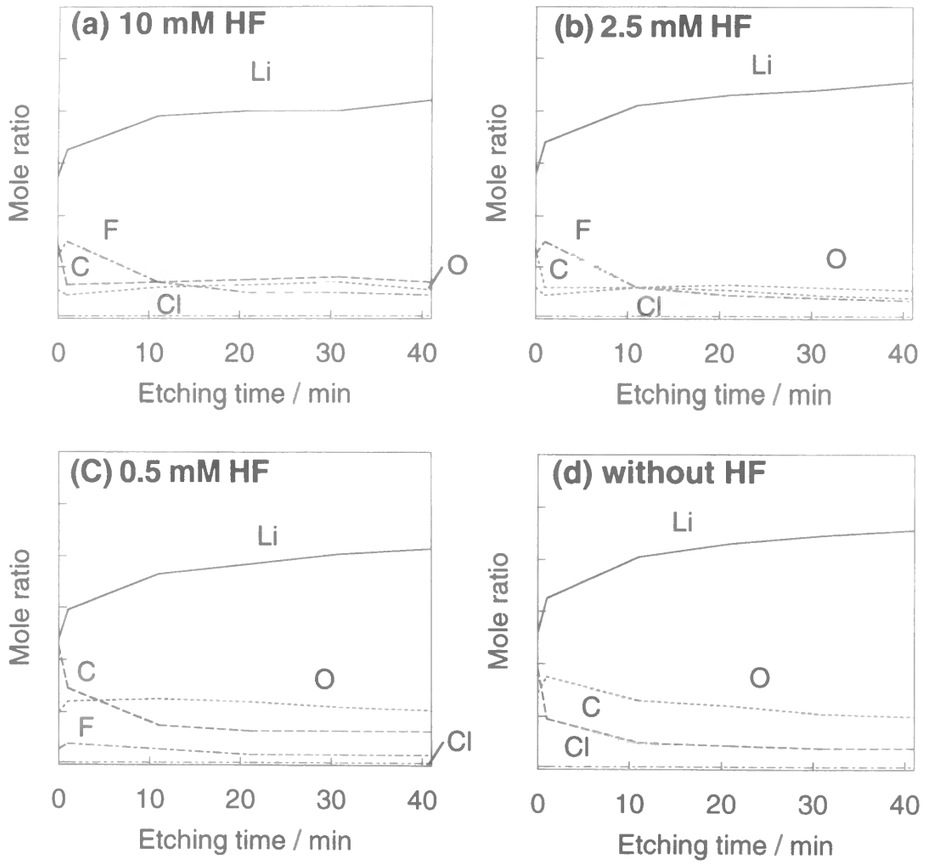

Figure 4-9 XPS depth profiles for the elements in the surface film formed on lithium deposited on the Ni substrate at 0.2 mA cm^{-2} from PC containing 1.0 M $LiClO_4$ and (a) 10 mM HF, (b) 2.5 mM HF, (c) 0.50 mM HF, or (d) without HF.

Figure 4-10 shows the dependence of condition of surface film and morphology of lithium on current density and HF content. This figure exhibits that the high concentration and the low current density were necessary for the smooth deposition of lithium particles. The local deposition of dendritic lithium (as same as shown in Figures 4-1 (c-e) and Figures 4-5 (c-e)) was observed at the relatively low content of HF and the relatively high current density.

In conclusion, HF in the PC electrolyte affects the modification of the surface of lithium during the electrodeposition. This effect can be attributed to the acid-base reaction of some organic or oxide compounds (these compounds are produced by the reactions of lithium with the electrolyte or residual moisture) in the surface film with HF, and the direct reaction of lithium metal with HF. From the XPS analysis and the SEM observations, it can be seen that dendrite formation takes place at localized sites on the surface, as illustrated in Figure 4-11. The surface film is mostly uniform, but there are several sites with an undesirable effect on the hemispherical lithium deposition when the concentration of HF is not adequate. If the dendrite formation of lithium is related to the current

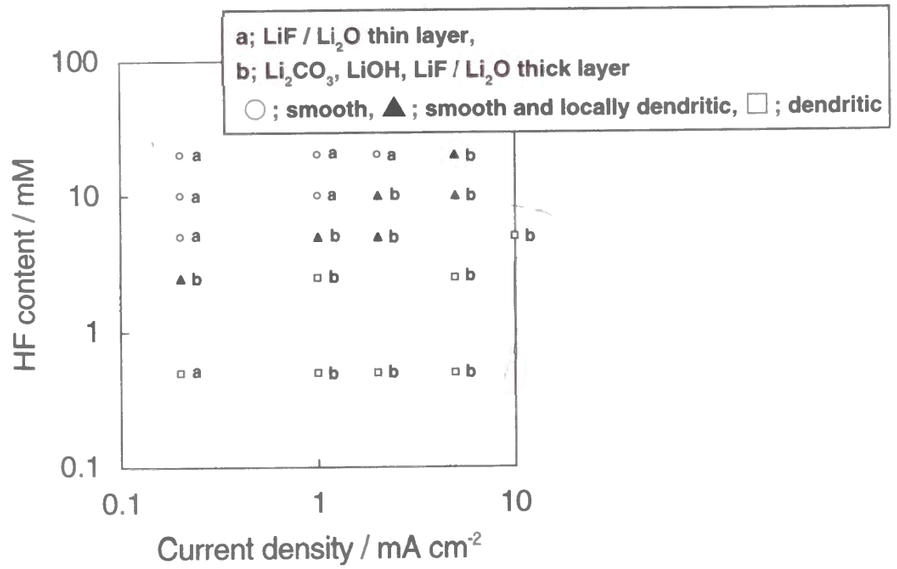

Figure 4-10 Dependence of condition of surface film and morphology of lithium on current density and HF content in 1.0 M $LiClO_4$ / PC.

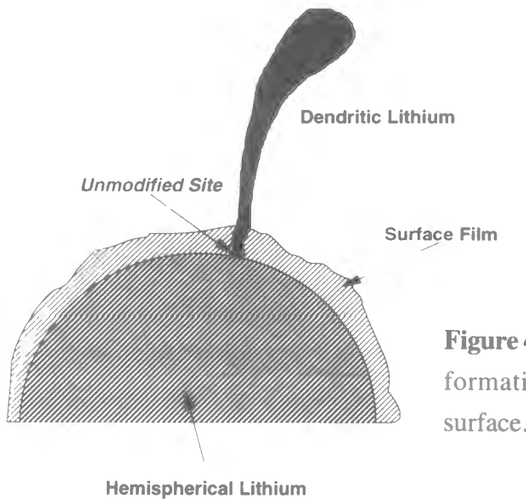

Figure 4-11 Schematic illustration of dendrite formation at a localized site on a lithium surface.

distribution, such variations in the surface film (e.g. cracks in the surface film) formed during the growth of lithium strongly influences dendrite formation.

4-3-3 Impedance behavior of lithium electrodeposited from PC electrolytes containing HF

Figure 4-12 shows the Cole-Cole plots for lithium deposited from propylene carbonate containing 1.0 mol dm^{-3} $LiClO_4$ (a) without HF or with (b) 0.50 mmol dm^{-3} HF, (c) 2.5 mmol dm^{-3}, or (d) 10 mmol dm^{-3}. The morphology of lithium was dendritic or hemispherical, depending on the concentration of HF in the PC electrolyte (see SEM Figures 4-5 and 4-6). Correspondingly, each Cole-Cole plot for lithium deposited from these four electrolytes was different, suggesting that the electrochemical property of the lithium-electrolyte interface depends on the HF content. Generally, a semicircle observed in the Cole-Cole plot is related to the charge-transfer process, or the surface film impedance when the surface film works as an ionic conductor [43-46]. Therefore, the diameter of a semicircle observed in the Cole-Cole plots corresponds to the resistance of the charge-transfer or the surface film. The charge transfer resistance can be calculated from the exchange current density using Equation (7) ;

$$R_{ct} = \frac{RT}{nFi_0} \qquad (7)$$

(R_{ct} , charge transfer resistance; R , molar gas constant; T , temperature; n , number of electrons,

F, Faraday constant; i_0, exchange current). Other researchers using microelectrodes have estimated the exchange current density of lithium to be in the range of about 3 mA cm^{-2} to 30 mA cm^{-2} [93-95]. Therefore, the charge transfer resistance may be in the range of about 0.9 to 9 Ω cm^2. As for frequency, it has been suggested that the characteristic frequency in a semi-circle is the inverse of the time constant of the interfacial electrochemical process [42-43]. Other researchers have suggested that the characteristic frequency for the charge transfer process of lithium is about several kHz [46]. On the other hand, when the electrode surface is very porous and highly rough, a large current distribution occurs on the electrode surface, leading to distortion of the semicircle [96]. A distorted semicircle in high frequency region and a highly distorted and overlapped impedance locus in low frequency region were observed for a dendritic lithium, as shown in Figure 4-12 (a). The semicircle at the high frequency may be due to the charge-transfer process or the surface film. The distortion of the semicircle and the forementioned complexity of the impedance at the low frequency may be due to variations in the shape of the deposition and the surface film. In Figure 4-12 (b), the slightly distorted semicircles were observed at the high and middle frequency regions. The appearance of the semicircle at mid-frequency range may be related to the change in structure of the surface film caused by HF addition. At the low frequency region, the complicated impedance locus was again observed. Since these lithium deposits were also dendritic, this complicated impedance behavior may be related to a complex situation in the surface state. On the other hand, the Cole-Cole plots in Figure 4-12 (c) and (d) show well defined semi-circles in the high frequency region. In the low frequency region, lines at an angle of about 45° were observed. From the comparison of these Cole-Cole plots with the XPS spectra in Figure 4-7 , it can be seen that the surface film consisting of LiF and Li_2O is adequately uniform for the formation of smooth lithium deposits on the

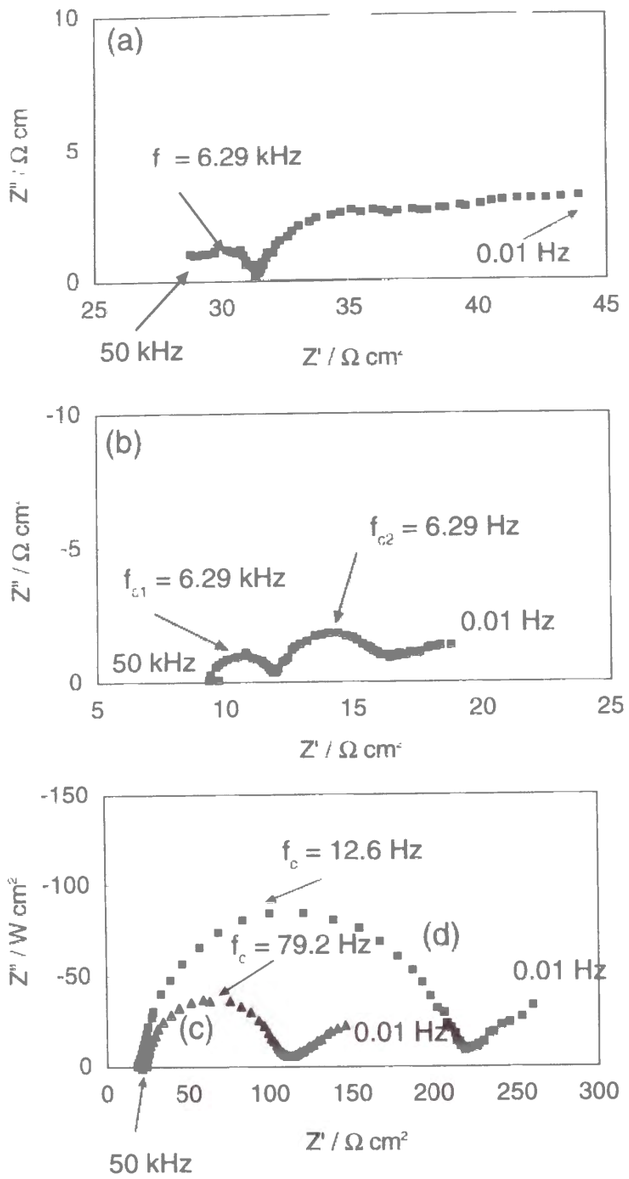

Figure 4-12 Cole-Cole plots for lithium deposited on the Ni substrate from PC containing 1.0 M $LiClO_4$ (a) without HF, or with (b) 0.50 mM HF, (c) 2.5 mM HF or (d) 10 mM HF at 0.2 mA cm^{-2} (charge ; 1.0 C cm^{-2}). Impedance measurement for lithium was performed at open circuit voltage after electrodeposition of lithium, the amplitude of the alternating current was 5 mV, and the frequency range was 50 kHz 0.01 Hz The sign fc indicates the characteristic frequency.

Ni substrate. The semicircles in the high frequency region are too large to be attributed to the charge transfer resistance and the characteristic frequency is too low to be attributed to the charge transfer process. Therefore, in these cases the resistances obtained from these Cole-Cole plots correspond to the resistance of the surface film. The diameter (70 Ω cm^2) of the semicircle in Figure 4-12 (c) was smaller than that (about 200 Ω cm^2) in Figure 4-12 (d). The low resistance of the surface film on lithium deposited from PC electrolyte containing 2.5 mmol dm^{-3} HF may be due to some dendritic lithium deposited at several localized points. The influence of the dendritic lithium on the resistance of the surface film is confirmed by the difference between the characteristic frequencies seen in Figure 4-11 (c) and (d).

4-3-4 Polarization-time transients during electrodeposition from PC electrolytes containing HF

The formation of the surface film and the morphology of lithium influences the polarization of lithium during the electrodeposition. Figure 4-13 shows the charge curves for propylene carbonate containing 1.0 mol dm^{-3} $LiClO_4$ and various HF concentrations at 0.2 mA cm^{-2}. The polarizations for the electrodeposition of lithium in a dendritic form were smaller than those for the same electrodeposition in a hemispherical shape. The overall polarization of electrodeposition is generally the result of a combination of the activation polarization, concentration polarization, electrolyte bulk resistance, and surface film resistance. From the charge transfer resistance of lithium (see the discussion of impedance), the activation overvoltage at 0.2 mA cm^{-2} can be estimated to be in the range of about 0.18 mV to 1.8 mV (at such a narrow overvoltage, the current is linearly related to overvoltage). Therefore, the activation overvoltage can not be a main component of the overvoltage in the electrodeposition of lithium at a high HF concentration. Furthermore, the concentration polarization in the electrolyte can be expected to be insignificant for the polarization of lithium deposition because the current density is low. The bulk resistance in our experiment was found to be 10 ~ 20 Ω cm^2 (see the impedance spectra in Figure 4-

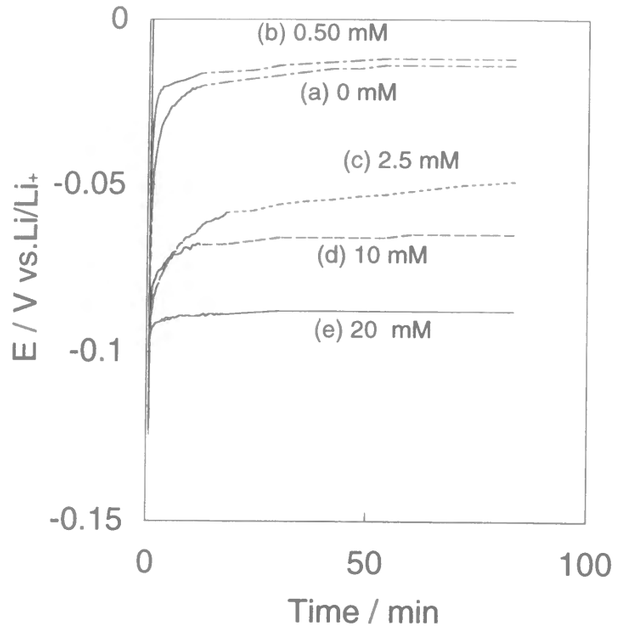

Figure 4-13 Charge curves on the Ni substrate from PC containing 1.0 M $LiClO_4$ (a) without HF, or (b) with 0.50 mM HF, (c) 2.5 mM HF, (d) 10 mM HF, or (e) 20 mM HF at 0.2 mA cm^{-2} (charge ; 1.0 C cm^{-2}).

12), leading to an overvoltage of 2 ~ 4 mV at most. Therefore, the polarization during the lithium electrodeposition must be due to changes in the surface area, which are related to the morphology of lithium, or to the surface film resistance, which is related to the physical properties of the surface film on lithium. The surface area of the dendritic lithium is much larger than that of the hemispherical lithium, as was seen in the scanning electron micrographs for both dendritic and hemispherical lithium (see in Figures 4-5 and 4-6). The differences in polarization thus seem to correlate with the surface areas of the lithium deposits, suggesting that the polarization can be explained by a simple geometrical area for the electrochemical deposition of lithium. However, the difference between the surface area of the two deposit forms is too large to explain the quantitative difference between the polarization of electrodepositions for two different morphologies. The characteristics of the surface film of lithium should therefore be taken into consideration for an explanation

of the polarization behavior of lithium electrodes. As a result, the resistance per true area for the surface film on lithium in the hemispherical form may turn out to be smaller than that in the dendritic form. A final observation in support of the argument presented here is that the surface film on the extremely smooth hemispherical lithium is much thinner than that on the dendritic lithium.

4-4 Conclusion

The morphology of lithium deposits is strongly related to the current distribution due to variations in the surface film on lithium. HF in PC electrolytes is very effective for the formation of surface films consisting of LiF/Li_2O which provide a more uniform current distribution. The attainment of such surfaces depends on to two factors:

(1) the surface reaction rate of HF with lithium compounds formed during the electrodeposition.

(2) the electrochemical deposition rate of lithium.

To suppress lithium dendrite formation during the charging process of lithium batteries, both kinetic factors need to be taken into consideration.

Chapter 5
Surface Composition of Highly Smooth Lithium Deposited in Various Carbonate Electrolytes Containing HF

5-1 Introduction

In the previous chapter, effects of deposition current density and HF concentration on the morphology of lithium deposits were discussed for understanding the deposition process. However, the surface composition of lithium deposited in electrolytes containing HF was not quantitatively clear. The HF effect in various kinds of nonaqueous electrolytes has not been also reported, yet. If the above interfacial reaction (LiF/Li_2O formation) is superior to other reactions, the HF effect will be independent of the kind of electrolyte. Therefore, in this chapter, the dependence of the surface and bulk composition and morphology of lithium on components of electrolyte was investigated to confirm the above supposition. Moreover, a semi-quantitative analysis for the surface film on lithium was performed in order to clarify an interfacial structure of lithium metal in nonaqueous electrolytes under a presence of a small amount of HF.

5-2 Experimental

5-2-1 Electrodeposition

A nickel plate (Nilaco Corporation, Japan) was used as a substrate electrode (6 mm × 20 mm). The nickel substrate was polished with fine alumina powders (0.05 μm) to obtain a mirror surface and then dipped in an ultra sonic bath containing pure water and acetone to remove residual alumina powders. Lithium metal foil (Honjoh Metal Company, Japan) was used as the reference and counter electrodes. Propylene carbonate containing 1.0 mol dm^{-3} $LiBF_4$ ($LiBF_4$/PC) or $LiCF_3SO_3$ ($LiCF_3SO_3$/PC), ethylene carbonate-dimethyl carbonate mixture (1:1 in volume ratio) containing 1.0 mol dm^{-3} $LiClO_4$ ($LiClO_4$/EC+DMC), and ethylene carbonate-diethyl carbonate mixture (1:1 in volume ratio) containing 1.0 mol dm^{-3} $LiClO_4$ ($LiClO_4$/EC+DEC) were used as base electrolytes (Mitsubishi Chemical

Co., Japan). The water contents in these electrolytes were less than 20 ppm (1 mmol dm^{-3}), determined by the Karl Fischer Moisture Titrator. Electrolytes containing HF were prepared by an addition of an aqueous hydrofluoric acid solution (46 weight %, Wako Pure Chemical Industries, Ltd., Japan) into these base electrolytes. Concentrations of HF and H_2O in the electrolytes containing HF were 10 mmol dm^{-3} and 14 mmol dm^{-3}, respectively. Therefore, the water content in these electrolytes increased after the addition of HF. An electrochemical deposition of lithium was performed under galvanostatic conditions at 1.0 mA cm^{-2}. The charge density for all electrodepositions was 1.0 C cm^{-2}. After the deposition of lithium , the electrode was washed with a pure PC, DEC, or DMC (Mitsubishi Chemical Co.) to remove electrolyte salts. All procedures were conducted in an argon dry atmosphere (dew point < -90 ˚C) at 30 ˚C.

5-2-2 XPS analysis and SEM observation

The surface condition of the lithium electrodepoisted on the Ni substarte was analyzed with XPS. The morphology of the lithium electrodepoisted was observed with SEM. The sample transfer from the argon dry box to the XPS or the SEM equipment was conducted in the same way as described in the chapter 1. The analysis condition for the XPS or the SEM were also the same as that in the chapter 1.

5-3 Results and Discussion

Figure 5-1 shows the scanning electron micrographs of lithium deposited in various electrolytes at 1.0 mA cm^{-2}. The morphology of lithium deposited on the Ni substrate electrodes in all electrolytes was a dendritic shape having 0.1~1 μm in diameter. On the other hand, the morphology of lithium electrodeposited in various electrolytes containing HF was a hemispherical, as shown in Figure 5-2. The diameter of particles was about 0.3~0.4 μm. The morphologies of deposits all in the tested electrolytes were almost similar except that the deposits in $LiBF_4$/PC containing HF had a slightly roughened shape. These results could mean that the effect of HF in carbonate electrolytes is a dominant component

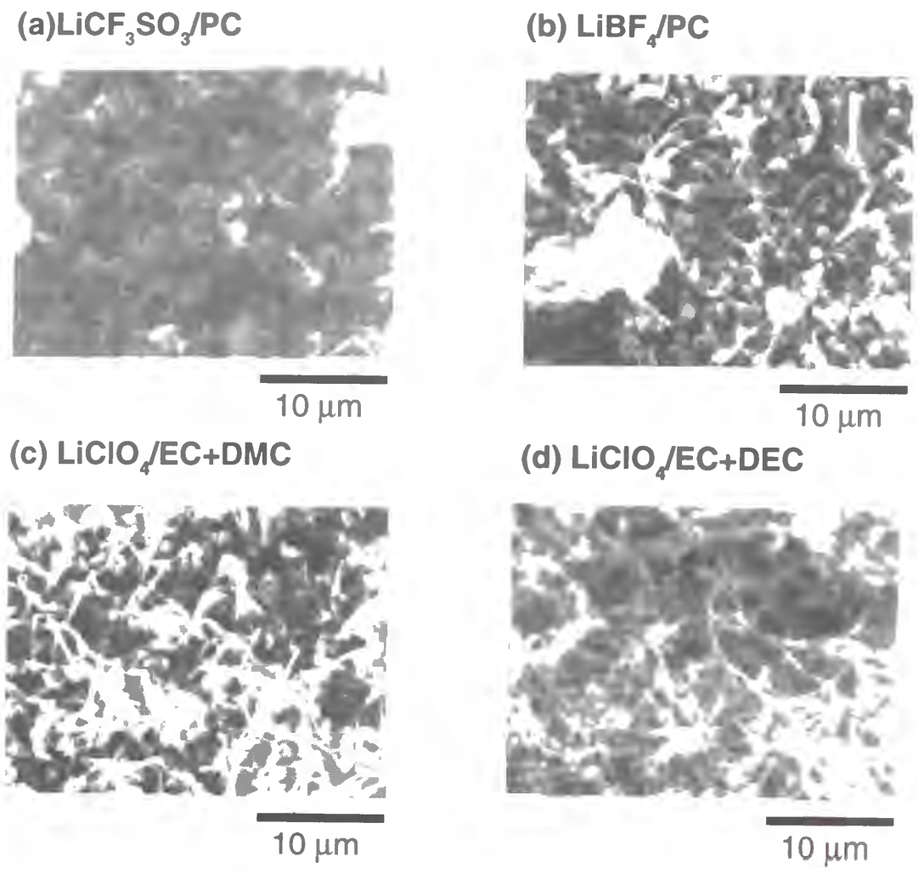

Figure 5-1 Scanning electron micrographs of lithium electrodepoisted (1.0mA cm^{-2}) on the Ni substrate in (a) 1.0 M $LiCF_3SO_3$ / PC, (b) 1.0 M $LiBF_4$ / PC, (c) 1.0 M $LiClO_4$ / EC+DMC, or (d) 1.0 M $LiClO_4$ / EC+DEC,

to the morphology of lithium deposits. As mentioned numerous times previously, the morphology of lithium is strongly related to the surface film composition. The effect of HF on the surface morphological change of the lithium deposits may be understood by elemental composition. In order to confirm this assumption, the deposits' elemental composition were determined by XPS.

Figure 5-3 shows the XPS spectra of Li1s, O1s, and C1s for lithium deposited from 1.0 M $LiCF_3SO_3$/PC at 1.0 mA cm^{-2}. Several depth profile spectra as shown in each figure were obtained by the argon ion etching for various times. Etching times were 0

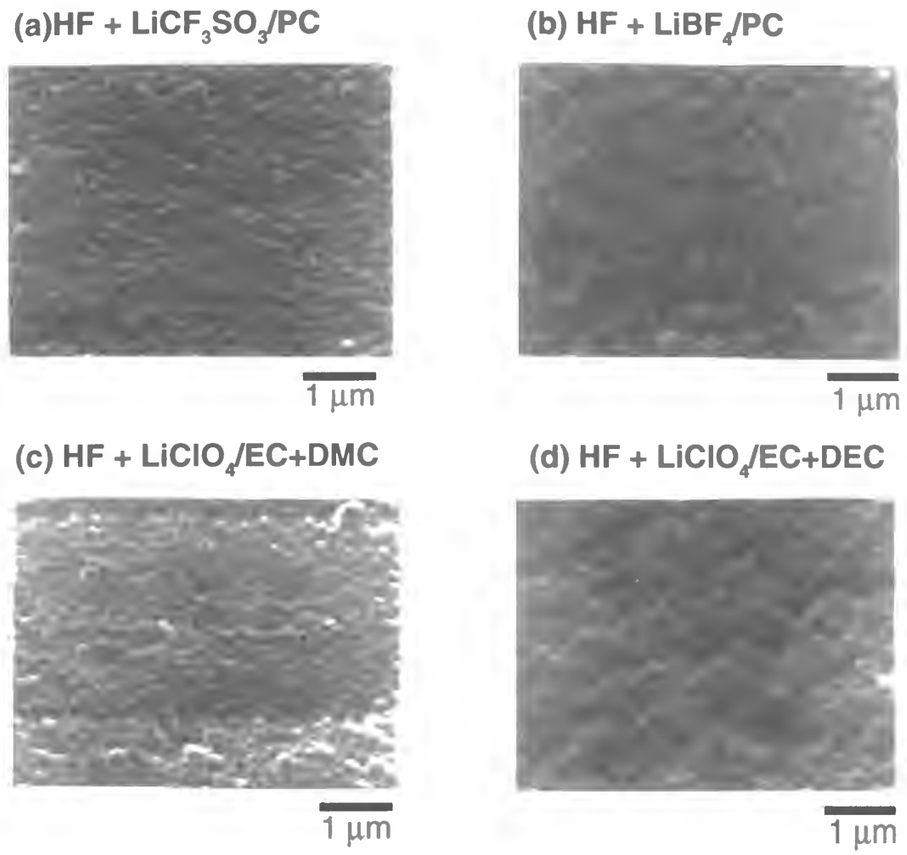

Figure 5-2 Scanning electron micrographs of lithium electrodepoisted (1.0mA cm^{-2}) on the Ni substrate in (a) 1.0 M $LiCF_3SO_3$ / PC, (b) 1.0 M $LiBF_4$ / PC, (c) 1.0 M $LiClO_4$ / EC+DMC, or (d) 1.0 M $LiClO_4$ / EC+DEC containing 10 mM HF and 14 mM H_2O.

min, 1 min, 11 min, 21 min, 31 min, and 41 min from top to bottom. The etching rate is roughly estimated to be 5 Å min^{-1} from the sputtering coefficient and the ion beam current. A peak at around 55.0 eV in the Li1s spectrum can be attributed to Li_2CO_3 or $LiOCO_2R$. This peak decreased with the argon ion etching, and then the peak at 53.7 eV attributed to Li_2O becomes prominent. Since this Li_2O peak was observed even after the argon ion etching for 41 min, the Li_2O layer thickness on lithium can be estimated to be more than 200 Å. A intense peak at 285.0 eV in the C1s spectrum was observed before the argon ion etching. If this peak is attributed to hydrocarbon adsorbed on the sample in the XPS

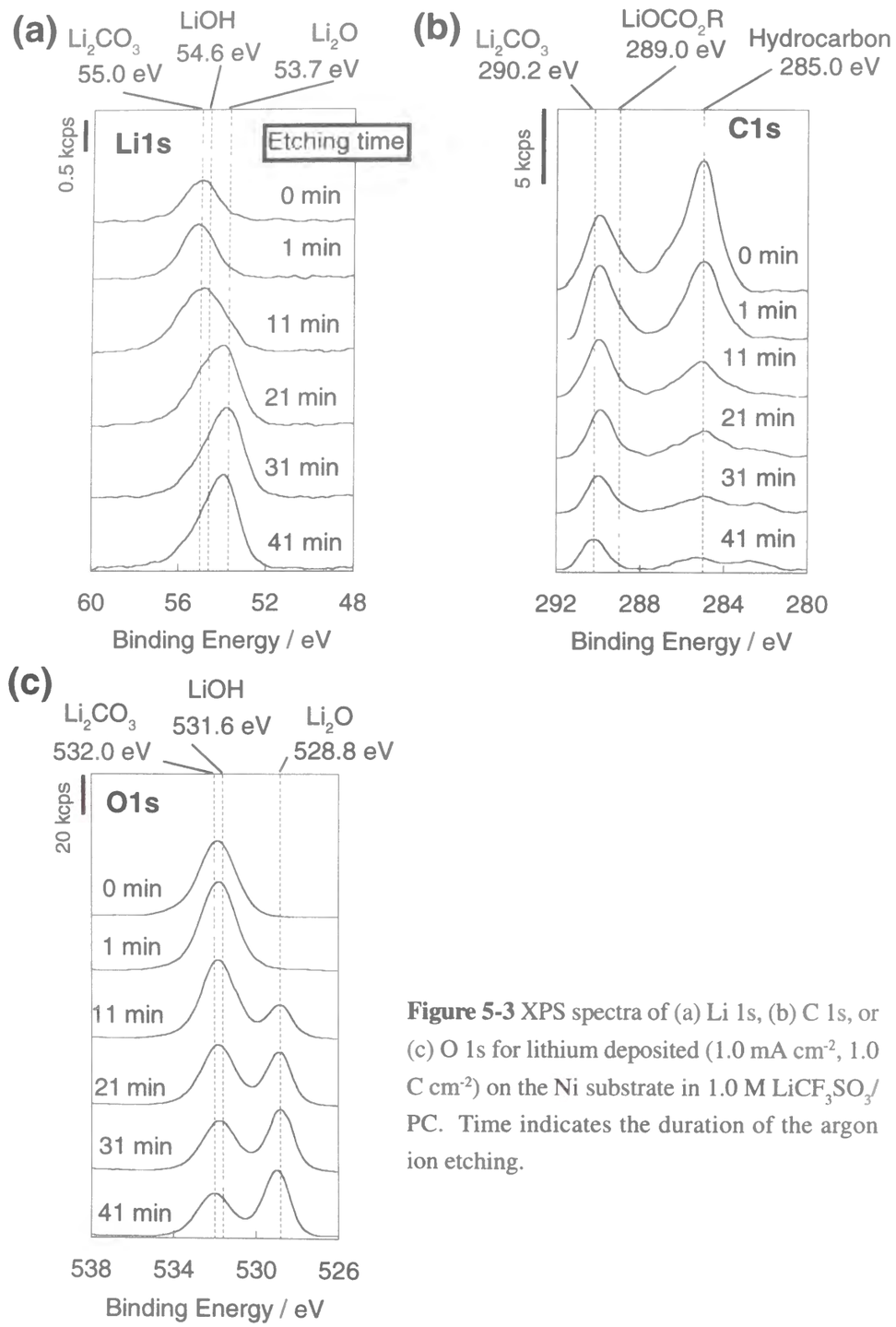

Figure 5-3 XPS spectra of (a) Li 1s, (b) C 1s, or (c) O 1s for lithium deposited (1.0 mA cm^{-2}, 1.0 C cm^{-2}) on the Ni substrate in 1.0 M $LiCF_3SO_3$/PC. Time indicates the duration of the argon ion etching.

analysis chamber, its peak intensity should be markedly decreased by the radiation of argon ion beam for a short time. In the C1s spectra, the peak at 285.0 eV decreased after the first argon ion etching, but did not completely diminished. This spectrum change shows that the peak at 285.0 eV corresponds to not only residual hydrocarbon gas adsorbed on the sample but also reduction products of solvent. A peak around 290~289 eV in the C1s spectra is assigned to Li_2CO_3 or $LiOCO_2R$. The intensities of these peaks decreased

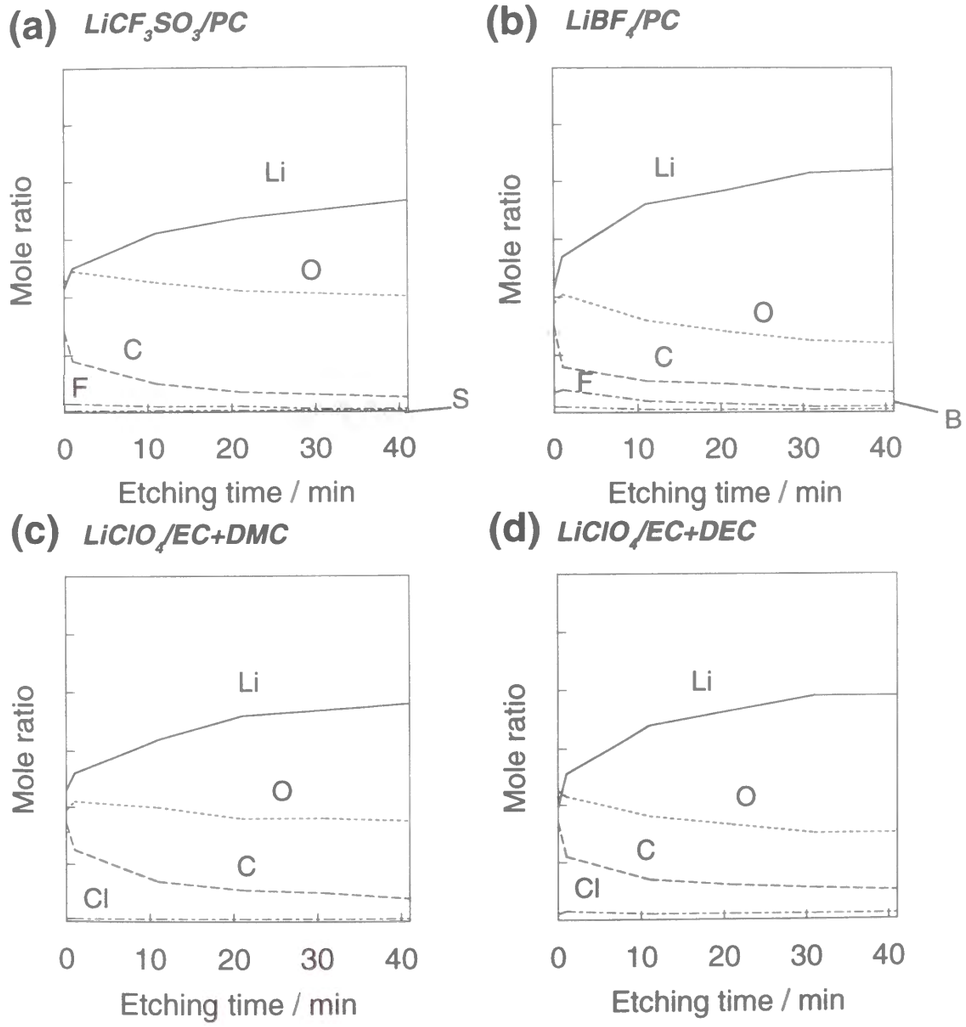

Figure 5-4 XPS depth profiles for each element in the surface film formed on lithium deposited (1.0 mA cm^{-2}, 1.0 C cm^{-2}) on the Ni substrata in (a) 1.0 M $LiCF_3SO_3$/PC, (b) 1.0 M $LiBF_4$/PC, (c) 1.0 M $LiClO_4$/EC+DMC, and (d) 1.0 M $LiClO_4$/EC+DEC.

after the argon ion etching. Therefore, the Li_2CO_3 or $LiOCO_2R$ layer is present at the outer portion of the deposits. The peaks attributed to Li_2CO_3, $LiOCO_2R$, or LiOH were observed around 532~531 eV in the O1s spectrum before the argon ion etching, and then decreased after etching for 1 min. On the other hand, the peak attributed to Li_2O was strongly observed at 528.8 eV after the consecutive argon ion etching. The information obtained in the Li1s, C1s, and O1s spectra are consistent. The lithium deposits formed in a 1.0 M $LiCF_3SO_3$/PC are covered with Li_2CO_3, or $LiOCO_2R$, LiOH, and Li_2O layers.

Figure 5-4 shows the XPS depth profiles for the deposits formed in various electrolytes ($LiCF_3SO_3$, $LiBF_4$/PC, $LiClO_4$/EC+DMC, and $LiClO_4$/EC+DEC). The depth profiles represent a distribution of the mole ratio of each element in the film. The amount of oxygen or carbon was lager than that of fluorine, chlorine, sulfur, or boron in the deposits formed in all the electrolytes. Moreover, the Li1s, O1s, and C1s spectra for lithium electrodeposited in three electrolytes ($LiBF_4$/PC, $LiClO_4$/EC+DMC, and $LiClO_4$/EC+DEC, (the spectra are not shown in this paper.) were similar to those in Figure 5-3. Therefore, the surface film formed on lithium electrodeposited in all electrolytes used consists of Li_2CO_3, $LiOCO_2R$ and Li_2O. According to literature [22,24] and the previous chapter, these compounds may be formed by the electrochemically reductive decomposition of solvent and moisture.

Figure 5-5 shows the XPS spectra of C1s for lithium deposited in various electrolytes containing a small amount of HF. Little differences were observed in these C1s spectra. All peaks attributed to hydrocarbon, Li_2CO_3, and $LiOCO_2R$ before the argon ion etching were weaker compared with those for lithium electrodeposited in electrolytes without HF. Peaks corresponding to Li_2CO_3 and $LiOCO_2R$ were diminished after the argon ion etching. These results clearly indicate that a small amount of Li_2CO_3 and $LiOCO_2R$ is present only at the outermost portion of the deposits.

Figure 5-6 shows the XPS spectra of F1s for lithium deposited in various electrolytes containing a small amount of HF. The peak observed at 685.5 eV in all spectra is attributed to LiF. The peak intensity of LiF was constant before and after the argon ion

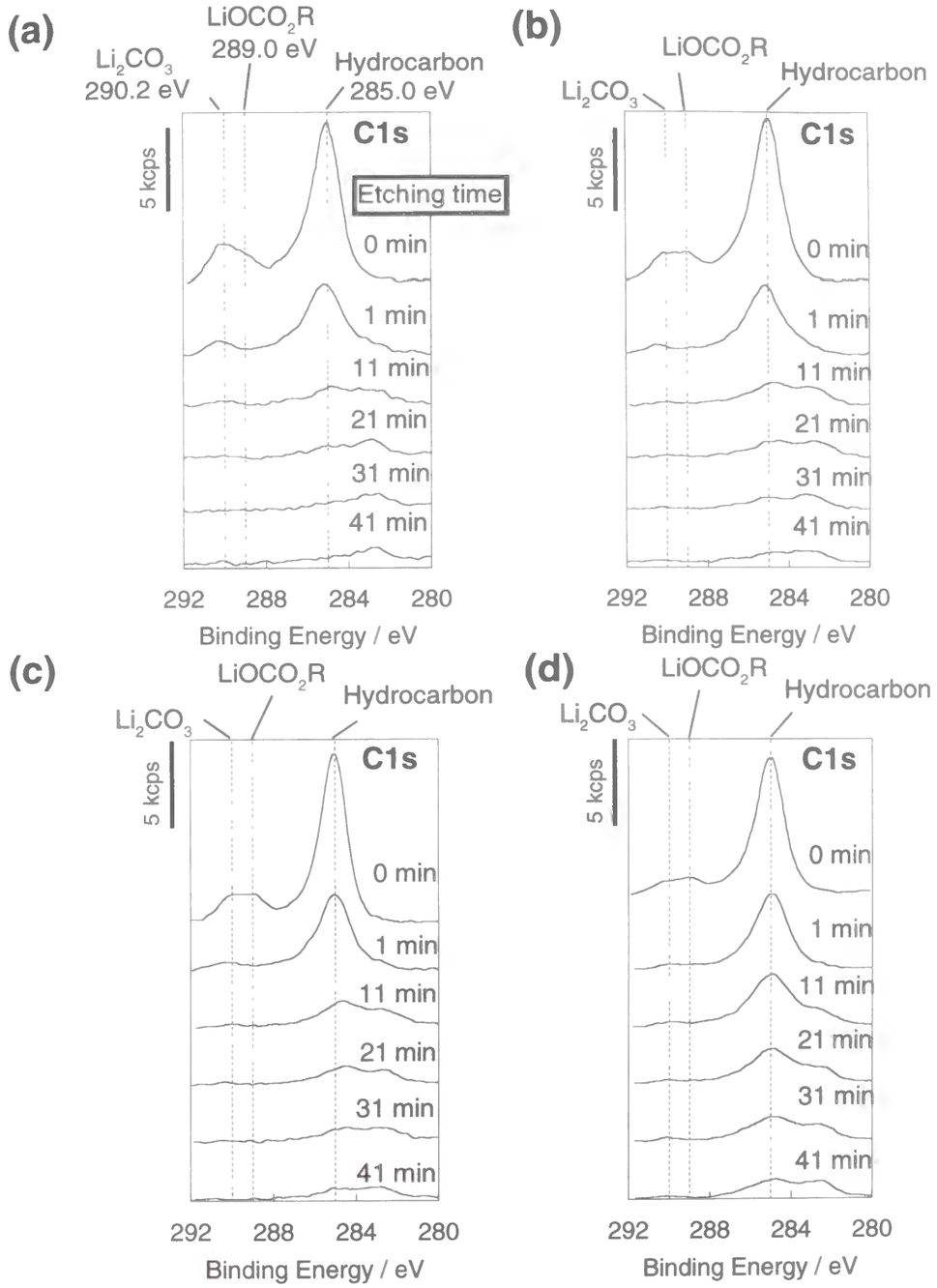

Figure 5-5 XPS spectra of C1s for lithium deposited (1.0 mA cm^{-2} , 1.0 C cm^{-2}) on the Ni substrate in (a) 1.0 M $LiCF_3SO_3$/PC, (b) 1.0 M $LiBF_4$/PC, (c) 1.0 M $LiClO_4$/ EC + DMC, and (d) 1.0 M $LiClO_4$/EC + DEC containing 10 mM HF + 14 mM H_2O.

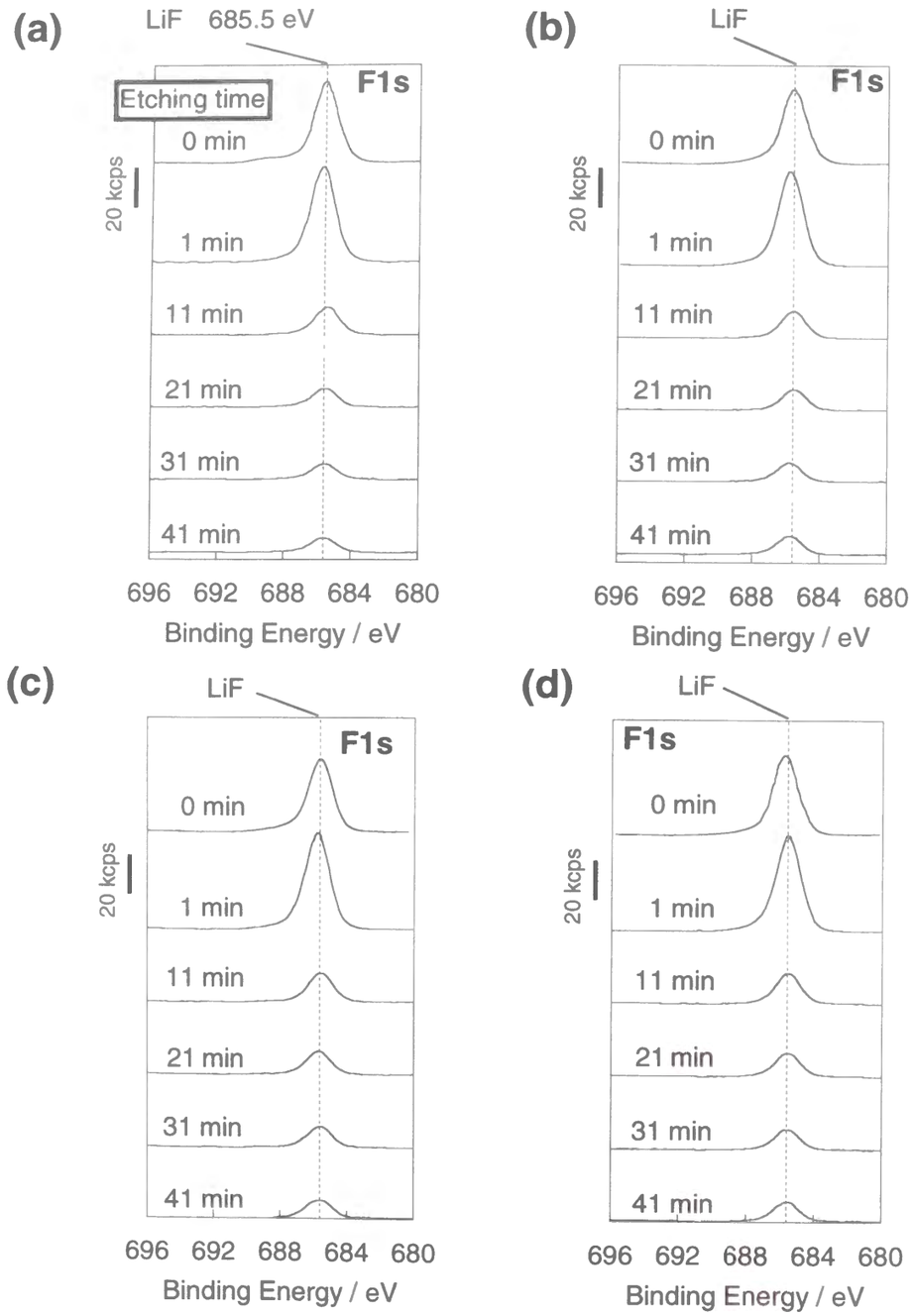

Figure 5-6 XPS spectra of F1s for lithium deposited (1.0 mA cm^{-2} , 1.0 C cm^{-2}) on the Ni substrate in (a) 1.0 M $LiCF_3SO_3$/PC, (b) 1.0 M $LiBF_4$/PC, (c) 1.0 M $LiClO_4$/ EC + DMC, and (b) 1.0 M $LiClO_4$/EC + DEC containing 10 mM HF + 14 mM H_2O.

etching for 1 min, but decreased markedly during further argon ion etching. This peak intensity change shows that lithium electrodeposited in the electrolytes containing HF is covered with a thin LiF layer.

Figure 5-7 shows the XPS spectra of O1s for lithium deposited in various electrolytes containing HF. No dependence of the surface film composition on the electrolyte was observed, consistent with the trends in the F1s and C1s spectra as shown previously. The peaks attributed to Li_2CO_3, $LiOCO_2R$, or LiOH were observed in the O1s spectra before the argon ion etching. The peak attributed to Li_2O became the main peak after the argon ion etching. The peak around 532 eV after the argon ion etching is attributed to LiOH because Li_2CO_3 or $LiOCO_2R$ is not observed after the argon ion etching for 11 min in the C 1s spectra as shown in Figure 5-5. These results demonstrate that LiOH, Li_2CO_3, or $LiOCO_2R$ are mainly present at the outermost portion of the deposits and Li_2O is exclusively mainly present in the bulk.

Figure 5-8 shows the XPS spectra of Li1s for lithium deposited in various electrolyte containing a small amount of HF. These spectra are much different from those for lithium deposited in the electrolytes without HF. The spectra in Figure 5-8 (a-d) were very similar for all electrolytes, and show that the surface film composition of lithium electrodeposited in electrolytes containing HF was independent of the kind of solvent or salt, consistent with the SEM observations (see Figure 5-2). The peak at 56.0 eV in Figure 5-8 (a-d) was attributed to LiF. The LiF peak markedly decreased after the argon ion etching, then the Li metal peak at 52.3 eV became more intense with the argon ion etching, accompanied by a shoulder peak around 54 eV. This shoulder peak is attributed to Li_2O at 53.7 eV because the O1s spectra in Figure 5-7 also indicated the presence of Li_2O in the surface film. This spectrum change with the argon ion etching represents that lithium electrodeposited in all these electrolytes containing HF is covered with the bi-layer surface film consisting of LiF (outer layer) and Li_2O (inner layer).

The spectra of Li1s was not changed with the argon ion etching for 11 min. Therefore, the thickness of the surface film is roughly estimated to be 50 Å. However,

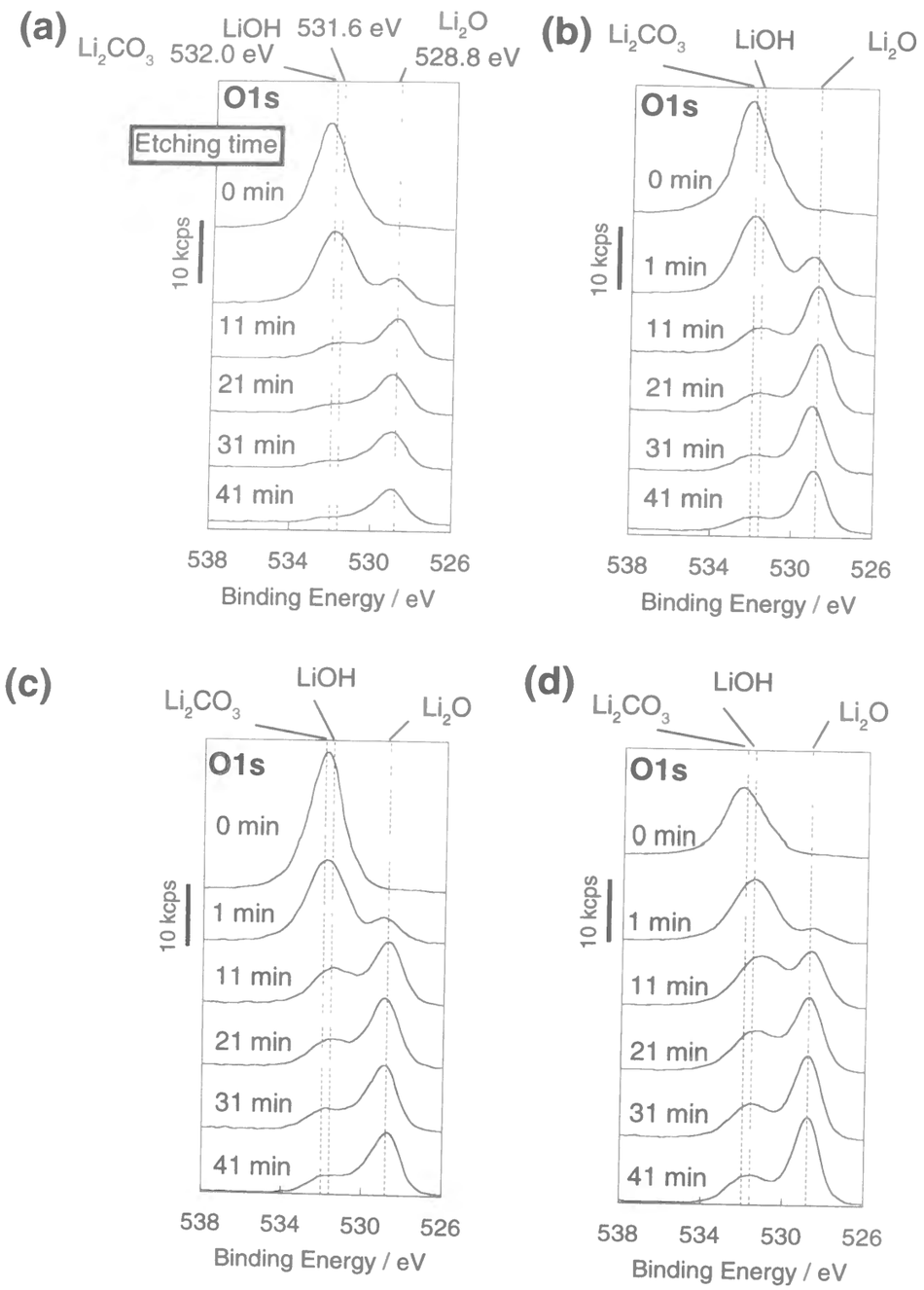

Figure 5-7 XPS spectra of O1s for lithium deposited (1.0 mA cm^{-2} , 1.0 C cm^{-2}) on the Ni substrate in (a) 1.0 M $LiCF_3SO_3$/PC, (b) 1.0 M $LiBF_4$/PC, (c) 1.0 M $LiClO_4$/ EC + DMC, and (d) 1.0 M $LiClO_4$/EC + DEC containing 10 mM HF + 14 mM H_2O.

considering variations in the argon ion beam radiation to the sample and the oxidation of lithium metal by residual oxygen and moisture in the XPS analysis chamber, it might be expected to be less than 50 Å. On the other hand, the thickness of the surface film may be estimated from the XPS spectra before the argon ion etching. The peak corresponding to lithium metal were already observed in Figure 5-8 before the argon ion etching. The observation of the peak at 52.3 eV is due to the detection of photoelectrons of Li1s from lithium metal under the surface film. Generally in the XPS analysis, peak intensities of elements in a substrate covered with surface film can be estimated using peak intensities of elements in a substrate without a surface film, an escape depth of photoelectron emitted from a substrate, and a film thickness [97]. Therefore, using the peak intensity of lithium metal before and after the argon ion beam radiation for 41 min, the thickness of the surface film on lithium metal was calculated by the follow equation (1) [97].

$$\frac{I_i}{I_0} = \exp\left(\frac{-d}{\lambda_{Li}}\right) \qquad (1)$$

I_i ; intensity of the peak of Li metal before Argon ion etching

I_0 ; intensity of the peak of Li metal after Argon ion etching for 41 min

(Intensity of the peak of bare lithium)

d ; thickness of surface film

λ_{Li} ; escape depth of Li1s photoelectron (14 Å for Li_2O or LiF) [97]

We performed the curve deconvolution of the XPS spectra in order to obtain the peak intensity of lithium metal, as shown in Figure 5-9. The Li1s XPS spectra before the argon ion etching were separated in three curves of LiF, LiOH/Li_2CO_3, and lithium metal. On the other hand, the Li1s spectra after the argon ion etching for 41 min were separated in four curves of LiF, Li_2O, LiOH, and lithium metal. The peak position and the full width at half maximum (FWHM) of LiF and Li_2O were referred to the XPS spectra of standard samples. The FWHM of the Li1s XPS spectra of lithium metal was reported by Armstrong et al. [98]. They reported that the FWHM of lithium metal is about 1.1 eV and the shape of the Li1s XPS spectra of lithium metal is asymmetric tailing to high energy [98]. We treated

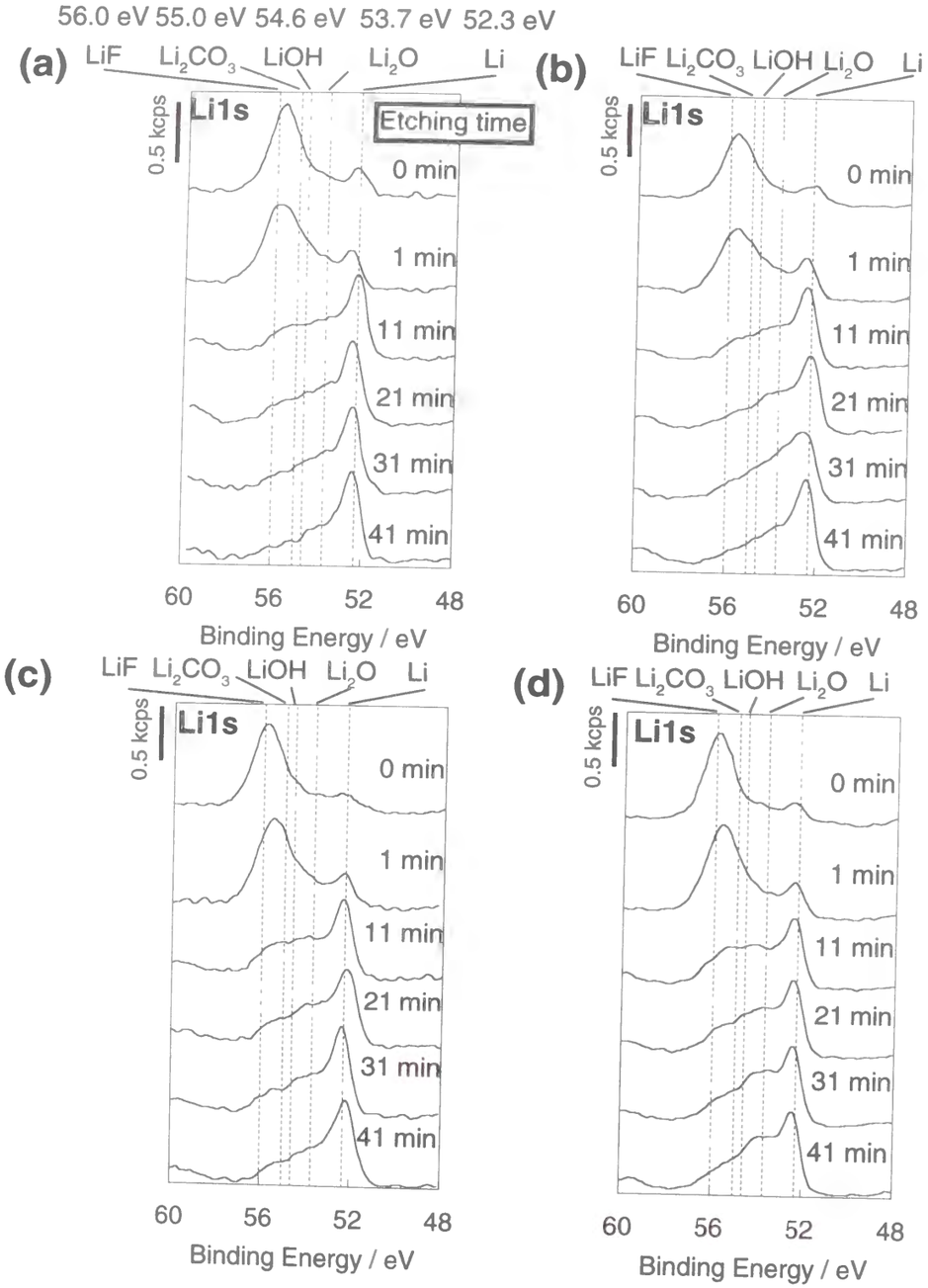

Figure 5-8 XPS spectra of Li1s for lithium deposited (1.0 mA cm^{-2} , 1.0 C cm^{-2}) on the Ni substrate in (a) 1.0 M $LiCF_3SO_3$/PC, (b) 1.0 M $LiBF_4$/PC, (c) 1.0 M $LiClO_4$/ EC + DMC, and (d) 1.0 M $LiClO_4$/EC + DEC containing 10 mM HF + 14 mM H_2O.

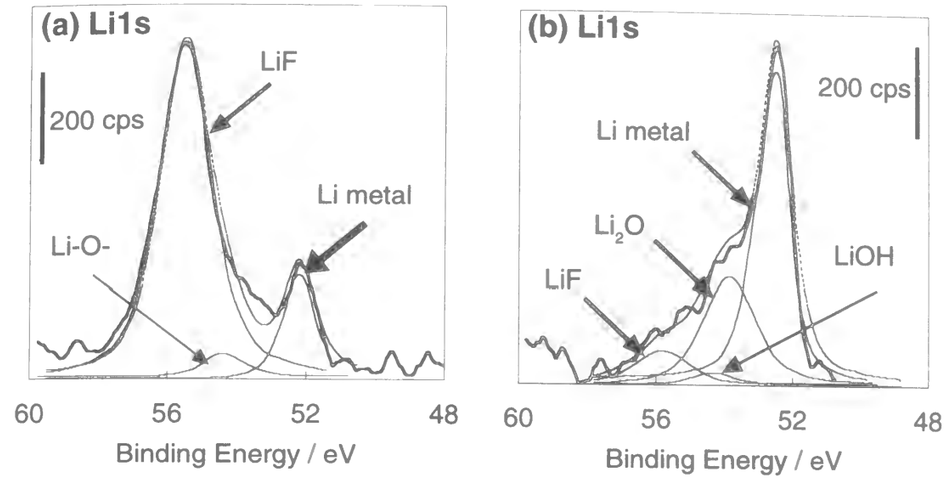

Figure 5-9 Curve separation of XPS spectra of Li1s (Fig. 5-8 (a)) for lithium deposited (1.0 mA cm^{-2} , 1.0 C cm^{-2}) on the Ni substrate in 1.0 M $LiCF_3SO_3$/PC containing 10 mM HF + 14 mM H_2O, (a) ; before the Argon ion etching, (b) ; after the Argon ion etching for 41 min. Dot line is the total locus of each separated curve. Li-O- in figure means Li_2CO_3 or LiOH. FWHM of LiF and Li_2O are 1.9 eV and 1.8 eV, respectively.

Table 5-1 The surface film thickness estimated by the XPS analysis

electrolyte*	d
HF + $LiCF_3SO_3$ / PC	16 Å
HF + $LiBF_4$ / PC	21 Å
HF + $LiClO_4$ / PC	16 Å
HF + $LiClO_4$ / EC+DMC	21 Å
HF + $LiClO_4$ / EC+DEC	18 Å

*all electrolytes contain 10 mM HF and 14 mM H_2O

d ; the thickness of the surface film estimated by the XPS analysis

the XPS spectra of lithium metal as symmetric peak. Table 5-1 shows the thickness of the surface film formed on lithium electrodeposited in various electrolytes containing HF. The thickness of the surface film was about 20 Å. However, this result is obtained under the assumption that an uniform surface film is formed on the substrate. The peaks of the compounds (LiF and Li_2O) in the surface film were in fact observed in the Li1s spectra

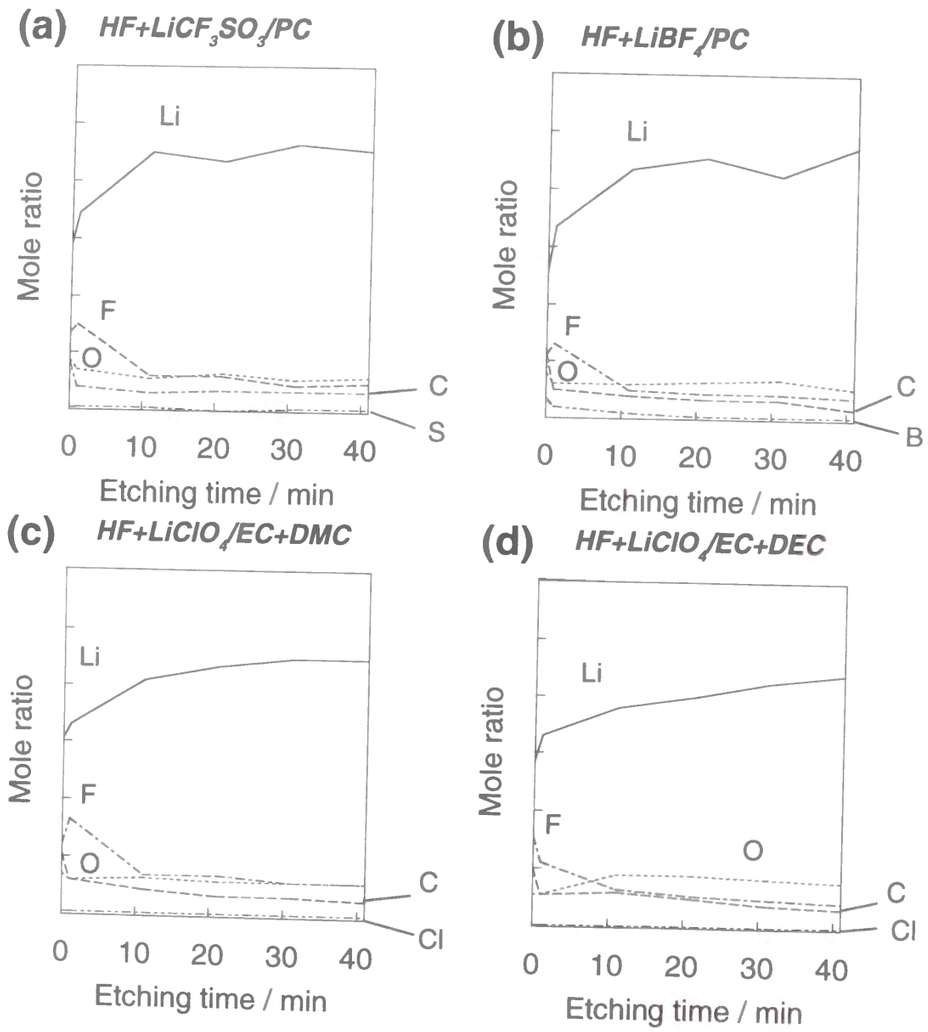

Figure 5-10 XPS depth profiles for each element in the surface film formed on lithium deposited (1.0 mA cm^{-2}, 1.0 C cm^{-2}) on the Ni substrata in (a) 1.0 M $LiCF_3SO_3$/PC, (b) 1.0 M $LiBF_4$/PC, (c) 1.0 M $LiClO_4$/EC+DMC, and (d) 1.0 M $LiClO_4$/EC+DEC containing 10 mM HF + 14 mM H_2O.

even after the argon ion etching for 41 min. Therefore, considering that the roughness of the deposits and the non-uniformity of the argon ion beam radiation and the oxidation of lithium metal by residual oxygen and moisture in the XPS analysis chamber, the true thickness may be larger than the above calculated thickness. From the XPS depth profiles and the above calculation, it can be said that the thickness of the surface film formed on lithium electrodeposited in electrolytes containing HF is the range from 20 to 50 Å. The LiF layer is so compact that further interfacial reaction does not occur, leading to the extremely stable presence of such ultra-thin film on lithium metal in nonaqueous electrolyte.

From the XPS depth profiles in Figure 5-10, it was observed that the distribution of fluorine, oxygen, and carbon in the surface film was independent of the kind of carbonate electrolyte containing HF and the amount of chlorine, boron, or sulfur was little in the surface film. Moreover, the amount of fluorine was large at the outer part of the surface film. From the XPS depth profiles and spectra, it can be said that the surface film formed of the lithium electrodeposited in all carbonate electrolytes containing HF consists of the outer LiF layer (contains a small amount of Li_2CO_3, $LiOCO_2R$, LiOH) and the inner Li_2O layer (contains a small amount of LiOH). This structure was also already found in lithium electrodeposited in PC containing 1.0 mol dm^{-3} $LiClO_4$ and a small amount of HF as shown in the chapter 3 and 4.

5-4 Conclusion

The morphology of lithium electrodeposited in various nonaqueous carbonate electrolytes was almost dendritic. The surface film formed on the dendritic lithium consisted of the outer layer of $LiOCO_2R$, Li_2CO_3, and LiOH and the inner layer of Li_2O. On the other hand, lithium having a hemispherical shape was smoothly electrodeposited in electrolyte containing a small amount of HF. This smooth lithium was covered with a ultra-thin (20-50 Å) surface film consisting of LiF/Li_2O layer. The surface film was independent of the kind of the carbonate electrolyte containing HF. These phenomena reveal that the surface composition of lithium is highly sensitive to HF existing as minor

species in nonaqueous electrolyte rather than carbonate solvent and salt as major species. This is because LiF is a final product in lithium surface and is highly stable in nonaqueous electrolytes. In conclusion, this study indicates that the stable and thin surface film on lithium formed by HF establish more uniform interface which provides the suppression of deposition of dendritic lithium.

Chapter 6
Surface Condition Changes in Lithium Metal Deposited in Nonaqueous Electrolyte Containing HF by Dissolution-Deposition Cycles

6-1 Introduction

Lithium electrodeposited in the electrolytes containing HF has a smooth hemispherical form. This is due to the modification of the surface film formed on the lithium metal. However, the surface film on lithium deposits may be changed by the discharge and charge cycle. In this case, the performance of discharge and charge cycling will not suitable for practical use. Therefore, the change in the surface film must be investigated in order to obtain a higher efficiency in the discharge and charge cycles. In this chapter, the surface condition change in lithium, which was deposited in propylene carbonate electrolyte containing HF, was investigated using scanning electron microscopy (SEM) and X-ray photoelectron spectroscopy (XPS), and electrochemical impedance spectroscopy (EIS) during the deposition and dissolution cycles.

6-2 Experimental

A nickel plate (Nilaco Corporation, Japan) was used as the substrate electrode (6 mm $\times$ 20 mm). Propylene carbonate containing 1.0 mol dm^{-3} $LiCF_3SO_3$ ($LiCF_3SO_3$/PC) was used as a base electrolyte (Mitsubishi Chemical Co., Japan). The water contents in these electrolytes were less than 20 ppm (1 mmol dm^{-3}). Electrolytes containing HF were prepared by the addition of an aqueous hydrofluoric acid solution (HF content is 46 weight %, Wako Pure Chemical Industries, Ltd., Japan) into the base electrolyte. The deposition and dissolution current densities were set at 1.0 mA cm^{-2}. The amount of electricity for each deposition process was 1.0 C cm^{-2}. The dissolution process was terminated at 1.0 V vs. Li/Li^+. The electrode after the deposition or dissolution process was washed with pure PC (Mitsubishi Chemical Co.) to remove electrolyte salts before the XPS and SEM analyses.

All procedures were conducted in an argon dry atmosphere (dew point < -90°C) at room temperature.

The surface analysis of the electrode after the deposition or dissolution process was carried out with XPS. The morphology of the lithium electrodeposited was observed with SEM. The sample transfer from the argon dry box to the XPS or the SEM equipment was conducted in the same way as described in the chapter 1. The analysis condition for the XPS or the SEM were the same as that in the chapter 1.

The electrochemical behavior of lithium metal deposited on the substrate electrode was also analyzed by an impedance measurement. The impedance measurement of lithium metal was performed at open circuit potential after the deposition or dissolution process. The analysis condition of the impedance measurement was the same as that in the chapter 4.

6-3 Result and Discussion

SEM photographs

Figure 6-1 shows the SEM photographs of the electrode before and after the deposition and dissolution cycles in 1.0 mol dm^{-3} $LiCF_3SO_3$/PC containing 10 mmol dm^{-3} HF and 14 mmol dm^{-3} H_2O. Figure 6-1 (a) shows the SEM photographs of lithium obtained by the first deposition. Smooth lithium particles were deposited on the entire surface of the electrode. These particles had a hemispherical shape of about 0.3 μm diameter. This smooth morphology is due to the effect of the surface modification by the small amount of HF in the electrolyte, as discussed in the previous chapters. Figure 6-1 (b) shows the SEM photographs of the electrode after the first dissolution process. A residual film was observed on the entire surface of the substrate electrode. In this case, a high resolution micrograph could not be obtained because of the strong charging-up of the sample. Figure 6-1 (c) shows the SEM photographs of the electrode after the second deposition. The particle size of these lithium deposits was larger than those obtained in the first deposition. In addition, shrinking areas on the lithium particles were also observed. These areas are indicated by

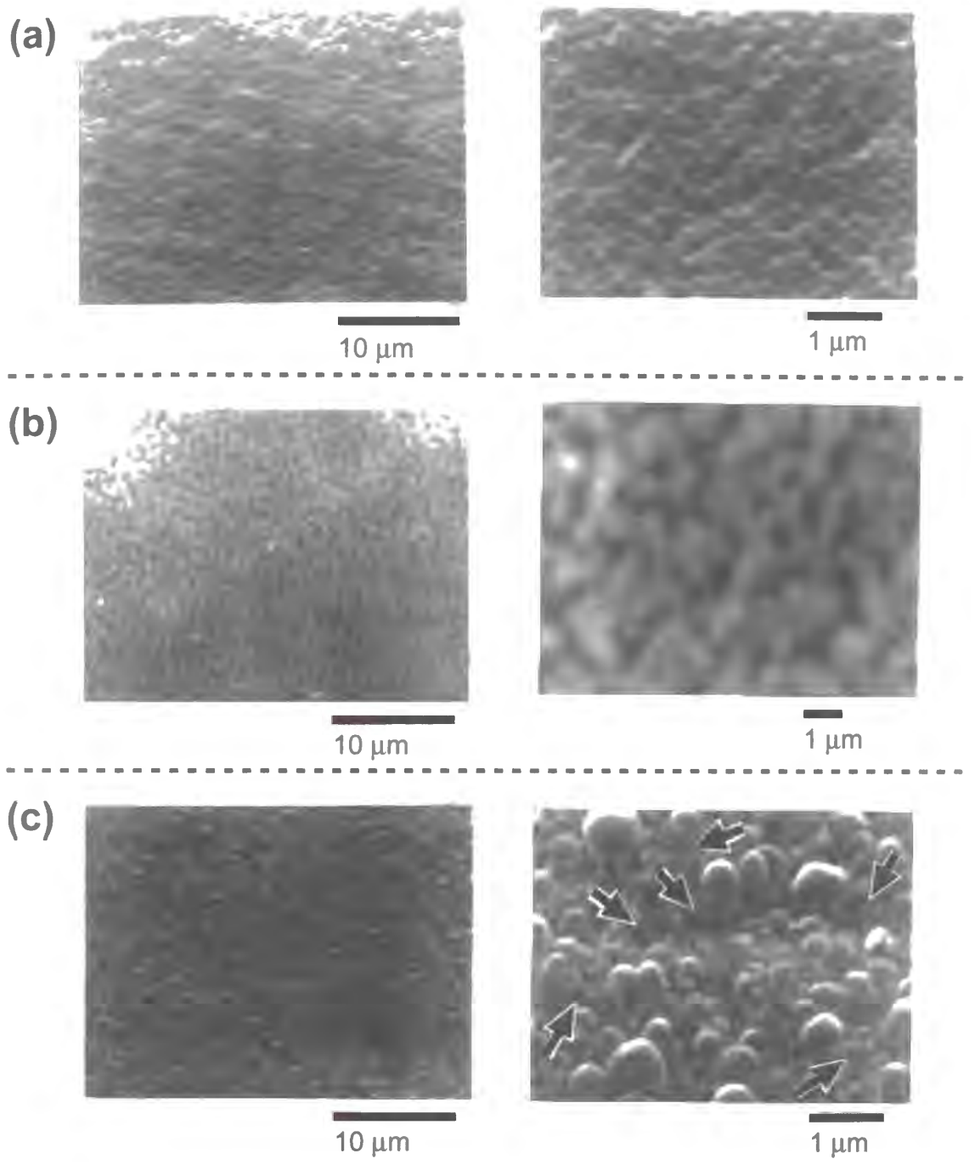

Figure 6-1 Scanning electron micrographs for the Ni substrate electrode in propylene carbonate containing 1.0 M $LiCF_3SO_3$, 10 mM HF, and 14 mM H_2O after (a) the first deposition of lithium, (b) the first dissolution of lithium, and (c) the 2nd deposition of lithium.

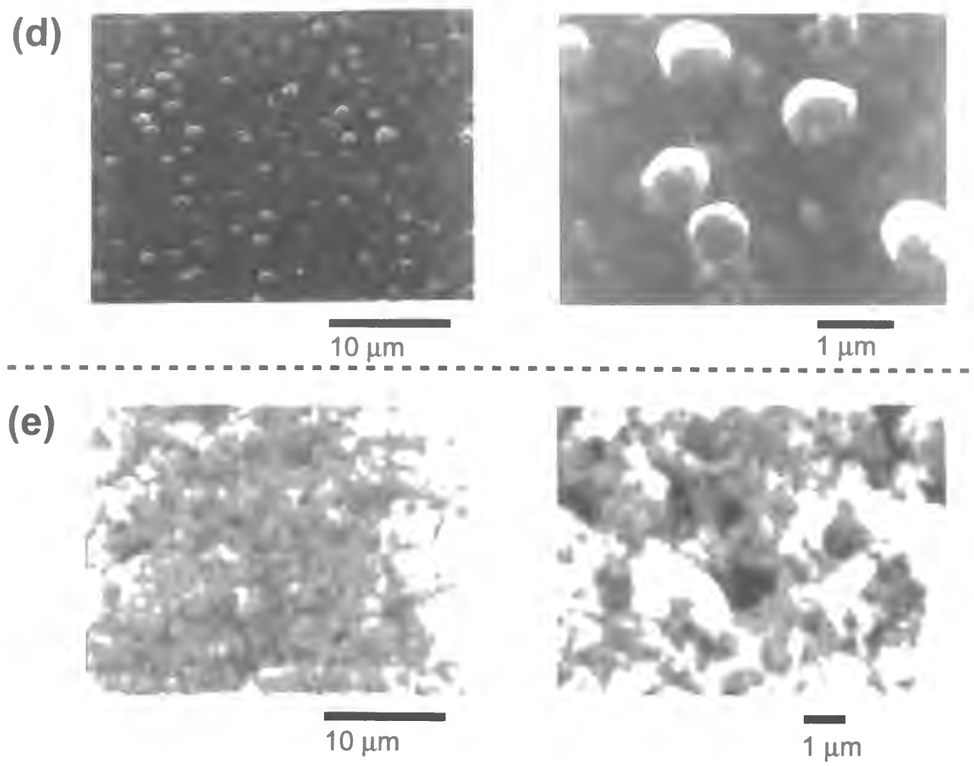

Figure 6-1 Scanning electron micrographs for the Ni substrate electrode in propylene carbonate containing 1.0 M $LiCF_3SO_3$, 10 mM HF, and 14 mM H_2O after (d) the 3rd deposition of lithium and (e) the 10th deposition of lithium.

the black arrows in Figure 6-1 (c). From a comparison of Figure 6-1(c) with Figure 6-1 (b), it can been seen that these shrinking areas resemble the residual film observed in Figure 6-1 (b). Probably, the residual film produced during the first dissolution remains on the electrode. Figure 6-1 (d) shows the SEM photographs of the electrode after the third deposition. Hemispherical lithium particles of about 1 µm diameter were formed on the electrode by the third deposition. However, the location of the lithium deposits was not uniform. Moreover, other deposits were also clearly observed where the hemispherical lithium particles were not observed. These deposits may correspond to the residual film produced by the first and second dissolution processes. Figure 6-1 (e) shows the SEM

photographs of the electrode after the 10th deposition. No lithium particles could be found anywhere. Only rough film was observed on the entire surface of the electrode. This film may be derived from the accumulation of the residual films produced during the previous dissolution processes. Perhaps, lithium metal is deposited under this thick accumulated residual film.

XPS spectra & Depth profiles

Figures 6-2 (a-e) show the XPS spectra for lithium electrodeposited on a fresh Ni substrate in 1.0 mol dm^{-3} $LiCF_3SO_3$/PC containing 10 mmol dm^{-3} HF and 14 mmol dm^{-3} H_2O. The times in the XPS figures correspond to the total Ar ion etching duration. The spectra labeled with a longer time reflect the information from innermost region of the surface film. These XPS spectra and depth profiles indicate that the surface film has the LiF/Li_2O bi-layer structure. Other compounds such as carbonate species and LiOH were present in minor amounts in the surface film.

The thickness of the surface film can be estimated by using the Li 1s spectra. In Figure 2(a), the peak assigned to lithium metal already appeared before the Ar ion etching. Because lithium metal is easily oxidized even in nonaqueous electrolytes, the peak could not be attributed to bare lithium metal. Generally, the photoelectrons from a substrate covered with a thin film are sometimes detectable when the film thickness is comparable to the escape depth of photoelectrons [97]. Therefore, the peak corresponding to lithium metal observed before the Ar ion etching can be attributed to the lithium metal under the surface film. In such a case, the thickness of the surface film can be estimated using XPS spectra. The thickness was calculated by the following equation [97].

$$\frac{I_i}{I_0} = \exp\left(\frac{-d}{\lambda_{Li}}\right) \qquad (6)$$

where I_i is the peak intensity of lithium metal observed in the Li 1s XPS spectrum before the Ar ion etching, I_0 is the peak intensity of lithium metal after the Ar ion etching for 41 min, d is the thickness of the surface film [Å], and λ_{Li} is the escape depth of photoelectrons

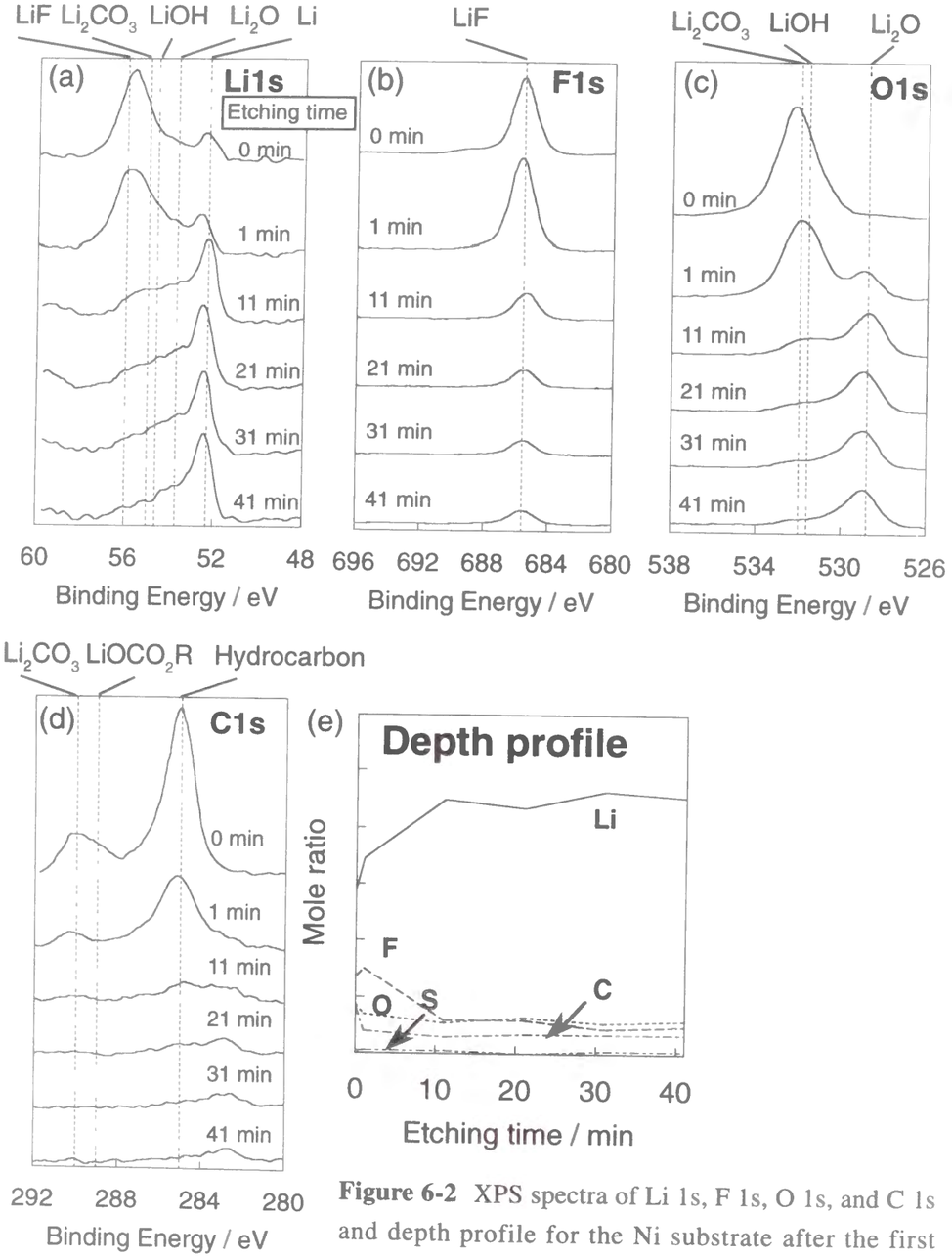

Figure 6-2 XPS spectra of Li 1s, F 1s, O 1s, and C 1s and depth profile for the Ni substrate after the first deposition of lithium in propylene carbonate containing 1.0 M $LiCF_3SO_3$, 10 mM HF, and 14 mM H_2O. Times in figures indicate the argon ion etching duration.

from the Li 1s level through the surface film (14 Å for Li_2O or LiF)[97]. This equation means that the attenuation of photoelectrons in the surface film is dependent on the thickness of the surface film. The calculation according to this equation indicates that the film thickness is approximately 20 Å. The surface film, however, could not be completely removed by the Ar ion etching, as shown in the Li 1s spectra in Figure 6-2 (a), so that the intensity I_0 is estimated to be smaller than the intensity for bare lithium metal. Therefore, the true thickness may be larger than 20 Å.

The film thickness was also deduced using another method based on the etching duration to remove the surface film completely. In this case, the thickness is calculated by the product of the etching duration and the etching rate. The Li 1s spectra in Figure 6-2(a) did not change after the Ar ion etching for 11 min, showing that the etching duration for complete removal of the surface film was estimated to be about 10 min. When the etching rate is 5 Å min^{-1}, the thickness of the surface film was estimated to be about 50 Å. However, the true etching rate is usually smaller than that obtained by a theoretical calculation (5 Å min^{-1}) because of surface roughness. Therefore, the true thickness should be smaller than 50 Å. From the two different methods, it can be said that the true thickness is in the range

Table 6-1 The surface film thickness estimated by the XPS analysis

Condition*	d_{XPS}
the first deposition	16 Å
the second deposition	22 Å
the third deposition	NC
the 10 th deposition	NC

* electrolytes was propylene carbonate containing 1.0 M $LiCF_3SO_3$, 10 mM HF, and 14 mM H_2O. The current density was 1.0 mA cm^{-2}, and the amount of the electricity for each deposition process was 1.0 C cm^{-2}. The cut of potential for the dissolution process was set at 1.0 V vs.Li/Li^+

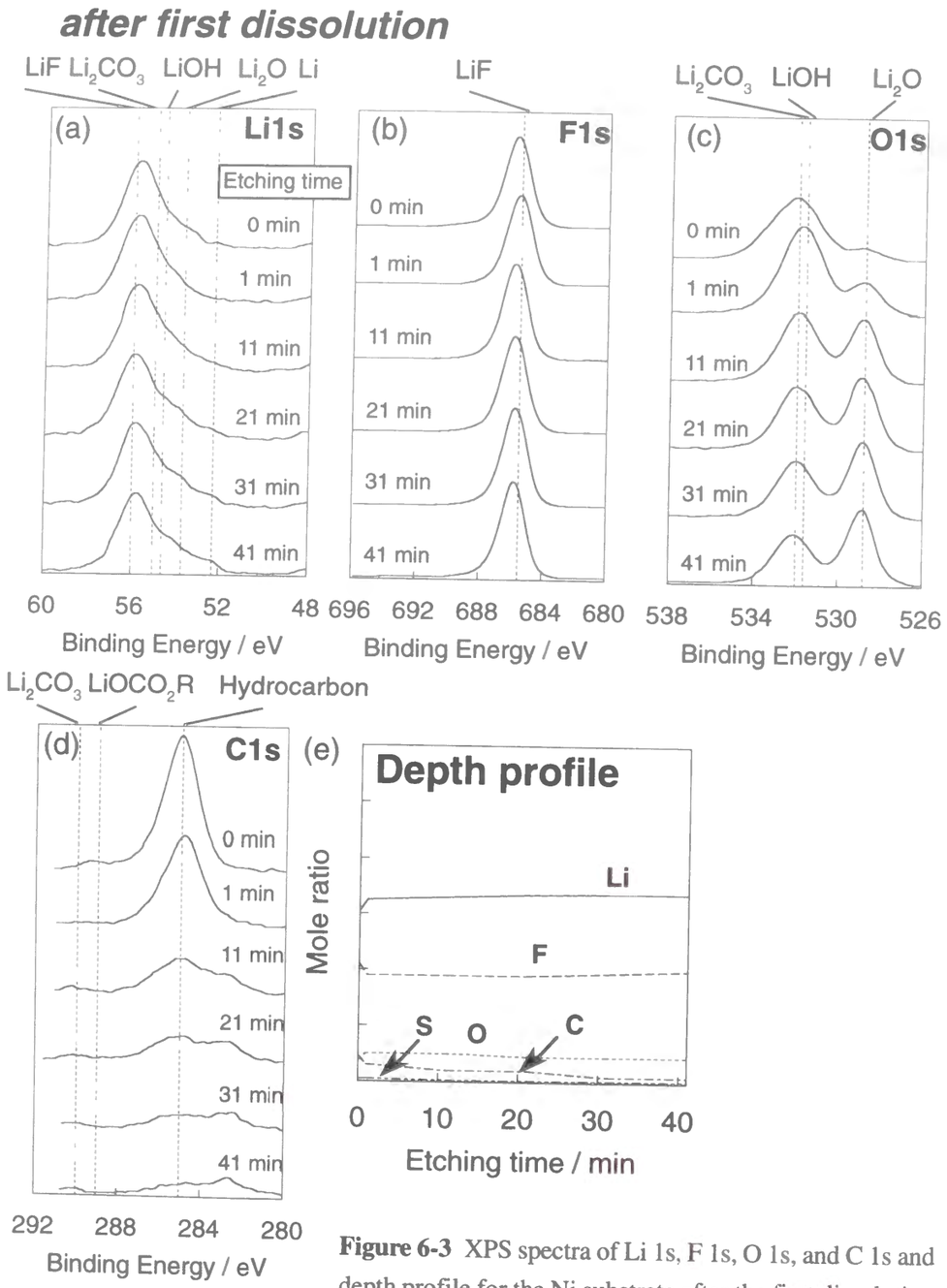

Figure 6-3 XPS spectra of Li 1s, F 1s, O 1s, and C 1s and depth profile for the Ni substrate after the first dissolution of lithium in propylene carbonate containing 1.0 mM $LiCF_3SO_3$, 10 mM HF, and 14 mM H_2O. Times in figures indicate the argon ion etching duration.

20-50 Å.

Figure 6-3 shows the XPS spectra for the electrode after the first dissolution of lithium. The SEM photographs in Figure 6-1 (b) showed that the electrode after the first dissolution was covered with the residual film, so that the XPS spectra and depth profile in Figure 6-3 reflect the chemical composition of the residual film. In the Li 1s or F 1s spectra, a strong peak attributed to LiF was observed before and after the Ar ion etching. The peak intensities of LiF did not change with the Ar ion etching for 41 min, indicating that the layer containing LiF is more than 200 Å in thickness. A tailing or shoulder peak was observed at lower energy around 55-53 eV in the Li 1s spectra after the Ar ion etching for 11 min. This is due to the contribution of the presence of a small amount of other lithium compounds as LiOH or Li_2O. The depth profile indicates that the atomic ratio of F is much more than those of other elements such as elemental O, C, and S. Therefore, the residual film consists mainly of LiF. In the O 1s spectra, peaks attributed to LiOH (or Li_2CO_3) and Li_2O were observed. The peak intensity of Li_2O increased with the Ar ion etching, showing that Li_2O is involved mainly at the inner region of the residual film. However, these oxygen compounds are minor species in the residual film, as shown in the depth profile. This is in good agreement with the information from the Li 1s spectra. In the C 1s spectra, a strong peak at 285.0 eV is attributed to organic species containing hydrocarbon structure. These species may be a adsorbed hydrocarbon gas which is a contaminant in the XPS analysis chamber or an high molecular weight polymer which may be derived from polymerization of propylene carbonate. Because the peak did not decrease remarkably with the Ar ion etching for 1 min, it can be seen that the polymer was present in the residual film. In addition, very small peaks attributed to Li_2CO_3 or $LiOCO_2R$ were observed at about 289-290 eV before the Ar ion etching. These peaks diminished after the Ar ion etching. This means that only a very small amount of carbonate species are present at the outer region of the residual film.

From these XPS spectra and depth profile, it can be said that the residual film consists of the thick LiF layer containing a small amount of Li_2CO_3, LiOH and Li_2O.

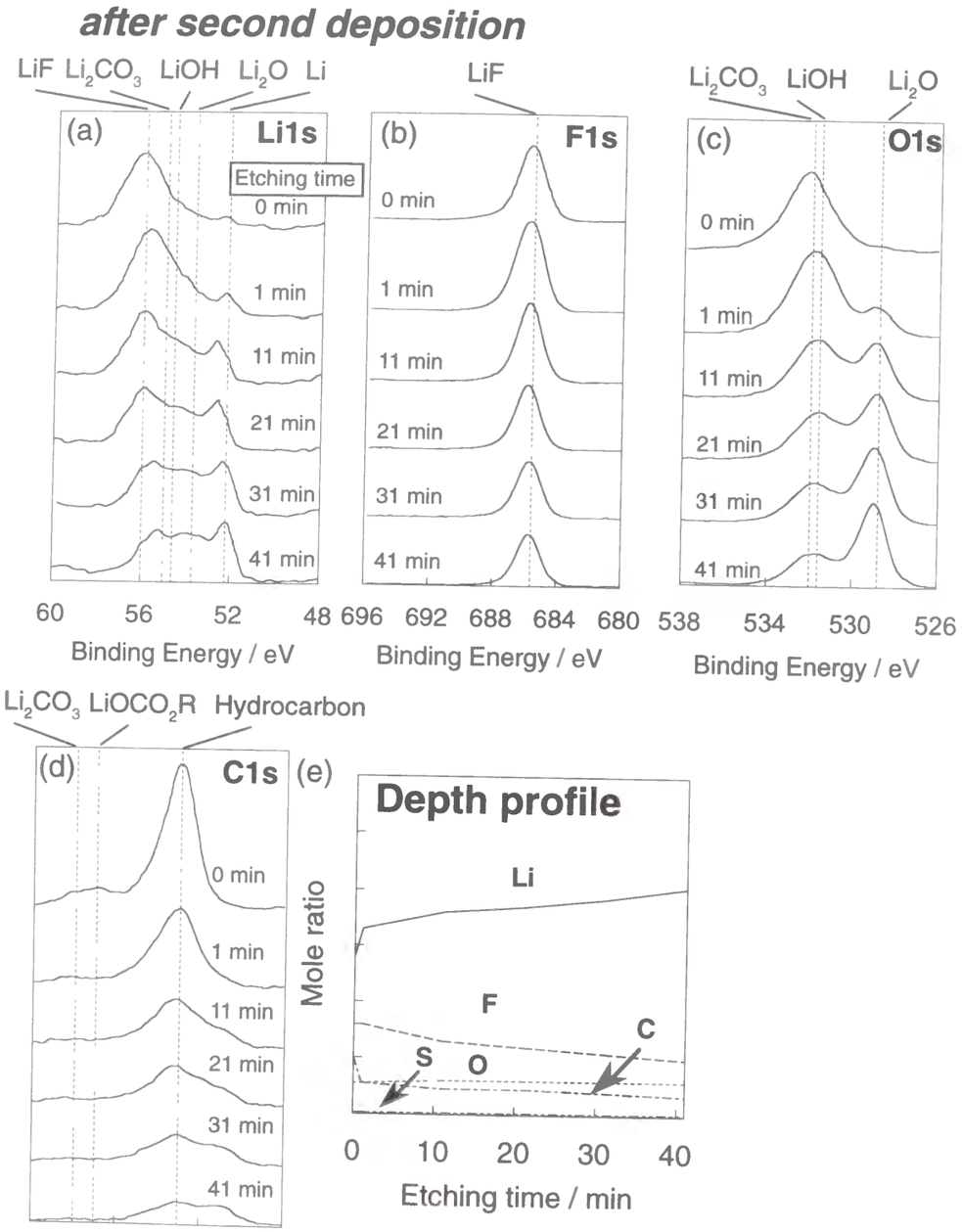

Figure 6-4 XPS spectra of Li 1s, F 1s, O 1s, and C 1s and depth profile for the Ni substrate after the 2nd deposition of lithium in propylene carbonate containing 1.0 M $LiCF_3SO_3$, 10 mM HF, and 14 mM H_2O. Times in figures indicate the argon ion etching duration.

These results indicates that the residual film is derived from the surface film on the lithium particles. However, it is unlikely that the surface film is the only origin of the residual film, because such compounds can also be produced by the decomposition reaction of lithium metal with the electrolyte containing HF during the dissolution process. This reaction will be enhanced by the breakdown of the surface film during the discharge process. On the other hand, Naoi et al. analyzed the deposition-dissolution behavior of lithium using an electrochemical quartz crystal microbalance (ECQCM)[52]. They have already reported that secondary reactions possibly occur during the dissolution process of lithium when propylene carbonate containing $LiPF_6$ (this electrolyte contains a small amount of HF as a contaminant) was used[52].

Figure 6-4 shows the XPS spectra and the depth profile for the electrode after the second deposition process. In the Li 1s spectra, the peak attributed to lithium metal was observed before the Ar ion etching. This peak is derived from the emission of a photoelectron from the Li 1s level of lithium metal through the surface film. However, this peak intensity was smaller than that for lithium deposits at the first deposition (shown in Figure 6-2(b)). The peak became intense with Ar ion etching, but the peaks assigned to LiF, LiOH, and Li_2O were still observed intensely even after Ar ion etching for 41 min. The F 1s spectra also showed a strong peak of LiF. This peak became weak with Ar ion etching, but the decrement in the peak intensity was smaller than that for the first lithium deposition. On the other hand, the SEM photographs in Figure 6-1 (b) indicated that the residual film partially remained on the electrode. Therefore, the strong peak of LiF after Ar ion etching for 41 min is due to the residual film. The thickness of the surface film on the lithium formed during the second deposition was also estimated using the same methods as described above. However, the estimated thickness included an uncertainty. Especially, the estimation based on the etching duration was more difficult. Therefore, only the estimation according to equation (6) was performed here. The estimated thickness is shown in Table 6-1. From this table, it can be seen that the thickness of the surface film on the lithium particles obtained in the second deposition is slightly larger than that obtained

in the first deposition. The O 1s and the C 1s spectra showed that the surface film contains Li_2CO_3 or LiOH in its outer region and Li_2O in the inner region. However, the amount of these compounds is smaller than that of LiF as shown in the depth profiles. From these results, it can be seen that the chemical composition of the surface film on the lithium deposits after the second charge process is not so different from that after the first charge process, except for the thickness of the surface film. Therefore, the deposition of the large lithium particles may be due to the increase in the thickness of the surface film. However, it is unlikely that only the increment in the film thickness is related to such morphology change in the lithium deposits. The existence of the residual film produced during the first dissolution process can be considered to be another possible reason for this morphology change. The residual film may affect nuclei formation and growth of the lithium particles.

Figure 6-5 shows the XPS spectra and the XPS depth profile for the electrode after the 10th deposition of lithium. From the SEM photographs in Figure 6-1(e), it can be seen that the electrode is covered with the residual film produced during the dissolution process. Therefore, the XPS spectra and the depth profile corresponds to the chemical compositions of the residual film. A strong peak attributed to LiF was observed in the Li 1s and the F 1s spectra. Their peak intensities did not change with Ar ion etching. The peak attributed to lithium metal was not observed even after Ar ion etching for 41 min. The peak around 533 eV in the O1s before the Ar ion etching can be attributed to the polymer containing C-O-C structure. The formation of the polymer may derived from the polymerization of propylene carbonate by reductive decomposition [43]. The O 1s spectra after the Ar ion etching and the C 1s spectra indicate the presence of LiOH and Li_2O (only in the inner region) in the residual film. The depth profile of Figure 6-5 (e) shows that the ratio of elemental Li and elemental F is almost 1:1 and that the amounts of the O, C, and S elements are smaller than that of Li and F over the whole region. Form these results, it can be concluded that the lithium deposits formed by the 10th deposition process are covered with a thick residual film consisting of LiF. Such a thick residual film indicates that part of the original surface film on lithium cannot be re-used as a stable surface film.

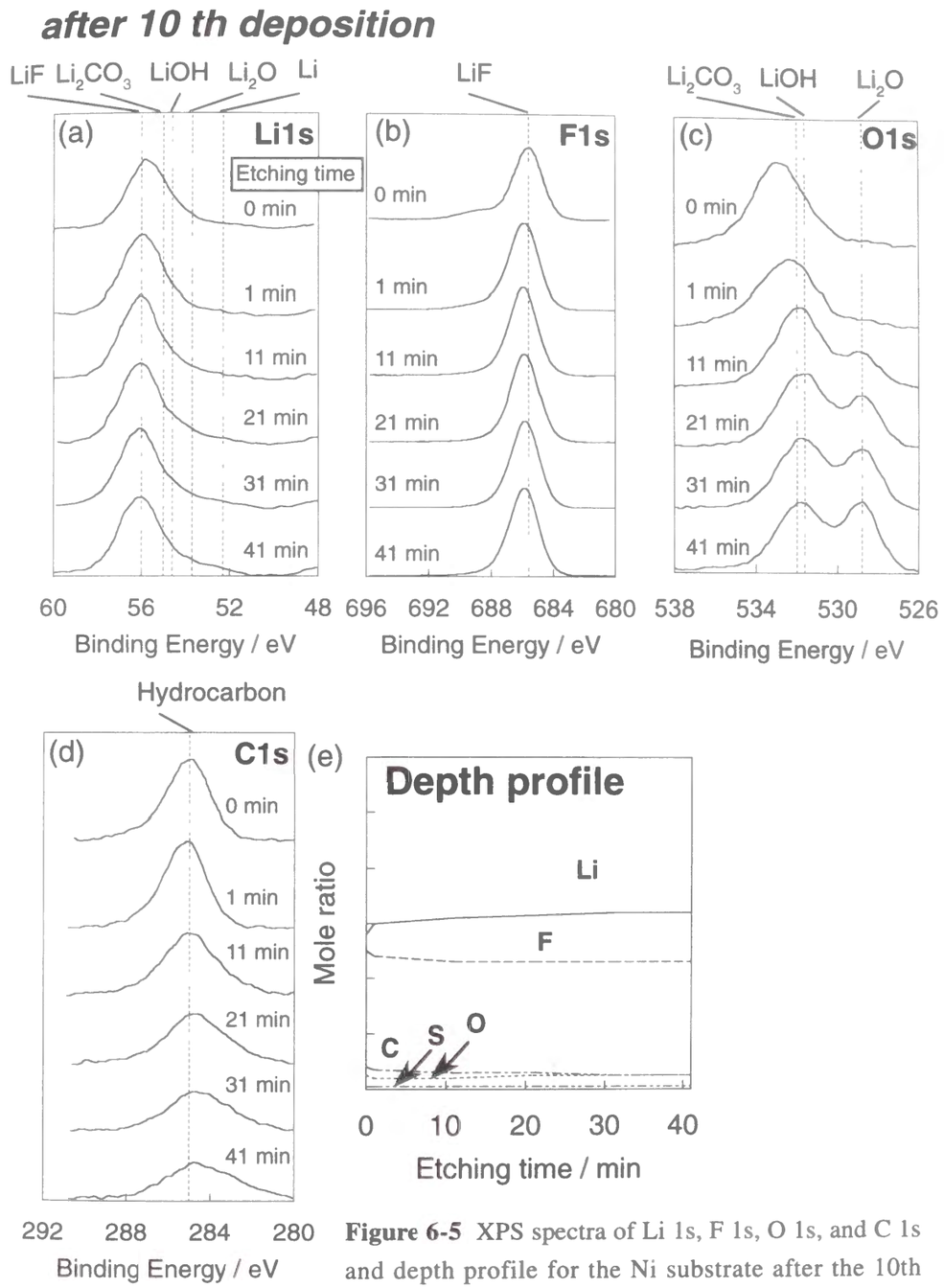

Figure 6-5 XPS spectra of Li 1s, F 1s, O 1s, and C 1s and depth profile for the Ni substrate after the 10th deposition of lithium in propylene carbonate containing 1.0 M $LiCF_3SO_3$, 10 mM HF, and 14 mM H_2O. Times in figures indicate the argon ion etching duration.

Electrochemical impedance spectroscopy (EIS)

Figure 6-6 shows the Cole-Cole plots for the electrode after deposition-dissolution cycles in 1.0 M $LiCF_3SO_3$/PC containing 10 mmol dm^{-3} HF and 14 mmol dm^{-3} H_2O. The Cole-Cole plots after the first dissolution process showed typical behavior for a blocking electrode, as shown in Figure 6-6 (b). This is because the electrode is covered with the residual film produced during the first dissolution (no active lithium was present on the electrode). On the other hand, all Cole-Cole plots after the deposition process showed a well-defined single semicircle. These semicircles can be attributed to the impedance due to the surface film, as discussed below. This was confirmed from the characteristic frequencies (ω_0), which were indicated in Figure 6-6. These values were much lower than those for the charge transfer process of Li/Li^+ redox (the frequency was several kHz) [43,46]. Therefore, the semicircles in the Cole-Cole plots correspond to the resistance caused by an ionically conductive surface film on lithium. Both the resistance after the first deposition and that after the second deposition were about 150 Ω cm^2. The film resistance after the third deposition process was about 200 Ω cm^2. The film resistance did not change after the consecutive deposition and dissolution cycles. For example, the Cole-Cole plot after the 10th deposition showed the film resistance to be about 200 Ω cm^2. The characteristic frequencies are also an important parameter, as stated above. Generally, the characteristic frequency in a Cole-Cole plot is independent of the film thickness and the surface area of the electrode when the semicircle is attributed to surface film impedance. The characteristic frequency can then be represented as follows [43].

$$f_c = \frac{\omega_c}{2\pi} = \frac{1}{2\pi RC} = \frac{\sigma}{2\pi\varepsilon_r\varepsilon_0} \qquad (7)$$

where f_c is the characteristic frequency [Hz], R is the resistance of the surface film [Ω cm^2], C is the capacity of the surface film [F cm^{-2}], ε_r is the relative permittivity of the surface film, ε_0 is the permittivity in vacuum (8.85×10^{-14} F cm^{-1}), and σ is the conductivity of the surface film [S cm^{-1}]. The characteristic frequency is related to both conductivity

and permittivity of the surface film which are determined by the chemical composition and the physical structure of the surface film. In Figure 6-6, the characteristic frequencies for all semicircles were 15.8 Hz. This result strongly indicates that the chemical composition and the structure of the surface film on lithium do not change through the deposition-dissolution processes. Therefore, the increment in the film resistance by cycles (as shown in Figure 6-6 (c) and (d)) is related to the increase in the film thickness or the decrease in the surface area of lithium particles.

An important characteristic of the residual film produced during each dissolution process can be deduced by a comparison of the Cole-Cole plot at the third deposition with that at the 10th. From the SEM photograph (Figure 6-1 (e)) and the XPS spectra (Figure 6-5), it was found that the lithium deposits obtained by the 10th deposition were covered with the thick residual film. Therefore, if the residual film functions as a resistive layer, the Cole-Cole plot at the 10th deposition must be different from that at the third one. However, the Cole-Cole plot measured after the 10th deposition was almost the same as that measured after the third one. This fact indicates that the residual film does not disturb the conduction of Li^+ ion. Therefore, it can be said that the residual film is very porous.

Coulombic efficiency

Figure 6-7 shows the coulombic efficiency changes in the deposition and dissolution cycles of lithium in 1.0 mol dm^{-3} $LiCF_3SO_3$/PC without any additives and with a small amount of HF. In this figure, the coulombic efficiency for the first cycles was about 80% when the electrolyte did not contain HF. However, it rapidly decreased with each cycle and became about 20 % at the 10th cycle. This is caused by the mechanical separation of lithium deposits from the Ni substrate electrode or the electrical insulation of lithium deposits from the substrate. These phenomena have often been observed for dendritic lithium. On the other hand, when HF was added to electrolyte, the coulombic efficiency at the initial cycle was also about 80%, but the high efficiency was maintained even after many cycles. These results may be related to the smooth morphology of the

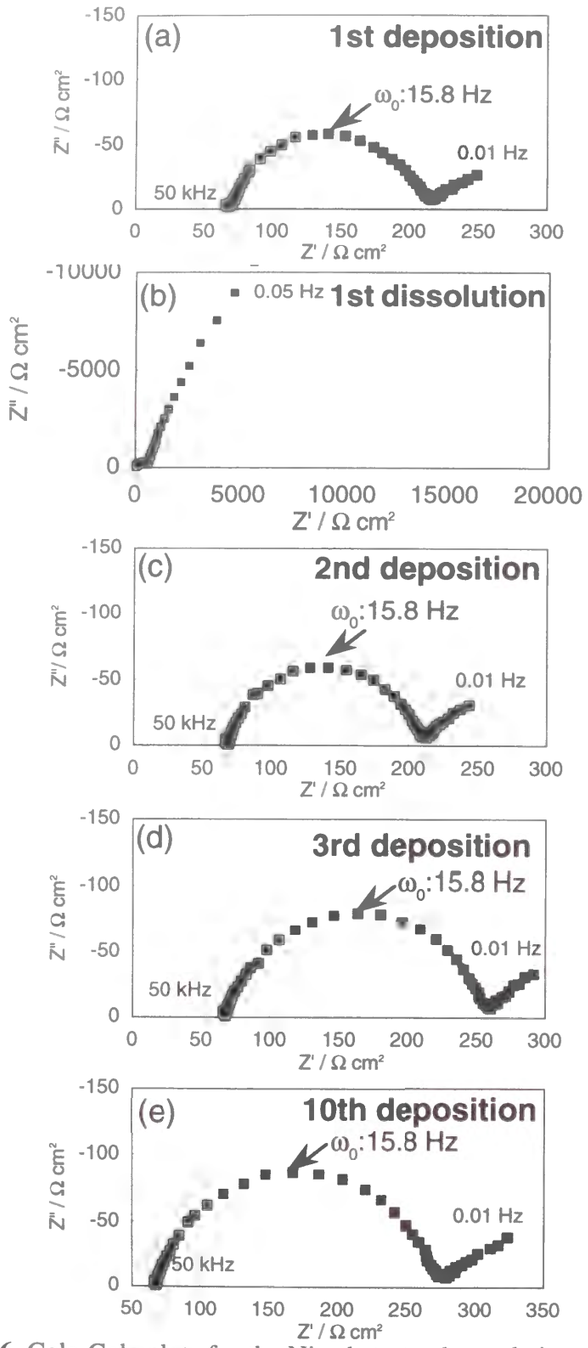

Figure 6-6 Cole-Cole plots for the Ni substrate electrode in propylene carbonate containing 1.0 M $LiCF_3SO_3$, 10 mM HF, and 14 mM H_2O after (a) the first deposition, (b) the first dissolution, (c) the 2nd deposition, (d) the 3rd deposition, and (e) the 10th deposition process. ω_0 indicates characteristic frequency.

lithium deposits. In the case of a higher content of HF, the coulombic efficiency gradually decreased after the 10th cycles and reached about 70% at the 40th cycle. In the case of a lower content of HF, the efficiency was more than 80 % during 20 cycles. However, the efficiency rapidly decreased at the 45th cycle. After the 60th cycle, the electrode surface was observed with SEM. The local formation of dendritic lithium was observed. Moreover, these dendrites exist in an agglomerate form which can be seen easily by the naked eye. Possibly, the rapid decrease in the coulombic efficiency is caused by the formation of the dendritic lithium during many deposition and dissolution cycles. Two possibilities have arisen for the formation of dendritic lithium.

(1) According to the acid-base reactions (1-5), HF in the electrolyte is consumed at each deposition processes while a new tight, compact surface film is formed. The consumption of HF in the electrolyte during many cycles causes the formation of dendritic lithium.

(2) The electrode after many cycles was covered with a thick residual film produced during

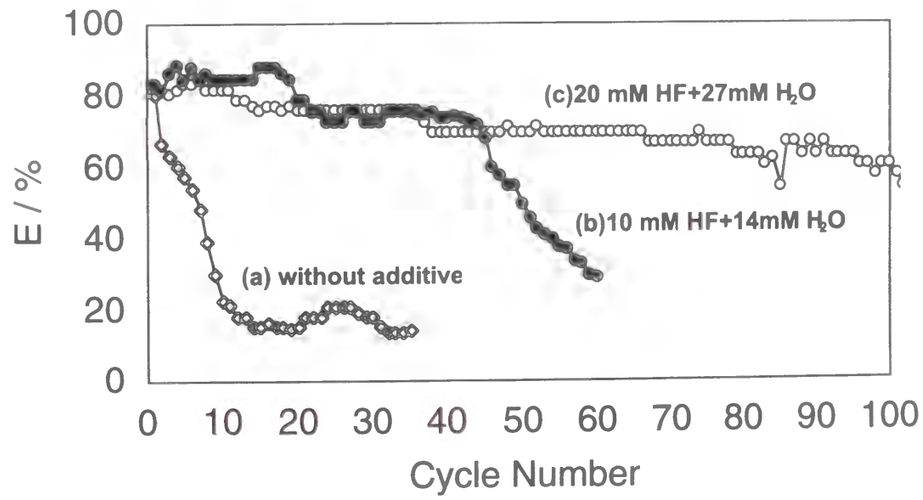

Figure 6-7 Coulombic cycle efficiency of lithium deposited on the Ni substrate electrode in propylene carbonate containing 1.0 M $LiCF_3SO_3$ (a) without additives, (b) with 10 mM HF and 14 mM H_2O, (c) 20 mM HF, and 27 mM H_2O, the total charge; 1.0 C cm^{-2}, the cut off potential; 1.0 V vs. Li/Li^+.

the dissolution process. These thick residual films did not disturb the conduction of Li^+ ion, as described above (migration). However, they may disturb the supply of HF to the interface (diffusion). The lack of HF at the interface due to the existence of the residual film causes the formation of dendritic lithium.

The following experiment was performed to confirm the above two possibilities After the cycle test, the substrate electrode was changed to a fresh one and then the electrodeposition of lithium was performed again. Figure 6-8 shows the SEM photograph of lithium electrodeposited on a new fresh Ni electrode. The morphology was smooth and no dendritic lithium was observed. This result indicates that the second explanation is more reasonable.

6-4 Conclusions

The surface condition change during the deposition and dissolution cycles is schematically summarized in Figure 6-9. In the first deposition process, fine lithium particles were deposited on the Ni substrate electrode through a migration of Li^+ ions in a surface film consisting of an LiF/Li_2O bi-layer. In the first dissolution process, a residual

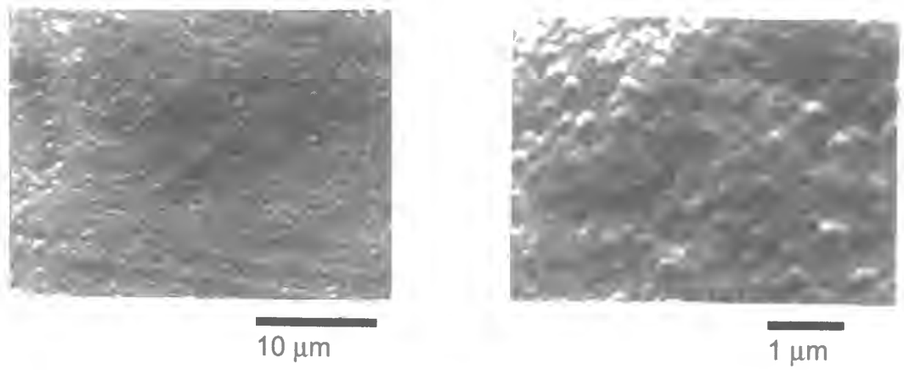

Figure 6-8 Scanning electron micrographs for lithium deposited in propylene carbonate containing 1.0 M $LiCF_3SO_3$, 10 mM HF, and 14 mM H_2O on the fresh Ni substrate electrode after 60th cycle was finished in the same electrolyte.

film was observed on the electrode. This film may be derived from the surface film on the lithium particles because it consisted mainly of LiF. The residual film affected the morphology of lithium particles produced in the following deposition process. The residual film accumulated thickly on the electrode during each dissolution process. The thick residual films do not have significant resistance to Li^+ ion conductivity, but they disturb the supply of HF to the lithium interface, leading to the formation of lithium dendrites. Therefore, it can be concluded that the accumulation of the residual film produced during the dissolution process is a serious problem for many deposition-dissolution cycles in the electrolyte containing HF.

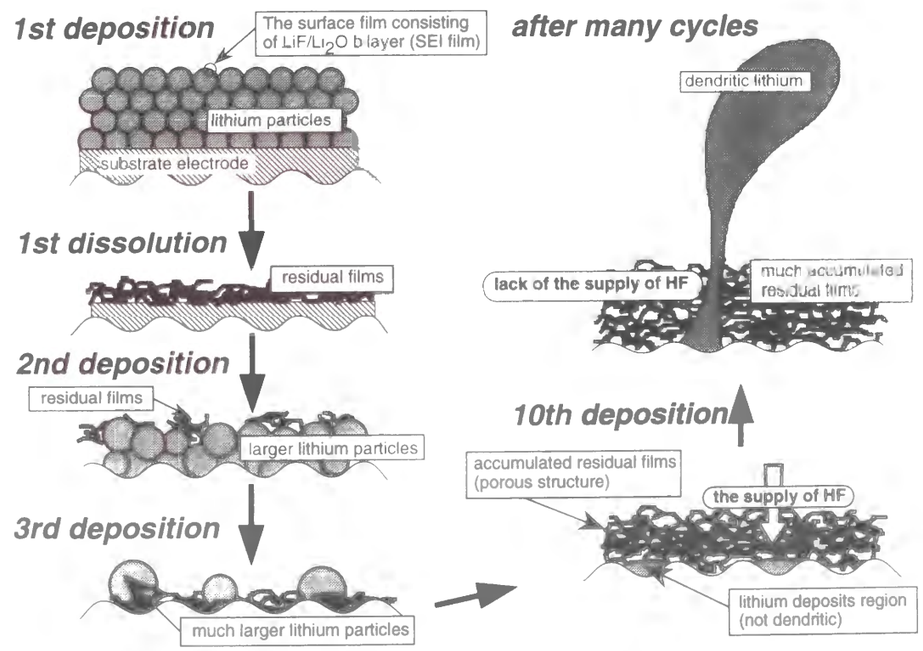

Figure 6-9 Schematic illustration for the surface condition changes of lithium deposits on the Ni substrate electrode by deposition-dissolution cycles.

Chapter 7
Clear Imaging for Uniformity of Lithium Metal Surface using Tapping Mode-Atomic Force and Surface Potential Microscopy

7-1 Introduction

The addition of a small amount of HF into nonaqueous electrolytes was effective in suppressing the dendrite formation of lithium. This effect is realized by the thin and compact surface film consisting of LiF/Li_2O bi-layer which is formed by the addition of HF. Such a surface film is enough uniform to avoid the concentrated current. By the way, this discussion is supported by indirect proofs obtained from XPS, SEM, and electrochemical analyses as seen at the chapter 4. However, no direct proofs for the high uniformity of the surface film modified by HF has been obtained in the previous chapters.

Scanning Probe Microscopes (SPMs) have got much attention as a new tool for surface analyses since scanning tunnel electron microscope (STM) was developed in 1982 [99]. SPMs provide two-dimensional images for various physical/chemical conditions of sample surfaces using a microprobe scanning on a sample surface [101,101]. In the case of Atomic Force Microscope (AFM) which is one of famous SPMs, a pull or repulsion force between atoms in a microprobe and a sample surface is detected without its electronic conductivity [102]. Thus, the AFM is used in a wide surface scientific field. However, the sample surface is often damaged by a scanning microprobe. Recently, in order to avoid such a problem, a new type AFM called "Tapping Mode AFM (TMAFM)" was developed by Digital Instruments Co. In TMAFM, the microprobe is oscillated mechanically by a vibration of a bi-morph piezo device in order to attain an intermittent contacts of the microprobe with a sample surface. The intermittent contact extremely minimizes such damages caused by a friction.

Recently, a new type SPM, which can measure a surface potential, has been focused in a surface analysis for an electrically functional thin film. This SPM is called "Kelvin Probe Microscope" [103], "Scanning Maxwell Stress Microscope (SMM)" [104], or "Scanning

Surface Potential Microscope (SSPM)" [105]. In these SPMs, the distribution of the surface potential on the sample is displayed as an image. The surface potential is generally derived from the contact potential difference between the prove and the sample, but it is also much affected by dielectric moment of adsorbent or surface film on the sample. This means that the surface potential is very sensitive to the surface chemical composition of the sample. So, the surface potential measurement can be considered as a very useful tool for a microscopic analysis in a surface chemistry.

As above discussion, TMAFM and surface potential microscopy (SPoM) are promising analytical methods for the surface film on lithium metal. Therefore, in this chapter, the surface film on lithium metal was analyzed by using TMAFM and SPoM. Especially, the difference between the surface film on lithium deposited in nonaqueous electrolytes with and without HF was detected in order to discuss the relationship between the uniformity of the surface film and the morphology of lithium.

7-2 Experimental

Lithium metal was deposited on a Ni substrate electrode (15 mm diameter disk) by a galvanostatic condition. Propylene carbonate containing 1.0 mol dm^{-3} $LiClO_4$ ($LiClO_4$/PC) was used as a base electrolyte. The electrolyte containing HF was prepared by an addition of a small amount of hydrofluoric acid to the base electrolyte. After the deposition, the samples were washed by a pure PC and dried in vacuum for 30 min to remove the electrolyte on the sample. All procedures were performed in a high pure argon dry box. After the dry process, the samples were transferred to another Ar dry box. TMAFM and SPoM equipment were set in this dry box. A glass transfer vessel was used to avoid undesirable reactions with air.

Extended multi-mode SPM unit (Digital Instruments), Nanoscope IIIa control station (Digital Instruments), and Phase-01 phase-detection module (Digital Instruments) were used for TMAFM and SPoM. The microprobe was a silicon microcantilever coated with thin CoCr film (MESP type, Digital Instruments). The scan rate was set at 1 scan line

Hz^{-1}. At the TMAFM measurement, the amplitude and frequency of the alternating voltage for the mechanical oscillation of the probe were 500 mV and 70 kHz (this condition is near to a resonant frequency of the probe), respectively. On the other hand, at the SPoM measurement, the amplitude and frequency of the alternating voltage for the electric oscillation were 5 V and 70 kHz, respectively. The SPM system used in this study has two merits for AFM/SPoM analysis. One merit is a simultaneous measurement of the TMAFM and SPoM [106]. In this system, the topographical data along a scanning line are taken by the TMAFM in the first scan and the surface potential data on the same scanning line are obtained by the SPoM in the second scan. Another merit is the independence of surface potential data from the topographical data. Generally, undesirable influences of a surface topography on a surface potential is a serious problem [106]. In this SPM system, it is minimized by maintaining a constant distance (in this study, 20 nm) between the sample surface and the tip of the probe during SPoM analysis.

7-3 Theoretical details

Detection of Surface Potential

The surface potential measurement used in this study is based on the detection of the oscillating electrical static force working on the conductive probe when the alternating voltage is applied to the probe. This is similar to a technique in Scanning Maxwell Stress Microscopy, developed by H. Yokoyama. et. al. [104]. The surface potential obtained by the SPoM can be determined according to the following equation (1) [106].

$$F_\omega = \frac{d\,C}{dz}(V_s - V_{DC})\,V_{AC}\sin\omega t \qquad (1)$$

F_w : the oscillating force of the tip

dC/dz : the vertical derivative of the tip/sample capacitance

V_s : the surface potential

V_{DC} : the applied dc bias voltage

V_{AC} sinwt : the applied alternating voltage with angular frequency.

This equation means that the oscillation force working on the probe depends on the product of the ac drive voltage (V_{AC}sinwt) and the voltage difference between the applied dc voltage and the surface potential (V_s - V_{DC}). If the applied dc voltage is equal to the surface potential, the oscillation force will be zero. Therefore, the surface potential can be determined by adjusting the dc voltage on the probe until the oscillation amplitude become zero. This applied dc voltage is recorded to provide a voltage map of the surface.

7-4 Results and Discussion

Distribution of Surface Potential on Lithium Metal Surface

In the SPoM, a surface potential for a bare metal is equal to a contact potential difference (CPD) between the bare metal and the metal film on the probe. In this case, the CPD is derived from the difference in the work functions of both metals. Generally, a metal with a smaller work function is positively charged by an electron-transfer to another metal with a lager work function. In this study, the sample is lithium metal which has a small work function (2.8 eV) [107]. On the other hand, the metal film on the probe consists of cobalt and chrome alloy which have a relative large work function (about 5 eV). Therefore, the lithium metal is positively charged to the prove. Figure 7-1 (a) shows the potential slope (electric field) between the tip and the lithium metal surface. For bare lithium metal, the CPD is equal to the surface potential measured with the probe (Figure 7-1(a)). On the other hand, if the lithium metal surface is covered with a thin surface film, the surface potential does not correspond to the CPD. Figure 7-1 (b) shows the change of the potential slope under the presence of the thin surface film. The surface potential may become smaller than the CPD because of a screening effect to the electric field by the surface film. The screening effect is larger when the film thickness is larger or the permittivity of the film is smaller. From the discussion above, it can be understood that the surface potential of lithium metal depends on the thickness and the chemical composition of the surface film on the lithium metal.

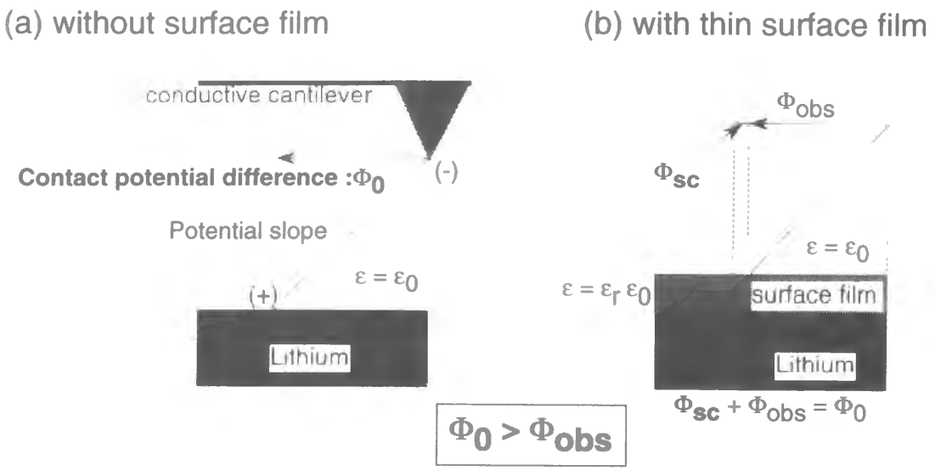

Figure 7-1 Schematic illustrations for contact potential difference (CPD) and potential slope, (a) without the surface film, (b) with the thin surface film. Φ : CPD between lithium metal and CoCr film on tip (= about 2 V), Φ_{obs} : observed CPD (equal to the surface potential), and Φ_{sc} : screening CPD.

TMAFM image and SPoM image for lithium deposits

Figures 7-2 (a) and (b) show the TMAFM image and the SPoM image for lithium electrodeposited on the Ni substrate electrode in 1.0 mol dm^{-3} $LiClO_4$/PC containing 10 mM HF and 14 mM HF. The current density is 1.0 mA cm^{-2}. The total charge for the deposition was set at 1.0 C cm^{-2}. The TMAFM images show that fine lithium particles with 0.3 μm diameter deposit on the Ni substrate electrode. This image is in good agreement with the SEM observation in the previous chapter. Therefore, it is found that the TMAFM is available to the microscopic observation for the lithium deposits. Some irregular parts were observed in the TMAFM image. For example, some particles marked with white-circles were present in a like valley. This irregularity is caused by the irregularity on the Ni substrate. On the other hand, the SPoM image shows the very small potential distribution for the lithium particles, except for slight lower potential at the outlines of particles. This SPoM image directly proves the high uniformity of the surface films on the lithium particles

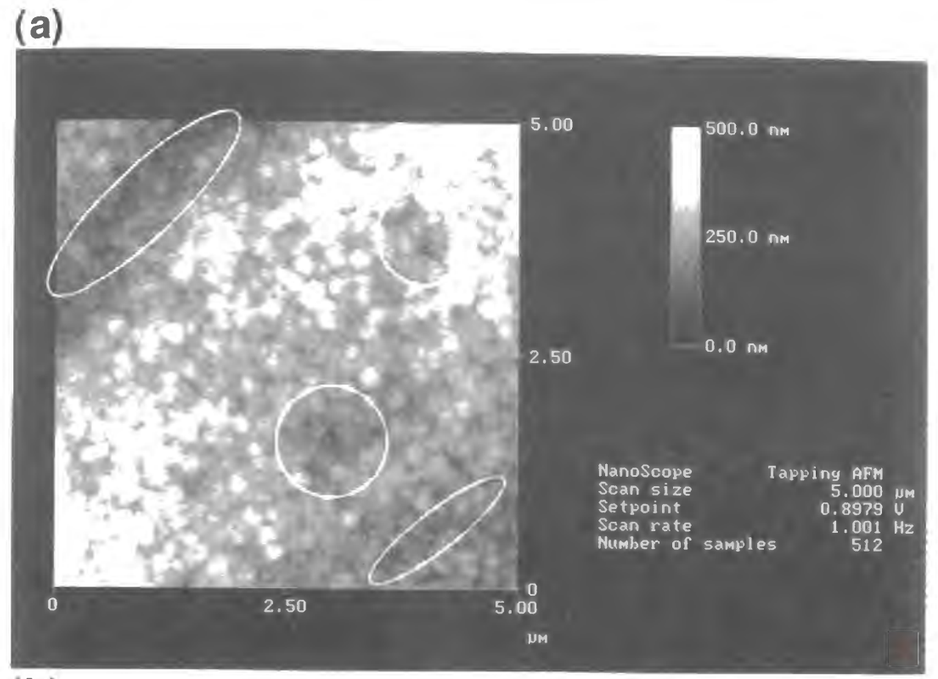

Figure 7-2 Tapping Mode-AFM image and SPoM image (5 μm × 5 μm) for lithium electrodeposited (1.0 mA cm^{-2}, 1.0 C cm^{-2}) on the Ni substrate in 1.0 M $LiClO_4$ / PC containing 10 mM HF and 14 mM H_2O.

deposited in electrolyte containing HF. The lower potential on outlines of particles may be due to an influence of the probe shape (in the SPoM, the probe tip is not a point, but it is a pyramid).

The following TMAFM/SPoM measurement was carried out to clarify the uniformity of the surface film on the dendritic lithium deposits. Figures 7-3 (a) and (b) are the TMAFM image and the SPoM image for lithium electrodeposited on the Ni substrate electrode in 1.0 mol dm^{-3} $LiClO_4$/PC without any additives. The current density was 1.0 mA cm^{-2}. The total charge for the deposition was 20 mC cm^{-2}. Such small total charge was used in order to avoid crash of the well-grown dendritic lithium and the probe. In the TMAFM image, many deposits like a cone or a pyramid are observed on the Ni substrate. However, these deposits are not uniform in both size and distribution. Especially, some large deposits were about 1 mm height. These deposits are in initial stage of the formation of the dendritic lithium. In fact, the typical dendritic lithium was observed after more charge pass. On the other hand, in the SPoM image, the large distribution of the surface potential was clearly observed. The well-grown deposits have a more positive surface potential compared with other deposits. This result reflects the ununiformity of the surface film for the deposits. As discussed above, the distribution of the surface potential is due to the difference in the chemical composition or the film thickness. In the chapter 3, it was already found that Li_2CO_3, LiOH, and Li_2O are main species for the surface film on the dendritic lithium in 1.0 M $LiClO_4$/PC electrolyte. Moreover, other researcher already reported that the permittivity of these lithium compounds are not so different, for example, Li_2CO_3 ; 6.9, LiOH ; 8.5, and Li_2O ; 7.4 [44]. So, the potential distribution observed in Figure 7-3(b) is related to the difference in the film thickness. It can be considered that the thickness of the surface film are thinner for the well-grown lithium deposits than that for other ingrown deposits. Since the thinner surface film has a lower resistance for Li^+ ion conduction, the current is easily concentrated on the deposits covered with such thin surface film. Therefore, the TMAFM/SPoM image in Figure 7-3 strongly suggests that

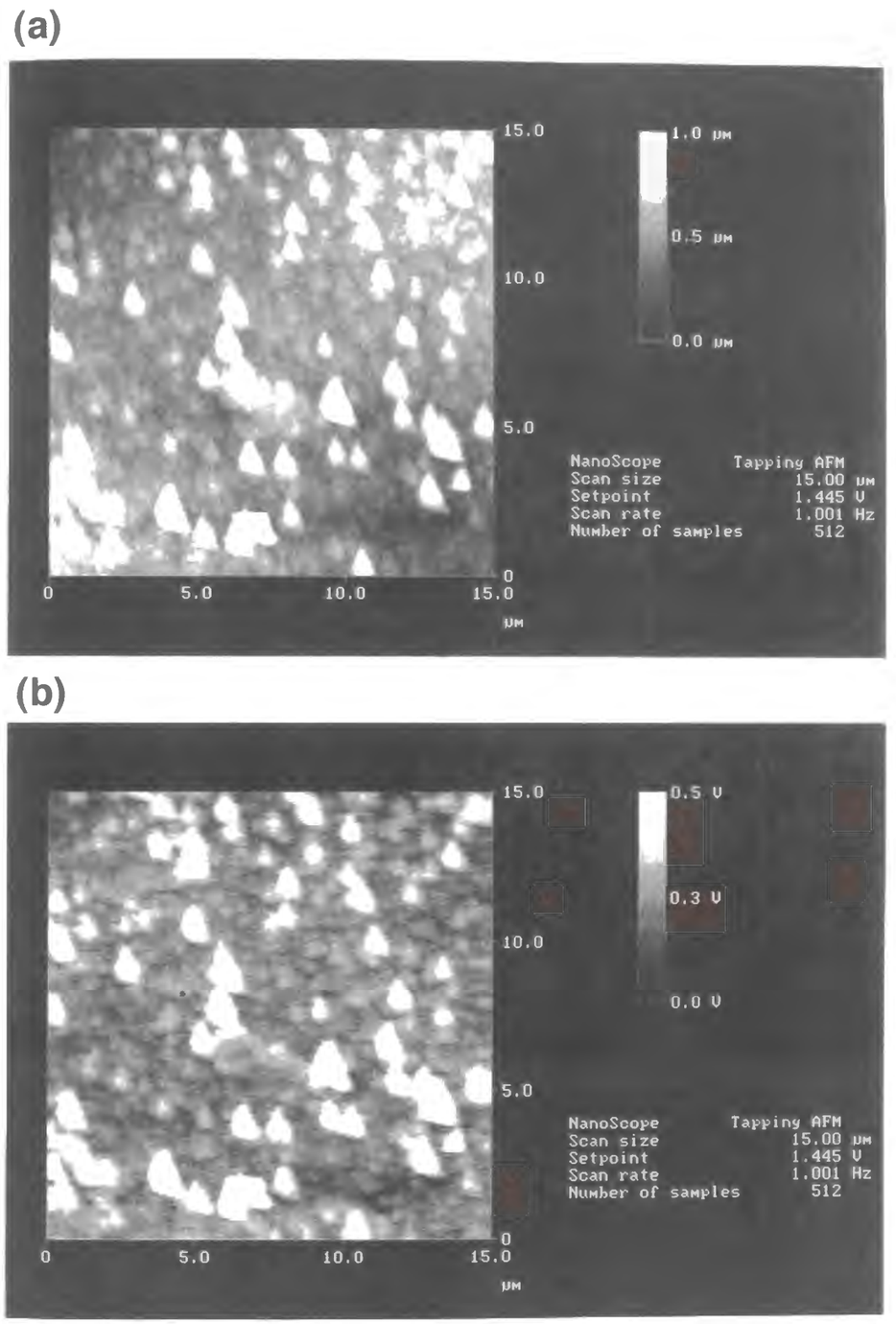

Figure 7-3 Tapping Mode-AFM image and SPoM image (15 μm × 15 μm) for lithium electrodeposited (1.0 mA cm^{-2}, 20 mC cm^{-2}) on the Ni substrate in 1.0 M $LiClO_4$ / PC without HF.

the distribution in the surface film condition promotes the formation of dendritic lithium.

7-5 Conclusion

In this chapter, the surface film on lithium metal was analyzed by using Tapping mode Atomic Force microscopy (TMAFM) and Surface Potential Microscopy (SPoM). The difference between the surface film on lithium deposited in nonaqueous electrolytes with and without HF was detected in order to discuss the relationship between the uniformity of the surface film and the morphology of lithium. The TMAFM/SPoM images indicate a much higher uniformity of the surface films on the lithium particles deposited in electrolyte containing HF. This results directly prove that the HF in electrolyte has the effect of forming the high uniform surface film on electrodeposited lithium.

Chapter 8
The Observation of Electrochemical Dissolution of Lithium Metal Using Electrochemical Quartz Crystal Microbalance and *in-situ* Tapping Mode Atomic Force Microscopy

8-1 Introduction

The morphological change with the addition of HF produces a significant improvement in the reversibility of the lithium metal anode. However, even in this case, the coulombic efficiency of the discharge and charge cycles is still not sufficient (≈ 80%) for practical use. On the other hand, the residual film is formed on the substrate electrode during the dissolution process. The accumulated residual film affects the morphology of the lithium particles electrodeposited after the second deposition (charge) process. From the results of XPS analyses, it was found that the residual film was derived from the surface film on the lithium particles. However, the formation mechanism of the residual film is not clear, because the XPS analysis is *ex-situ*. Thus, the electrochemical dissolution of lithium metal in the presence of the HF additive must be investigated using *in-situ* methods. Therefore, in this chapter, the electrochemical behavior of lithium metal during the dissolution process was examined using two *in-situ* methods: Electrochemical Quartz Crystal Microbalance (ECQCM) and Fluid Tapping Mode Atomic Force Microscopy (F-TMAFM). In the former one, a mass change in an electrode can be measured from a change in a resonance frequency of the quartz crystal disk [108,109]. The latter is a new type of *in-situ* atomic force microscopic (AFM) analyses [110,111], which provides a excellent observation for soft samples in solution without damage due to the scanning probe [112-114]. Especially, this study is the first demonstration for the application of the F-TMAFM to the electrochemistry of the lithium surface.

8-2 Experimental

Preparation of electrolytes

Lithium metal was deposited in an electrolyte containing a small amount of HF. Propylene carbonate containing 1.0 mol dm^{-3} $LiClO_4$ ($LiClO_4$/PC) was used as the nonaqueous electrolyte. The water contents in the base electrolyte was less than 20 ppm (1 mmol dm^{-3}) as determined by the Karl Fischer Moisture Titrator (MKC-210, Kyoto Denshi Kogyo Co., Japan). The electrolyte containing HF was prepared by the addition of a small amount of hydrofluoric acid (46 weight % aqueous solution, Wako Pure Chemical Industries, Ltd., Japan) to the base electrolyte. The concentrations of HF and H_2O in the electrolyte were 10 mmol dm^{-3} and 14 mmol dm^{-3}, respectively.

Electrochemical quartz crystal microbalance (ECQCM)

The mass change in the quartz crystal electrode is calculated from the following equation which is so-called the Sauerbrey equation [108,109]

$$\Delta f = - 2 \Delta m f_0^2 / \sqrt{\mu_q \rho_q} \qquad (1)$$

where Δf is the resonance frequency change of the quartz crystal electrode [Hz], Δm is the mass change, f_0 is the vacuum resonance frequency [Hz], μ_q is the shear modulus of quartz (2.947×10^{11} g cm^{-1} s^{-2}), and ρ_q is the density of quartz (2.648 g cm^{-3}). The decrease in the resonance frequency is proportional to the increase in the mass of the electrode. However, the frequency response deviates from the Sauerbrey equation when electrolyte is trapped in the many crevices formed by an increase in the surface roughness of the electrode [109].

In this chapter, the working electrode was made of a 6 MHz At-cut quartz covered with a Ni thin film (obtained from Hokuto-Denko industry). The electrochemical deposition and dissolution of lithium were performed by a galvanostatic technique. A frequency analyzer (HQ-301, Hokuto Denko), the oscillation synthesizer (HQ-101B, Hokuto Denko), and the potentio/galvanostat (HA-501, Hokuto Denko) were used in this ECQCM study. The counter electrode was lithium foil (8 cm^2). The reference electrode was also lithium metal (Li/Li^+). The current density was 1.0 mA cm^{-2}, and the amount of electric charge was 250 mC cm^{-2} for the deposition (charge) process. The dissolution (discharge) was terminated at 1.0 V vs. Li/Li^+. The ECQCM measurement was conducted in a pure argon

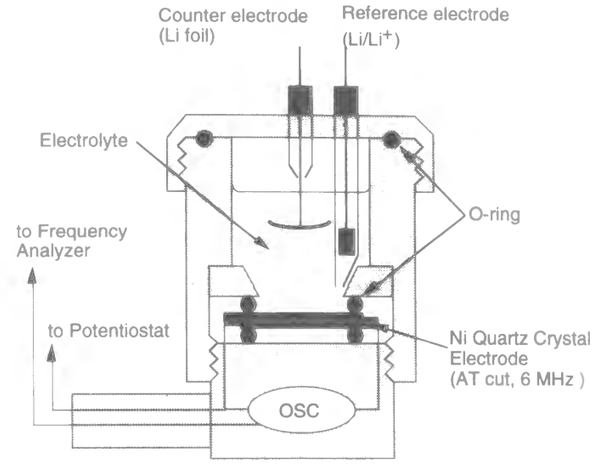

Figure 8-1 Schematic illustration of the electrochemical cell for electrochemical quartz crystal microbalance.

atmosphere at room temperature. The ECQCM equipment used in this study is shown in Figure 8-1.

In-situ Fluid Tapping Mode Atomic Force Microscopy (F-TMAFM)

In an AFM, a surface of a soft sample is often damaged by a scanning microprobe. A Tapping Mode AFM (TMAFM) is useful to avoid such a problem. In the TMAFM, the microprobe (cantilever) is mechanically oscillated by the vibration of a bi-morph piezo device in order to attain an intermittent contact of the microprobe with a sample surface. The intermittent contact significantly minimizes such damage (a friction). A Fluid-TMAFM is a TMAFM extended for the microscopic observation of samples in liquid. In the F-TMAFM, the entire cantilever holder is mechanically oscillated because it is difficult to only oscillate the microprobe by the vibration of the bi-morph piezo in a liquid.

A Nanoscope IIIa control station (Digital Instruments), extended multi-mode SPM unit (Digital Instruments), the cantilever folder for the F-TMAFM (Digital Instruments), and the potentio/galvanostat (HA-501, Hokuto Denko) were used for F-TMAFM. The microprobe was oxide sensor type Si_3N_4 microcantilever (NP-S type, Digital Instruments).

(a) Cross section

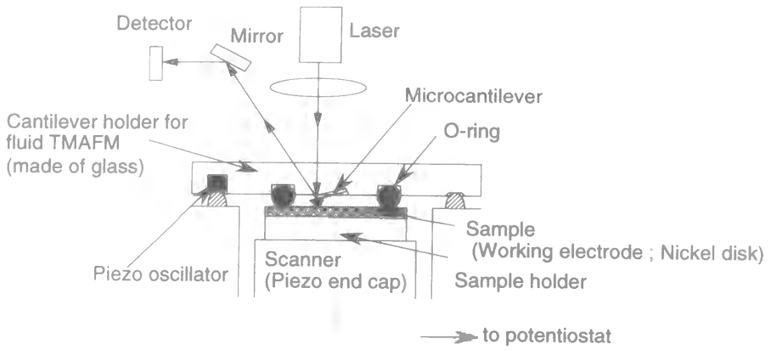

(b) Top View

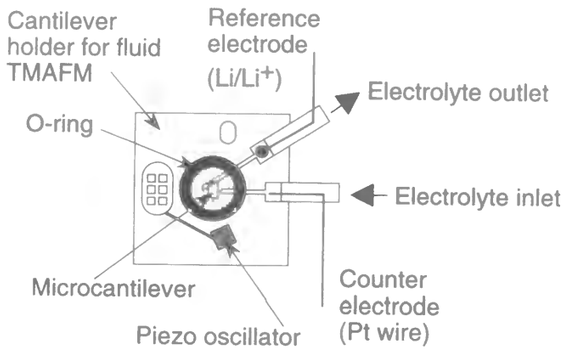

Figure 8-2 Schematic illustration of the cantilver holder for Fluid Tapping Mode Atomic Force Microscopy for the electrochemical operation, (a) cross section, (b) top view.

The scan rate was set at 1 scan line Hz^{-1}. The amplitude and frequency of the alternating voltage for the mechanical oscillation of the probe were 500 mV and between 50-100 kHz, respectively. The electrochemical deposition and dissolution of lithium metal was conducted on a Ni substrate electrode (15 mm diameter disk) under galvanostatic control. The counter electrode was a Pt wire and the reference electrode was lithium metal (Li/Li^+). The current density was 1.0 mA cm^{-2}. Since the AFM unit and the cantilever holder offered by Digital Instruments were not designed for electrochemical operations, these

instruments were modified.

(1) the counter electrode and the reference electrode were set at the injection and the drain of the liquid (electrolyte) in the cantilever holder, respectively.

(2) the piezo end cap under the sample substrate (corresponding to the working electrode of Ni disk) was connected to the terminal for the working electrode of the potentiostat through the interior of the AFM unit.

The modified cantilever holder is shown in Figure 8-2. The F-TMAFM observation was performed in a pure argon dry box at room temperature. In this study, the microprobe was moved away from the target area during the electrochemical deposition and dissolution process to obtain a uniform current distribution.

8-3 Results and Discussion

Observation of the electrochemical deposition and dissolution of lithium using ECQCM

Figure 8-3 (a) shows the electrode potential changes of the 6 MHz Ni quartz crystal microbalance electrode in $LiClO_4$ /PC containing 10 mmol dm^{-3} HF and 14 mmol dm^{-3} H_2O during the deposition and dissolution processes. At the beginning of the electrodeposition, the electrode potential rapidly dropped from the OCV (≈ 3 V vs. Li/Li^+), and became flat at about -270 mV vs. Li/Li^+ through a minimum potential of - 280 mV vs. Li/Li^+. This type of potential change may be caused by the nuclei formation of lithium deposits. During the dissolution process, the potential curve showed a flat potential at +300 mV vs. Li/Li^+. This dissolution process was terminated when 180 mC cm^{-2} had passed. Based on the electrode potential change, the coulombic efficiency of the deposition (charge)/dissolution (discharge) was estimated to be 72 %.

Figure 8-3 (b) shows the changes in the resonance frequency of the 6 MHz Ni quartz crystal microbalance electrode in $LiClO_4$/PC containing 10 mmol dm^{-3} HF and 14 mmol dm^{-3} H_2O during the deposition and dissolution processes. The dotted line in Figure 8-2 (b) is the theoretical line when the mass change per a unit amount of electricity is ± 7 g F^{-1} which corresponds to the ideal electrochemical deposition/dissolution of lithium metal.

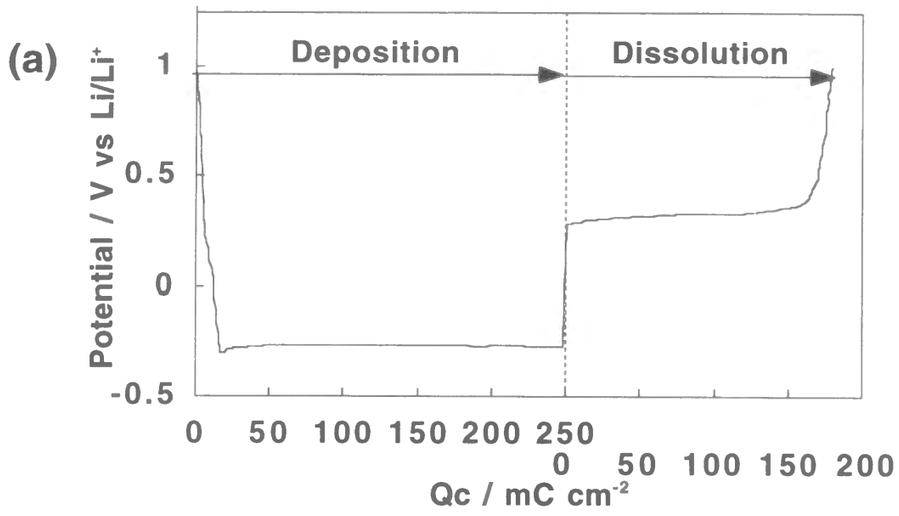

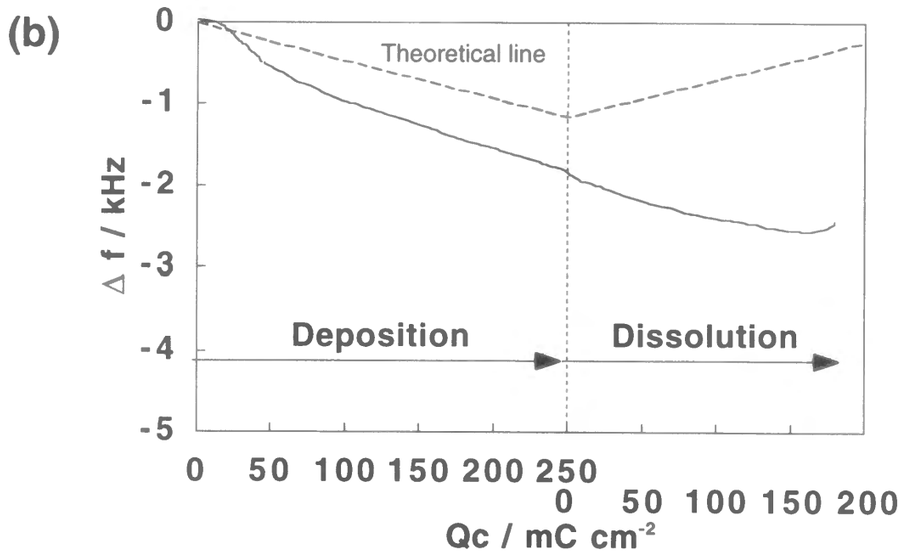

Figure 8-3 (a) Potential changes and (b) frequency changes of 6 MHz Ni quartz crystal microbalance electrode at the electrodeposition and dissolution (current density:1.0 mA cm^{-2}) of lithium in 1.0 M $LiClO_4$/ PC containing 10 mM HF and 14 mM H_2O, dotted line is theoretical line if only lithium metal (mass:7) is deposited.

During the initial deposition process (Q_c < 20 mC cm^{-2}), the frequency gradually decreased with increasing electrical charge. In the region of 50 mC cm^{-2} > Q_c > 20 mC cm^{-2}, the frequency rapidly decreased. The slope of the frequency change in this region was larger than that of the theoretical one. If the surface roughness did not change in this region, it follows that lithium compounds, which have a larger molecular weight per one mole lithium than that of lithium metal, were formed in this region. The potential change in Figure 8-3 (a) shows that the bulk deposition of lithium metal already occurs in the region of 50 mC cm^{-2} > Q_c > 20 mC cm^{-2}. Therefore, these lithium compounds may be produced by the chemical reactions of lithium metal with electrolytes or the electrochemical reduction of electrolytes at the beginning of the electrodeposition process. In the region of Q_c > 50 mC cm^{-2}, the frequency change was constant, which was nearly equal to the theoretical slope. This indicates that the electrodeposition of lithium metal proceeds with the coulombic efficiency of about 100% in the electrolyte containing HF in the region of Q_c > 50 mC cm^{-2}. This ideal lithium deposition continued to the end of deposition process (Qc = 250 mC cm^{-2}).

During the dissolution process, the resonance frequency decreased with increasing amount of electrical charge by Q_c < 150 mC cm^{-2}. This is a surprisingly unexpected result. The resonance frequency change must increase during the electrochemical dissolution as indicated by the theoretical line if the ideal lithium dissolution takes place. This result indicates that extra phenomena occur during the lithium dissolution process. We considered the following two points to explain this frequency change.

(1) Trapping of electrolytes in crevices formed on an electrode surface during the dissolution of lithium. (Such crevices can be formed by an increasing surface roughness. The trapped electrolyte can be detected as the mass change in the electrode because it also oscillated at the resonance frequency as well as the quartz crystal electrode.)

(2) Accumulation of reaction products formed by the chemical reactions of lithium metal with the electrolyte. (If the reaction products on the electrode have a large molecular weight, the electrode mass increases even during the lithium dissolution

process.)

K. Naoi et al. also investigated the electrochemical deposition and dissolution of lithium with ECQCM, and they have already reported that secondary reactions possibly occur during the dissolution process of lithium when using propylene carbonate containing $LiPF_6$ (this electrolyte contains a small amount of HF as the contaminant) [52]. In the previous chapter, it has been already learned that the thick residual film consisting of mainly LiF (a reaction product of lithium with the electrolyte) had accumulated on the substrate electrode during the dissolution of lithium. Therefore, the irreversible chemical reactions of lithium metal with the electrolyte are a possible explanation for the mass increment during the dissolution process. If the residual deposits consisting of LiF contribute to the mass increment, the amount of lithium atoms in the residual deposits is quantitatively related to the amount of lithium metal consumed by electrochemical deposition-dissolution cycle. The amount of lithium atoms included in LiF can be calculated by the frequency decrease (= -2.44 kHz). The amount of lithium consumed by the electrochemical dissolution can be calculated by the loss in the cycle efficiency (= 28% which corresponds to 70 mC cm^{-2}). As a result of this calculation, the former was 1.01×10^{-5} g cm^{-2}, while the latter was 5.0×10^{-6} g cm^{-2}. The former was larger than the latter. So, the influence of the trapped electrolyte is also somewhat related to the mass increment in the electrode. Consequently, based on these ECQCM results, the following two points are suggested.

(1) The consumption of lithium metal during the lithium deposition process occurs only during the initial period.

(2) A part of the electrodeposited lithium metal is consumed by the irreversible chemical reaction of lithium metal with the electrolyte during the dissolution process.

Observation of the electrochemical dissolution of lithium using F-TMAFM

Figure 8-4 (a) shows the F-TMAFM image of the Ni substrate electrode. The surface of the substrate electrode was flat and smooth. Figure 8-4 (b) shows the F-TMAFM image of the lithium electrodeposited on the substrate electrode. The amount of electricity

for the electrodeposition was 300 mC cm^{-2}. The lithium particles with a 0.3-0.4 μm radius were deposited on the substrate electrode. No dendritic lithium was observed anywhere. Such lithium deposits were already observed using SEM or *ex-situ* TMAFM in the previous chapter. This means that the F-TMAFM observation of the lithium particles deposited in the electrolyte containing HF can be performed without any damage by the scanning probe. The electrochemical dissolution of the lithium particles was also conducted. Figure 8-4 (c) shows the F-TMAFM image of the lithium deposits after the electrochemical dissolution of 20 mC cm^{-2}. The center of the image area observed in Figure 8-4 (c) was slightly shifted to the right compared with that in Figure 8-4 (b). This is due to the procedure that the probe is moved out of the target area during the electrochemical dissolution as described in the experimental section. However, it can be said that there are no serious problems for observing the electrochemical dissolution of lithium deposits because the degree of the shift is not very large. Some holes and defects were observed in Figure 8-4 (c), which are marked by white circles. Figure 8-4 (d) and Figure 8-4 (e) show the F-TMAFM images of the lithium deposits after the electrochemical dissolution of 60 mC cm^{-2} and 110 mC cm^{-2}, respectively. The holes and defects observed in Figure 8-4 (c) were enlarged by the consecutive dissolution process. Moreover, many new holes and defects were observed on the lithium particles. Especially, in Figure 8-4 (e), shrinking of the lithium particles was also observed in addition to the formation of holes and defects. Figure 8-4 (f) shows the F-TMAFM image of the lithium deposits after the electrochemical dissolution of 190 mC cm^{-2}. When 190 mC cm^{-2} had passed, the electrode potential was 1.0 V vs. Li/Li^+. Therefore, Figure 8-4 (f) is the F-TMAFM image after the complete dissolution of the lithium particles. The shrinking of the lithium particles significantly proceeded, leading to the very angular morphology of the deposits in this image. These results indicate that residual deposits still remained on the electrode even after the complete dissolution. However, some scratches were also observed in the below part of the image in Figure 8-4 (f). This is because the residual deposits are very soft therefore, they can be easily scratched by the probe. It can be said that *in-situ* observation can not be perfectly conducted for the

(a) Before Deposition

(b) 300 mC cm^{-2} deposition

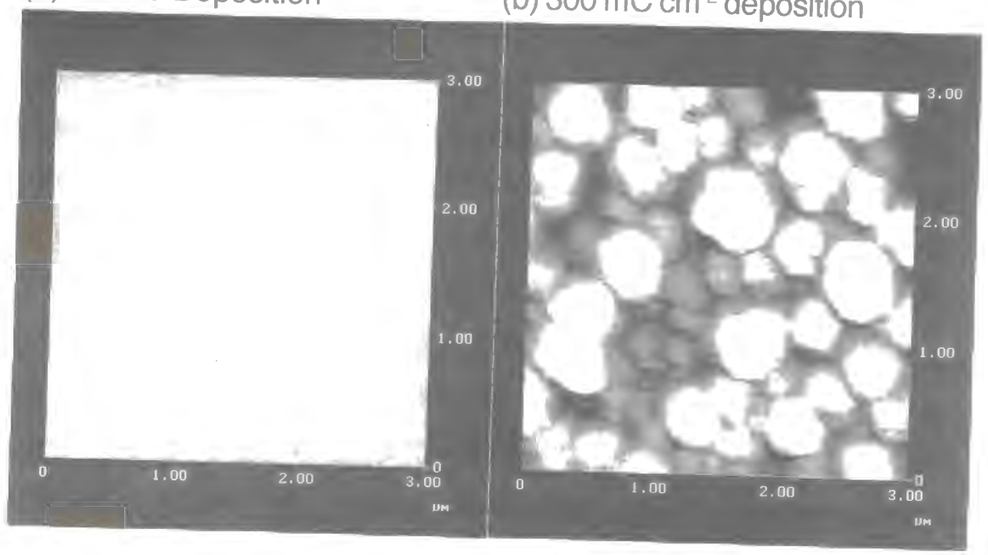

(c) 20 mC cm^{-2} dissolution

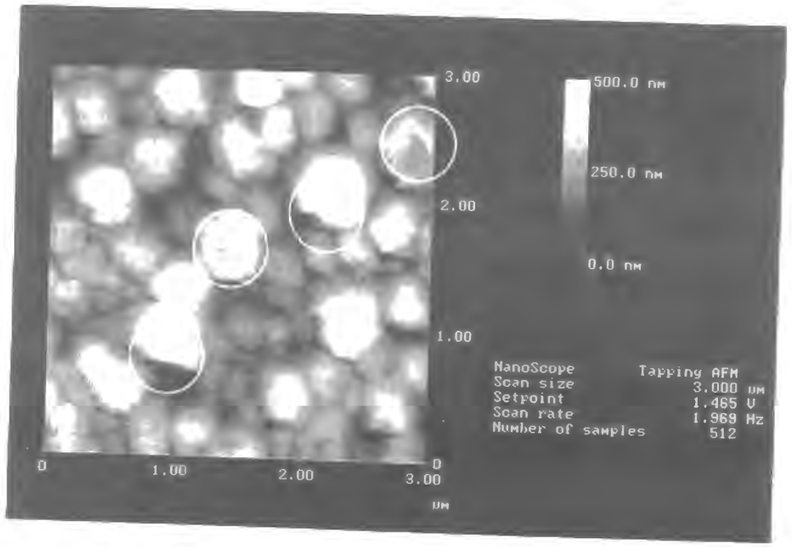

Figure 8-4 Fluid-Tapping Mode-Atomic Force Microscopic (Fluid-TMAFM) image (3 × 3 μm) of electrodeposition and dissolution (current density:1.0 mA cm^{-2}) of lithium on Ni substrate electrode in 1.0 M $LiClO_4$/ PC containing 10 mM HF and 14 mM H_2O, for deposition of (a) 0 mC cm^{-2} and (b) 300 mC cm^{-2}, consecutive dissolution of (c) 20 mC^{-2}.

(d) 60 mC cm^{-2} dissolution

(e) 110 mC cm^{-2} dissolution

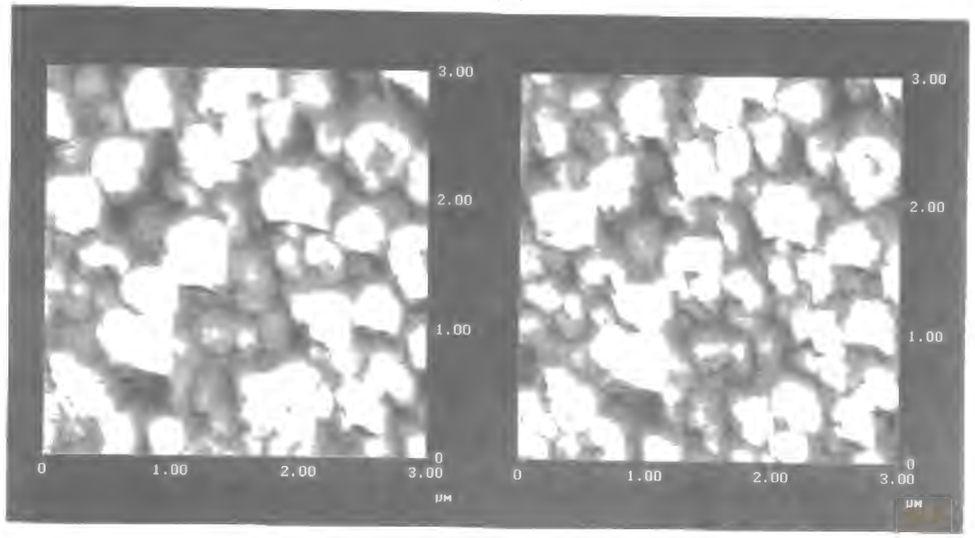

(f) 190 mC cm^{-2} dissolution

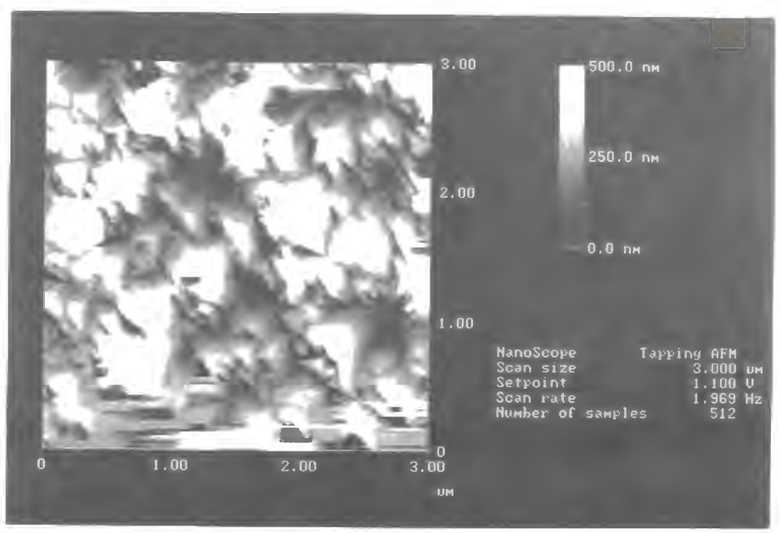

Figure 8-4 Fluid-Tapping Mode-Atomic Force Microscopic (Fluid-TMAFM) image (3 × 3 μm) of electrodeposition and dissolution (current density:1.0 mA cm^{-2}) of lithium on Ni substrate electrode in 1.0 M $LiClO_4$/ PC containing 10 mM HF and 14 mM H_2O, for consecutive dissolution of (d) 60 mC cm^{-2}, (e) 110 mC cm^{-2}, and (f) 190 mC cm^{-2}.

complete dissolution of the lithium particles even using F-TMAFM. On the other hand, D. Aurbach et al. also observed the morphology of the lithium deposits in PC containing $LiPF_6$ after the complete dissolution (discharge) with *in-situ* AFM [56]. They reported that undissolved and corroded lithium deposits were clearly observed on the electrode after the complete dissolution. The differences between their results and ours may be caused by the type of AFM or the electrochemical conditions (current density, total amount of electricity for deposition, substrate electrode type, etc.).

Based on these F-TMAFM results, it is found that the lithium particles are dissolved not only with shrinkage of the particles but also with formation of hole and defects. This drastic morphology change generates an increase in the surface roughness of the electrode and a breakdown of the surface film on the lithium particles. Especially, the latter leads to

the chemical reaction of lithium metal with the components in the electrolyte. Such roughening of the electrode surface and chemical reaction are already confirmed from the mass change in the electrode obtained with ECQCM. Therefore, the F-TMAFM images obtained here suggest that a part of the lithium metal in the lithium particles is irreversibly consumed during the electrochemical dissolution process, namely, the discharge process of the anode.

8-4 Conclusion

The results obtained in this chapter can be summarized in Figure 8-5. In this chapter, the observations with ECQCM and F-TMAFM have revealed for the first time the cause for the loss in cycle efficiency of the lithium particles deposited in the electrolyte containing HF. The loss is strongly related to the consumption of the lithium metal through a chemical reaction with the electrolyte during the dissolution process.

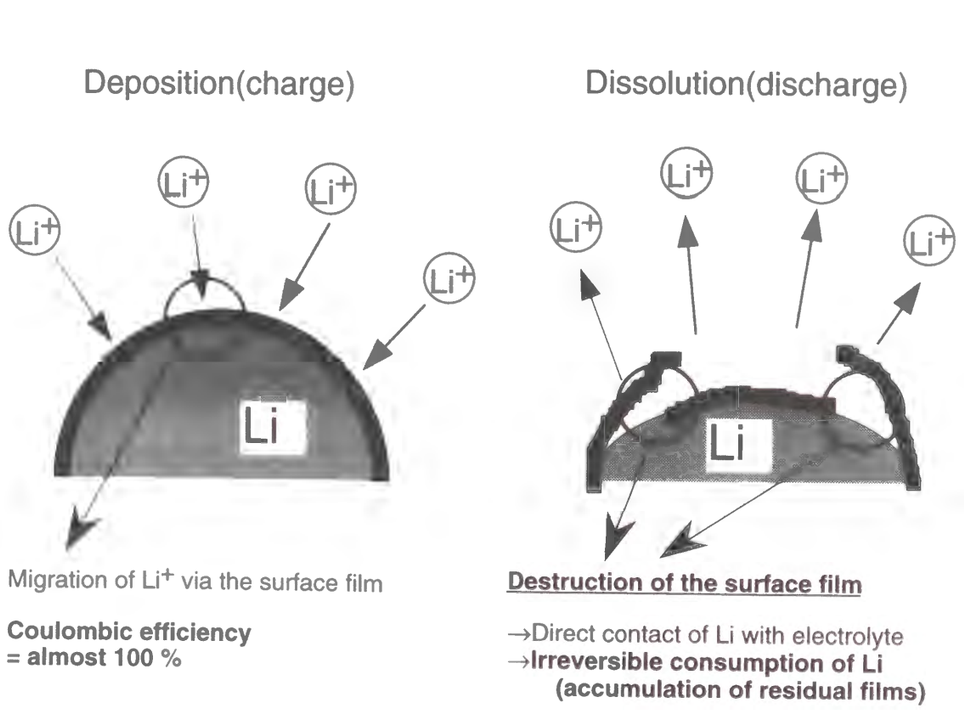

Figure 8-5 Schematic illustration of the despotion and dissolution process of lithium metal in the electrolyte containing HF.

Chapter 9
Electrochemical Deposition of Lithium Metal in Nonaqueous Electrolyte Containing $(C_2H_5)_4NF(HF)_4$ Additive

9-1 Introduction

In the previous chapters, it was discussed that a new surface modification of lithium for a smooth deposition of lithium by adding of hydrofluoric acid (aqueous HF solution). This modification was based on acid-base reactions of HF with basic lithium compounds existing on the lithium metal surface. However, it was found that the coulombic efficiency (utilization) of lithium was only about 80% even with the addition of HF to the electrolytes. This utilization is quite low for practical use, and may be related to H_2O added into the electrolytes together with HF. Theoretically, anhydrous HF might be suitable as an additive, but it is too dangerous and harmful to be used it as a practical additive. Therefore, a new safe source of HF without H_2O would be very useful to examine the effect of species involved in electrolytes with easier handling for an additive.

Recently, some new agents containing HF have been developed for the fluorination of organic compounds, for example, liquid pyridine-anhydrous HF[115], tetraalkylammonium fluoride-anhydrous HF (R_4NF-mHF)[116], and so on. These agents actively promote fluorination, but are safe and do not contain water, and R_4NF-nHF in particular has been used successfully as an electrolyte salt for the electrochemical fluorination in nonaqueous electrolyte solutions, so that it was thought that R_4NF-nHF could be used as an additive for the surface modification of lithium metal. In this chapter, the electrochemical deposition of lithium in a nonaqueous electrolyte containing a new additive $(C_2H_5)_4NF(HF)_4$ (tetraethylammonium fluoride-tetrakis hydrogen fluoride; TEAFHF) was performed and the resultant improvement in the rechargeability of lithium anode was discussed.

9-2 Experimental

Propylene carbonate (PC) containing 1.0 mol dm^{-3} $LiCF_3SO_3$ and dimethoxy ethane

(DME) containing 0.4 mol dm^{-3} $LiClO_4$, supplied by Mitsubishi Chemicals Corporation, were used as base electrolytes. $(C_2H_5)_4NF(HF)_4$ (TEAFHF) was supplied by Morita Kagaku Industrial Company. TEAFHF in concentrations of 1.3 mmol dm^{-3}, 2.5 mmol dm^{-3}, 5.0 mmol dm^{-3}, or 10 mmol dm^{-3} was added to the electrolytes as an additive. Water content in the electrolytes containing TEAFHF, measured with the Karl Fischer titration method ranged from 20 to 30 ppm (1.0~1.5 mmol dm^{-3}) H_2O before and after the addition of TEAFHF at various concentrations. When 10 mmol dm^{-3} of hydrofluoric acid (46 wt %), which was also used as an additive, was added to the base electrolytes, the water content became more than 14 mmol dm^{-3}. Lithium metal was deposited on a Ni substrate (0.6 cm × 1.0 cm) in these electrolytes. A galvanostatic method was used for the electrochemical deposition of lithium metal at a current of 1.0 mA cm^{-2}. In addition, a discharge and charge cycling test of lithium was conducted in the same electrolyte used for the electrochemical deposition. The discharge and charge currents were 1.0 mA cm^{-2} and the discharge terminated at 1.0 V vs. Li/Li^+. Utilization was then calculated by dividing the discharge capacity by the charge capacity (1.0 C cm^{-2} or 7.2 C cm^{-2}). All the procedures were conducted in an argon dry box at room temperature (dew point < -90 °C).

The surface analysis of the electrode after the deposition or dissolution process was carried out with XPS. The morphology of the lithium electrodeposited was observed with SEM. The sample transfer from the argon dry box to the XPS or the SEM equipment was conducted in the same way as described in the chapter 1. The analysis condition for the XPS or the SEM was the same as that in the chapter 1.

The electrochemical behavior of lithium metal deposited on the substrate electrode was also analyzed by an impedance measurement. The impedance measurement of lithium metal was performed at open circuit potential after the deposition or dissolution process. The analysis condition of the impedance measurement was the same as that in the chapter 6.

9-3 Results and Discussion

9-3-1 Lithium deposited in PC electrolyte containing TEAFHF

Figures 9-1 (a), (b), and (c) show the electron micrographs of lithium deposited in 1.0 mol dm^{-3} $LiCF_3SO_3$/PC without any additives, with the addition of hydrofluoric acid ($HF+H_2O$), and with TEAFHF, respectively. The lithium deposited in $LiCF_3SO_3$/PC without an additive showed a typical dendrite shape of lithium particle, but that deposited in $LiCF_3SO_3$/PC with hydrofluoric acid with a flat surface consisting of fine particles. In addition, the lithium deposited in $LiCF_3SO_3$/PC containing TEAFHF yielded the same morphology of the lithium particles as that for $LiCF_3SO_3$/PC with aqueous HF.

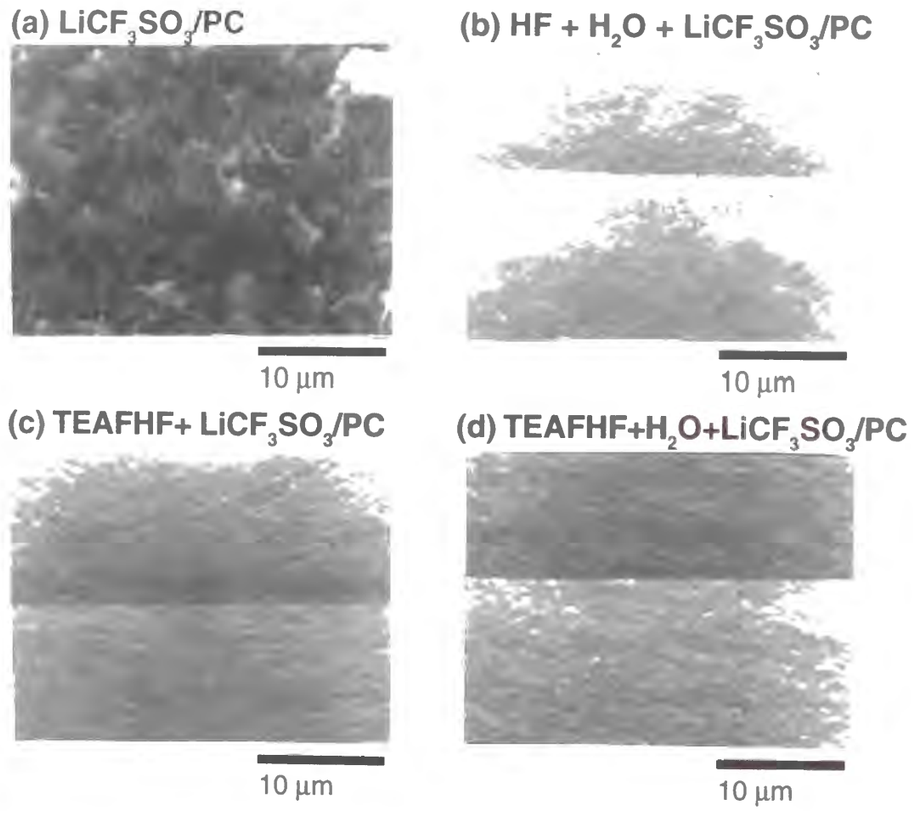

Figure 9-1 Scanning electron micrographs of lithium deposited in various nonaqueous electrolytes, (a) propylene carbonate containing 1.0 M $LiCF_3SO_3$, (b) propylene carbonate containing 1.0 M $LiCF_3SO_3$, 10 mM HF and 14 mM H_2O , (c) propylene carbonate containing 1.0 M $LiCF_3SO_3$ and 2.5 mM TEAFHF, (d) propylene carbonate containing 1.0 M $LiCF_3SO_3$, 2.5 mM TEAFHF, and 10 mM H_2O,

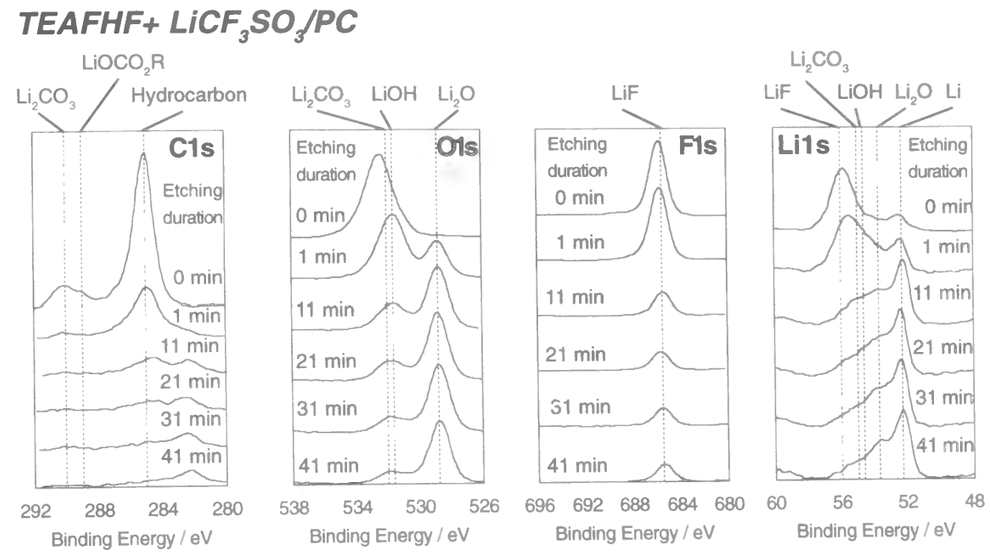

Figure 9-2 XPS spectra of Li 1s, C 1s, O 1s, and F 1s electrons for lithium deposited in propylene carbonate containing 1.0 M $LiCF_3SO_3$ and 2.5 mM TEAFHF. Times in figures indicates the argon ion etching duration.

Figure 9-2 shows the XPS spectra of the surface film on lithium deposited in $LiCF_3SO_3$/PC containing 2.5 mmol dm^{-3} of TEAFHF at 1.0 mA cm^{-2}. The C 1s XPS spectra included three peaks at 290.0 eV, 289.0 eV, and 285.0 eV, the last of which was attributed to hydrocarbon remaining in the XPS analysis chamber as an impurity. The peaks at 290.0 eV and 289.0 eV were assigned to Li_2CO_3 and lithium alkylcarbonate ($LiOCO_2R$), respectively, and both peaks disappeared by etching even for only 1 min. The peak at 532.0 eV in the O 1s XPS spectra also shows the presence of Li_2CO_3 as well as of LiOH in the outer layer of the surface film on lithium. The peak at 528.8 eV for Li_2O appeared after 1 min of etching and became more intense during the argon ion etching process, suggesting that Li_2O was distributed over the inner layer of the surface film. While the XPS spectra of F 1s showed that LiF was included in the outer surface film. The peak at 56.0 eV in the spectra of Li 1s was attributed to LiF. The LiF peak markedly decreased after the argon ion etching for 1 min, indicating that the LiF layer was very thin. The peak at 52.3 eV in the same spectra of Li 1s was attributed to Li metal, the peak of

which was already observed before the argon ion etching. This does not mean, however, that lithium metal as such is exposed before the argon ion etching, because all lithium metal is always covered with a surface film, otherwise it would not be stable in nonaqueous solvents. This observation is based on the detection of Li 1s photoelectrons from lithium metal under the surface film, indicating that the surface film is very thin (a few nanometers thick). The Li metal peak intensified with argon ion etching, accompanied by a shoulder peak around 54 eV, which corresponds to Li_2O (the binding energy of Li 1s corresponding to Li_2O is 53.7 eV). These peaks in the Li 1s XPS spectra demonstrated that the Li_2O layer lies underneath the LiF layer, a structure which could also be confirmed from the O 1s XPS spectra. From these XPS spectra changes during the argon ion etching, it was found that the lithium deposit is covered with a surface film consisting of LiF (outer layer) and Li_2O (inner layer). Similar XPS spectra of Li 1s, C 1s, O 1s, and F 1s have been observed for the surface film on lithium deposited in nonaqueous electrolytes containing an aqueous HF additive, as shown in the chapter 5 and 6. These results indicate that the surface reactions occurring on the lithium particles deposited in the $LiCF_3SO_3$/PC with TEAFHF are similar to those in nonaqueous electrolytes containing aqueous HF.

Figure 9-3 (a) shows the depth profiles of Li, C, O, F, S, and N elements involved in the surface film on lithium deposited in $LiCF_3SO_3$/PC with TEAFHF. A main element on the outside of the surface film was fluorine in addition to Li, indicating that the outer layer of the surface film consisted of LiF. Oxygen element was a major component of the inner layer of the surface film, while sulfur and nitrogen were not present in the surface film. It can therefore be said that the outer layer of the surface film consists of LiF and the inner layer of Li_2O. This surface film was thus completely different from that on lithium deposited in $LiCF_3SO_3$/PC without any additives as shown in the chapter 5. A similar LiF/ Li_2O bi-layered structure has been observed for lithium deposited in nonaqueous electrolytes containing HF+H_2O. In the previous chapters, it was discussed that this surface film yields hemispherical lithium particles because the suppression of lithium dendrites is attained as a result of a uniform current distribution. Since the surface film on lithium consisting of

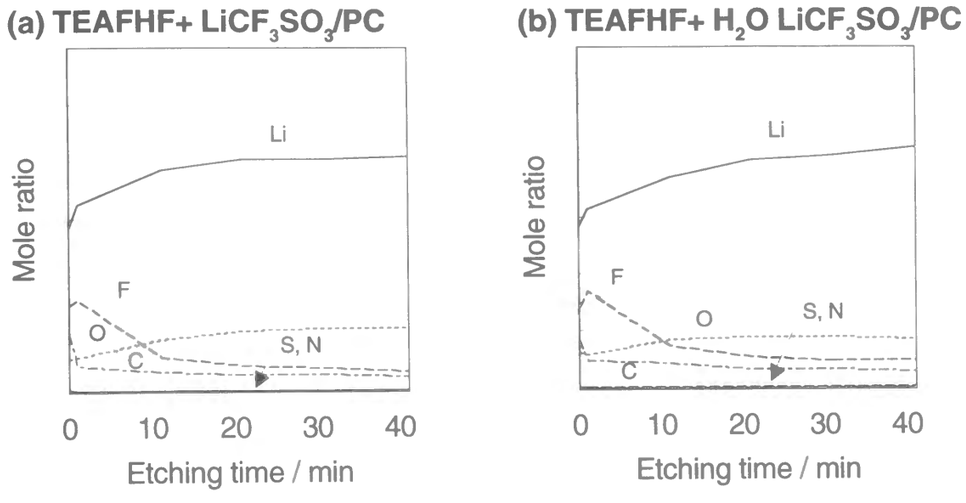

Figure 9-3 Depth profiles of the elements involved in the surface film on lithium deposited in (a) propylene carbonate containing 1.0 M $LiCF_3SO_3$ and 2.5 mM TEAFHF, and (b) propylene carbonate containing 1.0 M $LiCF_3SO_3$, 2.5 mM TEAFHF, and 10 mM H_2O.

several lithium compounds has a high resistance (a low ionic conductivity), the current distribution is determined by the distribution of resistance in the surface film formed on lithium deposited in the nonaqueous electrolyte. A more uniform surface film may result in a more uniform current distribution which is good for the electrodeposition of lithium in a hemispherical particle shape. Therefore, it can be concluded that the TEAFHF additive promotes a uniform surface film on lithium.

The formation of LiF can be explained by the acid-base reactions of lithium or lithium compounds with HF. HF is produced by a chemical equilibrium of $F(HF)_4^-$ ions and HF_2^-. $F(HF)_4^-$ ions, which are formed by the ionic dissociation of $[(C_2H_5)_4N^+ - F(HF)_4^-]$ salt in $LiCF_3SO_3$/PC, as expressed by the formula

$$(C_2H_5)_4NF(HF)_4 \rightarrow (C_2H_5)_4N^+ + F(HF)_4^- \rightarrow (C_2H_5)_4N^+ + F(HF)_n^- + (4 - n)HF \quad (4 \leq n \leq 0)$$ [116]

This equilibrium can maintain a constant concentration of HF in the electrolytes.

The scanning electron micrographs showed that the addition of TEAFHF to the electrolyte promoted the formation of smooth and flat lithium deposits. The morphology

of lithium particle deposited in $LiCF_3SO_3$/PC with TEAFHF may indicate that the discharge and charge characteristics of lithium metal can be improved with this additive. In order to investigate the effect of TEAFHF on the discharge and charge cycle performance of lithium metal anodes, a galvanostatic charge and discharge cycle test was employed to elucidate their performance. The utilization for each cycle in the electrolytes with the aqueous HF, with TEAFHF, or without any additives are shown in Figure 9-4. The utilization for the first cycle was about 80% when $LiCF_3SO_3$/PC did not contain any additives. However, it rapidly decreased with each cycle, reaching 20% at the tenth cycle. This decrease can be explained by the mechanical sloughing off of lithium from the Ni substrate or the electrical insulation of lithium from the Ni substrate, phenomena which are often observed when lithium dendrites are formed, and are typical when lithium is deposited in dendrite form. When $LiCF_3SO_3$/PC was used with the HF+H_2O additive, the initial utilization was also about 80%, but after 35 cycles, it was still about 70%. On the other hand, when $LiCF_3SO_3$/PC was used with TEAFHF, the initial utilization was only about 70 %, but this utilization was maintained until the 18th cycle, and at the 30th cycle, it had been reduced to 20%.

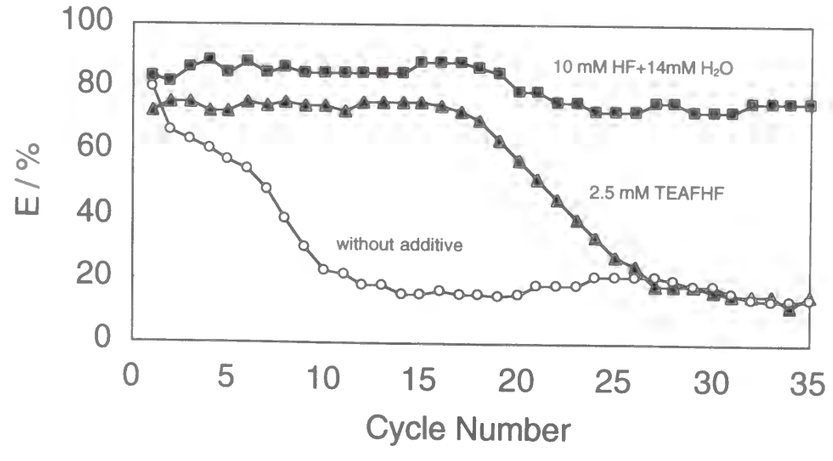

Figure 9-4 Utilization of lithium deposited in propylene carbonate containing 1.0 M $LiCF_3SO_3$ without additive, with 10 mM HF and 14 mM H_2O, or with 2.5 mM TEAFHF. The current density; 1.0 mA cm^{-2}, the total charge; 1.0 C cm^{-2}, the cut off potential; 1.0 V vs. Li/Li^+.

Dendrite formation was observed at the electrode surface after the 30th cycle in this case. This result suggests that the following two important points. First, the additives did not affect the initial utilization of lithium. On the other hand, the decrease in the utilization of lithium during dissolution and deposition cycles seemed to be strongly affected by the presence of HF, TEAFHF, and H_2O. In the case of a lithium metal anode, the low utilization is due to lithium dendrite formation and major consumption of lithium metal by undesirable reactions with electrolytes. It is likely that a breakdown of the surface film occurs as a result of a decrease in volume of lithium particles during the discharge (the dissolution) process of the lithium metal anode, leading to an acceleration of lithium dendrite formation and a direct reaction of lithium with electrolytes. Second, the addition of HF+H_2O to the PC electrolyte is more effective in suppressing the dendrite formation than is the addition of TEAFHF. This indicates that lithium dendrite formation and major consumption of lithium metal by undesirable reactions with electrolytes are influenced by the presence of H_2O.

5-3-2 Lithium deposited in PC electrolytes containing TEAFHF and H_2O

Figure 9-5 shows the utilization changes in $LiCF_3SO_3$/PC containing TEAFHF with various quantities of H_2O. The utilization was improved most when the water content was 10 mmol dm^{-3}: it was maintained at 80 % even after 35 cycles. The utilization in $LiCF_3SO_3$/PC containing 2.5 mmol dm^{-3} TEAFHF with 10 mmol dm^{-3} H_2O was higher than that containing 10 mmol dm^{-3} aqueous HF. This is because, when the aqueous HF solution is used as the additive, water content cannot be controlled. Therefore, TEAFHF is more useful additive. A comparison of the utilization in $LiCF_3SO_3$/PC containing 2.5 mmol dm^{-3} TEAFHF with various H_2O concentrations demonstrates that the appropriate addition of H_2O is effective for stabilizing the surface film on lithium.

The morphology of lithium deposited in $LiCF_3SO_3$/PC containing 2.5 mmol dm^{-3} TEAFHF and 10 mmol dm^{-3} H_2O was observed with SEM. Figure 9-1 (d) shows the electron micrograph of lithium deposited in this electrolyte. All of the lithium particles

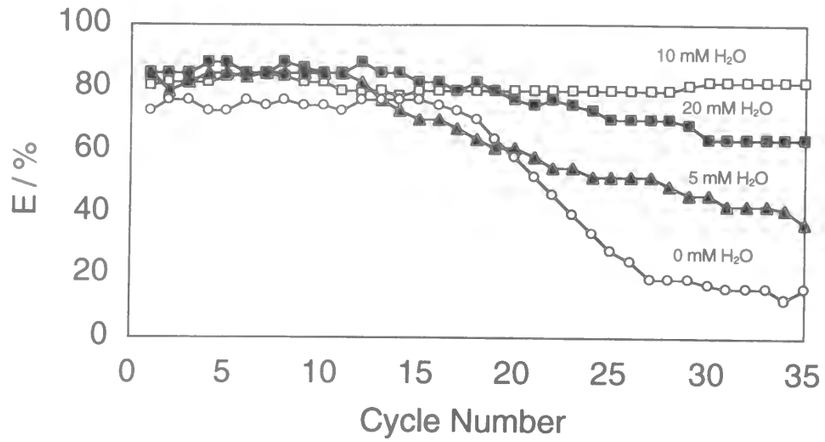

Figure 9-5 Utilization of lithium deposited in propylene carbonate containing 1.0 M $LiCF_3SO_3$, 2.5 mmol dm^{-3} TEAFHF, and various content of H_2O. The current density; 1.0 mA cm^{-2}, the total charge; 1.0 C cm^{-2}, the cut off potential; 1.0 V vs. Li/ Li^+.

deposited in the electrolytes containing various concentration of H_2O had the same morphology as observed for the electrolyte containing only TEAFHF. This SEM observation, thus indicates that the initial morphology of lithium deposited in these electrolytes is not influenced by a presence of H_2O.

XPS spectra for lithium deposited in $LiCF_3SO_3$/PC containing TEAFHF and H_2O are shown in Figure 9-6. The C 1s XPS spectra show the presence of carbonate compounds in the outer layer of the surface film on lithium. The O 1s XPS spectra show the presence of LiOH and Li_2CO_3 at the outer layer of the surface film. The peak intensity for LiOH and Li_2CO_3 was reduced by argon ion etching, while that corresponding to Li_2O was enhanced. Whereas the F 1s XPS spectra show the presence of LiF in the outer layer of the surface film, those of Li 1s indicate the presence of LiF in the outer surface film as well as the existence of Li_2O in the inner layer. These XPS spectra indicate that the surface film on lithium deposited in the electrolyte containing H_2O is the same as that observed for lithium deposited in the electrolyte without addition of H_2O. In other words, the surface films on lithium deposited in $LiCF_3SO_3$/PC containing TEAFHF with or without the addition of H_2O did not show any differences, and that both surface films consist of bi-layered LiF/

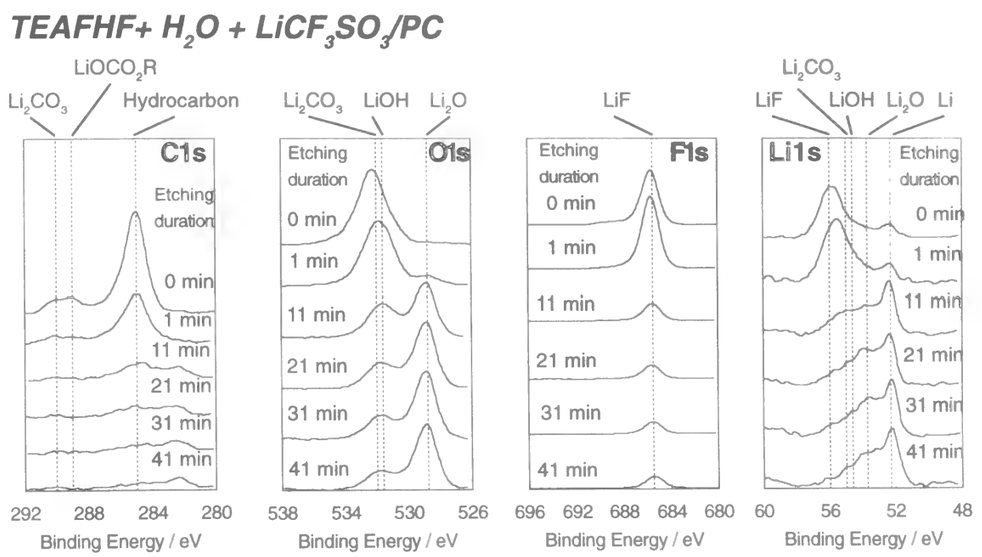

Figure 9-6 XPS spectra of Li 1s, C 1s, O 1s, and F 1s electrons for lithium deposited in propylene carbonate containing 1.0 M $LiCF_3SO_3$, 2.5 mM TEAFHF, and 10 mM H_2O. Times in figures indicate the argon ion etching duration. The current density; 1.0 mA cm^{-2}, the total charge; 1.0 C cm^{-2}.

Li_2O. The depth profiles of the elements shown in Figure 9-3(b) are similar to those in Figure 9-3(a). These results show that the outer layer of the surface film mainly consists of LiF and the inner one of Li_2O. Furthermore, these XPS and SEM analyses indicate that the difference in utilization is not related to the surface film on lithium during the first charge process (the first deposition process). The difference may therefore be due to the degree of stability of the surface film on lithium during the discharge and charge cycles.

5-3-3 Lithium deposited in DME electrolyte containing TEAFHF

Several results obtained for PC electrolytes containing TEAFHF or aqueous HF additives have demonstrated that less reactivity of the solvent with lithium metal is needed to obtain a higher rechargeability of lithium anodes. Furthermore, ether solvents, such as DME, are less active than ester solvents, such as PC, against a reduction by lithium metal [66]. Figures 9-7 (a) and (b) show the electron micrographs of lithium deposited in 0.4 mol

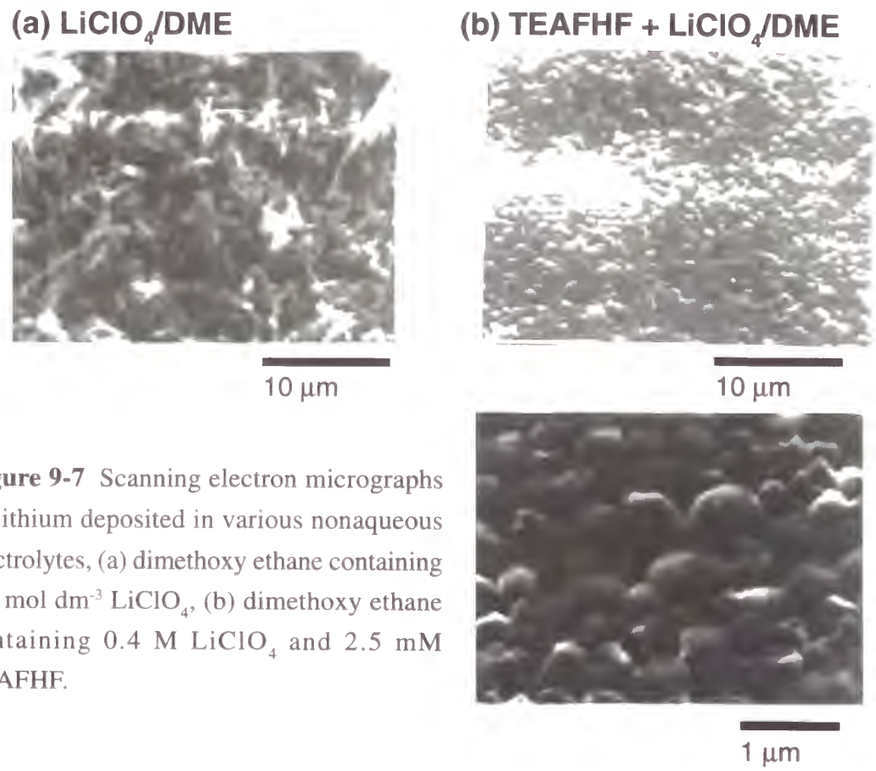

Figure 9-7 Scanning electron micrographs of lithium deposited in various nonaqueous electrolytes, (a) dimethoxy ethane containing 0.4 mol dm^{-3} $LiClO_4$, (b) dimethoxy ethane containing 0.4 M $LiClO_4$ and 2.5 mM TEAFHF.

dm^{-3} $LiClO_4$/DME without any additives and with TEAFHF as an additive, respectively. The morphology of lithium deposited in the DME electrolyte without TEAFHF exhibited a typical dendritic shape, while that in the DME electrolyte with TEAFHF consisted of particles 0.5 μm in diameter. This particle size was much larger than that obtained in the PC electrolyte with TEAFHF, as shown in Figures 9-1 and 9-7.

Figure 9-8 shows the XPS spectra for lithium deposits obtained in $LiClO_4$/DME containing TEAFHF. Figure 9-9 shows the depth profiles of the elements involved in the surface film on lithium deposited in this electrolyte. The C 1s XPS spectra show a very weak peak corresponding to the carbonate species. The atomic ratio of C in the depth profiles was smaller than that in the PC electrolyte containing TEAFHF (as shown in Figure 9-3(a)), indicating smaller amounts of carbonate or organic compounds in the surface film formed in DME electrolyte than of those in the surface film formed in PC electrolyte. These results are assumed to be due to a reduced reactivity of DME with

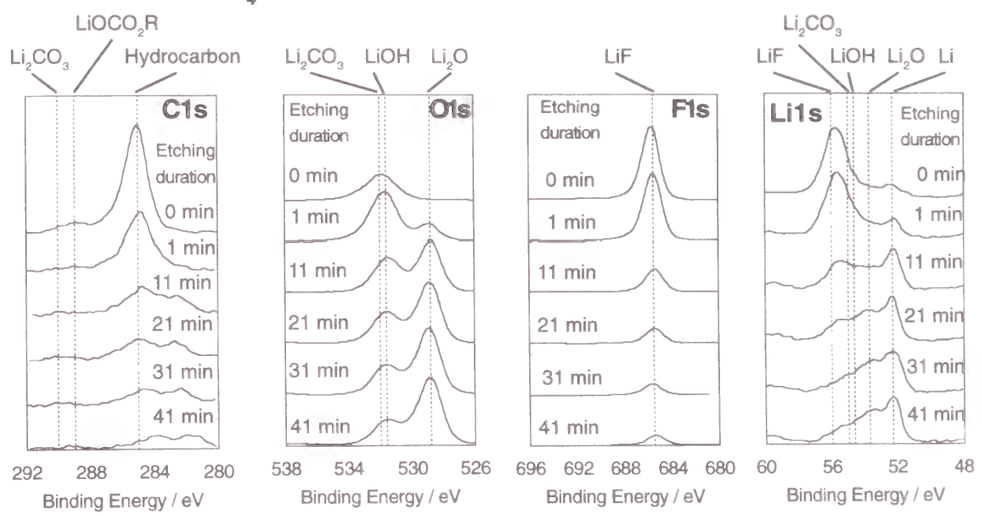

Figure 9-8 XPS spectra of Li 1s, C 1s, O 1s, and F 1s electrons for lithium deposited in dimethoxy ethane containing 0.4 M $LiClO_4$ and 2.5 mM TEAFHF. Times in figures indicate the argon ion etching duration. The current density; 1.0 mA cm^{-2}, the total charge; 7.2 C cm^{-2}.

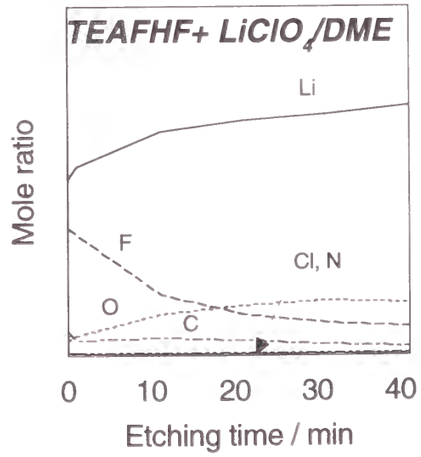

Figure 9-9 Depth profiles of the elements involved in the surface film on lithium deposited in dimethoxy ethane containing 0.4 M $LiClO_4$ and 2.5 mM TEAFHF.

lithium metal. On the other hand, the XPS spectra of Li 1s, O 1s, and F 1s and the mole ratio of Li, O, and F in the depth profiles were very similar to those observed for the surface film on lithium deposited in $LiCF_3SO_3$ or $LiClO_4$/PC containing HF+H_2O or TEAFHF. The depth profiles show that the surface film formed in $LiClO_4$/DME consisted of a LiF/Li_2O bi-layered structure. The particle size of lithium deposited in $LiClO_4$/DME was larger than that deposited in $LiCF_3SO_3$ or $LiClO_4$/PC containing HF+H_2O or TEAFHF, while the surface films formed in these electrolytes were

almost the same. From this result, it can be concluded that the selection of the solvent affects the particle size as well as the particle shape when TEAFHF is contained in the electrolyte. When the cycle of dissolution and deposition of lithium particles is repeated many times, the surface film may undergo a mechanical stress which can cause its breakdown. It can therefore be expected that the particle size of lithium influences the mechanical stress produced in the surface film during the dissolution and deposition cycles. Therefore, the discharge and charge cycle performance may be improved in terms of less reactivity of the $LiClO_4$/DME electrolyte and less mechanical stress due to the larger particle size of lithium.

Figure 9-10 shows changes in the discharge and charge cycle efficiency of lithium deposited in $LiClO_4$/DME containing various TEAFHF concentrations. The highest coulombic efficiency (92.5%) for the five different concentrations of TEAFHF was obtained with 2.5 mmol dm^{-3}. However, the efficiency decreased rapidly after the 5th cycle. When 5.0 mmol dm^{-3} TEAFHF was added into the electrolyte, the initial efficiency of more than 80 %, was maintained during up to the 15th cycle. These high utilization were obtained without the addition of H_2O. This is important because the addition of H_2O is usually detrimental for batteries using nonaqueous electrolytes.

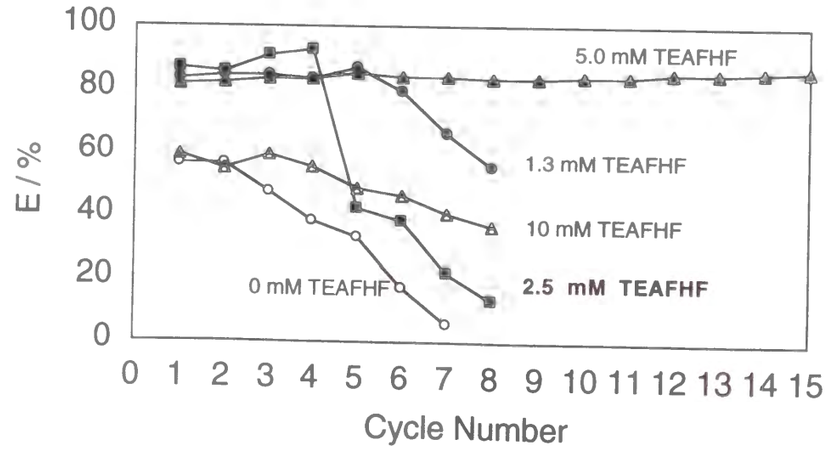

Figure 9-10 Utilization of lithium deposited in dimethoxy ethane containing 0.4 mM $LiClO_4$ and various contents of TEAFHF. The current density; 1.0 mA cm^{-2}, the total charge; 2.0 mA h cm^{-2} (7.2 C cm^{-2}), the cut off potential; 0.4 V vs. Li/Li^+.

According to the above results, the performance of lithium metal anode in the electrolyte containing DME and TEAFHF is highly significant for practical use. Therefore, the discharge and charge cycle tests were performed by using a electrochemical cell like practical coin type cell as shown in Figure 9-11. A solvent mixture of dimethoxy ethane and ethylene carbonate containing 0.6 mol dm^{-3} $LiClO_4$ ($LiClO_4$/DME+EC) was used as the base electrolyte. TEAFHF was added into the base electrolyte to obtain the electrolyte containing 5.0 mmol dm^{-3} TEAFHF. In this cell, $LiCoO_2$ was used as the cathode material and Ni substrate as the anode substrate. This means that this battery does not contain any lithium metal at first. The lithium metal was then prepared during the first charging of this battery, and $LiCoO_2$ cathode pellet was produced by pressing together a mixture of $LiCoO_2$, acetylene black, and PTFE binder with a weight ratio of 80:15:5. The amount of $LiCoO_2$ was much larger (more than 5 times in capacity) than that of lithium metal, so that the capacity of this battery was controlled by the capacity of the lithium metal anode. Therefore, the rechargeability of the lithium metal anode can be easily estimated by dividing the discharge capacity by the charge capacity. The Ni substrate was sandwiched between two

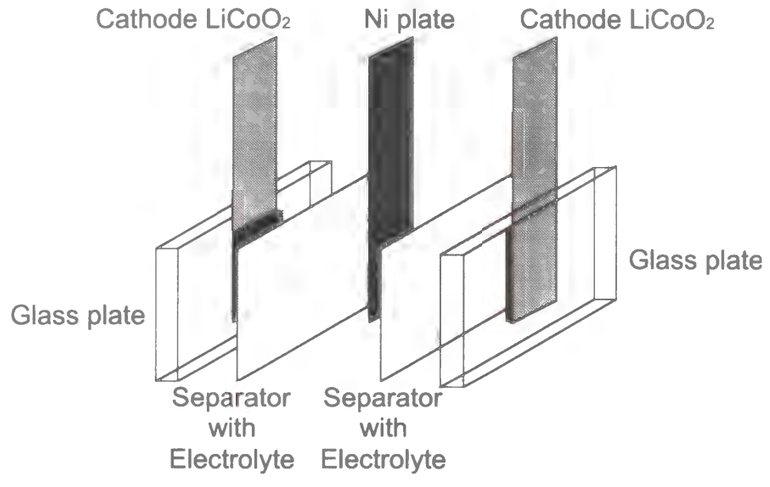

Figure 9-11 Schematic illustration for rechargeable lithium battery constructed by $LiCoO_2$ cathode, polypropylene separator, and Ni substrate.

cathode pellets covered with a separator. The discharge and charge currents were 1.0 mA cm^{-2}, and the discharge was terminated at 3.0 V cell voltage. The charging time was set at 2 hours, corresponding to a constant charge capacity of 2 mA h.

Figure 9-12 shows the charge-discharge curve during the discharge and charge cycles. The initial cell voltage was roughly 0 V. During the charging process, the cell voltage increased to be about 3.9 V, indicating that the deposition of lithium metal on the Ni substrate and the deintercalation of lithium from $LiCoO_2$ took place simultaneously. After two hours charging, the cell was discharged. The cell voltage decreased as the discharge proceeded, and the average voltage of this battery was about 3.8 V. The most important point is the rechargeability of the lithium metal anode. Figure 9-13 shows the efficiency obtained during the discharge and charge cycles. The efficiency was less than 100 % at the first or the second cycle, became 100 % after the third cycle, and stayed at nearly 100 % even more than 30 cycles. This result clearly indicates that lithium metal is used at 100 % utilization when the DME base electrolyte with TEAFHF is used. The 100 % efficiency for this battery indicates two important points. First, the dendrite formation of lithium is suppressed even during many discharge and charge cycles. In fact, no lithium dendrites were observed by scanning electron microscopic observation even after the 70th

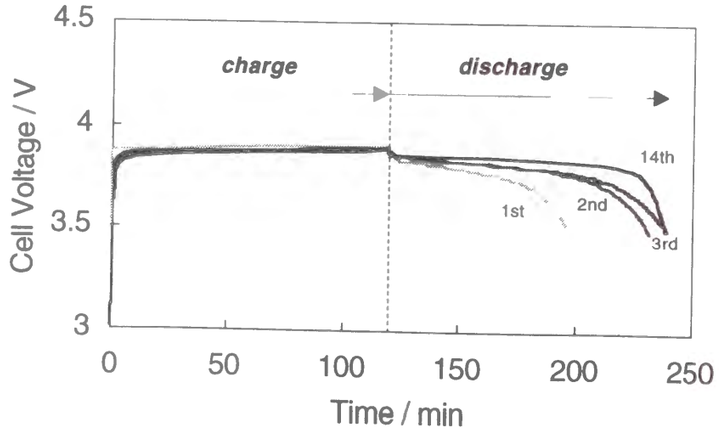

Figure 9-12 Charge-discharge curves for the battery in figure 9-11, in $LiClO_4$/ DME+EC containing 5 mmol dm^{-3} $(C_2H_5)_4NF(HF)_4$.

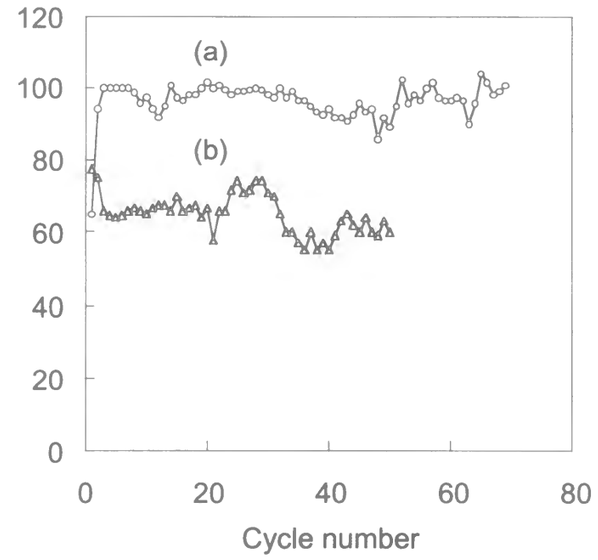

Figure 9-13 Efficiencies of lithium metal anodes obtained by using the battery in figure 9-11, in (a) $LiClO_4$/DME+EC containing 5.0 mM TEAFHF and (b) $LiClO_4$/ DME+EC.

cycle (Figure 9-14), a result which may be credited to the exceptionally uniform surface film on lithium metal formed during the initial cycles. Second, the surface film formed on the lithium metal anode remains highly stable during the discharge and charge cycles. In general, surface film is often affected by the discharge and charge cycles of the battery, which leads to the breakdown of the uniform surface film during the initial charging. However, when such a breakdown occurs during the discharge and charge cycles, the efficiency should become much less than 100 %.

9-4 Conclusion

The coulombic efficiency of lithium metal anodes during discharge and charge cycles was examined by using $LiCF_3SO_3$/PC containing various concentrations of HF, H_2O, and TEAFHF. TEAFHF was effective for suppressing the dendrite formation of lithium, leading to a high performance of the lithium anode. The appropriate proper

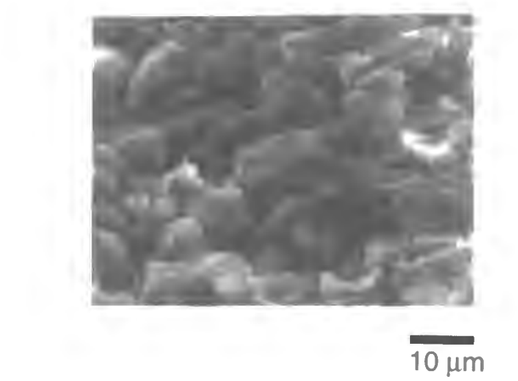

Figure 9-14 Scanning electron micrographs of lithium metal anodes in the battery, in (a) $LiClO_4$/DME+EC containing 5 mmol dm^{-3} $(C_2H_5)_4NF(HF)_4$, after 70 th cycles.

amount of H_2O in PC containing HF or TEAFHF promoted a long cycle life of the lithium anode, but the utilization was only about 80%.

In the case of a $LiClO_4$/DME base electrolyte, large lithium particles were deposited with the surface film consisting of bi-layered LiF/Li_2O. These lithium particles also exhibited the highest performance when 2.5 mmol dm^{-3} TEAFHF was added to the electrolyte, with a utilization of 92.5%.

As results of charge-discharge cycle test by quasi-practical battery cell, it was found that the rechargeability of batteries with lithium metal is extremely improved to almost 100%. This result indicates strongly the possibility to realize the practical lithium battery with lithium metal anode.

General Conclusion

In the present study, the author's objective was to improve the reversibility of deposition and dissolution of a lithium metal anode for lithium metal rechargeable batteries. The thesis is a summary of a study of the surface condition control of lithium metal anodes. The results obtained in this investigation are shown as follows.

1. The charge-discharge cycle efficiency (the reversibility of deposition and dissolution of lithium metal) and safety of the lithium metal anode are too low to be used for practical batteries. These are caused by both the high reactivity of lithium with nonaqueous electrolytes and the morphology of lithium electrodeposited during charging. The author suggested that the morphology of the electrodeposited lithium strongly depends on the physical and chemical conditions of the surface film. Thus various electrochemical and spectroscopic analyses (XPS, FTIR, and EIS) of the lithium metal surface have been conducted to obtain information about the chemical compositions and structure of the surface film. As a result, it was found that the surface film on lithium and the morphology of lithium seem to be sensitive to impurities such as acids in the nonaqueous electrolytes as well as the solvent and salt (Chapters 1 and 2).
2. The relationship between the morphology of the electrodeposited lithium in various nonaqueous electrolytes and the condition of the surface film on the electrodeposited lithium itself was investigated using SEM and XPS. As a result, the electrochemical conditions for the suppression of the dendritic lithium were found. A surface film consisting of various basic lithium compounds (Li_2CO_3, LiOH, Li_2O, etc.) was observed when dendritic lithium was deposited. On the other hand, when a small amount of hydrogen fluoride (HF) as an impurity was contained in electrolyte, an effective surface film (LiF/Li_2O thin bi-layer) for suppressing the dendrite lithium was produced by surface modification with HF. The electrochemical behavior of lithium metal in the presence of HF was investigated using various spectroscopic and electrochemical

analyses. Consequently, the deposition of lithium particles with an extremely smooth hemispherical form was accomplished by the addition of an adequate amount of HF into the electrolytes (Chapters 3 and 4).

3. The fine lithium particles electrodeposited in electrolytes containing HF were covered with a highly stable and ultrathin (20-50 Å) film consisting of a LiF/Li_2O bilayer. The formation of this surface film can be explained by the acid-base reactions of the various basic lithium compounds (Li_2CO_3, LiOH, Li_2O, etc.) with HF. Various surface analyses (XPS, SEM, EIS, AFM, and SPoM) revealed that the surface film was sufficiently uniform and smoothed the current distribution of Li^+ ions at the lithium/electrolyte interface (the current distribution promotes the dendritic lithium). Moreover, the fine lithium particles showed a high reversibility (the coulombic efficiency > 80%) of deposition and dissolution (Chapters 5, 6, and 7).
4. Some *in-situ* surface analyses (ECQCM and AFM) showed the cause for the loss (20% of the amount of electric charge) in cycle efficiency of the lithium particles deposited in an electrolyte containing HF. The loss is strongly related to the consumption of the lithium metal through a chemical reaction with the electrolyte during the dissolution process (Chapters 6 and 8).
5. The most effective additive (HF complex) was proposed based on the above investigations using HF, and the possibility to realize a practical rechargeable lithium battery with a lithium metal anode was demonstrated using the charge-discharge cycle test (Chapter 9).

The most characteristic point in the present paper is that a small amount of HF, which had been considered as the impurity in nonaqueous electrolytes, is used as an additive for surface modification of the lithium metal anode. The suppression of the formation of dendritic lithium was accomplished by the surface condition control of the lithium metal using HF or HF complex. Consequently, the present study shows light on the realization of a practical lithium metal anode for rechargeable lithium batteries.

Appendix 1
Binding energies of various lithium compounds

Table A-1 Binding energies of various lithium compounds

Compounds	Binding energy* / eV				
	Li1s	O1s	C1s	F1s	Cl2p
Li_2O	53.7±0.1	528.8±0.1			
LiOH	54.6±0.1	531.6±0.1			
Li_2CO_3	55.0±0.1	532.0±0.1	290.1±0.1		
LiF	56.0±0.1			685.5±0.1	
LiCl	56.0±0.1				199.0±0.1

*The binding energies were calibrated by the C1s peak (285.0 eV) of a residual hydrocarbon gas adsorbed on samples in XPS analysis chamber

Table A-2 The Volume of Lithium and Lithium Compounds per 1 mole Lithium Atom

Compounds	Molar Volume(cm³)	Volume per 1 mole Lithium Atom(cm³)
Li_2CO_3	35.2	17.6
LiOH	16.4	16.4
$LiOH•H_2O$	27.8	27.8
LiF	9.84	9.84
Li_2O	14.8	7.42
Lithium metal	13.0	13.0

Appendix 2

Influence of x-ray radiation and Ar ion beam radiation on lithium compounds

In general, decomposition of chemical compounds by x-ray radiation or Ar ion beam radiation are one of the serious problem for XPS depth analysis. Therefore, damage of some lithium compounds, such as Li_2CO_3, LiOH, LiF, by x-ray radiation and Ar ion beam radiation was checked before the XPS analysis. Powders of these pure compounds were pelletized in a 6 mm diameter disk shape, and then were exposed to x-ray radiation (8 kV, 30 mA) for 1 hour or Ar ion beam (acceleration voltage, 2 kV; ion beam current, 8 μA) for 40 min in the XPS analysis chamber. LiF and Li_2CO_3 powders were purchased from Wako Chemical Industries, Ltd., and LiOH was synthesized by a vacuum drying treatment of LiOH-H_2O powder (Wako Pure Chemical Industries, Ltd., Japan) for 24 hours at room temperature. Anhydrous LiOH was identified by an x-ray diffraction pattern under a dry atmosphere.

Influence of x-ray radiation and Ar ion beam radiation on lithium compounds

Figure A-1 shows the XPS spectra of Li 1s, O 1s, F 1s, and C 1s for LiF, LiOH, and Li_2CO_3 standard samples before and after the x-ray radiation and the Ar ion beam radiation (the Ar ion etching). Two peaks were observed at 56.0 eV and 685.5 eV in the XPS spectra of Li 1s and F 1s for LiF (Figure A-1 (a) and (b)), respectively, before either the x ray radiation or the Ar ion beam radiation. These spectra were not changed by the x-ray radiation and the Ar ion beam radiation. Two peaks were observed at 54.7 eV and at 531.6 eV in the XPS spectra of Li 1s and O1s for LiOH (Figure A-1 (c) and (d)), respectively These peaks were not significantly changed by the x-ray radiation, although a slight decomposition of LiOH to Li_2O (at 53.7 eV in Li 1s, at 528.8 eV in O 1s) was observed after the Ar ion beam radiation for 20 min. However, no serious decomposition was

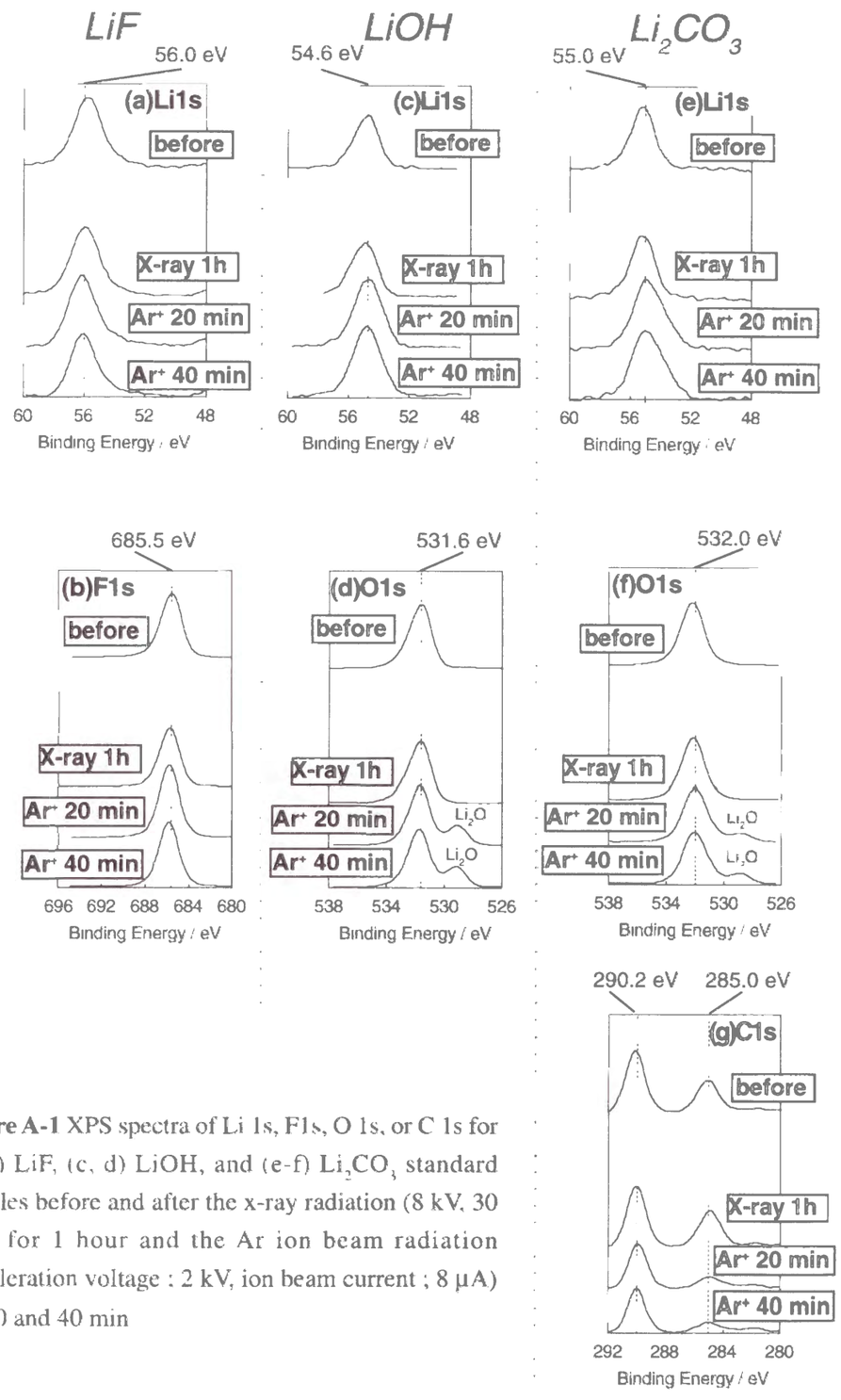

Figure A-1 XPS spectra of Li 1s, F1s, O 1s, or C 1s for (a, b) LiF, (c, d) LiOH, and (e-f) Li_2CO_3 standard samples before and after the x-ray radiation (8 kV, 30 mA) for 1 hour and the Ar ion beam radiation (acceleration voltage : 2 kV, ion beam current ; 8 μA) for 20 and 40 min

observed after the consecutive Ar ion beam radiation. These spectra indicate that the influence of the Ar ion beam radiation on LiOH is not significant. Peaks were observed at 55.0 eV, 532.0 eV, and 290.2 eV in the XPS spectra of Li 1s and O 1s, and C 1s for Li_2CO_3 (Figure A-1 (e), (f), and (g)), respectively. A peak at 285.0 eV in the C 1s spectra is due to a hydrocarbon gas adsorbed on the sample in the XPS analysis chamber. A slight decomposition of Li_2CO_3 to Li_2O was observed in the spectra after the Ar ion etching. This decomposition of Li_2CO_3 by the Ar ion beam radiation is negligible. From these results, it can be concluded that all compounds are sufficiently stable for the present study of the surface chemical conditions of lithium metal from XPS depth profiles.

References

[1] J. P. Gabano, in *Lithium Batteries*, J. P Gabano, Editors; Academic Press, London, (1983), Chapter 1

[2] Z. Takehara and K. Kanamura, *Electrochm. Acta*, **38**, 1169 (1993).

[3]J. R. Dahn, A. K. Sleigh, H. Shi, B. M. Way, W. J. Weydanz, J. N. Reimers, Q. Zhong, and U. von Sacken, in *Lithium Batteries-New Materials, Developments and Perspectives*, G. Pistoia, Editor, Elsevier Science, Amusterdam (1994), Chap. 1.

[4] S. Megahed and B. Scrosati, *Interface*, **4**, 34 (1995).

[5] D. Fauteux and R. Koksbang, *J. Applied. Electrochem.*, **23**, 1 (1993)

[6] K. Kanamura, *Denki Kagaku*, **65**, 722 (1997)

[7] R. D. Rauch and S. B. Brummer, *Electrochim. Acta*, **22**, 75 (1977).

[8] V. R. Koch, *J. Power Sources*, **6**, 357 (1981).

[9] I. Yoshimatsu, T. Hirai, and J. Yamaki, *J. Electrochem. Soc.*, **135**, 2422 (1988)

[10] M. Arakawa, S. Tobishima, Y. Nemoto, M. Ichimura, and J. Yamaki, *J. Power Sources*, **43-44**, 27 (1993).

[11] R. Selim and P. Bro, *J. Electrochem. Soc.*, **121**, 1457 (1974).

[12] M. Ue, in *Lithium Ion Battery*, M. Yoshio and A. Kozawa, Editors, Nikkan Kogyo Shinbunsha, Tokyo (1996), Chapter 6.

[13] M. Ue and S. Mori, *J. Electrochem. Soc.*, **142**, 2577 (1995).

[14] S. Tobishima and T. Okada, *Electrochim. Acta*, **30**, 1715 (1985).

[15] L. G. Scanlon, Jr., in *Batteries and Fuel Cells for Stationary and Electric Vehicle Application*, A. R. Landgebe and Z. Takehara, Editor; PV 93-8, The Electrochemical Society Proceedings Series, Pennington, NJ (1993), P.36.

[16] R. F. Scarr, *J. Electrochem. Soc.*, **117**, 295 (1970).

[17] M. Garreau, J. Thevenin and D. Warin, *Prog. Batt. Solar Cell*, **2**, 54 (1979).

[18] S. G. Meibuhr, *J. Electrochem. Soc.*, **118**, 1320 (1971).

[19] V. R. Koch and J. H. Young, *J. Electrochem. Soc.*, **125**, 1371 (1978)

[20] J. M. Sullivian, D. C. Hanson, and R. Keller, *J. Electrochem. Soc.*, **117**, 779 (1970).

[21] E. Peled, *J. Electrochem. Soc.*, **126**, 2047 (1979).

[22] D. Aurbach, M. L. Daroux, P. Faguy, and E. Yeager, *J. Electrochem. Soc.*, **134**, 1611 (1987).

[23] D. Aurbach and O. Chusid (Youngman), *J. Electrochem. Soc.*, **140**, L1 (1993).

[24] D. Aurbach, Y. Ein-Ely, and A. Zaban, *J. Electrochem. Soc.*, **141**, L1 (1994).

[25] D. Aurbach, A. Zaban, A. Schechter, Y. Ein-Ely, E. Zinigrad, and B. Markovsky, *J. Electrochem. Soc.*, **142**, 2873 (1995).

[26] K. Kanamura, H. Takezawa, S. Shiraishi, and Z. Takehara, *J. Electrochem. Soc.*, **144**, 1900 (1997).

[27] K. Morigaki, T. Fujii, and A. Ohta, *Denki Kagaku*, **66**, 824 (1998).

[28] D. Aurbach, B. Markovsky, A. Shechter, and Y. Ein-Eli, *J. Electrochem. Soc.*, **143**, 3809 (1996).

[29] G. Nazri and R. H. Muller, *J. Electrochem. Soc.*, **132**, 1385, (1985).

[30] G. Nazri and R. H. Muller, *J. Electrochem. Soc.*, **132**, 2050, (1985).

[31] D. Aurbach and Y. Gofer, *J. Electrochem. Soc.*, **138**, 3529 (1991).

[32] D. Aurbach, I. Weissman, and O. Chusid, *Electrochim. Acta*, **39**, 51 (1994).

[33] D. Aurbach, I. Weissman, and H.Yamin, and E. Elster, *J. Electrochem. Soc.*, **145**, 1421 (1998).

[34] M. Odziemkowski, M. Krell, and D. E. Irish, *J. Electrochem. Soc.*, **139**, 3052 (1992).

[35] S. Yen, D. Shen, R. Vasquez, F. Grunthander, and R. Somoano, *J. Electrochem. Soc.*, **128**, 1434 (1981).

[36] R. D. Zavadil and N. R. Armstrong, *J. Electrochem. Soc.*, **137**, 2371 (1990).

[37] K. Kanamura, H. Tamura, and Z. Takehara, *J. Electroanal. Chem.*, **333**, 127 (1992).

[38] T. Fujieda, N. Yamamoto, K. Saito, T. Ishibashi, M. Honjo, S. Koike, N. Wakabayashi, and S. Higuchi, *J. Power Sources*, **52**, 197 (1994).

[39] D. Aurbach, I. Weissman, and A. Schechter, *Langmuir*, **12**, 3991 (1996).

[40] T. Osaka, T. Momma, Y. Matsumoto, and Y. Uchida, *J. Electrochem. Soc.*, **144**, 1709

(1997).

[41] K. Wang, G. S. Chottiner, and D. A. Scherson, *J. Phys. Chem.*, **97**, 11075 (1993).

[42] K. Wang, P. N. Ross, Jr., F. Kong, and F. McLarnon, *J. Electrochem., Soc.*, **143**, 422 (1996).

[43] J. G. Thevenin and R. H. Muller, *J. Electrochem. Soc.*, **134**, 273 (1987).

[44] D. Aurbach and A. Zaban, *J. Electroanal. Chem.*, **367**, 15 (1994).

[45] C. Fringant, A. Tranchant, and R. Messina, *Electrochim. Acta*, **40**, 513 (1995).

[46] T. Osaka, T. Momma, T. Tajima, and Y. Matsumoto, *J. Electrochem. Soc.*, **140**, 2745 (1995).

[47] M. Ishikawa, Y. Takaki, M. Morita, and Y. Matsuda, *J. Electrochem. Soc.*, **144**, L90 (1997).

[48] M. Mori, Y. Naruoka, K. Naoi, and D. Fauteux, *J. Electrochem. Soc.*, **145**, 2340 (1998).

[49] N. Yamamoto, H. Hirasawa, H. Ishida, T. Tatsuma, and N. Oyama, *Bull. Chem. Soc. Jpn*, **67**, 1296 (1994).

[50] Y. Mo, Y. Gofer, E. Hwang, Z. Wang, and D. A. Scherson, *J. Electroanal. Chem.*, **409**, 87 (1996).

[51] D. Aurbach and Z. Zaban, *J. Electrochem. Soc.*, **142**, L 108 (1995).

[52] K. Naoi, M. Mori, and Y. Shinagawa., *J. Electrochem. Soc.*, **143**, 2517 (1996).

[53] D. Aurbach and M. Moshkovich, *J. Electrochem. Soc.*, **145**, 2629 (1998).

[54] M. Ishikawa, S. Yoshitake, M. Morita, and Y. Matsuda, *J. Electrochem. Soc.*, **141**, L159 (1994)..

[55] N. Koura, S. Tamura, and M. Yoshitake, *Denki Kagaku*, **63**, 623 (1995).

[56] D. Aurbach and Y. Cohen, *J. Electrochem. Soc.*, **143**, 3525 (1996).

[57] D. Aurbach and Y. Cohen, *J. Electrochem. Soc.*, **144**, 3355 (1997).

[58] K. Morigaki, A. Morita, and A. Ohta, *Denki Kagaku*, **66**, 831 (1998).

[59] D. Aurbach and Y. Cohen, *Electrochem. Solid. Lett.*, **2**, 16 (1998).

[60] K. Kanamura, H. Tamura, S. Shiraishi, and Z. Takehara, *J. Electrochem. Soc.*, **142**,

340 (1995).

[61] M. Odziemkovski and D. E. Irish, *J. Electrochem. Soc.*, **139**, 3063 (1992).

[62] M. Odziemkovski and D. E. Irish, *J. Electrochem. Soc.*, **140**, 1546 (1992).

[63] K. Kanamura, H. Tamura, S. Shiraishi, Z. Takehara, *J. Electroanal. Chem.*, **394**, 49 (1995).

[64] A. N. Dey, *Thin Solid Films*, **43**, 131 (1977).

[65] V. R. Koch, *J. Electrochem. Soc.*, **126**, 181 (1979).

[66] D. Aurbach, M. Daroux, P. W. Faguy, and E. Yeager, *J. Electrochem. Soc.*, **135**, 1863 (1988).

[67] Y. Malik, D. Aurbach, P. Dan, and A. Meitav, *J. Electroanal. Chem.*, **282**, 73 (1990).

[68] D. Aurbach, *J. Electrochem. Soc.*, **136**, 1606 (1989).

[69] D. Aurbach, O. Youngman, Y. Gofer, and A. Meitav, *Electrochim. Acta*, **35**, 625 (1990).

[70] Y. E. Ely and D. Aurbach, *Langmuir*, **8**, 1845 (1992).

[71] D. Aurbach, Y.Gofer, and J. Langzam, *J. Electrochem. Soc.*, **136**, 3198 (1989).

[72] K. Kanamura, S. Shiraishi, H. Tamura, and Z. Takehara, *J. Electrochem. Soc.*, **141**, 2379 (1994).

[73] D. Aurbach and A. Zaban, *J. Electrochem. Soc.*, **141**, 1808 (1994).

[74] K. Kanamura, S. Shiraishi, and Z. Takehara, *J. Electrochem. Soc.*, **143**, 2187 (1996).

[75] D. Aurbach and E. Granot, *Electrochim. Acta*, **42**, 697 (1997).

[76] J. M. Diggle, A. R. Despic, and J. O'M. Bockris, *J. Electrochem. Soc.*, **116**, 1503 (1969).

[77] A. R. Despic, J. W. Diggle, and J. O'M. Bockris, *J. Electrochem. Soc.*, **115**, 507 (1968).

[78] J. Yamaki, S. Tobishima, K. Hayashi, K. Saito, Y. Nemoto, and M. Arakawa, *J. Power Sources*, **74**, 219 (1998).

[79] D. Aurbach, Y. Gofer, M. Ben-Zion, P. Aped, *J. Electroanal. Chem.*, **339**, 451 (1992).

[80] T. Osaka, T. Momma, T. Tajima, and Y. Matsumoto, J. Electrochem. Soc., **142**, 1057 (1995).

[81] T. Osaka, T. Momma, T. Tajima, and Y. Matsumoto, *Denki Kagaku*, **62**, 450 (1994).

[82] K. M. Abraham, J. S. Foos, and J. L. Goldman, *J. Electrochem. Soc.*, **131**, 2197 (1984).

[83] M. Morita, S. Aoki, and Y. Matsuda, *Electrochim. Acta*, **37**, 119 (1992).

[84] H. Nakamura, C. Wang, E. Mitani, T. Fujita, and M. Yoshio, *J. Surf. Finish. Soc. Jpn.*, **46**, 1187 (1995).

[85] T. Hirai, I. Yoshimatsu, and J. Yamaki, *J. Electrochem. Soc.*, **141**, 2300 (1994).

[86] A. T. Ribes, P. Beaunier, P. Willmann, and D. Lemordant, *J. Power Sources*, **58** (1996) 189.

[87] S. Hofmann, in *Practical Surface Analysis*, Vol. 1, D. Briggs and M. P. Seah, Editors; Wiley, Chichester (1983), Chap. 4.

[88] B. Beden and C. Lamy, in *Spectroelectrochemistry*, R. J. Gale, Editors; Plenum Press (1988), P. 47.

[89] T. Kudo and K. Fueki, in *Solid State Ionics*, Kodansha, Tokyo (1986), P. 73.

[90] D. W. A. Sharp, in *Advances in Fluorine Chemistry*, Vol. 1, M. Stacey, J. C. Tatlow, and A. G. Sharpe, Editors; Butterworths Scientific Pub., London (1960), P.69.

[91] D. H. Aue and M. T. Bowers, in *Gas Phase Chemistry*, Vol. 2, M. T. Bowers, Editors; Academic Press, New York (1979), Chap. 9.

[92] D. Pletcher, J. F. Rohan, and A. G. Ritchie, *Electrochim. Acta*, **39**, 1369 (1994).

[93] M. W. Verbrugge and B. J. Koch, *J. Electroanal Chem.*, **367**, 123 (1994).

[94] D. Pletcher, J. F. Rohan, and A. G. Ritchie, *Electrochim. Acta*, **39**, 2015 (1994).

[95] X. Wang, T. Nishina, and I. Uchida, *The Journal of the Surface Finishing Society of Japan*, **46**, 941 (1995).

[96] W. H. Mulder and J. H. Sluyters, *Electrochim. Acta*, **33,** 303 (1988).

[97] M. P. Seah, in *Practical Surface Analysis*, Vol. 1, D. Briggs and M. P. Seah , Editors; John Wiley & Sons : Sussex (1983), Chapter 5.

[98] K.R. Zavadil, N. R. Armstrong, *Surface Science*, **230**, 47 (1990).

[99] G. Binnig, H. Rohrer, C. Gerber, and E. Weibel, *Appl. Phys. Lett.*, **40**, 178 (1982).

[100] D. Sarid, *Scanning Force Microscopy*, Oxford Univ. Press (1991).

[101] R. Wiesendanger, *Scanning Probe Microscopy and Spectroscopy*, Cambridge Univ Press (1994)

[102] G. Binnig, C. F. Quate, and C. Gerber, *Phys. Rev. Lett.*, **56**, 930 (1986).

[103] M. Nonnenmacher, M. O'Boyle, and H. K. Wickramsinghe, *Appl. Phys. Lett.*, **58** 2921 (1991).

[104] H. Yokoyama and T. Inoue, *Thin Solid Films*, **242**, 33 (1994).

[105] M. Fujihira and H. Kawate, *Thin Solid Films*, **242**, 163 (1994).

[106] *Magnetic & Electric Force Imaging with SPMs-Phase and Amplitude Detection Techniques*, Support Note No.201, Rev. C, Digital Instruments, Inc.

[107] G. K. Wertheim, P. M. Th. M. Van Attekum, and S. Basu, *Solid State Commun.*, **33** 1127 (1980).

[108] D. A. Buttry and M. D Ward, *Chem. Rev.*, **92**, 1355 (1992).

[109] D. A. Buttry, in *Electroanalytical Chemistry*, Vol. 17, A. J. Bard, Editors; Marcel Dekker, Inc., New York (1990), P.1

[110] C. Chen , S. Vesecky, and A. Gewirth, *J. Am. Chem. Soc.*, **114**, 451 (1992).

[111] R. M. Rynders and R. C. Alkire, *J. Electrochem. Soc.*, **141**, 1166 (1994).

[112] I. Schmitz, M. Schreiner, G. Friedbacher, and M. Grasserbauer, *Anal. Chem.*, **69** 1012 (1997).

[113] K. N-Dejanovic and P. A. Maurice, *Colloids Surf. A*, **120**, 77 (1997)

[114] S. Boussaad, N. J. Tao, and R. Arechabaleta, *Chem. Phys. Lett.*, **280**, 397 (1997).

[115] G. A. Olar, J. T. Welch, Y. D. Vanker, M. Nojima, I. Kwewkwa, and J. A. Olar, *J. Org. Chem.*, **44**, 3872 (1979).

[116] K. Momota, M. Morita, and Y. Matsuda, *Electrochim. Acta*, **38** (1993) 1123.

List of Publications

The content of each chapter has been or will be published as follows.

Chapter 1

Influence of Initial Surface Condition of Lithium Metal Anodes on the Surface Modification
S. Shiraishi, K. Kanamura, and Z. Takehara,
J. Applied Electrochemistry, accepted.

X-ray Photoelectron Spectroscopic Analysis and Scanning Electron Microscopic Observation of the Lithium Surface Immersed in Nonaqueous Solvent
K. Kanamura, S. Shiraishi, H. Tamura, and Z. Takehara
J. Electrochem. Soc., **141**, 2379-2385 (1994)

Chapter 2

Effect of Surface Modification Using Various Acids on Electrodeposition of Lithium
S. Shiraishi, K. Kanamura, and Z. Takehara
J. Applied Electrochem., **25**, 584-591 (1995).

Chapter 3

Morphology and Chemical Composition of Surface Films of Lithium Deposited on an Ni Substrate in Nonaqueous Electrolytes
K. Kanamura, H. Tamura, S. Shiraishi, and Z. Takehara
J. Electroanal. Chem., **394,** 49-62 (1995).

Chapter 4

Electrochemical Deposition of Very Smooth Lithium Using Nonaqueous Electrolytes Containing HF
K. Kanamura, S. Shiraishi, and Z. Takehara
J. Electrochem. Soc., **143**, 2187-2197 (1996)

Chapter 5

The Study for Surface Condition of Highly Smooth Lithium Deposited in Various Carbonate Electrolytes Containing HF
S.Shiraishi, K. Kanamura, and Z. Takehara
Langmuir, **13**, 3542-3549 (1997)

Chapter 6

Surface Condition Changes in Lithium Metal Deposited in Nonaqueous Electrolyte Containing HF by Dissolution-Deposition Cycles
S. Shiraishi, K. Kanamura, and Z. Takehara
J. Electrochem. Soc., in press.

Chapter 7

Clear Imaging of Uniformity of Lithium Metal Surface using Tapping Mode-Atomic Force and Surface Potential Microscopy,
S. Shiraishi, K. Kanamura, and Z. Takehara,
Submitted for publication to *Electrochem. Solid. Lett.*

Chapter 8

The Observation of Electrochemical Dissolution for Lithium Metal Using *in-situ* Tapping Mode Atomic Force Microscopy and Electrochemical Quartz Crystal Microbalance
S. Shiraishi, K. Kanamura, and Z. Takehara,
Langmuir, **14**, 7082-7086 (1998).

Chapter 9

Electrochemical Deposition of Lithium Metal in Nonaqueous Electrolyte Containing $(C_2H_5)_4NF(HF)_4$ Additive
K. Kanamura, S. Shiraishi, and Z. Takehara,
J. Fluorine Chemistry, **87**, 235-243 (1998).

Related Publications

Surface Modification of Lithium Metal by Using $(C_2H_5)_4NF(HF)_4$ additive to Propylene Carbonate Containing $LiClO_4$
S. Shiraishi, K. Kanamura, and Z. Takehara
Recent Research Developments in Pure & Applied Chemistry, **1**, 45-53 (1997).

XPS Analysis for the Lithium Surface Immersed in γ-butyrolactone Containing Various Salts
K. Kanamura, H. Tamura, S. Shiraishi and Z. Takehara
Electrochim. Acta, **40**, 913-921 (1995)

Morphology Control of Lithium Deposited in Nonaqueous Media
K. Kanamura, S. Shiraishi, and Z. Takehara
Chemistry Letters, No.3, 209-210 (1995).

Electrochemical Deposition of Uniform Lithium on an Ni Substrate in a Nonaqueous Electrolyte
K. Kanamura, S. Shiraishi, and Z. Takehara
J. Electrochem. Soc., **141**, L108-110 (1994).

Acknowledgment

The author would like to express my sincerest gratitude to Professor Yasuhiko Ito, Kyoto University, for his helpful advice and encouragement on publishing the thesis. The present studies have been carried out under Professor Zen-ichiro Takehara and Associate Professor Kiyoshi Kanamura at Kyoto University.

The author would like to express special thanks to Professor Zen-ichiro Takehara, Kansai University, and Associate Professor Kiyoshi Kanamura, Tokyo Metropolitan University, for helpful advice, suggestion and careful reading of the manuscript.

The author is deeply indebted to Mr. Hideharu Takezawa for *in-situ* FTIR measurements.

Finally, the author would like to express hearty gratitude to Professor Asao Oya and Associate Professor Jun-ichi Ozaki at Gunma University for their kind support and encouragement.

Soshi Shiraishi

Department of Chemistry, Faculty of Engineering

Gunma University,

Kiryu, Gunma 376-8515, Japan

1999